Universidad de Valladolid

IMG PHARMA

LIPID RAFTS IN BRAIN CELLS

FROM ENZYMATIC ACTIVITY TO LIPIDOMIC ASSAYS IN A NOVEL PRINTED RAFTS PLATFORM

Ph.D. Thesis

Laura Sánchez Sánchez

Supervised by:
María Dolores Ganfornina Álvarez
Gabriel Barreda-Gómez

December 2023

Universidad de Valladolid

Escuela de Doctorado Universidad de Valladolid

PhD PROGRAM IN BIOMEDICAL RESEARCH

DOCTORAL THESIS

LIPID RAFTS IN BRAIN CELLS: FROM ENZYMATIC ACTIVITY TO LIPIDOMIC ASSAYS IN A NOVEL PRINTED RAFTS PLATFORM

By Laura Sánchez Sánchez

To apply for Ph.D. degree at the

University of Valladolid

Supervised by:

María Dolores Ganfornina Álvarez, PhD

Gabriel Barreda Gómez, PhD

INDEX

FIGURE INDEX

TABLE INDEX

ABBREVIATIONS

%	Percentage
A.U	Arbitrary units
AA	arachidonic acid
AChE	Acetilcholinesterase
AD	Alzheimer disease
Akt	Protein kinase B
ANOVA	Analysis of variance
ApoD	Apolipoprotein D
ApoE	Apolipoprotein E
APP	Amyloid precursor protein
APS	Ammonium persulfate
ATCC	American Type Culture Collection
ATP	Adenosine 5′-triphosphate
Aβ	Amyloid-β
BMP	Bis(monoacylglycerol)phosphate
BSA	Bovine serum albumin
BuChE	Butyrylcholineserase
CCD	Charge-coupled device
CCo	Cytochrome c Oxidase
CD	Cluster of differentiation
CE	Calibration error
Cer	Ceramide
CerP	Ceramide Phosphate
CGT	UDP-galactose:ceramide galactosyltransferase
ChE	Cholinesterase
CL	Cardiolipin
cm	Centimeter
CMMA	Cell Membrane Microarray

ABBREVIATIONS

CoQ	Coenzyme Q
COX	Cyclooxygenase
cPLA2	Cytosolic phospholipase A2
CRAC	Cholesterol Recognition/interaction Amino acid Consensus sequence
CYP	Cytochrome P450
CytC	Cytochrome C
Da	Dalton
DAB	3,3-Diaminobenzidine Tetrahydrochloride hydrate
DAN	1,5-diaminophtalene
DF	Deviation factor
DG	Diacylglycerols
dH_2O	Distilled wáter
DMEM	Dulbecco's Modified Eagle Medium
DMSO	Dimethylsulfoxide
DTT	Dithiothreitol
DUOX	Dual oxidase
dUQ	Decylubiquinone
ECL	Enhanced Chemoluminiscence
EDTA	Ethylenediaminetatraacetic acid
FA	Fatty acid
FBS	Fetal Bovine Serum
FC	Fold change
FWHM	Full width at half maximum
g	Universal gravitational force
G_3P	Glyceraldehyde-3-phosphate
GAPDH	Glyceraldehyde-3-phosphate dehydrogenase
GL	Glycerolipids
GP	Glycerophospholipids

GPCR	G protein-coupled receptors
GPI	Glycosylphosphatidylinositol
h	Hour
Hex2Cer	Dihexosylceramide
HexCer	Hesoxylceramide
HflK	High-frequency lysogenization Kinase
HRP	Horseradish peroxidase
IF	Immunofluorescence
IGF	Insulin-like growth factor
IL-4	Interleukin 4
IL-6	Interleukin 6
IP	Integral protein
kNN	k-Nearest neighbors
LCPUFA	long-chain polyunsaturated fatty acids
LD	Liquid-disordered
L-Glut	L-Glutamine
LGP	Lysoglycerophospholipid
LO	Liquid-ordered
LOX	Lipoxygenase
LPA	Lysophosphatidic acid
LPC	Lysophosphatidylcholine
LPE	Lysophosphatidylethanolamine
LPG	Lysophosphatidylglycerol
LPI	Lysophosphatidylinositol
LRRK2	Leucine-rich repeat kinase 2
LTQ	Lineal ion trap
m/z	Mass to charge ratio
MALDI	Matrix-Assisted Laser Desoprtion Ionization
MAO	Monoamine-oxidase

ABBREVIATIONS

MBT	2-mercaptobenthiazole
mETC	Mitochondrial electron transport chain
min	Minute
ml	Milliliters
MS	Mass spectrometry
MS-	Ion-negative mode in mass spectrometry
MS+	Ion-positive mode in mass spectrometry
N/A	Not applicable
NAD+	Nicotinamide adenine dinucleotide
NADH	Nicotinamide adenine dinucleotide reduced form
NAPDH	Nicotinamide adenine dinucleotide phosphate reduced form
NBT	Nitrotetrazolium blue chloride
NEAA	Non-essential amino acid
NOX	NADPH-oxidase
O.D	Optical density
°C	Celsisus Degree (centigrade)
OL	Outlier limit
OXPHOS	Oxidative phosphorylation
P/S	Penicillin/Streptomycin
PA	Phosphatidic acid
PAGE	Polyacrylamide gel electrophoresis
PB	Phosphate buffer
PBS	Phosphate-buffered saline
PBST	PBS-Tween 20
PC	Phosphatidylcholine
PCA	Principal component analysis
PC-PLC	PC-specific phospholipase C
PD	Parkinson's disease
PDGF	Platelet-derived growth factor

PE	Phosphatidylethanolamine
PG	Phosphatidylglycerol
PI	Phosphatidylinositol
PI	Phosphatase inhibitor
PI3K	Phosphatidylinositol 3 kinase
PIP	Phosphoinositol phosphate
PLC	Phospholipase C
PP	Peripheral protein
PQ	Paraquat
PQ+	Paraquat mono-cation
PRPSC	The scrapie prion protein
PS	Phosphatidylserine
PUFA	Polyunsaturated fatty acid
PVDF	Polyvinylidene difluoride
R.I	Relative intensity
ReLu	Rectified linear unit function
RET	Reverse electron transort
RMMA	Raft and non-raft microarray
ROS	Reactive oxygen species
Rpm	Revolutions per minute
RT	Room temperature
S.E.M	Standard error of the mean
S-1-P	Sphingosine-1-phosphate
SDH	Succinate dehydrogenase
SDS	Sodium Dodecyl Sulfate
SHexCer	Sulfatide
SL	Sphingolipid
SM	Sphingomyelin
SMase	Sphingomyelinase

SOL	Spectra outlier limit
SPFH	Stomatin/prohibitin/flotillin/HflK/C
SRP	Signal recognition particle
STD	Standard deviation
SW	Swinging bucket
TBS	Tris-Buffered saline
TEMED	N,N,N,N-Tetramethylethylenediamine
TG	Triacylglycerol
TIC	Total Ion Current
TNE	Tris-HCl, NaCl, EDTA
TNF-α	Tumor necrosis factor alpha
TX-100	Triton X-100
TX-114	Triton X-114
ULC	Ultra-long chain
V	Volt
VLCFA	Very long chain fatty acid
Vs	*Versus*
α-syn	α-synuclein
λ	Wavelength

SUMMARY

SUMMARY

Lipid rafts are liquid-ordered membrane domains where specific enzymes are located. These membrane platforms play crucial roles in a variety of signaling pathways. Thus, alterations in the lipidic environment, such as those elicited by oxidative stress, can lead to important functional disruptions in membrane proteins.

In this sense, the dysregulation of the Reactive Oxygen Species (ROS) levels derived from the impairment of cellular homeostasis can trigger lipid peroxidation, oxidative modification of proteins, and DNA damage. Mitochondrial electron transport chain (mETC), as well as certain oxidoreductase enzymes, can be source of oxidative stress by the production of ROS. Many of these enzymes are located lipid rafts, being a key players in certain signaling pathways. However, the difficulties inherent to work with this very specific and scarce fraction of membranes limit their study.

Cell membrane microarrays (CMMAs) has emerged in the last decade as a powerful methodology for the study of both lipids and membrane proteins. Lipidomic and enzymatic activity assays have been successfully performed in CMMAs. Based on that technology and the importance of liquid-ordered subdomains, we have developed a printed lipid raft and non-raft platform (raft membranes microarrays, RMMAs), with preserved native protein structure and lipidic environment.

To evaluate the differences over lipidic environment in raft and non-raft subdomains in control, metabolic and oxidative stress conditions MALDI-MS assay was performed on RMMAs. Raft and non-raft subdomains presented a distinguishable fingerprint in every condition in both cell types (astrocytes and neurons). Distinguishable lipid fingerprints were also observed comparing printed raft subdomains obtained from cells in control, metabolic and oxidative stress situations. In the same way, raft and non-raft printed domains from control astrocytes and neurons are also distinguishable. Therefore, the lipidomic data obtained with this RMMA methodology can be used as a classification tool for samples of raft and non-raft subdomains with different treatments.

As the lipidic environment is a key aspect for proper physiological enzymatic activity, changes over lipidome can lead to differences between enzymatic activities.

SUMMARY

To evaluate the differences in enzymatic activities inside the raft domains between stressed and non-stressed astrocytes, NADH oxidoreductase, GADPH, and cholinesterase (ChE) activity assays were performed on RMMAs. Higher NADH oxidoreductase activity in raft domains from metabolically stressed astrocytes was observed, whereas no differences were observed in Glyceraldehyde-3-phosphate dehydrogenase (GAPDH) and acetylcholinesterase activities. By contrast, rafts from neuronal samples presented high activity of both GAPDH and acetylcholinesterase. Furthermore, NADH and GAPDH activities revealed a positive correlation between them and specific phospholipids, but surprisingly not with sphingolipids, one of the main components of lipid rafts. Thus, these data show the close relationship between lipidic structure in liquid-ordered domains and enzymatic activities, and also that both analyses can be performed using a single platform with minimal amount of sample.

The results presented in this Ph.D. thesis reveal the importance of a proper lipidic environment in lipid raft domains, and the impact over enzymatic activities, in two major cell types of the nervous system. This thesis demonstrates the suitability of this newly-developed technology to make high-throughput analysis of lipid environment-function relationships in printed RMMAs of neuronal and astrocyte membranes.

INTRODUCTION

1 Biological membranes

Biological membranes are a group of structures derived from a combination of proteins, lipids, and sugar species, organized in two layers or leaflets (reviewed by Honigmann & Pralle, 2016; Rothfield & Finkelstein, 1968), which are non-homogenously distributed and present asymmetry in each leaflet (reviewed by Emmelot & van Hoeven, 1975; Holthuis & Menon, 2014; Honigmann & Pralle, 2016; Quinn, 2002). The presence of membranes is a key aspect of cellular physiology, architecture maintenance (reviewed by Casares et al., 2019), and compartmentalization of biochemical reactions (reviewed by Honigmann & Pralle, 2016), as they provide a physical barrier between intracellular and extracellular compartments (reviewed by Chiu, 2012). Membrane formation has been widely studied using model membranes composed of phospholipids, as they are their major constituent and can associate themselves spontaneously. The auto-organization of model membranes can be accomplished in three different states or phases: hydratated crystal (Lc or high order phase), gel (L_β or disordered phase), and liquid crystal (L_α or more fluid state)(Matsuki et al., 2019), which can be transformed into each other (Matsuki et al., 2019). Concerning the lipid component of animal's membranes, heterogeneity in lipid states or phases has been observed (A. Lee, 2001) similar to those described in model membranes.

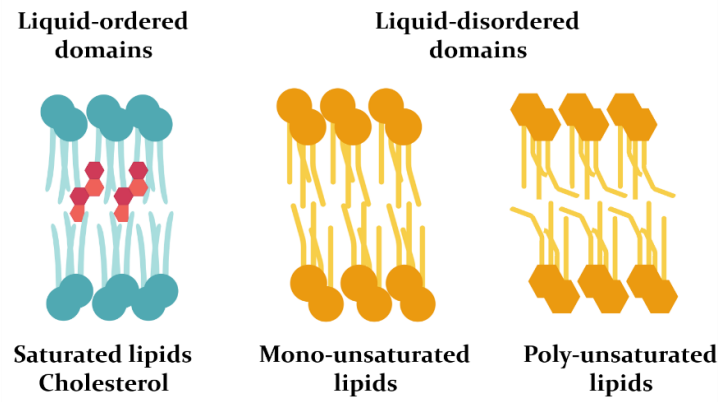

Figure 1: Liquid-ordered and liquid-disordered phases produced by different types of lipids and their degree of unsaturation (Figure adapted from Harayama & Riezman, 2018).

Therefore, depending on lipid composition, this structure can be in a solid, liquid-ordered (LO), or liquid-disordered state (LD) (reviewed by Honigmann & Pralle, 2016; Owen et al., 2012) (Figure 1). These membrane states (LO and LD) involve different intrinsic properties such as the level of membrane packing (reviewed by

Kaiser et al., 2009), lipid composition, permeability (Anderson, 1966), diffusion of fluid-soluble particles (Almeida et al., 1992), and homogeneity or heterogeneity in membrane proteins distribution among others. Regarding membrane proteins, although a general random mixture has been observed due to their diffusion capacity in plasma membrane, they can also be heterogeneously distributed in different regions of these membranes, called domains, associated with specific lipids with different rate of unsaturation (Popov-Čeleketic & van Bergen en Henegouwen, 2014). In these domains, proteins decrease their diffusion ability, contributing in this way to the compartmentalization of membranes in different types of domains, and, as a consequence, compartmentalization of cellular processes (reviewed by Patel et al., 2008).

1.1 Membrane proteins

Membrane proteins, which represent up to 30% of protein-encoding genes (Curnow, 2019; Souda et al., 2011), are associated with plasma and organelles' membranes (Smith, 2017). These proteins are essential for the maintenance of cell physiology as they transport nutrients, ions, and residues across compartments, and participate in inter and intra-cellular communication (reviewed by Chiu, 2012).

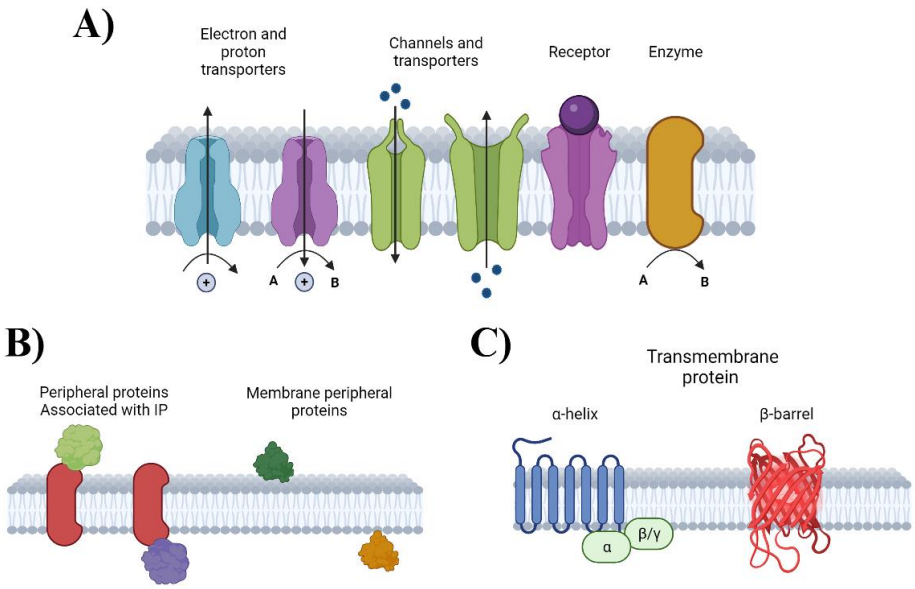

Figure 2: Function and types of different membrane proteins. A) Integral membrane protein types. B) Peripheral membrane proteins, associated with integral proteins (IP) or with membranes. C) structures of integral proteins (Figure adapted from Hedin et al., 2011).

Depending on the interaction with the membrane bilayer, proteins can be classified as integral (partially or fully embedded in the membrane) and peripheral (do not

pass through the membrane) (Hedin et al., 2011; Ohlendieck, 1996; Smith, 2017)(Figure 2). Integral membrane proteins (IP), which includes receptors, channels, and transporters (Shinoda et al., 2016) interact with cell membranes (CM) via their hydrophobic helix structures and their interaction with lipids acyl chain (E. Cybulski & de Mendoza, 2011). Unlike them, peripheral proteins (PP) interact with membranes in a reversible way, thus they can be found in soluble or membrane-bound state. The later state can be mediated by covalent (lipid-anchor) (Larsen et al., 2022) or non-covalent interactions with the lipid components, which will be different depending on the leaflet (inner or outer). In the inner membrane leaflet, anionic-headed lipids, such as phosphatidylserines (PS) or phosphatidylinositol phosphates (PIP) (Larsen et al., 2022), interact with positively charged aminoacids (Vorobyov & Allen, 2011). On the other hand, the outer membrane leaflet mainly present zwitterionic lipids (Vorobyov & Allen, 2011; Wodlej et al., 2019), such as phosphatidylcholines (PCs) interacting with proteins by electrostatic and other forces (Nicolson & Ferreira de Mattos, 2021), or through a Glycosilphosphatidylinositol (GPI)-lipid anchors (Critchley et al., 2004). In addition, the origin and synthesis of each type is different, PPs that associate to the cytosolic site are generally synthesized in the ribosomes present in the cytoplasm, whereas extracellular PPs or IPs are synthetized in the endoplasmic reticulum (ER) (Brumley & Marchase, 1991). After synthesis, the integration of IP in the membrane is carried out by different pathways, such as signal recognition particle (SRP) dependent pathway, secretase traslocon (Sec) pathway (Hedin et al., 2011), or mitochondrial twin-pore translocase (Rehling et al., 2004).

1.2 Membrane Lipids

Lipids are key molecules for function and structure of proteins in cell membranes. Lipids are organic amphipathic molecules which compose the membranes (reviewed by Harayama & Riezman, 2018) and are implicated in varied functions like energy storage (reviewed by Mesa-Herrera et al., 2019), signaling reactions, or post-translational protein-modifications (reviewed by Harayama & Riezman, 2018). As described above, asymmetry in membrane lipids has been found between inner and outer leaflet. Positively charged or zwitterionic phospholipids and sphingolipids are present in the outer membrane leaflet (Emmelot & van Hoeven, 1975) while negatively charged phospholipids such as PSs and PIs are present in the inner membrane leaflet (Op den Kamp, 1979; Sebastian et al., 2012). Lipids interact with

each other via cohesive and repulsive forces. The later are implicated in the interaction of phospholipids and water, whereas London-van der Waals forces (attractive) are implicated in lateral cohesion. Thus, the forces implicated in lipid membrane cohesion are decisive for proteins lateral diffusion and protein organization in membrane domains.

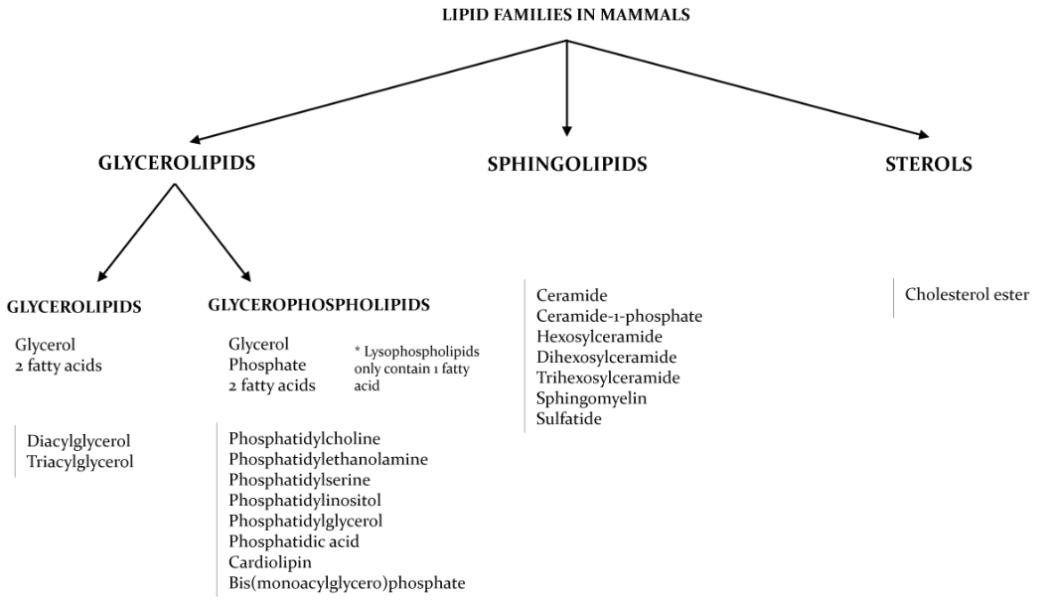

Figure 3: Principal lipid classes in mammalian cells.

There are four main families of lipids in all animal membranes: glycerophospholipids (GPs), sphingolipids (SLs), glycerolipids (GLs) and sterols (STs) (Spector & Yorek, 1985) (Figure 3). Within the families, there are different molecular compositions, the mixture of those lipids exhibits an asymmetry inside the membrane (due to the presence of membrane domains) (Gupta et al., 2020) and between both leaflets. Within a family, lipids can be differentiated by their head group, number of carbons, and number of double bonds (Figure 4). GPs are the main constituent of membranes. This family combines 9 different types of lipid species. Figure 4 shows the structure of six common GPs, that contains two fatty acids besides the head group linked to a glycerol molecule. Fatty acids attached to the glycerol group in GPs usually present a saturated and unsaturated fatty acid in C1 and C2 positions respectively (Ziegler & Tavosanis, 2019). In contrast, Lyso-glycerophospholipids (LGPs), have lost one of the fatty acid chains. All GPs are found in plasma and organelle's membranes, but only cardiolipins (CLs) (not shown) (Lucken-Ardjomande Hasler, 2012) and bis(monoacylglycerol)phosphates

(BMP)(Tengstrand et al., 2010), are specifically enriched in mitochondria and endosomal-lysosomal membranes respectively (Casares et al., 2019).

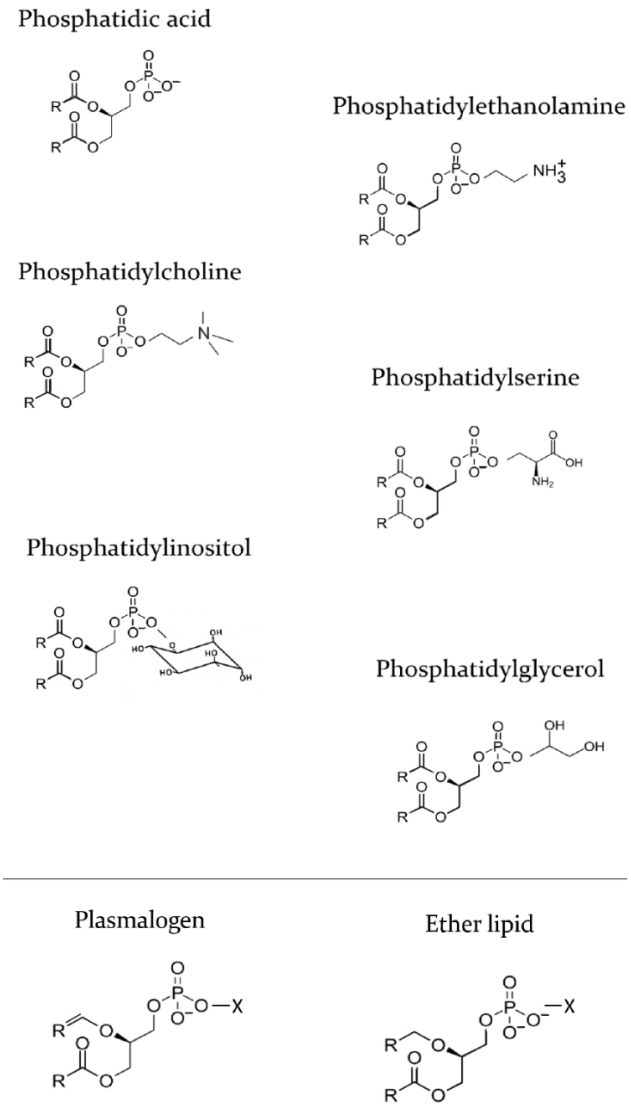

Figure 4: Different types of glycerophospholipids present in cellular membranes. Phosphatidic acid (PA), Phosphatidylethanolamine (PE), Phosphatidylcholine (PC), Phosphatidylserine (PS), Phosphatidylinositol (PI), Phosphatidylglycerol (PG). R in figure refers to fatty acid chain. Every type of GP could be normal GP, ether GP or plasmalogen (images at the bottom), X represent the headgroup.

Most abundant GPs in human brain are PCs, followed by phosphatidylethanolamines (PEs), lysophosphatidylglycerols (LPGs), phosphatidic acids (PAs), and phosphatidylglycerols (PGs) (Ziegler & Tavosanis, 2019). PE ethers (O-PEs), PC ethers (O-PCs), and plasmalogens are also common in brain tissues (Chan et al., 2012) (Figure 4). Moreover, plasmalogens are a subclass of GPs whose alkyl and acyl chains are linked to the glycerol molecule by a vinyl-ether bond to the first and second positions respectively (Udagawa & Hino, 2022), and are described

to be a component of lipid raft domains. The second most abundant lipid membrane components are SLs, a group which comprise 6 main groups of lipids that are classified by their head group (Table 1).

Table 1: Sphingolipid classification by different head groups. Ceramide (Cer), Ceramide phosphate (CerP), Sphingomyelin (SM), Hexosylceramide (HexCer), Dihexosylceramide (Hex2Cer), Sulfatide (SHexCer).

Sphingolipid	Head group
Ceramide	
Ceramide Phosphate	Phosphate
Sphingomyelin	Phosphocholine
Hexosylceramide	Neutral Sugar molecule
Dihexosylceramide	Neutral disaccharide molecule
Sulfatide	Sulfated Galactose sugar molecule

The head group can be absent or present and it is composed by one or more molecules attached to the sphingoid base (sphingosine, the most common, sphinganine or hydroxysphinganine) (Figure 5). SLs includes Ceramides (Cer), sphingomyelins (SM), hexosylceramides (HexCer), dihesoxyl ceramides (Hex2Cer), and sulfatides (SHexCer).

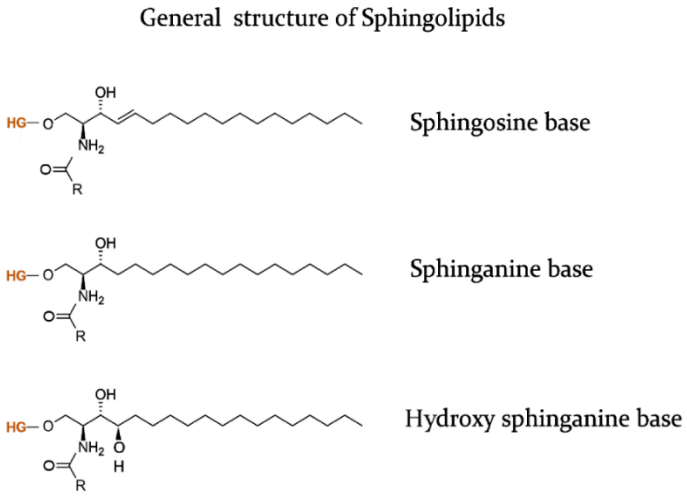

Figure 5: General structure of sphingolipids. Sphingolipids present a sphingoid base that can be Sphingosine, sphinganine or 4-hydroxysphinganine. Classification of the different types of sphingolipids are made by its head group (HG in figure).

GLs include mainly diacylglycerol (DG) and triacylglycerol (TG), which are composed of a glycerol molecule and 2 or 3 fatty acids linked to it, with no head group. GLs and SLs are also intermediaries in diverse second messenger signaling cascades, such as the case for lysophosphatidic acid (LPA) or sphingosine-1-phosphate (S-1-P)(Ghosh et al., 1997). Nevertheless, various GPs can be related to

different biosynthetic pathways (Figure 6) (Farooqui et al., 2000; Hishikawa et al., 2014). That is the case for the synthesis of LGPs from GPs in the remodeling pathway (Figure 6) or the synthesis of PEs, PCs or PSs from DGs in the *de novo* pathway (Figure 6), implying the possibility of lipid transformation (Hishikawa et al., 2014).

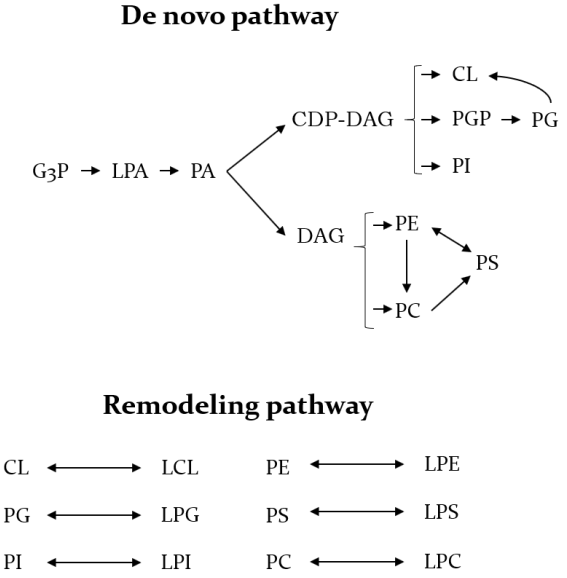

Figure 6: Biosynthetic pathways of glycerophospholipids. De novo pathway (up), glycerophospholipid synthesis from glyceraldehyde-3 phosphate. Remodeling pathways (down) glycerophospholipids processed to obtain lysophospholipids. Abbreviation: Glyceraldehýde-3-phosphate (G3P); Lysophosphatidic acid (LPA); phosphatidic acid (PA), diacylglycerol (DAG), Cytidine diphosphate - diacylglycerol (CDP-DAG), cardiolipin (CL); glycerophosphoglycerol phosphate (PGP), glycerophosphoglycerol (PG), glycerophosphoinositol (PI), glycerophosphoethanolamine (PE), glycerophosphocholine (PC), glycerophosphatidilserine (PS). Abbreviations mentioned before preceded by an L (LCL, LPG…) are lysoglycerophospholipids of the molecules mentioned. (Figure adapted from Hishikawa et al., 2014).

Finally, STs are a group of organic compounds derived from isoprenoids. Sterol lipid family can directly interact with GPs and proteins and serves as metabolic precursor of steroid hormones. STs also have a key role in the regulation of membrane structure, permeability and in some hormones signaling pathways (L. Yu et al., 2021). Cholesterol, the most abundant sterol, is present in different amounts depending on the membrane. The range varies from 5% in mitochondrial membranes to 40 % in plasma membrane (Chakraborty et al., 2020). It can be found in free form (mainly associated to the cytosolic leaflet) or esterified to long-chain fatty acids forming cholesterol esters (CEs). CEs can interact with acyl chains from other lipids and the membrane properties (Marquardt et al., 2016), in particular fluidity, that affect ion channels, and modulates signal transduction processes (Eckert et al., 2003; Gimpl et al., 1997). Distribution of intra-membrane cholesterol is strictly regulated,

however changes in the abundance of cholesterol are related with ageing processes. In this sense, the ratio between cholesterol and phospholipids is crucial to maintain a correct fluidity in neuronal membranes (Eckert et al., 2003).

2 Membrane domains: Lipid rafts

The combination of GPs, SLs, GLs, and cholesterol constitute the complete lipidome that can be organized in liquid-ordered and disordered domains within membranes (Lu & Fairn, 2018). To form the domains, lipid associations are influenced by the cytoskeleton, specific proteins, and electrostatics forces (Lu & Fairn, 2018). Those domains can be classified by their size as lipid ligands, lipid shells, nanodomains, diffraction limited structures or visible structures (Figure 7). Although, in those groups there are different classification depending on their characteristics such as the shape, lipid and protein composition.

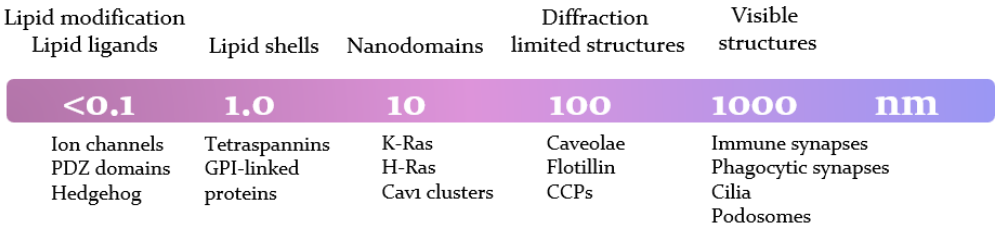

Figure 7: Length scale of cholesterol and other lipids assemblies in the plasma membrane (Figure adapted from Lu & Fairn, 2018).

Membrane raft microdomains, also known as lipid rafts, are heterogeneous and metastable (Kusumi et al., 2020) domains with a dynamic structure (George & Wu, 2012), enriched in SLs and cholesterol (Simons & Ikonen, 1997). raft domains, can reach between 10 and 200 nm, because small raft can be stabilized into larger platforms (Schmid, 2017). Those domains correspond with the diffraction limited structured defined by Lu & Fairn (2018) and more specifically with flotillin enriched domains (Figure 7). Their main characteristic apart from its composition and their resistance to detergent disruption (Levental et al., 2010), is the reduction of lateral mobility, forming an LO domain. rafts are present in the external part of the plasma membrane leaflet (reviewed by Patel et al., 2008), in endosomal compartments of yeast, and could be found in mammalian cells endosomes (Diaz-Rohrer et al., 2014; Levental et al., 2010). In addition, raft-like domains have been observed in various organelles, such as the ER (Browman et al., 2006) or mitochondria (Sorice et al.,

2009). Raft formation can be produced by lipid-lipid interactions via different mechanisms based on the phase separation or the dynamic heterogeneity (Baoukina et al., 2017), such as membrane recycling (Schmid, 2017). Most relevant interactions take place between saturated lipids, SLs and STs rather than *cis*-unsaturated lipids (substituent groups in the same direction) (Alves et al., 2018; Levental et al., 2020). *Cis*-unsaturated lipids interact more loosely with ST molecules than *trans*-unsaturated ones (substituent groups in opposite directions) (Alves et al., 2018), which have a larger contact area. However, in mammalian membranes, it is more common to have different fatty acids in the same GP: one saturated and one unsaturated (Levental et al., 2020), thus in disordered phases highly polyunsaturated GPs and very short lipids are observed (Alves et al., 2018). Beside cholesterol-SL and cholesterol-ganglioside (ceramides with a sugar molecule) (Figure 8a) lipid-protein interactions also play roles in the regulation of the lipid raft domain. Moreover, lipid raft structure and size can change through protein-protein or protein-lipid interactions. Some of these interactions are protein-SL and protein-cholesterol binding motifs that can regulate raft distribution (Figure 8b). On the other hand, covalent attachment of palmitic acid to cysteine, serine or threonine amino acids (also known as palmitoylation) (J. Jin et al., 2021) in lipid raft domains was described to be a mechanism for lipid raft recruitment to synaptic sites (Figure 8c). Non-enzymatic-driven reactions are also responsible for lipid raft structure. In this sense, hydrophobic mismatch between longer saturated lipids and shorter unsaturated lipids inside and outside rafts can regulate the size of coexisting domains (Figure 8d) (Sezgin et al., 2017).

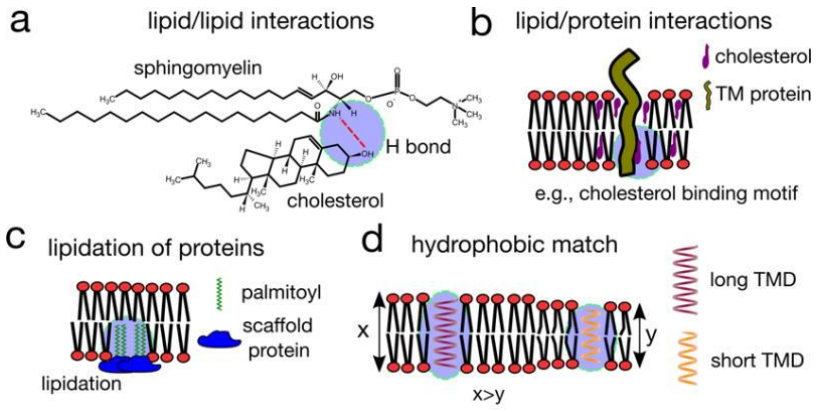

Figure 8: Main interactions in lipid raft domains. A) Lipid-lipid interaction between sphingomyelin and cholesterol. B) Lipid-protein interaction through cholesterol-binding motifs. C) Lipidation of proteins by the addition of fatty acid to a scaffold protein, such as palmitoylation. D) Hydrophobic mismatch interactions. Abbreviations: TM: *trans*-membrane, TMD: *trans*-membrane domain. (Figure obtained from Sezgin et al., 2017).

2.1 Raft proteins

Depending on the protein composition there are a variety of subtypes of microdomains, such as caveolae or clathrin-coated pits that has specific proteins (Lu & Fairn, 2018; Patel et al., 2008) or even lipid raft domain without proteins (Lucero & Robbins, 2004). Generally, raft domains present an enrichment in different protein classes that can be classified in three categories: scaffolding proteins, proteins integrated into the LD phase, and shifting proteins that go in and out the microdomains (Mesa-Herrera et al., 2019). Raft platforms can recruit or exclude signaling proteins, kinases, and phosphatases as a response to certain intra or extra-cellular stimuli (Martellucci et al., 2020). The protein integration in lipid rafts is dependent of specific protein-lipid interactions (Díaz et al., 2015), as these microdomains are highly regulated by lipid metabolism changes, receptor activation and cytoskeleton interactions (Sviridov et al., 2020). Raft proteins include glycosylphosphatidylinositol (GPI)-anchored proteins, specific members of src-kinases family (Van Der Goot & Harder, 2001), platelet-derived growth factor (PDGF) receptors (Alves et al., 2018), and various types of G protein-coupled receptors (GPCR) protein among others (Patel et al., 2008). GPCR can be located in lipid raft domains via cysteine-palmitoylation, also protein G α-subunits are present in lipid raft domains through fatty acylation and caveolin-interaction mechanisms (Barnett-Norris et al., 2005). These receptors are associated with a variety of signaling pathways, such as the endocannabinoid system (Barnett-Norris et al., 2005). Cyclooxygenase (COX) 2 is localized in lipid raft and caveolae domains, making its inhibition a target for some anti-inflammatory drugs (Tsuchiya & Mizogami, 2020). Fas death receptors can be present in raft domains (Castro et al., 2011; Gajate & Mollinedo, 2015), and promote other receptors to co-cluster and activate apoptotic pathways (Gajate & Mollinedo, 2014). But not only apoptotic pathways, survival signal pathways including insulin-like growth factor-I/phosphatidylinositol 3-kinase (PI3K/Akt) are also found in raft microdomains (Gajate & Mollinedo, 2015). Moreover, acetylcholinesterase (AchE), a protein which performs the hydrolysis of acetylcholine neurotransmitter (D. Hicks et al., 2011), can be in rafts and stay linked to GPI molecules (Moral-Naranjo et al., 2008) an interaction required for certain neural functions (D. Hicks et al., 2011). Lastly, flotillin also named reggie protein is a transmembrane protein that has two isoforms (flotillin-1 and 2) (Figure 9). Flotillin has a wide tissue distribution, especially

enriched in brain, heart, lung and placenta, and low in liver and pancreas (Banning et al., 2011). It is specifically located in lipid rafts, making it a raft biomarker (Banning et al., 2011; Yokoyama & Matsui, 2020) implicated the correct functioning of raft domains, signal transduction, organization, membrane trafficking (Yokoyama & Matsui, 2020) and activation of receptors inside and outside of the domains (Alves et al., 2018). The integration of flotillin-1 into raft microdomains may be due to the Golgi-independent and stomatin/prohibitin/flotillin/HflK/C domain (SPFH) dependent way (Banning et al., 2011; Morrow et al., 2002) (Figure 9).

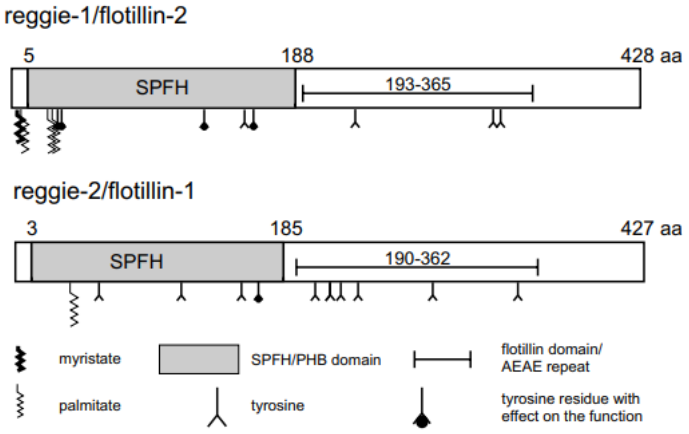

Figure 9: Domain structure of human flotillins-1 and 2. (Figure obtained from Banning et al., 2011).

Other proteins, associated to lipid raft domains are lipid-binding proteins such as apolipoprotein D (ApoD) and E (ApoE). On one hand, ApoD has been described as a peripheral protein that interacts with raft domains (del Caño-Espinel, 2014; Pascua Maestro, 2018) and can act as an antioxidant protein reducing free radical-generating lipid hydroperoxide molecules (Bhatia et al., 2012). On the other hand, ApoE can transport lipids through lipoprotein complex formation (S. I. Lee et al., 2021). The different isoforms of this protein have been related with alteration in lipid raft structural components (Igbavboa et al., 2005; S. I. Lee et al., 2021).

Proteins in raft domains can assemble forming macromolecular complexes, changing their functional properties in response to changes in metabolic conditions (Sviridov et al., 2020) which can lead to a dysregulation.

2.2 Raft lipids

Originally, rafts are formed by the interactions between cholesterol and SLs, being SMs the main component of these domains. In model membranes raft and raft-like

domains, can contain saturated GPs, or gangliosides (Sezgin et al., 2017). The requirement of cholesterol for raft formation entails the necessity of higher cholesterol content. In plasma membranes, concentration around 35 to 45% is needed to ensure lipid raft normal functionality, however, concentrations under 25% maintains the lipid raft structure but its functionality is compromised (Kusumi et al., 2020). In this sense, as other organelles such as ER are poor in raft-forming lipids it is less probable that they contain raft-like structures (Levental et al., 2020), however raft microdomains in mitochondria associated membranes has been reported (Garofalo et al., 2016). In regard to SLs, not only SMs have importance in lipid raft formation, but also ceramides. An increase in the production of this lipid is related with the consumption of SMs (Döhr et al., 2001) through the action of acid sphingomyelinase (SMase) activated by PC-specific phospholipase C (PC-PLC) (Cuschieri & Maier, 2007; Schütze et al., 1992). In this sense, the ceramides can form their own ceramide-enriched domains which can coalescence to form larger platforms or displace cholesterol from its interaction with SMs (Castro et al., 2014). Cholesterol displacement results in ceramide-rich cholesterol-poor rafts, an alteration affecting protein associations to these rafts (Megha & London, 2004). In this sense, lipid environment in cell membranes leads to lipid raft microdomain formation, whose activity as signaling platforms is a key aspect for homeostasis maintenance of different cell types, such as neurons. This homeostasis maintenance is performed by lipid mediators derived from GPs, SLs, and cholesterol, as well as transporters and different enzymatic pathways. However, some alterations in the lipid environment can lead onto changes affecting both raft and non-raft domains.

Another factor altering the structure and function of lipid rafts is the exposure to oxidant molecules, that can alter the lipidome, producing lipid peroxidation and externalization of PSs (Cuschieri & Maier, 2007), an important event for apoptosis (Adayev et al., 1998). In general, lipid peroxidation alters the composition, structure, and assembly of the lipids inside cellular membranes (Gaschler & Stockwell, 2017), as oxidant molecules can react with head groups and even destroy them (Yusupov et al., 2017). Lipidome alterations directly affect certain lipid second messengers or mediators that modulate divers enzyme activities, immune responses, mitogenesis, apoptotic pathways, and susceptibility to oxidative stress (Frisardi et al., 2011).

3 Importance of membranes and their lipid raft in the nervous system

3.1 Lipid raft in disease

3.1.1 Raft domains in neurodegenerative diseases

Regarding neurodegenerative diseases, it has been observed that lipid homeostasis is altered in pathologies such as Alzheimer disease (AD) and Parkinson's disease (PD)(Mesa-Herrera et al., 2019). Modifications in lipid raft organization can alter membrane's local microenvironment (Marin et al., 2016) and entail disturbances over its functionality, particularly in neurotransmission, neurotransmitter signaling, or protein clustering, among others. Alteration of these processes can contribute to neuropathological events (Díaz et al., 2018).

AD, it is a neuropathology that is characterized for cortical atrophy, loss of motor and cognitive skills, and formation of amyloid plaques and neurofibrillary tangles. Furthermore, in addition to macroscopic changes, brain tissue of AD patients presents alterations of GPs and cholesterol metabolism, that can affect other pathways or even mitochondrial activity (Mesa-Herrera et al., 2019). Nevertheless, the amyloid cascade hypothesis blames amyloid-β (Aβ) oligomerization and its accumulation as the principal factor of AD pathogenesis. In this sense, amyloid precursor protein (APP), a transmembrane protein present in lipid raft domains (Arbor et al., 2016; Wahrle et al., 2002), can produce the soluble amyloid Aα (physiological) or the Aβ peptide that triggers amyloid plaques (pathological) (Figure 10), depending on the action of α secretase or β- and γ-secretases, also found in lipid rafts (S. I. Kim et al., 2006; Vetrivel et al., 2004). In this sense, cholesterol, as a major component of raft domains, has been found to be increased in brain tissue of AD patients, as well as in amyloid plaques (Marquer et al., 2011). In fact, APP integration in lipid rafts seems to be dependent on cholesterol concentration (D. A. Hicks et al., 2012), as this protein contain Cholesterol Recognition/interaction Amino acid Consensus sequence (CRAC) domains (Díaz et al., 2015), which bind cholesterol molecules (Marquer et al., 2011). Furthermore, APP protein in raft domain can be modified with a palmitic moiety, which may enhance the Aβ production and oligomerization, as described by Mesa-Herrera (2019) (Figure 10).

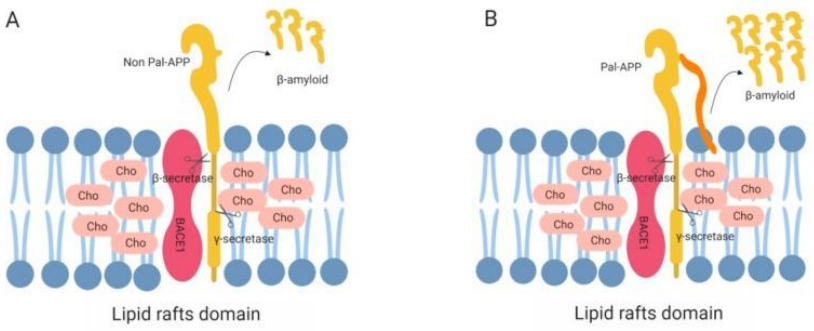

Figure 10: Schematic representation of APP palmitoylation modulating both APP processing and Aβ generation in lipid rafts. (A). Without APP palmitoylation BACE1 (red) in lipid rafts cleaves APP at the β-cleavage site. (B) When APP is palmitoylated (pal-APP), exhibits a palmitic moiety (orange), and is recruited to lipid rafts. This may produce an increase in β-amyloid production and oligomerization (Figure obtained from Mesa-Herrera et al., 2019).

SMs also presented changes in AD-affected brains. In this sense, SM metabolism pathway is altered leading to a decrease of SMs and S-1-Pand an increase in ceramides. This increase can be produced by the activation of acid and neutral SMases by Aβ40 and Aβ42 as described by Malaplate-Armand et al. (2006). Changes in the amount of ceramides, can lead onto cholesterol exclusion, as described above, which fluctuation can modulate γ-secretase activity (Wahrle et al., 2002). Additionally, higher ceramide presence changes membrane physical properties by activation of cytosolic phospholipase A2 (cPLA2)(Frisardi et al., 2011), as well as by promotion of interleukines IL-2 and IL-6 (Haughey et al., 2010). Those changes, in particular IL-6 levels has been related with an increase in APP synthesis (Vandenabeele & Fiers, 1991).

In Parkinson's disease, α-synuclein (α-syn), a highly conserved neural protein that is the major component of Lewy bodies, interacts with raft domains (Kubo et al., 2015). The interaction is based on the presence of PSs preferently containing oleic acid and a polyunsaturated fatty acid. Moreover, α-syn protein can oligomerize inside lipid raft domains forming a calcium channel called amyloid pore (Di Scala et al., 2016; Yahi et al., 2022). Oligomerization process is controlled by gangliosides and cholesterol (Jakubec et al., 2019), one of the major components of raft domains. Other PD-related proteins are LRRK2 and DJ-1 proteins. LRRK2 is located in lipid raft domains and has been found to be altered in brain regions associated with PD (caudate-putamen, and *substantia nigra)* (Higashi et al., 2007). LRRK2 mutants can alter the lipid raft normal function (Kubo et al., 2015) which contributes to the pathogenesis of PD (Hatano et al., 2007). On the other hand, DJ-1 proteins is a raft

associated protein (Nash et al., 2017) that belongs to THiJ/Pfp1/DJ-1 family which mutations are PD related (Kubo et al., 2015).

Prion diseases are a set of disorders characterized by the transformation of physiological proteins to abnormally folded/shaped proteins (known as prions or PRPSC) which are protease resistant (Baldwin & Correll, 2019). Cellular form of prion protein (PRPC) is a type of GPI-anchored glycoprotein mainly expressed in central and peripheral nervous systems (Martellucci et al., 2019; Mattei et al., 2017) and located in lipid raft domains (Lewis & Hooper, 2011). In this sense, lipid raft microdomains are associated in the physiological to pathological transformation of prion proteins (Y. C. Kim et al., 2021). Furthermore, it is involved in numerous cellular processes, including synaptic plasticity, neurite regulation, apoptosis, resistance to oxidative stress among others (Martellucci et al., 2019). Despite the effects over different signaling pathways or cellular processes, lipids such as PEs (Y. C. Kim et al., 2021) or cholesterol (Hannaoui et al., 2014) seem to be also involved in PRPSC formation.

3.1.2 Raft domains in cancer

Even though lipid raft-related problems have been reported mainly in neurodegenerative pathologies, this signaling platform domain has important roles in several other diseases, such as cardiac diseases (Das & Das, 2009), cancer (Mollinedo & Gajate, 2015) or aging (Mesa-Herrera et al., 2019).

In relationship to cancer development, lipid rafts are implicated in cell proliferation and survival pathways such as the PI3K/Akt and Insulin-like growth factor (IGF) system pathway (Figure 11) , but also with pro-apoptotic pathways. In this sense, death receptors have been shown to be recruited to lipid rafts, such as CD95 or Fas. Those receptors can recruit Fas-associated protein with death domain, which initiates an apoptotic cascade (B. Li et al., 2022) However, rafts are not only implicated in cell survival but also in cell migration and adhesion, essential in cancer metastasis, e.g.: CD44 signaling pathway. In tandem with this, higher levels of cholesterol have been reported in cancer cells and their lipid rafts (Li et al., 2022; Li et al., 2006; Mollinedo & Gajate, 2020). The regulation of cholesterol plays a key role in the correct lipid raft assembling and signaling, as its depletion leads to a dysfunctional raft. This disfunction affects Akt inactivation in cancer cells (Y. C. Li et al., 2006), and mesenchymal-epithelial transition factor (c-Met) signaling may

also be compromised. Additionally, raft domains' quantity is disparate from one cancer to another, being breast and prostate cancer the ones with more lipid raft domains (Y. C. Li et al., 2006; Mollinedo & Gajate, 2020).

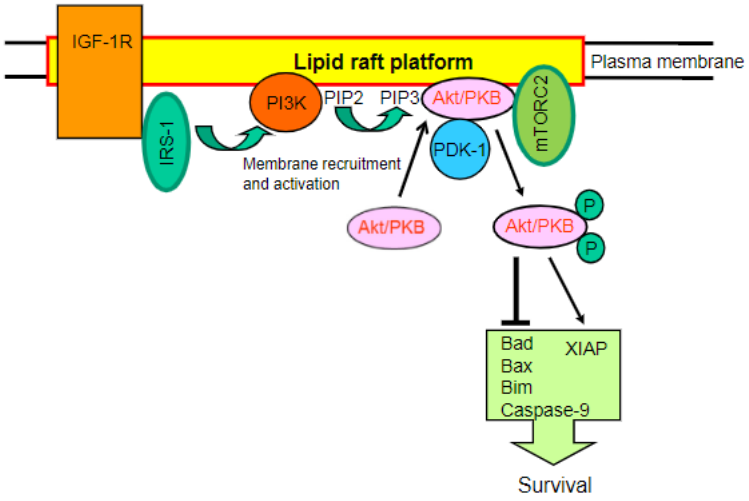

Figure 11: Schematic model of raft-mediated IGF-IR/PI3K/Akt signaling in the generation of cell survival and antiapoptotic signals (Figure obtained from Mollinedo & Gajate, 2015).

3.2 Oxidative stress and reactive oxygen species formation

Oxidative stress has been related with the development of a variety of diseases, from aging or neurodegenerative diseases to autoimmune disorders or cancer among others (Islam, 2017). Oxidative stress is the result of the overproduction of reactive species or free-radicals over the anti-oxidant defenses. Free-radicals formation is a physiological process that comprises a variety of pathways and antioxidant control mechanism, which might dysregulate leading into an imbalance between oxidant and antioxidant compounds (Checa & Aran, 2020). This pathological process, known as oxidative stress, entails a macromolecular damage (Jones, 2008) that impairs healthy aging (Vatner et al., 2020). Oxidative stress can be produced by reactive oxygen species (ROS) formation, a group of radical and non-radical oxygen species which forms upon incomplete oxygen reduction (Ray et al., 2012). ROS can be generated by a variety of enzymatic mechanisms, such as NADPH oxidase (NOX) enzyme family (Yang & Lian, 2020), monoamine oxidase (MAO)(Youdim et al., 2006), dual oxidase (DUOX)(Lambeth, 2004), peroxisomes, cytochrome P450 enzymes (He et al., 2017) and the mitochondrial electron transport chain (mETC) (Brieger et al., 2012; Kudryavtseva et al., 2016), which is the main ROS source (Dan Dunn et al., 2015; Elexpe et al., 2021, 2022; He et al., 2017). More in detail, NOX

enzyme family is located in a variety of tissues including brain, specifically NOX2, NOX3, and NOX 4 are expressed in nervous system (Bedard & Krause, 2007). In addition, MAO enzymes (MAO-A and MAO-B) also present in brain tissue and located in the mitochondrial outer membrane are related with PD (Mallajosyula et al., 2008) and Alzheimer disease among others (Chaturvedi & Beal, 2013). Monoaminoxidase main activity is the oxidation of its substrate accompanied by the reduction of oxygen to H_2O_2 (Antonucci et al., 2021; Tipton, 2018). The accumulation of this toxic sub-product provokes the damage of different cells, including neural (Fan et al., 2019; Tipton, 2018), and astrocytic cells such as the ones present in the *substantia nigra* (Mallajosyula et al., 2008). Furthermore, as the brain has a high metabolic rate, a low cellular regeneration capacity and a lack of enrichment in antioxidant defenses its cells are particularly susceptible to be damaged by oxidative stress (He et al., 2017). In addition, high oxidative damage has been reported in Alzheimer disease, and closely correlated with amyloid and tau pathologies (Chen & Zhong, 2014).

A major source of ROS is the mitochondrial electron transport chain or respiratory chain. It constitutes an oxidative phosphorylation (OXPHOS) system that ends in ATP generation (Annesley & Fisher, 2019; Chenna et al., 2022). The mETC is composed of four different complexes (from I to IV, see below) (Figure 12) which transport electrons through them (reviewed by Angelova & Abramov, 2018) and a fifth complex, the ATP synthase, which uses the electrochemical gradient to generate ATP molecules. Electrons are taken from different substrates from tricarboxylic acid cycle (TCA) or beta oxidation (Hirst, 2013), such as NADH (Rich & Maréchal, 2010) or succinate, used by complexes I and II respectively. Electron flows through the different complexes generate a proton transfer from the mitochondrial matrix to the intermembrane space, producing a transmembrane potential (reviewed by Angelova & Abramov, 2018). Generally, electrons that enter from complexes I or II are transferred to coenzyme Q (CoQ), and then they are donated to complex III and subsequently, to cyt c and complex IV. This whole process, known as mitochondrial respiration (reviewed by R.-Z. Zhao et al., 2019), can also produce reactive oxygen species by two mechanisms: the premature leak of electrons from complexes I to III or the reverse electron transport (RET) produced in complex I (see below)(reviewed by Nolfi-Donegan et al., 2020). Mitochondrial reactive oxygen species has been related to various pathologies, such as neurodegenerative diseases

(Lin & Beal, 2006), aging (Boveris & Navarro, 2008), and cancer (Costa et al., 2014; Hadrava Vanova et al., 2020).

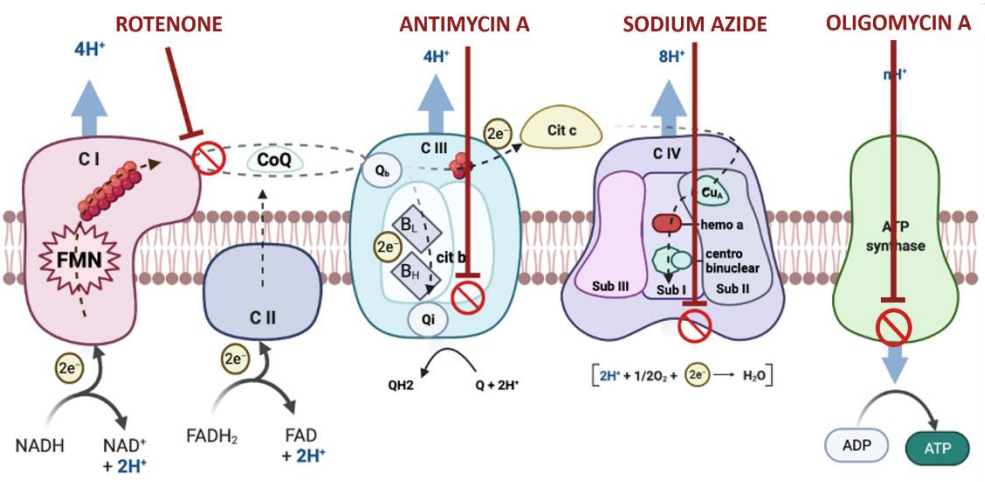

Figure 12: Mitochondrial electron transport chain complexes and inhibitors. The specific inhibitors (text in red) are rotenone (complex I), antimycin A (complex III), and sodium azide (complex IV).

Complex I. It is a group of enzymes located in the mitochondrial inner membrane, which main protein is NADH-ubiquinone oxidoreductase, which oxidizes NADH to NAD+ with parallel reaction of ubiquinone transporter reduction to ubiquinol (QH_2) (Hirst, 2013; reviewed by Murphy, 2009). Complex I is composed by a main protein, the NADH dehydrogenase, that has 14 conserved core subunits in eukaryotes and up to 45 in mammals' case due to the content of accessory subunits (Carroll et al., 2002, 2006; Hirst et al., 2003; Sousa et al., 2018). Complex I has been related to oxidative stress conditions as is the main source of ROS production inside the mitochondria (Sousa et al., 2018). ROS are produced by the leak of electron and its reaction with oxygen to form a superoxide molecule ($O_2^{\bullet -}$), which can produced in the FMN cofactor or in the ubiquinone (Q) binding site (Murphy, 2009) (Figure 12) and its dependent on the ratio NADH/NAD+ (reviewed by Nolfi-Donegan et al., 2020). Other mechanism for ROS generation is the reverse electron transport, that only occurs when the Q transporter is highly reduced and electrons are going backwards from reduced form of Q transporter (QH_2) back to mETC complex I (reviewed by Nolfi-Donegan et al., 2020; Scialò et al., 2017).

Complex II. Complex II is composed of Succinate dehydrogenase (SDH) A, B, C and D subdomains, that catalyze the transformation of succinate to fumarate (Huang & Millar, 2013) inside Kreb's cycle and is one of the entrances of electrons in the mETC (Bezawork-Geleta et al., 2017). SDH subdomains C and D are embedded in the inner

membrane of mitochondria , subdomain A is anchored to them and, B is protruded into mitochondrial matrix (reviewed by Bezawork-Geleta et al., 2017). SDHA is the first electron acceptor of the complex and start the oxidation of succinate, whereas C and D subdomains mediates the ubiquinone oxidoreductase activity (SQR) (Schwall et al., 2012). The production of ROS by this complex is not as much as in complexes I and III (main sources of ROS in the mETC), however its production has important implications in physiology and pathology (reviewed by Hadrava Vanova et al., 2020). The ROS production in complex II occurs by the uncoupling of SDH and SQR activities (Schwall et al., 2012).

Complex III. Mitochondrial complex III, also known as cytochrome bc_1, is an homo-dimeric complex (reviewed by Stephan & Ott, 2020) that transfers electrons from reduced ubiquinol (QH_2) to cyt c. Complex III has three highly conserved subunits and up to 8 accessory subunits (Trumpower, 1991), all of the enzymes that make up the complex II are PP proteins, except the cytochrome b (Sousa et al., 2018). Complex III dimers can interact with complexes I and IV to form mitochondrial supercomplexes (see below). Regarding ROS generation, the leak of electrons in this complex results in the generation of superoxide, similarly to complex I. This mETC complex has the particularity of emit superoxide to both sites of the mitochondrial inner membrane (intermembrane space (IMS) and mitochondrial matrix). In the IMS the superoxide molecules are transformed into H_2O_2, a second messenger in signaling pathways (Banerjee et al., 2022). The ROS production can be enhanced by the inhibition of the complex, caused by Antymicin A (Figure 12)(Bleier & Dröse, 2013), stigmatellin or myxothiazol (Degli Esposti et al., 1993).

Complex IV. This complex of the mETC also knowns Cytochrome c oxidase (CCo) is the terminal complex (Y. Li et al., 2006) of the mETC, it has 14 different subunits in mammal mitochondria (Sousa et al., 2018), being 3 of them which transport the electrons to catalyze the reduction of oxygen to H_2O. In total, 4 electrons are transferred from the cytochrome c to the di-oxygen molecule and 4 protons are translocated from the MM to the IMS (R.-Z. Zhao et al., 2019).

Supercomplexes. Furthermore, complexes I, III and IV can be associated forming mitochondrial supercomplexes or respirasome (Formosa et al., 2018; Lenaz et al., 2016). Respirasome is the supercomplex association that contains the minimal complexes required for mitochondrial respiration ($I_1III_2IV_1$), although other types of

supercomplexes with different number and type of complexes can be detected (Althoff et al., 2011; Sousa et al., 2018). In some tissues, such as bovine heart, it has been observed that a third of complex III quantity and the 85 % of the complex IV exist as free enzymes whereas all complex I forms the supercomplex superstructure (Schägger & Pfeiffer, 2001). Structural evidence of mitochondrial supercomplexes has been reported, additionally, oxidative stress-related pathologies have alteration of supercomplexes (Lenaz et al., 2016). The reorganization of the mETC in supercomplex structure can be produced to enhance the catalytical activity of the mETC by two major mechanisms: reduction of substrate diffusion distance and specific substrate channeling (Schägger, 2001).

Cytochrome P450 (CYP) can be another source of ROS in presence of certain molecules such as paraquat (PQ). In this sense paraquat toxic effects are related to oxidative stress, by the generation of ROS through paraquat mono-cation (PQ^+) reduction or the inhibition of mitochondrial complexes (Blanco-Ayala et al., 2014). CYP is an enzyme part of the heme-containing monooxygenases family which has been found in brain, retina, and trabecular meshwork among others (Song et al., 2022). CYP family catalyzes diverse reactions, including reduction, desaturation, ester cleavage, and rearrangement of fatty acids, and are implicated in metabolic homeostasis (Guengerich, 2001), and leukotriene metabolism (Dobon et al., 2019). More in detail, CYP1B1 enzyme carried out the catalysis of xenobiotic in a NADPH-dependent phase, however alternative version of this CYP use NADH as a co-factor (Döhr et al., 2001).

3.3 Antioxidant systems

Levels of ROS are maintained in a physiological level by the action of endogenous or exogenous antioxidants. Antioxidant systems are the main defense against oxidant molecules, by inhibiting the electron transfer from one molecule to another (Oyewole & Birch-Machin, 2015). Antioxidants can be categorized as endogenous or exogenous, being the first group enzymatic antioxidants (superoxide dismutase, Glutathione peroxidase, and catalase) and non-enzymatic antioxidants (glutathione, vitamin E, and bilirubin)(Oyewole & Birch-Machin, 2015; Shindo et al., 1994). Concretely, vitamin E or its predominant form α-tocopherol has lipoperoxyl radical scavenging activity (Jiang, 2014; Niki & Noguchi, 2021; P.-Y. Zhang et al., 2014). This antioxidant compound has an effective mechanism against oxidation mediated by

free radicals (Niki & Noguchi, 2021; P.-Y. Zhang et al., 2014), which consists in the donation of a hydrogen atom to lipoperoxyl radicals, generating their own radical (Miyazawa et al., 2019).

3.4 Oxidative stress and lipid rafts

Redox molecules, such as ROS, can alter lipid raft signaling platforms by the activation of PI3k/Akt pathway and ERK 1/2 by H_2O_2 or by the enrichment of ceramides due to superoxide molecules (S. Jin et al., 2011). Indeed, oxidative stress is a complex mechanism which produces several changes that can be related with membrane rafts in pathologic conditions. In this sense, oxidative stress can up-regulate PS1 proteins that can promote γ-secretase activity and therefore the production of Aβ (Wong et al., 2019). However, the main effect of oxidative stress on lipid rafts is the lipid peroxidation of certain species.

Lipid peroxidation is a physiological chain reaction process that can turn out into pathological and affect cell membranes and other lipid-containing structures (Kudryavtseva et al., 2016). Most common targets for this process are polyunsaturated fatty acids (PUFAs) present in GLs, GPs and cholesterol (Anthonymuthu et al., 2016). In contrast, more resistance to free-radical attack has been observed in monounsaturated and saturated fatty acids (Halliwell & Chirico, 1993). This oxidation reaction can take place due to enzymatic and non-enzymatic mechanisms (Girotti, 2021). An example of enzymatic mechanism is the peroxidation reaction produced by lipoxygenases (LOX), cyclooxygenases (COX), cyt c (Niki, 2008) or cytochrome P450 (Gaschler & Stockwell, 2017; Senoner & Dichtl, 2019). On the other hand, the main non-enzymatic mechanism for lipid peroxidation is mediated by oxygen free radicals (Ramana et al., 2014), such as superoxide or hydroxyl radicals among others (Halliwell & Chirico, 1993). This reaction, if produced inside raft domains, can disrupt them and provoke functional and structural changes affecting different signaling pathways (Morris et al., 2016).

4 Analytical techniques used to study whole membranes in microarrays

4.1 Printing membrane microarrays

Cell membrane microarray (CMMA) technology has been successfully applied to the simultaneous characterization and analysis of lipid fingerprints in samples from different species, in both tissues and cell cultures (Fernández et al., 2019). In addition to lipidomic analyses, this technique can be combined with enzymatic and immunochemistry assays as the proteins remain active and in their native form. The CMMA technology has already been used combined with autoradiography (Manuel et al., 2015) and mitochondrial activity colorimetric assays (Elexpe et al., 2021), being a powerful tool for drug screening and the identification of possible drug side effects in early stages of drug discovery process (Elexpe et al., 2022).

4.2 Lipidomic analysis in cell membrane microarrays

Mass spectrometry (MS) is an analytical technique used to measure the mass to charge (m/z) ratio of ions. This technique combined with matrix assisted laser desorption/ionization (MALDI) methodology, has been successfully applied to the analysis of scarce membrane samples printed on CMMAs, as the printed spots maintain a representative lipidome of the original membranes (Fernández et al., 2019), and overcome previous technological limitations (Lai et al., 2016). In addition, data acquisition time is significantly reduced compared to standard bulk MS analysis due to the size of the printed spots and the reduction of the laser shots required for the analysis (Fernández et al., 2019).

The mass spectrometer is formed by three components: the ion source, the mass analyzer and the detector.

Ion source. The ion source is a part of the mass spectrometer which ionizes the analyte converting it from liquid or solid state to a gas phase. The gas-phase ions, can be easily manipulated by magnetic or electric fields and transported to the mass analyzer. There are four main types of ionization depending on how the type of ionization and the sample used:

- **Electron ionization:** Used in MS for organic molecules in solid or gas phase, the electrons interact with the atoms to produce ions (Griffiths, 2008).

- **Chemical ionization:** There are a variety of methods for chemical ionization, but only ion attachment is used for mass spectrometry assays. The analyte molecule get attached to a cation by a reactive collision (Selvin & Fujii, 2001).

- **Gas-discharge ion sources:** This ion sources use a plasma source or an electric discharge to ionize the analyte. In mass spectrometry microwave-induced plasma ion source is used to create ions for trace elements (Okamoto, 1994).

- **Desorption ionization:** The neutral molecules in solid state are gasificated and ionized, detaching the molecules from the surface. The most common desorption ion source is MALDI source (explained below) (Usmanov et al., 2017).

Mass analyzer. The ions are sorted and separated according to a m/z ratio, using electric or magnetic fields, depending on the analyzer. The most common mass analyzers are:

- **Time of flight (TOF):** uses electric field and charges the ions with the same charge, for accelerating the ions and measure the time it takes them to reach the detector. Lower mass ions will reach the detector before higher mass ions (Wollnik, 1993).

- **Ion trap:** the ions are trapped by electrostatical forces around the trap, depending on the type of trap, they can be ejected sequentially (quadrupole) or trapped in an orbit around an electrode (orbitrap). The m/z is calculated using the excitation voltage frequency or the orbit frequencies (orbitrap) respectively.

Detector. Finally, the detector records the charge induced when an ion hit the surface and that signal produce a mass spectrum. The mass spectrum represents the m/z ratios and the relative intensity of each peak.

The different types of mass spectrometers, and the improvements in MS technology entailed the creation of "omic" analysis. Thus, the study of the whole lipidome by lipidomic analysis has become relevant due to the importance of lipids in structural function, apoptosis, and signaling pathways among others. In this sense, the MS can analyze the lipidome and the changes in lipid composition due to the exposure of

different agents in membrane subdomains. More in detail, MALDI is a high throughput analytical technique used to ionize the sample analyzed using an energy-absorbing matrix. This matrix allows the laser to create the ions of proteins, carbohydrates or lipids with minimal fragmentation. Allowing the ionization, and measurement of molecules below 300 kDa in a solid state without fragment them (Karas & Hillenkamp, 1988; Tanaka et al., 1988). With the possibility of analyzing the lipidome in solid samples, a variety of immobilized samples can be analyzed using the same platform.

4.3 Technological challenge for the study of lipid rafts in microarrays

The development of a high-throughput system for analysis of lipid rafts will be of much interest, but it involves various challenges. First, the analysis of lipid rafts is dependent on the raft isolation method, as the small size make them impossible to be visualized or captured by light microscopy (Lu & Fairn, 2018). The most popular raft isolation method is the detergent extraction with Triton X-100 (TX-100) or Triton X-114 (TX-114) due to its simplicity. However, some authors had described artefacts in raft formation due to low temperature (Mohamed et al., 2018) or cells treatment with Tx-100 (Heerklotz, 2002). In fact, the use of detergents can alter the concentration of some raft lipids, such as cholesterol, changing their physiological lipid fingerprint and cause ion suppression (Chandler et al., 2017) which affects the signal obtained in mass spectrometry assays. Another challenge comes from the fact that the methods for sample preparation and handling can entail the excessive loss of protein (H. Yu et al., 2007) or changes in the protein native structure making them non-suitable for downstream enzymatic analysis (Kan et al., 2013). In addition, the direct imaging of cholesterol, one of the main lipids inside the raft domains, is difficult for conventional MS techniques without using fluorescent dyes or derivatizing cholesterol (Angelini et al., 2021; Quinlivan et al., 2017; X. Wang et al., 2019). This difficulties has been overcome recently with the improvement of nanoscale secondary ion mass spectrometry (nanoSIMS) which has a resolution of 50 nm, and allows the observation of cholesterol and SLs (Frisz, Klitzing, et al., 2013; Frisz, Lou, et al., 2013).

The size of lipid raft domains is also a limiting factor for several techniques, and require concentrations around 10^8 cells for HPLC-MS analysis (N. Li et al., 2004).

Moreover, for this HPLC technique not only size is determinant, but also the time required for data acquisition, with 2 hours per HPLC per sample (Martosella et al., 2006). The majority of lipid raft analyses have been performed on raft proteome. Those assays has been performed isolating first proteins and peptides from raft samples, and then performing MS/MS (N. Zhang et al., 2008), with or without HPLC separation (N. Li et al., 2004). In this regard, the proteomic analysis has revealed that the lipid raft and cytoskeleton proteins are interdependent (N. Li et al., 2004), however, as the analysis depends on the extraction method, not all the proteins associated with lipid rafts are observed in all the assays. Lipid raft lipidome analysis has been performed on glycosphingolipids, one of their principal components, by extracting the lipid of interest before the mass spectrometry assay. Those analyses have been performed sample by sample hampering the evaluation of a huge amount of sample (Nagatsuka et al., 2006).

Making the microarray format compatible with lipid raft analysis represents a relevant improvement, allowing the analysis of many and varied samples in the same platform. However, the method for purification of lipid raft needs to be adapted to ensure the compatibility of the samples with the printing method, and with MS and enzymatic assays techniques.

4.4 Performing enzymatic assays in cell membrane microarrays

Enzymatic assays are based on the ability of a protein to break a substrate or produce an intermediate product that reacts with some salts producing a color in the reaction solution (Baehner et al., 1976). Colorimetric assays are commonly used with membrane homogenates, to determine kinetics properties of transmembrane or membrane-associated enzymes. This detection method has been successfully applied to CMMAs allowing the study of multiple samples simultaneously with a reduced amount of sample compared with conventional assays (Elexpe et al., 2022). Common examples of enzymatic assays are 3-(4,5-dimethylthiazol-2-yl)-2,5-diphenyl tetrazolium bromide (MTT) colorimetric assay or Nitro blue tetrazolium (NBT) reaction. NBT is a yellowish reagent that can be reduced by ROS electrons forming blue compound called formazan. Therefore, it is considered an indicator of ROS levels produced by the sources explained above, and using mETC inhibitors it can take the electrons that has altered their normal course through the mETC. In

this sense, NBT reaction can evaluate the activity of NADH dehydrogenase by using NADH as a substrate, with and without decylubiquinone (dUQ) to evaluate the ROS produced by the mETC (Elexpe et al., 2021, 2022). Moreover, succinate dehydrogenase activity can be observed by NBT colorimetric reaction using Succinate as a substrate. The mETC superoxide generation can be tested in presence of or rotenone, antimycin A or sodium azide, specific inhibitor of complexes I, III and IV.

Nevertheless, colorimetric assays can be used to test other enzymatic activities such as AChE or BuChE (Y. Li et al., 2011; M. Wang et al., 2009). This colorimetric technique can be performed by two ways. One is based in the measurement of thiocholine, a yellow color product, that is produced by the reaction of hydrolyzation of Ach and its reaction with dithiobisnitrobenzoate (Ellman et al., 1961). Whereas the other is based on the reduction of ferricyanide and its combination with copper ions (Cu^{2+}) to form brownish copper ferrocyanide precipitate (Karnovsky & Roots, 1964).

HYPOTHESIS AND OBJECTIVES

HYPOTHESIS AND OBJECTIVES

Several neurodegenerative diseases, as well as certain cancers, present metabolic changes such as an oxidant and antioxidant imbalance, which can be produced by an increase of reactive oxygen species (ROS). This oxidative stress can be triggered by different oxidoreductases, especially those that belong to the mitochondrial electron transport chain (mETC). ROS are known to modify membranes domains and their functions affecting important processes not only in neurodegenerative diseases but also in cancer. However, the intrinsic limitations to work with certain membrane subdomains, such as lipid rafts, constrain both their study and the development of targeted drugs.

Thus, the global hypothesis of this Doctoral Thesis is that the combination of membrane isolation protocols with cell membrane microarray technology, lipidomic and enzymatic assays could allow the development of a screening tool for the simultaneous analysis of membrane subdomains. This system will be particularly useful for screening of therapeutic agents specifically designed to target lipid rafts' proteins.

To demonstrate this general hypothesis, the following specific hypotheses are proposed:

- Liquid-ordered domains can be purified maintaining their native enzymatic composition, specifically the enzymes responsible for ROS production.
- Liquid-ordered domains can be purified maintaining the lipidic environment.
- Raft and non-raft subdomains can be immobilized using non-contact microarray printing methodology.
- Oxidative stress can lead to changes in enzymatic activities and lipidomic fingerprint in raft subdomains that can be detected in printed membrane subdomains.

The main aim of this study is to develop a platform which lead to characterize the differences between enzymatic activity and lipidomic fingerprint in raft and non-

raft domains with a minute amount of sample. To achieve this general aim, the following specific objectives were carried out:

SPECIFIC OBJECTIVES

- Validate a printed whole membrane microarray product (CMMA) as appropriate to evidence the effects of oxidative stress and antioxidant treatments in a high throughput-compatible format.
- Develop a printed raft and non-raft subdomain microarray product (RMMA) as appropriate to evidence the differential effects of metabolic and oxidative stress in a high throughput-compatible format.
- Explore the effects of metabolic and oxidative stress on the lipidome of lipid rafts in metabolic and oxidative stress conditions using RMMAs as a proof of concept.
- Evaluate the effects of metabolic and oxidative stress conditions over a variety of enzymatic activities using RMMAs as a proof of concept.

MATERIAL AND METHODS

1 Cell cultures

1.1 Cell lines

The 1321N1 cell line (ECACC-86030402) is a human astrocytoma cell line that was isolated as a subclone of the 1181N1 cell line, derived from U-118MG line isolated from human malignant glioma cultures (Pontén & Macintyre, 1968). 1321N1 cell line was culture at 37 °C in a humidity-saturated atmosphere containing 5% CO_2 using a cell culture incubator (Hera Cell 150, Heraeus, Hanau, Germany). Cells in normal conditions were grown in complete DMEM medium (Table 2-control situation).

The SH-SY5Y cell line (ATCC CRL-2266) is a human neuroblastoma cell line subcloned from the SK-N-SH cell line, which was established in 1970 from a metastatic bone tumor (Biedler et al., 1973). SH-SY5Y cell line was cultured as explained below but using DMEM:F12 medium as listed in Table 2.

1.2 Thawing cryopreserved cells

Cryopreserved cells were quickly thawed at 37 °C and mixed with 2 ml of medium (DMEM in case of 1321N1 and DMEM:F12 1:1 for SH-SY5Y) previously warmed at 37 °C. The mixture was centrifuged using a centrifuge (5810R, Eppendorf, Hamburg, Germany) with a rotor A-4-62 (Eppendorf, Hamburg, Germany) at 300 *g* for 5 minutes at room temperature (RT). The supernatant was discarded and 2 ml of complete medium: DMEM 1 g/l glucose, supplemented with 10% fetal bovine serum (FBS) heat-inactivated, 1% L-Glutamine (L-Glut), 1% Penicillin/Streptomycin (P/S) in case of 1321N1; DMEM:F12 1:1 supplemented with 10% FBS, 1% L-Glut, 1% P/S, and 1% Non-essential amino acids (NEAAs) for SH-SY5Y were added for pellet resuspension. The cell suspension was diluted 1:5 in a complete medium and then sowed in 2 culture flasks of 25 cm^2 for both cases. Cell culture was performed as explained above.

1.3 Cell subcultures

Cells were grown in 75 cm^2 cell-culture flasks using control situation medium listed in Table 2. For detaching the cells, the medium was collected, and cells were washed with warmed phosphate-buffered saline (PBS) (sodium dihydrogen phosphate di-hydrated 77 mM, sodium hydrogen phosphate monohydrated 24,2 mM, sodium chloride 1.4 M; pH 7.4) warmed at 37°C. After PBS was taken off, new PBS at 4°C was added and culture flasks were placed above an ice layer for 5 minutes. Cells, detached after gentle tapping the flask laterally, were reseeded at 1:4 dilution two

times a week in case of 1321N1 and one time a week in case of SH-SY5Y for cell culture maintenance or stored for other usages. For storage, detached cells were centrifuged using a centrifuge (5810R, Eppendorf, Hamburg, Germany) with a rotor A-4-62 at 300 *g*, for 5 minutes at RT.

1.4 Cell treatments

1.4.1 Low serum

When 1321N1 cell cultures reached confluence (around 10^5 cells/cm^2) the medium was removed, and low serum medium containing DMEM 1 g/l glucose, 0.2% charcoal-treated FBS, L-Glut (final concentration 2 nM), Penicillin (final concentration of 100 U/ml), and Streptomycin (final concentration of 100 U/ml) was added. Cells were treated for 24 hours and then harvested using the same detachment method as explained in section 1.3.

1.4.2 Paraquat treatment

When 1321N1 cell cultures reached confluence (around 10^5 cells/cm^2), the medium was removed and low serum medium with paraquat (final concentration: 0.5 mM) was added. Cells were treated for 24 hours and then harvested as explained above.

1.4.3 α -tocopherol treatment

The 1321N1 seeded at 10.000 cells/cm^2 was cultivated in 12 well plates in complete medium (Table 2-control situation) for 24 hours at 37 °C, 5% CO_2, and saturated-humidity atmosphere. Cells were habituated to low serum conditions (Table 2-low serum starvation) for 12 hours before treatments began. After adaptation, a pre-treatment of 3 hours with or without α-tocopherol (1 µM) prepared in low serum medium was performed before treatment with or without paraquat (500 µM) in low serum conditions for different times (24, 48, 72, 96, and 120 hours).

1.5 Cell freezing

Confluent cell cultures were harvested as usual, for freezing two confluent flasks of 75 cm^2 (7 million cells each approximately) were used. Pellets were resuspended in 6 ml of freezing medium (FBS + 5% DMSO) to get around 2 million cells/ml of freezing medium. Cells were frozen in 2 ml cryovials at -80°C using a container for cell freezing to allow for a slow freezing process. After 48 hours, frozen cell cryovials were stored in liquid nitrogen.

Table 2: List of mediums prepared for each condition. Reagents and concentration (v/v).

	Astrocytic 1321N1	Neuron SH-SY5Y
Control situation	DMEM 1 g/l glucose, 10% FBS heat-inactivated, 1% L-Glut, 1% P/S	DMEM:F12 medium 1:1, 10% heat-inactivated FBS, 1% NEAA, 1%P/S
Low serum	DMEM 1 g/l glucose, 0.2% FBS heat-inactivated charcoal-filtered, 1% L-Glut, 1% P/S	
Paraquat treated	DMEM 1 g/l glucose, 0.2% FBS heat-inactivated charcoal-filtered, 1% L-Glut, 1% P/S, Paraquat final concentration 0.5 mM	
Thawing medium	DMEM 1 g/l glucose, 15% FBS heat-inactivated, 1%L-Glut, 1% P/S	DMEM: F12 medium 1:1, 15% heat in-activated FBS, 1% NEAA, 1%P/S
Cryopreserving medium	FBS heat-inactivated with 5% DMSO.	FBS heat-inactivated with 5% DMSO.

1.6 Mycoplasma testing

To discard Mycoplasma contamination, cell lines were periodically tested (every 6 months) by using "Mycoplasma Gel form kit" (Biotools B&M Labs S.A, Spain).

2 Viability assays

To analyze cell viability, trypan-blue viability assays were performed. Cells were detached from the culture well by a mechanical method to avoid enzymatic treatments (described above for 1321N1 cells). The cell suspension was transferred to a microtube and diluted 1:1 with 0.4% trypan blue solution. The cells were counted using a Neubauer chamber in an inverted microscope Olympus CKX41 (Olympus Corporation, Tokyo, Japan). Dead cells (with a compromised membrane) were stained in dark blue. The percentage of live cells, with respect to total cells, was calculated. Viability data handling and analysis were carried out using Excel (Microsoft 365, Microsoft Co., Albuquerque, NM, USA) and GraphPad software (version 9.2, Dotmatics Inc, Bishop's Stortford, UK). Briefly, cell viability data were presented as a percentage of cell growth. The identification of outliers was carried out by applying the following formulas:

$$Y_1 = \bar{X} - DF * SD \qquad Y_2 = \bar{X} + DF * SD$$

DF: Deviation factor SD: Standard deviation $\overline{X}$: mean

Points were identified as outliers and excluded if Y_1 was higher than the point analyzed or Y_2 was lower than the point examined. We used a deviation factor of 1.25 in our analysis. Data were expressed as means of independent data points ± SD (standard deviation). The results were analyzed using one-way two-tailed ANOVA with Tukey's post-hoc. Statistical differences were indicated with *p*-values ≤ 0.05.

3 Membrane preparations

3.1 Membrane preparations for Cell Membrane Microarray development

In order to fabricate Cell Membrane Microarrays (CMMAs, see section 3.7 below), the 1321N1 cell line was cultivated in 25 cm^2 culture flask following the same conditions explained previously. Cells were cultivated until reached confluency of 80% (obtaining 10^6cells per flask) and one flask per condition was used, treated as described above. Cells were detached from the flasks and homogenized using a Teflon-glass grinder (RZR 2020, Heidolph, Schwabach,Germany) in 20 volumes of homogenization buffer (1 mM EGTA, 3 mM MgCl2, and 50 mM Tris-HCl, pH 7.4). The crude homogenate was subjected to a 3857 *g* centrifugation (AllegraTM X 22R centrifuge, Beckman Coulter, Brea, CA, USA) for 5 min at 4°C, and the resultant supernatant was collected and centrifuged at 18,000 *g* (Microfuge® 22R centrifuge, Beckman Coulter, Brea, CA, USA) for 15 min at 4 °C, obtaining membrane from the plasma membrane and internal organelles (mitochondria, endoplasmic reticulum). The tubes were finally decanted, and the pellets were frozen at -80°C, except for one aliquot, which was used to determine the protein concentration. Protein concentration was determined by the Bradford method and adjusted to a final concentration of 5 mg/ml.

3.1.1 Bradford protein quantification assay

Protein concentration was determined by the Bradford method, 10 µl of sample and 250 µl of Bradford reagent (Coomasie blue dissolved (final concentration 0.01%), in 95% ethanol (final concentration of 4.7%), and ortho phosphoric acid 85% (final concentration 8.5%) were added to a 96-well plate and mixed. Absorbance at 595 nm was measured 5 times for 15 minutes. To obtain protein concentrations a

calibration curve of bovine serum albumin (BSA) dissolved in H_2O_d was used. Each sample concentration was adjusted to 5 µg/ml for printing.

3.2 Membrane extraction for lipid raft purification

For membrane purification, one confluent 75 cm^2 flask was used for each lipid raft purification (around 10 million of cells per flask). Each pellet of the different cell types (1321N1 and SH-SY5Y) were resuspended in 5 ml of TNE buffer (Tris-HCl 50 mM, NaCl 150 mM, EDTA 5 mM, pH 7.4) with protease inhibitors and cells were homogenized using a potter S (Satorius AG, Göttingen, Germany), 20 strokes, rotating at 400 rpm. The tubes were centrifugated at 4°C and 4800 *g* (Rotanta 460RHettich, Westphalia, Germany) for 10 minutes to discard nuclei and big organelles. The supernatant was collected and used to fill a quick-seal centrifuge tube of 5.6 ml (ref 363963, Beckman Coulter, Brea, CA, USA). Tubes were centrifuged at 100,000 *g* using an optimal 100 XP ultracentrifuge (Beckman Coulter, Brea, CA, USA, 100Ti rotor) for 75 minutes. The supernatant was eliminated, and the membrane pellets were resuspended in 200 µl of TNE with protease inhibitors. In these experiments, protein concentration was determined by the BCA method.

3.2.1 Protein quantity determination by BCA

Firstly, in order to determine protein quantity, colorimetric assay Pierce MicroBCA Protein Assay kit (ref. 23235, ThermoFisher Sci., Waltham, MA, USA) was used. BSA standards at different concentrations were prepared following provider instructions, and membrane preparation pellets were resuspended in PBS + 2% sodium dodecyl sulfate (SDS). 150 µl of resuspensions (either standard or sample suspension) and 150 µl of working reagent were mixed together (ref. 23235, ThermoFisher Sci., Waltham, MA, USA). Absorbance was read at 562 nm.

Different cell membrane preparations pellets were merged to ensure sufficient protein quantity for lipid rafts extraction (300 µg). Each sample was divided into aliquots containing 300 µg of protein. Once protein concentration was known, aliquots of membrane preparations with 300 µg total protein were prepared for each lipid raft separation.

3.3 Lipid raft isolation

3.3.1 Detergent extraction method

For lipid raft extraction, each membrane preparation aliquot was incubated with the detergent (TX-100 or TX-114) at a final concentration of 1% at 4°C for 1 hour. A series of sucrose solution in TNE buffer was prepared as indicated in Table 3.

Table 3: Sucrose gradient reagents for lipid raft extraction per sample.

Reagent	80% Sucrose	35% Sucrose	5% Sucrose
Sucrose (g)	2.4	2.1	0.125
TNE (mL)	2.94	5.88	2.4
PI 50x (mL)	0.06	0.12	0.1
Final volume (mL)	3	6	2.5

To make the sucrose step gradient, first 2.25 ml of 80% sucrose was deposited carefully in the centrifuge ultra-clear 15 x 95 mm centrifuge tube. Samples (300 µg total protein) were then placed over the sucrose and vortexed gently to avoid bubbles, but thoroughly. On top of the sample sucrose mixture (now 55% of sucrose), 6 ml of 35% sucrose were placed, and finally 3 ml of 5% sucrose. Sucrose gradients were centrifuged at 4°C and 102,000 *g* (Beckman Coulter optimal 100 XP ultracentrifuge, SW40 rotor, Brea, CA, USA) for 20 hours.

Tube content was collected in 12 fractions of 1 ml from top to bottom. The fraction containing lipid raft locates at the interface between 5% and 35% sucrose. All the samples were stored at -20°C before analysis by Western blot.

3.3.2 Detergent-free extraction method

Membrane preparation (300 µg) were sonicated 5 times with 30% amplitude at intervals of 20 seconds with 1-minute cooldown period between sonication interval (Vibracell 75115, Thermo fisher Bioblock scientific S.L, Waltham, MA, USA) using a TipCB33-3363658 Tip (BochemLabordebarf, Weilburg, Germany). The sucrose gradient was prepared as indicated above immediately after sonication.

3.3.3 Direct isolation of lipid rafts from whole cell extracts

For membrane purification, one confluent 75 cm^2 flask was used for each lipid raft purification (around 10 million of cells per flask). Each pellet of the different cell types (1321N1 and SH-SY5Y) was resuspended in 5 ml of TNE buffer (Tris-HCl 50 mM, NaCl 150 mM, EDTA 5 mM, pH 7.4) with protease inhibitors and cells were

homogenized using a potter S (Satorius AG, Göttingen, Germany), 20 strokes, rotating at 400 rpm. The mixture was collected and used to fill a quick-seal centrifuge tube of 5.6 ml (ref 363963, Beckman Coulter, Brea, CA, USA,). Tubes were centrifuged at 100,000 *g* using a 100Ti rotor for 75 minutes. The supernatant was eliminated, and the membrane pellet was resuspended in 200 µl of TNE with protease inhibitor. In this case, only detergent free extraction method was used. When lipid rafts were extracted from the whole cell extract the preparation volume is 2 ml. This required a different design for the sucrose step gradient. Figure 13 displays a visual comparison of the two gradient designs used.

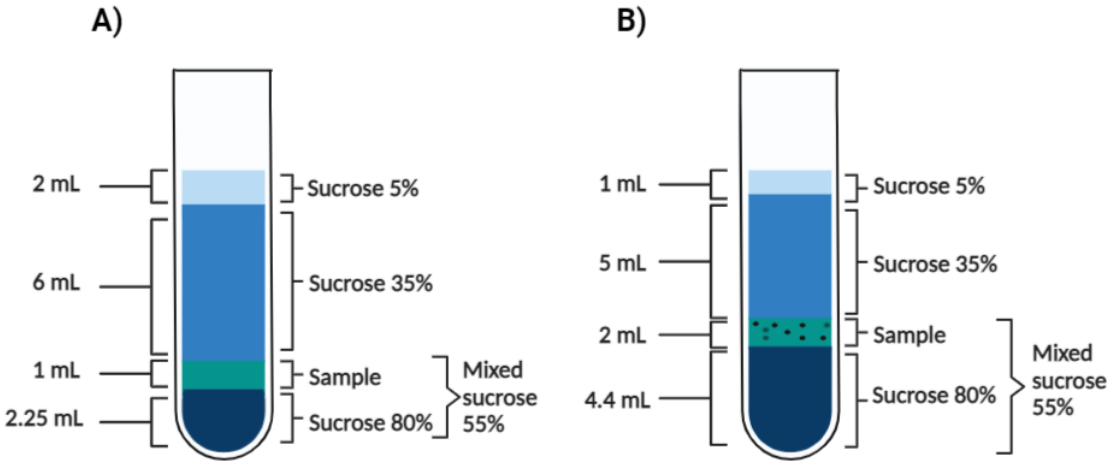

Figure 13: Volumes and concentrations of sucrose step gradients for lipid raft extractions. A) Sucrose gradient for lipid raft extraction from membrane preparations. B) Sucrose gradient for lipid raft extraction from whole cell extracts.

Lipid rafts extracted with TX-114 acquire a whitish color when placed at temperatures above 4°C, while in extraction performed with TX-100 or by sonication methods, the lipid raft fraction remains transparent.

3.4 Trichloroacetic acid protein precipitation

In order to analyze by Western Blot, the proteins present of fractions from the sucrose step-gradient, proteins were precipitated to then resuspend them in small volumes, compatible with the following steps. To precipitate proteins, 250 µl of 100% trichloroacetic acid was added for each ml of fraction, then vortexed and incubated at 4°C for 20 minutes. Next samples were centrifuged for 30 minutes at 16,100 *g*, 4°C (5415R centrifuge, Eppendorf, Hamburg Germany), the supernatant was removed and 1 ml of absolute ethanol at -20°C was added and mixed by inversion. Samples

were centrifuged again at 16,100 *g*, 4°C for 30 minutes, the supernatant was removed and 1 ml of absolute ethanol at -20°C was added to each sample and centrifuged another time under the same conditions. The supernatant of each sample was removed, and pellets were lyophilized at 35°C for 15 minutes (SPD Speed Vac, SPD111V, ThermoFisher Scientific, Waltham, MA, USA) and stored at -20°C until use.

3.5 Flotillin-1 Western Blot assay

Protein extracts were mixed with protein sample buffer adapted for raft and non-raft samples (63 mM Tris-HCl, 10% glycerol, 2% SDS, 100 mM DTT, 0.05% bromophenol blue) and heated at 70°C for 5 minutes. In the electrophoresis gel 15 ± 0.18 µg of protein was loaded per lane. SDS-Polyacrylamide gel electrophoresis (SDS-PAGE) technique was used to separate macromolecules according to the electrophoretic mobility (which varies depending on the length, conformation, and charge of the molecule). SDS is added to allow the proteins lose their native states and charge negatively, so their mobility depends only on their size. Gel electrophoresis was carried out using 12% and 3% polyacrylamide gels for resolving and stacking gel respectively (Table 4).

Table 4: List of reagents and volumes for resolving and stacking gel preparation for SDS-PAGE.

Reagent	Resolving gel (µL)	Stacking gel (µL)
Resolving Buffer	2500	-
Stacking Buffer	-	1500
SDS 1%	1000	600
Acrilamide 30 %	4000	600
$H20_d$	2500	3300
TEMED	7	10
APS 10%	75	50

Electrophoresis was performed with 80 V and amperage in excess to ensure the samples pass the stacking gel correctly. And then 120 V and amperage in excess for approximately 2 hours using an Electrophoresis power supply (Power Pac Basic, Bio-Rad Laboratories, Inc, Hercules, CA, USA), whole SDS-PAGE was carried out in electrophoresis buffer (25 mM Tris, 190 mM glycine, 1 % SDS, pH 8.3).For transferring the proteins in the gel to the Polyvinylidene difluoride (PVDF) membrane, the membrane had to be previously activated with methanol for 15 seconds. PVDF membrane was then washed in Tris-Buffered saline (TBS; 0.5M Tris, 1.5 M NaCl, pH 7.5) wash buffer at 4°C. Western Blot equipment was built up and

put in a tray filled with transfer buffer (25 mM Tris, 190 mM glycine, 20% Methanol, pH 8.5),400 mA current was applied for 1 hour and a half (Electrophoresis power supply, Power Pac Basic, Bio-Rad Laboratories, Inc., Hercules, CA, USA). After the proteins were transferred, the PVDF membrane was washed with TBS with 0.05% of Tween20 solution once. For the immunoblot assay, the membrane was immersed in blocked solution (5% of powdered milk in TBS with 0.05% Tween20) with primary antibody Mouse α-Flotillin-1 1:1000 (0.25 µg/ml) (BD laboratories, Franklin Lakes, NJ, USA) for 2 hours at RT or O.N at 4°C. After the incubation with the primary antibody, the membrane was washed in TBS-Tween20 0.05% buffer for 10 minutes four times. Afterward, it was incubated with the blocked solution with secondary antibody Goat α-Mouse-HRP 1:10,000 for 1 hour at room temperature. Finally, the membrane was washed with TBS-Tween20 0.05% buffer for 10 minutes four times. The presence of flotillin-1 was revealed using Enhanced Chemiluminescence (ECL) reagents (Millipore, Burlington, MS, USA) for bound peroxidase activity visualization. The signal was visualized with Versadoc Molecular Imager coupled with a high-sensitivity CCD camera (Versadoc Imaging System 5000, Bio-Rad Laboratories, Inc., Hercules, CA, USA). The integrated optical density of the immunoreactive protein bands was measured in images taken within the linear range of the camera, avoiding signal saturation.

4 Cell Membrane Microarrays (CMMA). Complete membranes standard method.

Membrane preparations were resuspended in printing buffer (IMG Pharma, Zamudio, Spain), adjusted to a concentration of 5 mg/ml, and incubated for 2 hours in ice. Then, the preparations were printed onto pre-activated glass slides using a non-contact microarrayer (Nanoplotter NP 2.1, GeSiM Bioinstruments and Microfluidics, Radeberg, Germany) using a solenoid tip, placing 2 replicates of each sample (30 nl/spot), into pre-activated glass microscope slides (Rodriguez-Puertas et al., 2009). Printing was carried out under controlled humidity (relative humidity 60%) at a controlled temperature of 4 °C. To ensure correct spot adherence, after printing CMMAs were let dry at 4°C and 60% of relative humidity for 30 minutes, and then stored at -20°C until usage. CMMAs were validated before usage by different methods including Bradford staining for protein determination, enzyme

activity assays (NADH oxidoreductase, succinate dehydrogenase, GAPDH, and cytochrome c oxidase), and MALDI mass spectrometry analysis.

4.1 Bradford staining

After two days at -20°C, Bradford staining is performed in CMMAs for correct membrane adherence and analyze the protein concentration of each spot after printing. CMMAs are defrosted inside a desiccator chamber for 45 minutes at RT. Afterwards, CMMAs are completely immersed in Bradford staining at 4°C (Coomasie blue dissolved (final concentration 0.01%), in 95% ethanol (final concentration of 4.7%), and ortho phosphoric acid 85% (final concentration 8.5%) for 1 hour in darkness, and dipped in H_2O_d at RT. Stained CMMAs were dried out with small fan, the color signal was acquired with an Epson V750 pro scanner (Seiko Epson Corporation, Suwa, Nagano, Japan), and digital images were analyzed and quantified using the software ImageScanner (IMG Pharma S.L, Zamudio, Spain). The total quantity of protein of each spot is determined representing the total color signal of each rat brain cortex spot with respect to its concentration.

5 Adaptations of methods to develop a novel Cell Membrane Microarray of lipid rafts *vs* non-raft membranes (RMMA)

raft and non-raft membranes preparations obtained from the sucrose gradient were unable to reach a correct adherence to the pre-activated glass slide due to the sucrose content. In addition, raft and non-raft membranes extracted by the detergent method spread over whole CMMAs and were incompatible with the MALDI-MS experiments. Thus, in order to remove the detergent and the remaining sucrose in the samples of raft and non-raft membranes two methods were tested: dialysis followed by concentration, and direct ultra-centrifugation method followed by resuspension in detergent-free and sucrose-free solution.

5.1 Lipid raft and non-raft membranes preparation by dialysis and concentration

For detergent and sucrose removal in lipid raft and non-raft membrane fractions, the dialysis of the samples was done using Slide-a-Lyzer dialysis cassettes (Thermofisher, Waltham, MA, USA). The starting volume of membrane fractions

was 1 ml, which was introduced in the cassette, two dialyses of 1 hour were done, changing the external media, afterward, 2 dialysis of 2 hours at RT and 1 dialysis overnight at 4°C. Final volume of dialyzed sample obtained was 2.5 ml approximately. After dialysis, samples were concentrated using Amicon Ultra 0.5 centrifugal filter pack (Merck Millipore, Burlington, MA, USA), following provider instructions. Final volume of the concentrated membrane fractions was around 300 µl, they were centrifuged at 18,000 *g* (Microfuge® 22R centrifuge, Beck-man Coulter, Brea, CA, USA) for 1 hour at 4 °C and raft and non-raft pellets were stored at -80 °C until usage.

5.2 Lipid raft and non-raft membranes preparation by ultracentrifugation

Once the lipid raft and non-raft samples from the whole extract were collected, 1 ml of sample was added in an ultra-clear 15 x 95 mm centrifuge tube, and 10 ml of TNE with protease inhibitors was added above the sample and gently mixed. The samples were centrifuged at 4°C, 120,000 *g* (Beckman coulter optimal 100 XP ultracentrifuge, SW40 Ti rotor) for 2.5 hours. Afterward, the supernatant was discarded, and pellets were resuspended in 100 µl TNE buffer with protease inhibitors and centrifuged at 4°C, 6 hours, and 16,100 *g* (5415R microcentrifuge, Eppendorf, Hamburg, Germany). Upper fractions were discarded, and samples were stored as pellets.

5.3 Lipid raft and non-raft microarrays fabrication

Lipid raft and non-raft fractions obtained by detergent and detergent-free method, and processed by dialysis or centrifugation method were printed in order to develop RMMAs. raft and non-raft fractions' pellets were defrosted in ice and resuspended in printing buffer (IMG Pharma S.L, Zamudio, Spain) and adjusted to a final concentration of protein of 3.5 mg/ml in the case of dialysis method and 5 mg/ml in case of centrifugation method. After resuspension, fractions were incubated in printing buffer O.N at 4 °C. raft and non-raft resuspended fractions were printed onto glass slides using a non-contact microarrayer (Nanoplotter NP 2.1, GeSiM Bioinstruments and Microfluidics, Radeberg, Germany) with solenoid Tip (GeSiM Bioinstruments and Microfluidics, Radeberg, Germany). Printing buffer (IMG Pharma Biotech S.L, Zamudio, Spain) allows the immobilization of samples maintaining protein functionality and lipid environment of samples (Elexpe et al., 2021; Fernández et al., 2019; Hebert-Chatelain et al., 2016; Rienda et al., 2021). For

each microarray 3 replicates of each sample were placed into pre-activated glass microscope slides (Rodriguez-Puertas et al., 2009) (Figure 14), each spot contains 30 nl of sample suspension (10 drops of 0.3 nl), one biological replica.

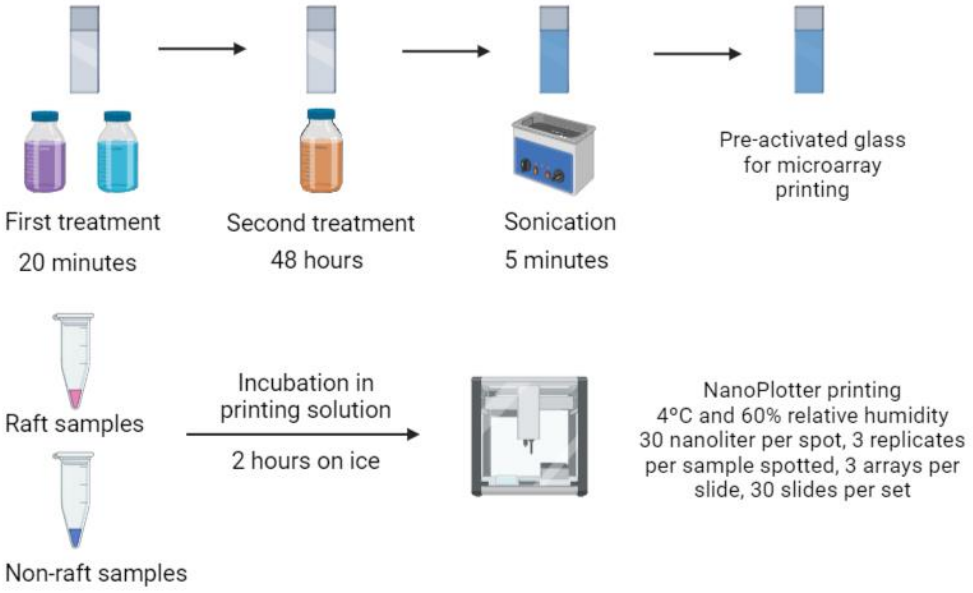

Figure 14: Time schedule of sample printing preparation. Pre-activation of glass slides for immobilization of solid compounds and printing conditions.

Printing was carried out under controlled humidity (relative humidity 60%) at a controlled temperature of 4°C during whole procedure. Distance between spots was 950 µm. After printing, microarrays stay at 4°C for 30 minutes and they were stored at -20°C until usage. Each microarray also included cell membrane homogenates from rat brain cortex at different concentrations for inner control and printing solution buffer as a negative control. 3 microarrays were printed per slide (Figure 15). After printing, one of the slides per batch was used to determine the quantity of protein. For this purpose, microarrays were immersed inside Bradford reagent for 1 hour. Then they were washed twice with distillated water for 1 minute and dried out at RT using a small fan. The color signal was acquired with an Epson V750 pro scanner (Seiko Epson Corporation, Suwa, Nagano, Japan) and digital images were analyzed and quantified using the ImageScanner software (IMG Pharma S.L, Zamudio, Spain). The total quantity of protein of each spot is determined representing the total color signal of each rat brain cortex spot respect to its concentration.

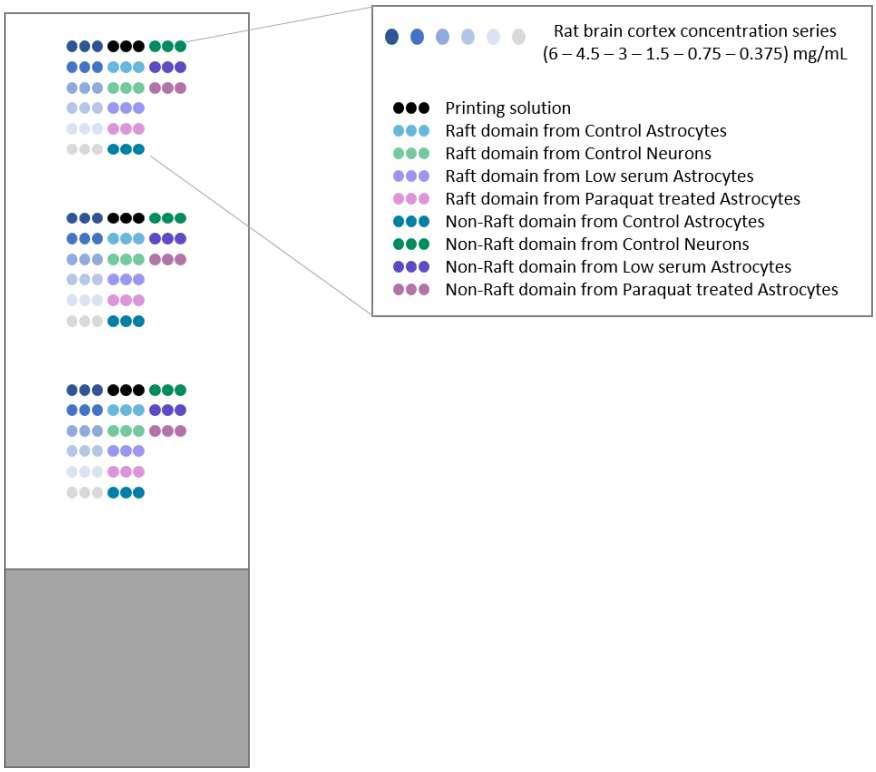

Figure 15: Microarray design for sample printing. Rat brain cortex was used as a positive control to ensure the correct impression of the samples, and for protein quantity normalization. Printing solution was used as a blank.

6 Lipidomic analysis in CMMAs or RMMAs

To perform lipidomic analysis by MALDI-MS, firstly the slides for positive ion mode were incubated with a solution of CsCl (300 mM) for 30 minutes, and then let them dry. Afterward, cell membrane microarrays (CMMAs or RMMAs) had to be coated with a the MALDI matrix forming a uniform film of approximately 0.2 mg/cm^2 with the aid of a standard glass sublimator (Ace Glass 8233, Vineland, NJ, USA), producing. For positive-ion and negative-ion modes, 2-mercaptobenzothiazole (MBT) and 1,5-diaminoaphtalene (DAN) were used, respectively. The CMMAs were scanned, as in the MALDI imaging experiment (Figure 16). Coverage, pixel quantity, and resolution of each experiment depends on the spot's diameter, separation between spots and quality of the samples analyzed.

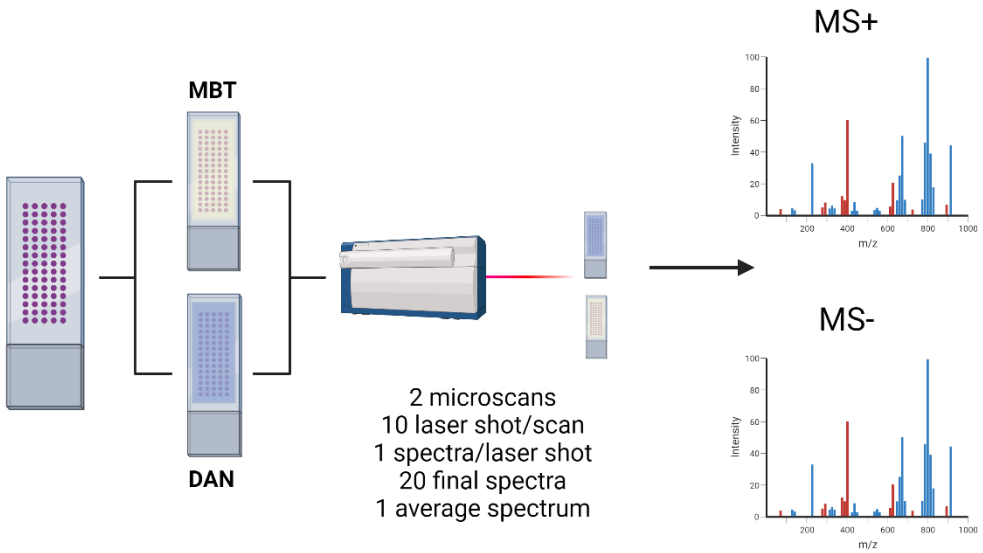

Figure 16: Schedule of matrix deposition and mass spectrometry procedure.

6.1 MALDI-MS – Whole plasma membrane of astrocytic cells

The area of the array was explored following a grid coordinate separated by 250 µm; as each spot has a diameter of 600 µm, six pixels were recorded at each spot. The mass spectrometer used was an LTQ-Orbitrap XL (Thermo Fisher Scientific, Waltham, Massachusetts, USA), equipped with a MALDI source with a N_2 laser (60 Hz, 100 µJ/pulse maximum power output). The laser spot is an ellipsoid of approximately 50–60 µm × 140–160 µm. Two microscans of 10 shots/pixel were used, with a laser power output of 20 µJ for positive ion mode (MS^+) and 30 µJ for negative ion mode (MS^-) and a resolution of 250 µm. Data loading included spectra normalization by total ion current (TIC), spectra alignment, and peak picking, filtering all the m/z with intensity < 0.5% of the strongest peak in the spectrum. The mass range collected was between 500 m/z and 1400 in ion positive mode and between 550 m/z and 1400 ion negative mode.

6.2 MALDI-MS – raft and non-raft membranes of astrocytic and neuronal cells

MALDI-MS experiment was carried out as explained above, but the area of the array was explored following a grid coordinate separated by 150 µm, the diameter of the pot was 500 µm and 12 pixels were obtained.

6.3 Data processing

6.3.1 Calibration

Before data processing, calibration of data might be performed to ensure correct data treatment.

6.3.2 Reference mass list calibration

A list of theoretical reference masses is used for calibration in MS^+ and MS^- separately. Theoretical masses are searched, and spectra are adjusted to a second-grade polynomial (if more than 3 masses are found) or first-grade polynomial (2 masses are found). Then, the error of calibration (CE) is calculated, as follows:

$$CE = \frac{m/z_e - m/z_t}{m/z_t}$$

*m/z_e: experimental m/z value of peak m/z_t: theoretical m/z value of peak

If CE is below 0.05 mass experimental mass is considered equal to theoretical mass, and peak alignment is carried out as explained below.

6.3.3 Peak smoothing

Once the aligned spectra are obtained, peaks of each spectrum were smoothed using a gaussian function with a window length of 10 points that convoluted along the whole spectrum. Maximum intensity of the peak gets lower when peak is smoothed but the whole peak area is maintained (Figure 17). The smoothing is necessary to convert the peaks into centroids for analyzing the data.

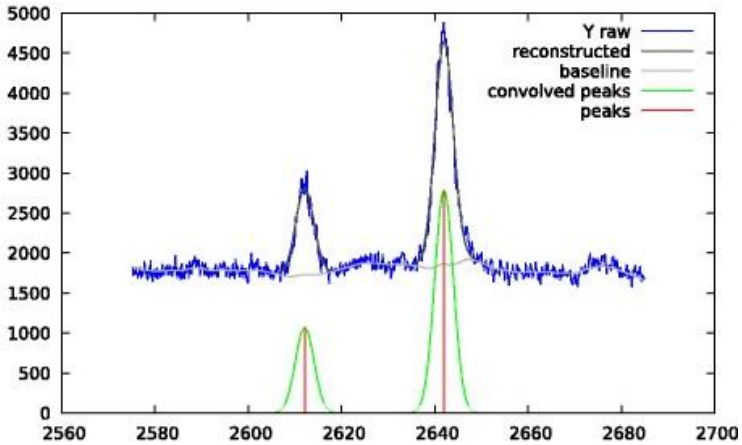

Figure 17: Gaussian smoothing for peaks obtained from MALDI-MS experiment (Figure obtained from Picaud et al., 2018)**.**

6.3.4 Peak alignment

All the mass spectrometry data was acquired and processed using IMG Pharma software built in MATLAB (MathWorks, Portola Valley, CA, USA). The average spectrum obtained from each sample was aligned to other samples by the following procedure (Figure 18).

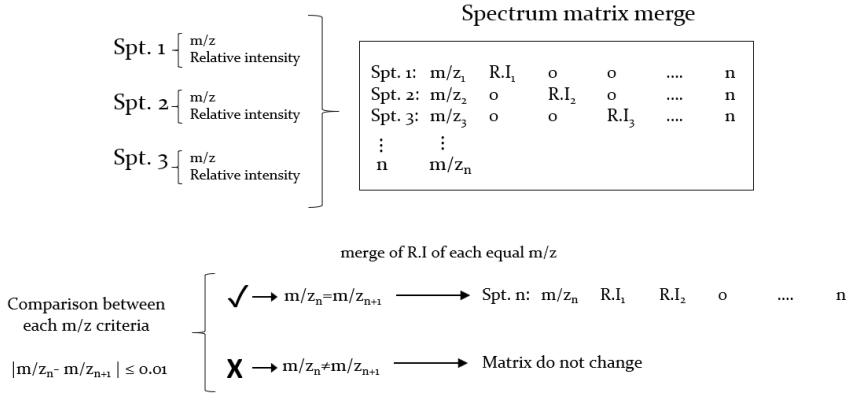

Figure 18: Different steps for spectra alignment for each MALDI-MS experiment.

Each spectrum from each sample was converted into a matrix of m/z and relative intensity signal, all matrixes were merged onto a bigger matrix of n columns and m rows. To avoid peak duplicity due to experimental error in proximal m/z values, each m/z peak was compared with the others. Due to the full width at half maximum (FWHM) of 60.000 of the equipment, a mass window between 0.01 and 0.03 Da was used. Thus, if the difference between them is ≤ |0.01|, the peak is considered to be the same.

6.3.5 Outlier identification

Subsequently, peak outliers were identified and discarded by the following method. Correlation matrix of all peaks obtained from the mean spectrum of all samples was performed. The median and the standard deviation of the correlation of each average peak is calculated. Outliers were identified with the following formula.

$$OL = median - 1.5 * STD$$

**OL: outlier limit STD: standard deviation*

The peaks (value of m/z) that were below the outlier limit (OL) were discarded. Afterward, the relative intensity value of remaining peaks was normalized to their

TIC, and new relative intensities of each lipid from each spectrum were calculated using following formula.

$$\frac{x_i}{\sum_i^n x_i}$$

x_i: relative intensity of a peak

Subsequently, peaks with less than 0.1%-1% (value was chosen depending on the noise of the spectrum, but generally was 0.5%) of the strongest peak in the spectra were considered as noise and discarded. Regarding the normalization, each lipid was re-normalized to its TIC and relative intensities of each lipid from each spectrum were calculated, as explained previously. Moreover, the identification of outlier spectra was carried out with similar method as outlier peak identification. Correlation matrix of all the spectra is obtained and correlation values mean and standard error of the mean (SEM) are calculated, and spectra outlier limit (SOL) is obtained by following formula, for outlier spectra rule out.

$$SOL = mean - SEM$$

If value was below SOL, spectrum was considered an outlier and discarded.

6.3.6 Isotopic distribution elimination

To avoid peak duplicity due to the presence of various isotopes from the same molecule, isotopic distribution elimination was carried out using IMG Pharma software built in MATLAB (MathWorks, Portola Valley, CA, USA). For each peak, three different criteria were taken into account for considering them an isotope.

- Distance between two peaks compared between 0.99 and 1.01 Da
- Intensity of one peak less than 75% the intensity of the other peak
- Correlation between both peaks is higher than 80%

If a combination of peaks fulfilled three criteria, the peak was considered an isotope, and isotopes with lower intensity were discarded.

6.3.7 Lipid tentative assignment

Online tools from LIPID MAPS data base were used to assign each m/z value to a lipid ion based on accuracy mass. Tool used was the LIPID MAPS database of computationally-generated “bulk” Lipid Species (COMP_DB) with a mass tolerance

of ± 0.005 m/z, ions with losses of H– and CH_3 – were selected for ion-negative mode and Cs^+ were selected for ion-positive mode, as we used Cesium in excess for ensure the spectrum displacement.

The lipid classes selected for each search were: Glycerophosphoserines (PS), Glycerophosphoglycerols (PG), Glycerophosphoinositols (PI), phosphoinositols (PIP), Glycerophosphoethanolamines (PE), Glycerophosphates (PA), Ceramides (Cer), Spingomyelins (SM) and Sulfatides (SHexCer) for ion-negative mode. Whereas Glycerophosphocholines (PC), Triacylglycerols and Tryalkylglycerols (TG), Diacylglycerols and dialkylglycerols (DG), Ceramides (Cer), Hexosylceramides (HexCer), Dihexosylceramides (Hex2Cer) and Spingomyelins (SM) were selected for ion-positive mode.

7 Lipidomic data analysis

7.1 Statistical analysis

Statistical analysis was performed using Graphpad Prism Software from Dotmatics (Boston, Massachussets, USA). To test the normality of each variable, Saphiro-Wilk normality test was performed, with α set at 0.05. For possible outlier spectrum detection, Pearson correlation test, two-tailed was performed for each ionization mode separately and α was set at 0.05. Correlation of less than 0.7 between replicates were considered as outlier value and discarded.

To calculate the reproducibility between microarrays measured, Pearson correlation test was performed between the two different arrays, α was set at 0.05. Lowest correlation percentage obtained between arrays was considered as the method reproducibility. To elucidate if there was any statistically significant difference in lipid relative abundance between the different spectra obtained, Mann-Whitney Rank non-parametric test was performed for every comparison, α was set at 0.05.

7.2 Unsupervised methods

7.2.1 Principal Component Analysis

Principal component Analysis is an unsupervised method for multivariate analysis which compress the original number of variables into a smaller subset of composite variables that are orthogonal to each other, called principal components. Each new

variable obtained explain the largest amount of variability as possible, thus the lowest the variable number, the higher the variability explained (Figure 19).

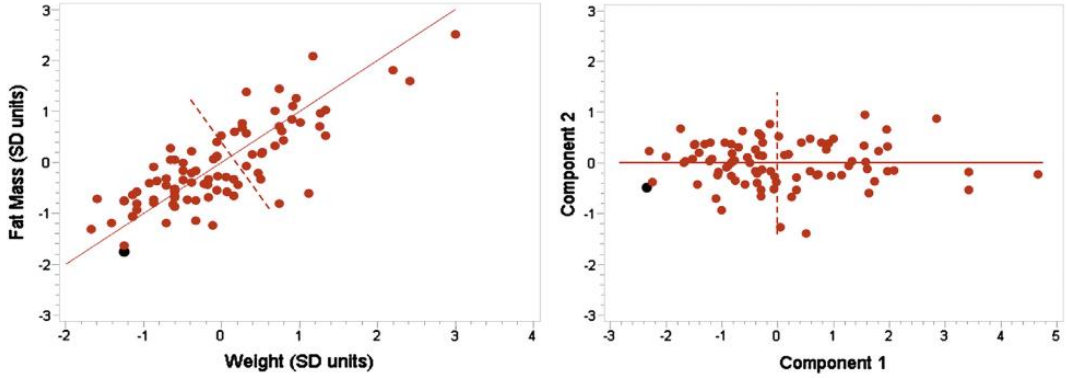

Figure 19: Two first principal component calculation from data collection (Figured obtained from Sainani, 2014).

Multivariate describing analysis were performed using Orange open-source software tools from the University of Ljubljana (Ljubljana, Slovenia). The number of principal components obtained in the analysis has to explain more than the 90% of variability and each one has to explain more than the 0.5% of the variability. The specific values of principal components obtained in each analysis are reported in the Appendix. The PCA analysis was performed using 2 different sets of data: first one was the whole lipid spectra and other one was the 50-best ranked lipids (ranking obtained by a one-way ANOVA analysis). The value of the differences between the variances obtained was the one used to rank the variables.

7.2.2 Supervised methods

Supervised classification methods were performed using Orange open-source software tools from the University of Ljubljana (Ljubljana, Slovenia). For supervised classification methods k-nearest neighbors (kNN), Naïve Bayes, Neural Networks, and Random Forest algorithms were used. All supervised methods were validated using cross-validation of 10-folds.

7.2.3 K-nearest neighbors

The k-Nearest neighbors' algorithm is a supervised classification method where each data is classified to the class that is most prevalent out of the points that are closest. For measuring the distance between each point and its neighbors, in our case

Euclidean distance was used to calculate the distance between two samples compared. Euclidean distance, calculated by following equation.

$$D(p,q) = \sqrt{(p_1 - q_1)^2 + (p_2 - q_2)^2 + \cdots + (p_n - q_n)^2}$$

Moreover, number of neighbors has to be chose, for kNN algorithm, larger k reduces impact of variance caused by randomness but can ignore small patterns (Zhang, 2016). K number of neighbors was set as 5 using Euclidean distance and uniform weight, as the variables have been normalized before.

7.2.4 Naïve Bayes

The Naïve Bayes classifier is one of the simpler machine learning techniques, based on the conditional probability Theorem of Bayes.

$$\mathrm{P(A|B)} = \frac{\mathrm{P(B|A)} * \mathrm{P\ [A]}}{\mathrm{P(B)}}$$

The method used this equation to calculate if a feature belongs or not to a certain class based in different classifiers (Carpenter & Huang, 2018). The classifier was used using the PC obtained for each analysis, not the pre-processed data.

7.2.5 Random Forest

The random forest supervised classificatory is a method based on decision trees: graphs that are used to divide data into different classes (Carpenter & Huang, 2018). Random forest classifies an input data subset using decision tress, the higher the decision tress number, the higher the classification accuracy. For our analysis number of decision tress was set as 10, subsets with less than 5 features do not split into new decision tree.

7.2.6 Neural Networks

Neural network algorithm model is composed by different layers of neurons, first layer takes the input data and is followed by a number of hidden neuron layer until the output layer which give the classification. Each neuron from each layer performs the data processing on its own, every neuron can receive multiple inputs, and different functions can be used for activate the input (Figure 20).

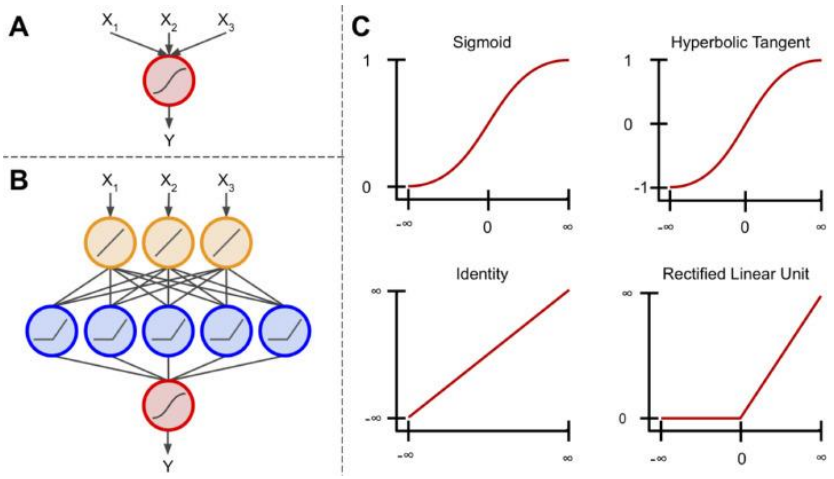

Figure 20: Components of artificial neural network. A) Basis of the neural network, algorithm with a sigmoid function (red circle) which transform multiple inputs in one output. B) Artificial neural network with different layers, the input of one layer is the output of another. C) Most used activation function: sigmoid, hyperbolic tangent, identity, and Rectified linear Unit (ReLU) (Figure obtained from R. Y. Choi et al., 2020)

For lipidomic data, the number of neurons per hidden layer was set at 200, neuronal input is processed using rectified linear unit function (ReLu) as its activation function. Stochastic gradient descent as the solver for weight optimization, and a maximum of 350 iteration were set. The regularization parameter alpha was set as 0.05. In this case, we did not use a different training data set for the neural network, all the supervised methods were validated using cross-validation of 10 folds.

8 Enzymatic activity assays on printed membrane subdomains

8.1 NADH-oxidoreductase activity assay

RMMAs were placed in a desiccator for 30 minutes to ensure correct defrosting and the area of each microarray was delimited with a hydrophobic barrier pen (Merck, Darmstadt, Germany). To study the NADH oxidoreductase activity, 4 different pH (7.2, 7.4, 7.6, and 7.8), 4 different solution buffer concentrations (0.1 M, 50 mM, 10 mM, and 5 mM), 2 reactive concentrations (0.1 mM and 0.35 mM), and 3 different decylubiquinone concentrations (10 µM, 25 µM and 50 µM) were tested with or without the presence of sodium azide, the inhibitor of the mETC complex IV. Final reaction solution contains the different concentrations of β-nicotinamide adenine dinucleotide (NADH), and decylubiquinone (dUQ), 0.1 mg/ml of Nitrotetrazolium Blue Chloride (NBT), and phosphate buffer at the concentrations and pH described before, with or without 10 mM of sodium azide (Sigma-Aldrich, St. Louis, MO, USA).

Reaction solution was added cautiously to the microarrays and were incubated inside a humidity chamber at a controlled temperature of 24 °C for times between 4 and 16 hours in darkness. The colorimetry of the reaction was evaluated every two hours. The reaction was stopped by removing the reaction solution and washing gently the microarrays in distilled water and dried at RT. The color signal was acquired with an Epson V750 pro scanner and digital images were analyzed and quantified using the software ImageScanner (IMG Pharma S.L, Zamudio, Spain).

8.2 Succinate dehydrogenase activity assay

Microarrays were placed in a desiccator for 30 minutes to ensure correct defrosting and the area of each microarray was delimited with a hydrophobic barrier pen (Merck, Darmstadt, Germany). To study the succinate dehydrogenase activity, 4 different pH (7.2, 7.4, 7.6, and 7.8), 4 different solution buffer concentrations (0.1 M, 50 mM, 10 mM and 5 mM) and 2 reactive concentrations (1 mM and 10 mM) were tested, with or without the presence of sodium azide, the inhibitor of the mETC complex IV. Final reaction solutions contain the different concentrations of sodium succinate dibasic, 50 µM of decylubiquinone (dUQ), 0.1 mg/ml of NBT, and phosphate buffer at the concentrations and pH described before, with or without 10 mM of sodium azide (Sigma-Aldrich, St. Louis, MO, USA). Reaction solution was added cautiously to the microarrays and them were incubated inside a humidity chamber at a controlled temperature of 24 °C for 16 hours in darkness. The colorimetry of the reaction was evaluated every hour. The reaction was stopped by removing the reaction solution and washing gently the microarrays in distilled water and dried at RT. The color signal was acquired with an Epson V750 pro scanner and digital images were analyzed and quantified using the software ImageScanner (IMG Pharma S.L, Zamudio, Spain).

8.3 Glyceraldehyde-phosphate dehydrogenase activity assay

Microarrays were placed in a desiccator for 30 minutes to ensure correct defrosting and the area of each microarray was delimited with a hydrophobic barrier pen (Merck, Darmstadt, Germany). To study the glyceraldehyde-3-phosphate dehydrogenase (GAPDH) activity, 4 different pH (7.2, 7.4, 7.6, and 7.8), 4 different solution buffer concentrations (0.1 M, 50 mM, 10 mM, and 5 mM) and 2 reactive concentrations (10 mM and 20 mM) were tested, with or without the presence of sodium azide, the inhibitor of the mETC complex IV. Final solution of the reactions

contains increasing concentrations of G3P, different concentrations of dUQ, 0.1 mg/ml of NBT, and phosphate buffer at the concentrations and pH described before, with or without 10 mM of sodium azide (Sigma-Aldrich, St. Louis, MO, USA). Reaction solution was added cautiously to the microarrays and them were incubated inside a humidity chamber at a controlled temperature of 24 °C for 16 hours in darkness. The colorimetry of the reaction was evaluated every hour. The reaction was stopped by removing the reaction solution and washing gently the microarrays in distilled water and dried at RT. The color signal was acquired with an Epson V750 pro scanner and digital images were analyzed and quantified using the software ImageScanner (IMG Pharma S.L, Zamudio, Spain).

8.4 Acetylcholinesterase activity assay

Microarrays were placed in a desiccator for 30 minutes to ensure correct defrosting. The area of each microarray was delimited with a hydrophobic barrier pen (Merck, Darmstadt, Germany). Microarrays were washed using Tris-maleate buffer (Tris-maleate (Sigma-Aldrich, St. Louis, MO, USA) at 0.1 M and pH 6) twice. Reaction solution contains 65 mM pH 6 of Tris-maleate, 5 mM sodium citrate,3 mM of copper sulfate and 5 mM of potassium ferricyanide, with or without acetylcholine iodide (Sigma-Aldrich, St. Louis, MO, USA) at a final concentration of 0.74 mg/ml. BW284 was used as Acetylcholinesterase at final concentration of 1 mM. The reaction was incubated for 16 hours in humidity chamber in darkness. Reaction was stopped removing cautiously the reaction solution and washing twice the microarrays with Tris-maleate buffer for 10 minutes. Microarrays were dipped onto distilled water and dried at RT. The color signal was acquired with an Epson V750 pro scanner and digital images were analyzed and quantified using the software ImageScanner (IMG Pharma S.L, Zamudio, Spain).

8.5 Data processing and statistical analysis

Data obtained were normalized respect its total protein quantity obtained by Bradford assay directly onto the microarray. Printing solution present in microarrays is used as blank for each experiment. Data handling and analysis was carried out using Excel and GraphPad software (version 9.2). All data were normalized respect their total amount of protein in the spot, obtained by Bradford assay. The identification of outliers was carried out as explained in the section 2.

9 Reagents and resources

Table 5: Reagents and resources

REAGENT OR RESOURCE	SOURCE	IDENTIFIER
CHEMICALS		
(±)-α -tocopherol	Sigma-Aldrich	Cat#T3251
1,5-Bis(4-Allydimethylammoniumphenyl)5-3-1-2Br (Bw284CS1)	Sigma-Aldrich	Cat#A9013
1,5-diaminophthalene	Sigma-Aldrich	Cat# D21200
2-mercaptobenzothiazole	Sigma-Aldrich	Cat#M3302
3,3'-diaminobenzidine (DAB)	Sigma-Aldrich	Cat#D5637
Acetylcholine iodide	Sigma-Aldrich	Cat#01480
Acrylamide-bis ready-to-use solution 30% (37.5:1)	Merck	Cat#100639
APS 10%	Merck	Cat#7727-54-0
Beta-nicotinamideadeninedinucleotide (NADH)	Sigma-Aldrich	Cat#N8129
Bovine serum albumin	Sigma-Aldrich	Cat#A8022
Bromophenol blue	Sigma-Aldrich	Cat#34725-61-6
Cessium chloride	HoneyWell	Cat#289329
Chlorhidric acid (HCl) 37%	Merck	Cat#100317.1000
Coomasie blue	Sigma-Aldrich	Cat#B-0770
Copper (II) sulfate	Sigma-Aldrich	Cat#C1297
Cytochrome c from equine heart	Sigma-Aldrich	Cat#C2506
Decylubiquinone	Sigma-Aldrich	Cat#D7911
Dimethyl sulfoxide (DMSO)	Sigma-Aldrich	Cat#D2650
Di-sodium hydrogen phosphate di hydrated	Panreac	Cat#122507.1210
Dithiothreitol (DTT)	BioRad	Cat#1610610
DL-A-glycerol phoshphate magnesium	Sigma-Aldrich	Cat#17766

Dodecyl sulfate sodium salt, 99% for biochemistry	Acros Organics	Cat#230425000
Dulbecco's modified eagle medium with phenol red	Lonza	Cat#BE12917F
Dulbecco's modified eagle medium: nutrient mixture f-12 (dmem/f-12)	Gibco	Cat#21331020
EDTA, tetrasodium tetrahydrate salt	Calbiochem	Cat#34103
Enhanced chemiluminescencereagents	Millipore	
Ethanol	Panreac	Cat#251086.9914
Ethanol for molecular biology	Merck	Cat#108543
Ethyleneglycol-bis(β-aminoethylether)-N,N,N',N'-tetraaceticacid (EGTA)	Sigma-Aldrich	Cat#E4378
Fetal bovine serum	Gibco	Cat#11573397
Fetal bovine serum charcoal-filtered	Gibco	Cat#12676011
Glycerol	Sigma-Aldrich	Cat#G7893
Glycine	Thermo Fisher Scientific	Cat#10070150
L-glutamine	Merck	Cat#56-85-9
Magnesium chloride hexahydrate	Sigma-Aldrich	Cat#M2670
Methanol (reag. Ph. Eur) for UHPLC	PanReac	Cat#221091
Methyl viologen dichloride hydrate (paraquat)	Sigma-Aldrich	Cat#856177
Nitrotetrazolium blue chloride (NBT)	Sigma-Aldrich	Cat#N6876
Non-essential amino acids	Sigma-Aldrich	Cat#M5550
Ortho-phosphoric acid 85%	Panreac	Cat#131032.1212
Penicillin/streptomycin	Gibco	Cat#15140122
Penicillin/streptomycin	Gibco	Cat#15140122
Phosphate-buffered saline	Gibco	Cat#11530546
potassium hexacyanoferrate (II) trihydrate	Sigma-Aldrich	Cat#P3289
Protease inhibitor cocktail	Sigma-Aldrich	Cat#P8340
Sodium azide	Sigma-Aldrich	Cat#S2002

Sodium chloride	Acros Organics	Cat#10478283
Sodium citrate tribasic dihydrate	Sigma-Aldrich	Cat#S4641
Sodium deoxycholate	Sigma-Aldrich	Cat#30970
Sodium di-hydrogen phosphate	Panreac	Cat#131965.1211
Sodium hydroxide pellets	Labkem	Cat#1310-73-2
Sodium succinate dibasic	Sigma-Aldrich	Cat#14160
Sucrose	Sigma-Aldrich	Cat#S0389
TEMED	Merck	Cat#110-18-9
Trichloroacetic acid (TCA)	Carlo ErbaReag.	Cat#307557
Tris-maleate	Sigma-Aldrich	Cat#T3128
Triton x-100	Acros Organics	Cat#10671652
Triton x-114	Sigma-Aldrich	Cat#93422
Trizima base	Sigma-Aldrich	Cat#T1378
Trypan blue solution 0.4% sterile filtered	Merck	Cat#T8154
Tween-20	BioRad	Cat#1706531
COMMERCIAL ASSAYS		
Micro BCA protein assay kit	ThermoFisher Scientific	Cat#23235
Mycoplasma get detection kit	BioTools	Cat#90021
EQUIPMENT		
Bioblock scientific ultrasonic processor	VibraCell	
Biorad electrophoresis system	BioRad	
Biorad gel transfer device	BioRad	
Centrifuge 5415r	Eppendorf	
Digital weight scale	Ohaus	
Plotter s	Sartorius	
Gs-800 calibrated densitometer	BioRad	
Optimal-100 xp ultracentrifuge	Beckman Coulter	
Rotanta 460R hettich centrifuge	Hettich	
Hera Cell 150	Heraeus	
Centrifuge 5810R	Eppendorf	
5810R rotor A-4-62	Eppendorf	

Olympus CKX41	Olympus Co.
Teflon-glass grinder RZR 2020	Heidolph
CentrifugeAllegra TM x 22R	Beckman Coulter
Microcentrifuge 22R	Beckman Coulter
Potter S	Satorius AG
100 Ti Optimal-100 XP rotor	Beckman Coulter
SW40 Optimal-100 XP rotor	Beckman Coulter
Vibracell 75115 sonicator	Thermo Fisher
Tipcb33-3363658 tip	BochemLabordebarf
Speedvac SPD	ThermoFisher
Electrophoresis power supply	BioRad
Veradoc Imaging System 5000	BioRad
Nanoplotter NP 2.1	GeSiMBioinstruments
Epson V750	Seiko Epson Co.
Solenoid Tip Nanoplotter	GeSiMBioinstruments
Standard Glass sublimator	AceGlass 8233
LTQ-Orbitrap XL	ThermoFisher

RESULTS

CHAPTER 1. LIPIDOMIC ANALYSIS IN CELL MEMBRANE MICROARRAYS FROM THE HUMAN ASTROCYTIC CELL LINE 1321N1

1 Lipidomic analysis in CMMAs confirms the correc immobilization of cell membranes and reveals paraquat-triggered changes in human astrocytic membranes

In this chapter, I present the results of the first specific objective of this thesis regarding the validation of CMMAs. Lipidomic analysis were performed on cell membranes from a human astrocytic cell line with different treatments in order to demonstrate not only the conservation of the lipid environment but also the potential of this technique to detect effects derived from metabolic and oxidative stress. Before proceeding with this analysis, a viability assay was carried out in order to determine the physiological effect of the studied conditions on the cell survival, whose membranes were further used for the CMMA development.

1.1 Viability of the Human astrocytic 1321N1 cell line upon different treatments. Selection of conditions to validate CMMAs.

For the analysis of cell viability, the culture medium was maintained along the treatments, and monitored until cells in every condition were dead, consequently, without medium refreshing cells could enter in senescence. To analyze cell viability, trypan-blue viability assays were performed as described in material and methods section. Paraquat treatment decreases cell viability at all time points with respect to control, decreasing cell viability from 86% ± 3 (control) to 68% ± 3 (paraquat-exposed) at 24 hours (Figure 21B and C), and reaching complete cell death at 72 hours (Figure 21B). Furthermore, with α-tocopherol pre-treatment, the viability was significantly improved at 24 hours (Figure 21C). At 72 hours, paraquat-induced viability is rescued up to 40% ± 3 if cells were pre-treated with α-tocopherol, whilst no viability differences were seen between α-tocopherol pre-treated cells and the control situation. Differences between paraquat-treated and control situations and between paraquat-treated cells with or without α-tocopherol pre-treatment were observed at all time points between 24h and 72h. Thus, the time chosen for MALDI mass spectrometry was 24 hours, when viability is still not much compromised, and quantitative differences between treatments were larger.

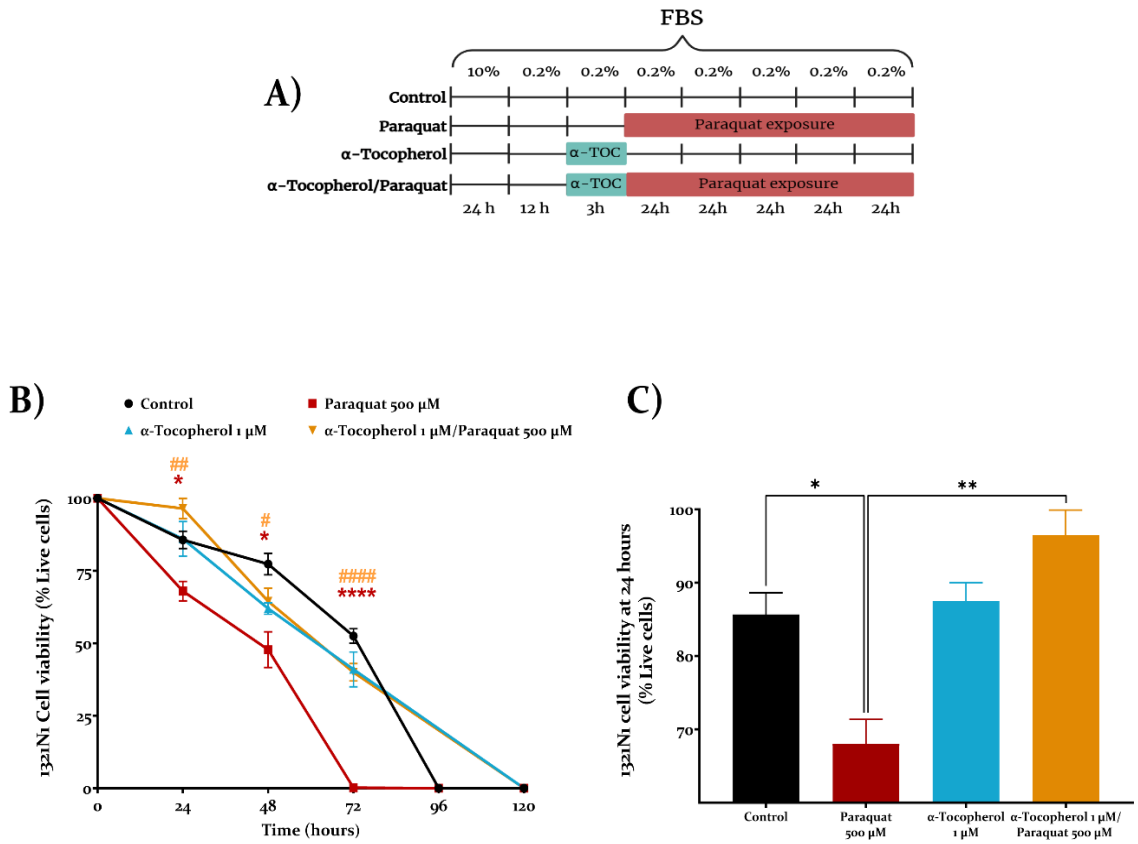

Figure 21: Effects of paraquat on 1321N1 cell viability with or without pre-treatment with α-tocopherol. A) Time course and design of treatments for the evaluation of cell culture viability. B) Time course of cell viability in control conditions and after treatment with paraquat (500 µM) with or without a pre-treatment with α-tocopherol (1 µM). Measurements were performed every 24 h using trypan blue cell viability assay. Asterisks symbols (*) refer to post-hoc comparisons with respect to control; hash symbols (#) refer to comparisons with respect to paraquat. The color of symbols alludes to the condition being compared. C) Cell viability results at 24 h expressed as percentage of live cells. Shapiro-Wilk test was performed to check the normality of distributions. One-way ANOVA analysis (two-tailed) and Tukey post-hoc were conducted, α set to 0.05. *p*-value < 0.05 (*), *p*-value < 0.01 (**), *p*-value < 0.0001 (****); *p*-value <0.05 (#), *p*-value < 0.01 (##), *p*-value < 0.0001 (####).

1.2 Lipidomic analysis in Cell Membrane Microarrays is able to reveal paraquat-triggered changes in human astrocytic membranes.

For MALDI-MS experiments, three experimental groups were selected: control situation, paraquat-exposed cells (500 µM, 24 hours), and paraquat-exposed cells preceded by 3-hours of α-tocopherol pre-treatment (1 µM, 3h). Cells were treated as explained above, and membranes were extracted for CMMAs development (see material and methods section). Once the CMMAs were generated, MALDI-MS technology was used to determine differences between membranes of paraquat-exposed human astrocytes with or without α-tocopherol pre-treatment and control situation. The immobilized samples which

composed the CMMAs were covered with MBT and DAN matrixes for positive and negative-ion mode respectively, as described previously. Using this technology, 103 lipid adducts were identified in a mass range of 500 m/z and 1400 m/z in MS^+ and 90 lipid adducts in a mass range between 550 m/z and 1400 m/z in MS^-. Data obtained were normalized to its TIC, and each ionization mode was analyzed separately. For lipid adducts assignation, lipid types that can be detected in both ionization modes were considered in the ionization mode whose relative signal is higher. Thus, PCs, SM, HexCer, Hex2Cer, TG, and DG were identified in MS^+, and PE, PI, PG, PS, PA, and its derivates such as plasmalogens, ethers, or LP, as well as Cer and SHexCer were analyzed in MS^-. Firstly, differences between lipid fingerprints of paraquat-exposed cells and control situation cells were analyzed in both MS^+ and MS^- modes separately.

Specific tentatively assigned lipids were detected in paraquat-exposed cells, in which 66 tentatively assigned lipids were only present in these membranes (Figure 22A, red arrows), in contrast to the control situation. Regarding to tentative lipid assignment, paraquat-exposed cells' membranes displayed very long ceramides (C > 26) Cer 40:0;O3, Cer 40:1;O3, and Cer 40:2; O3, which are absent in control membranes (Figure 22A, red arrows). Other SLs were increased in paraquat-treated samples, in particular unsaturated SMs with 34 to 42-carbon backbones, which contain fatty acids from 16 to 24 carbons (Figure 22A). Long-chain glycerophosphates also displayed a general increase, particularly evident in PA 40:6, with a very long chain and more than three unsaturations. In contrast, in PE family similar lipid species showed opposite behavior upon paraquat treatment. These changes were observed in pairs differing in their degree of unsaturation, such as PE 36:3, which was only present in paraquat-treated samples (Figure 22B, red arrows), whereas PE 36:2 showed a slight reduction, the same effect as with PE 38:3 and PE 38:2. Nevertheless, PE lipid family can be present as an ether version, which tentatively assigned lipids were generally increased in paraquat treated cells (Figure 22B). In contrast, m/z tentatively assigned as ether PG O-40:7 was present only in control samples (Figure 22B, black arrow), while normal PGs increase due to paraquat treatment (Figure 22B).

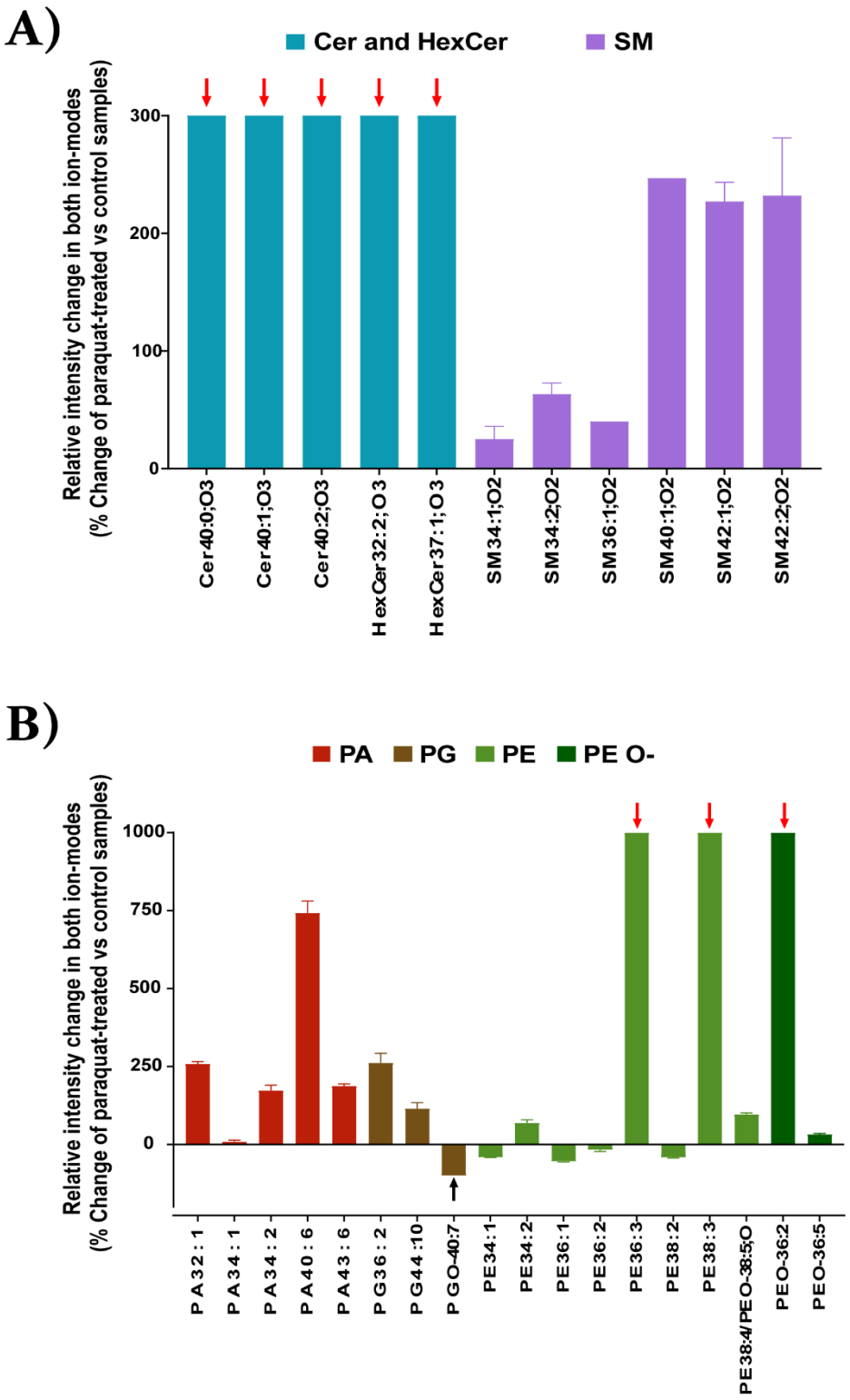
A)
Cer and HexCer
SM
Relative intensity change in both ion-modes
(% Change of paraquat-treated vs control samples)
300
200
100
0
Cer40:0;O3
Cer40:1;O3
Cer40:2;O3
HexCer32:2;O3
HexCer37:1;O3
SM34:1;O2
SM34:2;O2
SM36:1;O2
SM40:1;O2
SM42:1;O2
SM42:2;O2
B)
PA
PG
PE
PE O-
Relative intensity change in both ion-modes
(% Change of paraquat-treated vs control samples)
1000
750
500
250
0
PA32:1
PA34:1
PA34:2
PA40:6
PA43:6
PG36:2
PG44:10
PGO-40:7
PE34:1
PE34:2
PE36:1
PE36:2
PE36:3
PE38:2
PE38:3
PE38:4/PEO-38:5;O
PEO-36:2
PEO-36:5

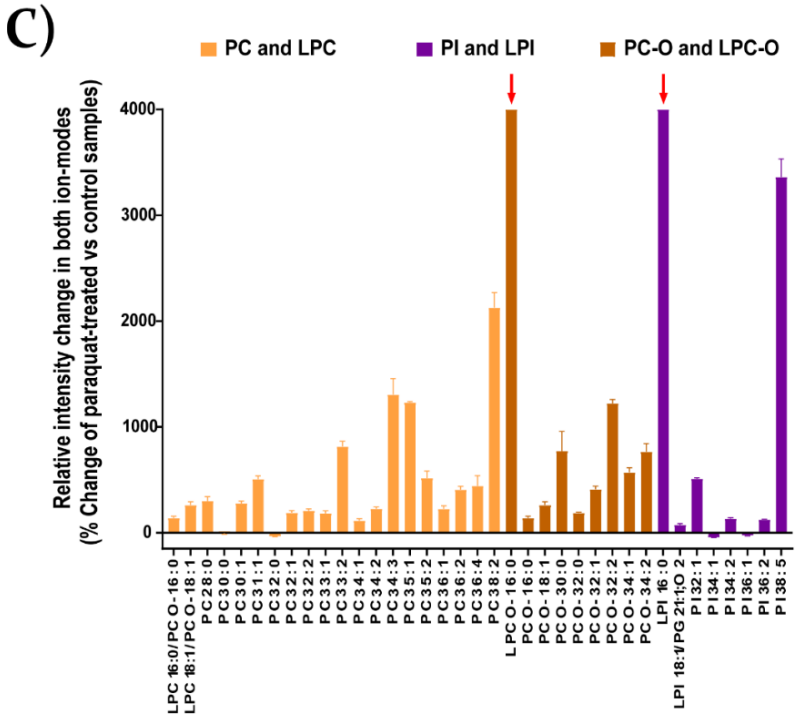

Figure 22: Relative intensity change in different lipids when comparing paraquat treated membranes with control samples printed in CMMAs. Data are shown as percentage of control values. A) Changes in sphingolipids (Cer, HexCer and SM). B, C) Changes in GPs. PA, PG, PE, and PE O- shown in B). LPC, PC, and PI shown in C). Oxygen number inside the lipid head and fatty acids in Ceramides and Sphingomyelins are indicated by O with a suffix. Bars with red arrows are only present in paraquat-treated samples, and Bars with black arrows are only present in control samples.

Nevertheless, very long-chain PCs are increased due to paraquat treatment: the higher the unsaturation number, the higher the change rates. Thus, PC with one or two unsaturations were increased in paraquat-treated samples, while saturated PCs were reduced or absent (Figure 22C). In addition, LGPs of PC family were detected, in particular LPC 16:0 and LPC 18:1 (Figure 22C), whose presented an increase of 38% ± 25 and 262% ± 43 respectively, whereas LPC 16:0 ether form appeared only upon paraquat treatment (Figure 22C, red arrows). Finally, PI adducts were presented as very long-chain lipids, with a general increase observed in the forms with more unsaturations, while their saturated forms or those with lower unsaturation were reduced or absent (Figure 22C).

1.3 Lipidomic analysis in CMMAs is able to reveal the effect of α-tocopherol pre-treatment on the paraquat-triggered signature

The effect of α-tocopherol pre-treatment in paraquat-treated cells not only affects viability but also involved changes over membrane lipidome that can be detected with the CMMA technology. The membranes from paraquat-treated cells with α-tocopherol pre-treatment,

showed a higher presence of unsaturated very long-chain ceramide Cer 40:0;O3 (271%), while Cer 40:1;O3 (–8.7% ± 4.9) and Cer 40:2;O3 (–35.4% ± 24) presented not significant changes or a slight reduction (Figure 23A). Also, HexCer 32:2;O3 and HexCer 37:1;O3 displayed a slight and pronounced increase in pre-treated cells respectively. However, these lipids were absent in control situation (Figure 23A). In regard to SMs, SM 35:1;O2, SM 36:2;O2 and SM 41:2;O2 appeared only in the α-tocopherol pre-treated cells (Figure 23A, red arrows). Moreover, SM 40:1, and 40:2 showed an increase in pre-treated (Figure 23A).

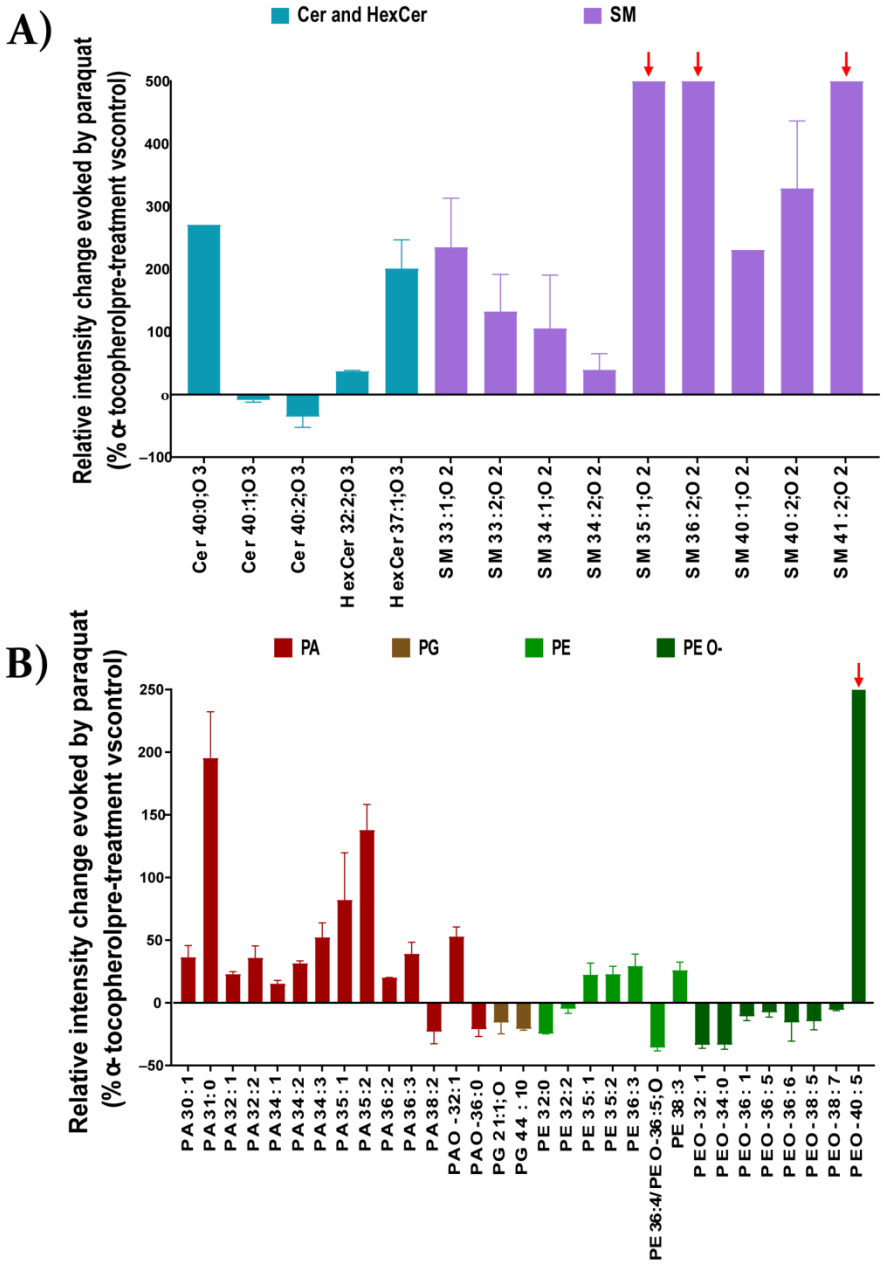

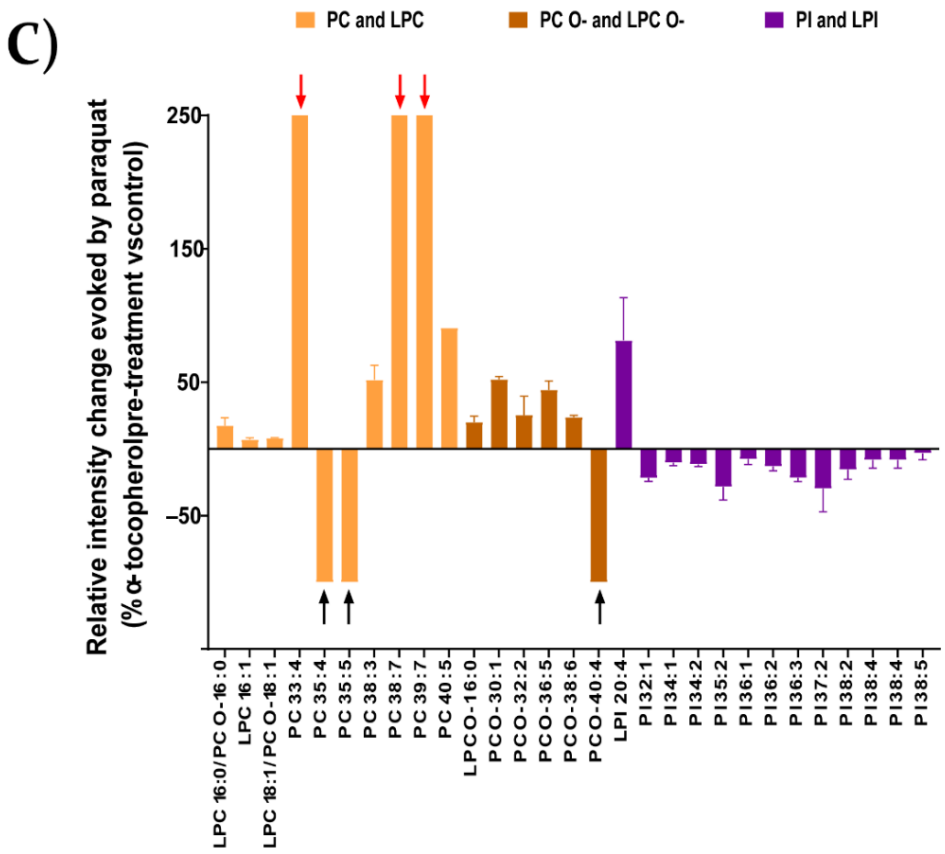

Figure 23: Relative intensity change in lipids when comparing paraquat-treated membranes preceded by an α-tocopherol pre-treatment with samples treated with paraquat only. Data are shown as percentage of control values. A) Change in sphingolipids (Cer, HexCer and SM). B, C) Changes in GPs. PA, PG, PE, and PE O shown in B). PC, PC O-, LPC, LPC O-, PI, and LPI shown in C). Ether forms indicated by the O-suffix. Oxygen number inside lipid head and fatty acids in Ceramides and Sphingomyelins is indicated by O with a suffix.

In contrast, saturated PAs generally increased; the lower number of double bonds, the higher change rate, in the case of PA with less than 32 carbons. Nevertheless, higher change rates were achieved with higher amount of unsaturation in the other PAs, with a general increase in all molecules except PA 38:2 (Figure 23B).

Furthermore, PG adducts generally decrease in α-tocopherol pre-treated samples, except PG O-40:7 whose only present in control situation. Two similar lipidic species were also found with opposite behavior upon α-tocopherol pre-treatment such is the case of ether PE generally decreased while normal forms displayed a mild increase (Figure 23B). The exception is PE O-40:5, an ether PE only present when paraquat treatment was preceded by α-tocopherol (Figure 23B, red arrows). Furthermore, due to the α-tocopherol pre-treatment, some very long-chain phosphocholines (PC 35:4, PC 35:5) disappeared from the astrocytic membranes (Figure 23C, black arrows). Ether phosphocholines generally showed a slight increase, with the exception of PC O-40:5, which was only present upon

α-tocopherol pre-treatment. LPC 16:1 and 18:0, which contains palmitoleic and stearic acid, were slightly increased (Figure 23C). Finally, the PI species showed a general mild decrease, whereas LPI 20:4, which contents arachidonic acid (AA, seemed to increase (81.3% ± 41.41) (Figure 23C). The complete data set of this section is listed in situation APPENDIX I, Table 6 and Table 7.

To summarize this chapter, clear differences triggered by paraquat in the lipid fingerprint were detected in our system in ceramides, SMs, glycolipids, and unsaturated phospholipids. In contrast, unsaturated ceramides and phospholipids were reduced when the cells were treated with α-tocopherol before the paraquat stress (Figure 24).

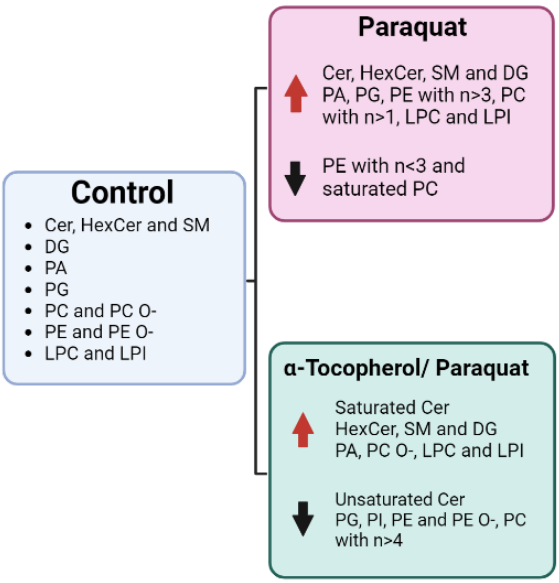

Figure 24: Graphic summary of lipid changes observed in CMMAs upon oxidative stress preceded or not by antioxidant treatment.

CHAPTER 2. DEVELOPMENT OF A METHOD TO PRINT MEMBRANES SEGREGATED IN LIPID RAFT AND NON-RAFT DOMAINS (RMMAs)

2 Development of RMMAs suitable for MALDI-MS analysis

As described in the Introduction section, lipid rafts have been described as membrane sub-domains with an enrichment in cholesterol and sphingolipids. However, as the lipid composition is a key feature for the correct function of signaling in lipid rafts, the lipid fingerprint may be different from the other parts of the membrane (here described as "non-raft membranes". An *in vitro* paradigm was used in which the astrocytic cell line 1321N1 was exposed to serum starvation and paraquat as metabolic and oxidative stress conditions respectively. These conditions were used since they can trigger changes in membrane lipid composition, in or out of the lipid raft domains. The challenge is to be able to detect these changes in printed subdomains.

MALDI-MS technology was used to determine the differences between the immobilized raft and non-raft membranes obtained from the human astrocytic cell line in control and under metabolic and oxidative stress conditions. We also used a human neuronal cell line to check whether our RMMA system is able to determine de expected differences in their lipid fingerprint due to cell-type differences. Samples were immobilized onto preactivated glass and then covered with MBT and DAN matrixes, as explained in material and method section. Samples were analyzed using MALDI-MS in positive and negative-ion modes. This mass spectrometry technology allowed the identification of 153 lipid adducts in a mass range between 500m/z and 1400 m/z in MS^+ and 388 lipid adducts in a mass range between 550 m/z and 1400 m/z in MS^-. Datasets obtained from both ionization modes were concatenated, spectrum by spectrum, to obtain the complete lipid fingerprint of every sample. Some lipids could be detected both in MS^+, MS^- ionization modes, in those cases, only the data from negative-ionization mode were maintained, in order to prevent peak duplicity, except in SM case in which only positive-ionization mode is maintained. Consequently, a unique data set of 536 different lipidic-adducts were kept for further analysis, as well as the separate MS^+ and MS^- datasets of 251 and 177 lipids respectively. To detect possible outliers among the spectra, for each ionization mode, two-tailed Pearson correlation test was performed, with a confidence interval of 95% and α set as 0.05 (Figure 25). For outlier consideration, values lower than 0.7 of the R-value in Pearson correlation

between replicates were considered outliers and discarded for statistical analysis. For negative ion-mode one of the replicates of non-raft domain from serum-starved astrocytes and one replicate of raft domain from control situation neurons were detected as outlier values (APPENDIX I; Table 8). Regarding the positive ion-mode, non-raft domain from paraquat treated astrocytes spectrum was considered as an outlier value (APPENDIX I, Table 9).

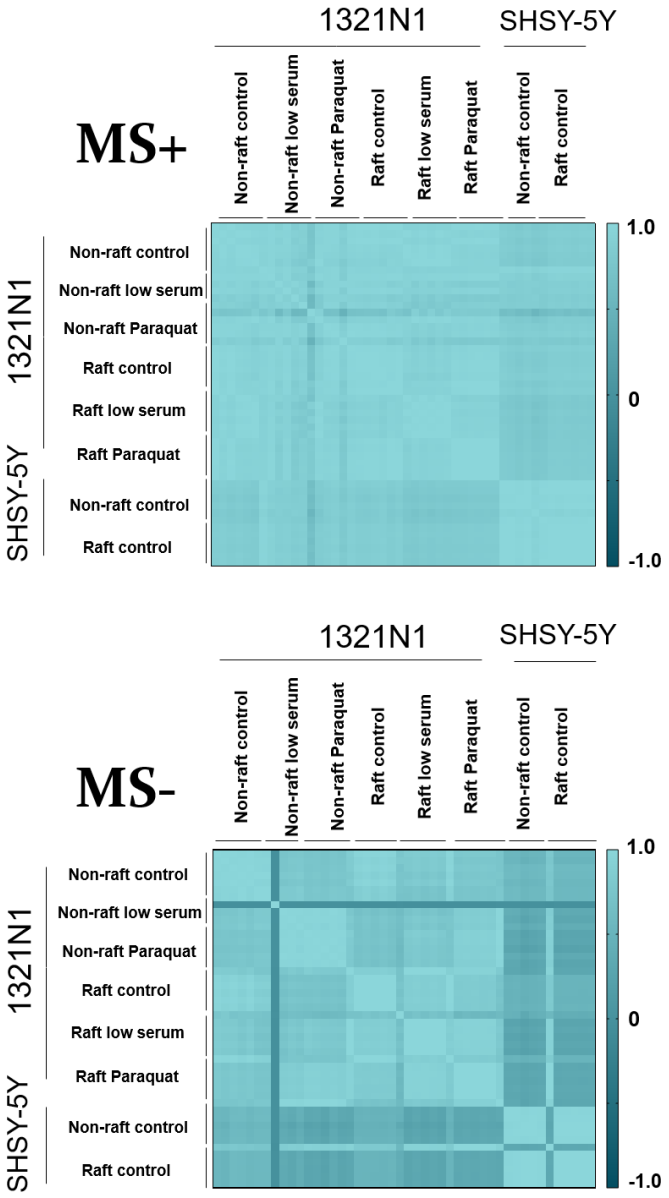

Figure 25: Reproducibility of RMMA printing technique analyzed by Pearson correlation. A) Negative ion-mode spectra Pearson correlation. B) Positive ion-mode spectra Pearson correlation. For both analysis, confidence interval was 95% and α was set at 0.05. Correlation of each spectrum is expressed as R-value in Pearson correlation; values are between -1 and 1. Correlation was performed using the whole spectra of Non-raft and raft samples obtained from human neuron cell line (control situation), and human astrocyte cell line (control situation, low serum-starvation and paraquat exposure).

In addition, to check the reproducibility of lipid raft printing technique, Pearson correlation matrix was calculated comparing the spectra each printed raft sample's replicates from two different RMMAs. For negative ion-mode, the correlation between non-raft obtained from astrocytes in control situation and with low serum-starvation and paraquat treatments reach 99%, 96%, and 99% respectively; raft domains from cells in the same conditions reach 95%, 98%, and 99% respectively; non-raft and raft domains from neurons in control situation reach 93% and 100% (APPENDIX II, Table 10). For positive ion-mode, correlation between non-raft astrocytes in control situation and with low serum and paraquat treatments reach 97%, 96%, and 79% respectively; raft domains in the same conditions reach 99%, 99%, and 99% respectively; non-raft and raft domains from neurons in control situation reach 99%, and 100% (APPENDIX II, Table 10). Thus, with the experimental conditions detailed in the material and methods section, we ensure a minimum reproducibility of 93% and 79% between the replicates from different arrays in negative and positive ion modes respectively. Considering the whole spectra, we performed a Pearson correlation-based hierarchical clustering of the variables, segmenting them into eight groups (Figure 26).

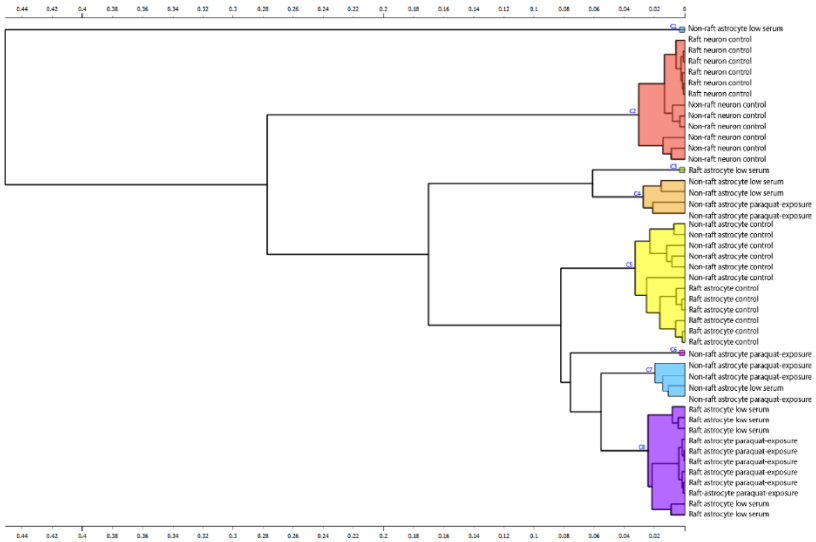

Figure 26: Pearson correlation-based hierarchical cluster of lipidomic fingerprint of all samples in both ionization modes.

To further characterize the differences in the lipid profile between printed raft and non-raft membranes in neuronal human cell line, Principal Component Analysis (PCA) was performed. PCA analysis was carried out over each ionization modes separately, plus with the whole data set in order to detect possible alterations. Clear grouping depending on the domain was observed in whole spectra analysis (Figure 27, Figure 29, Figure 31, Figure 33), as well as in the spectra from both ionization modes independently for every condition

and cell type (APPENDIX II, Figure 50-59). Comparisons between raft and non-raft domain lipidome were performed on one hand, in control situations from neurons and astrocytes, and on the other hand, in astrocytes exposed to low serum starvation in absence or presence of paraquat. For each comparison, all variables were assumed as non-parametric, as the number of data was small, and a Mann-Whitney test was performed with α set as 0.05

In the next sections we have analyzed more in detail each condition and cell population.

2.1 Lipidomic analysis of printed raft and non-raft membranes from neurons

To evaluate the differences between printed raft and non-raft first we performed a PCA analysis to elucidate whether the printed raft and non-raft samples can be classified using their lipid fingerprint.

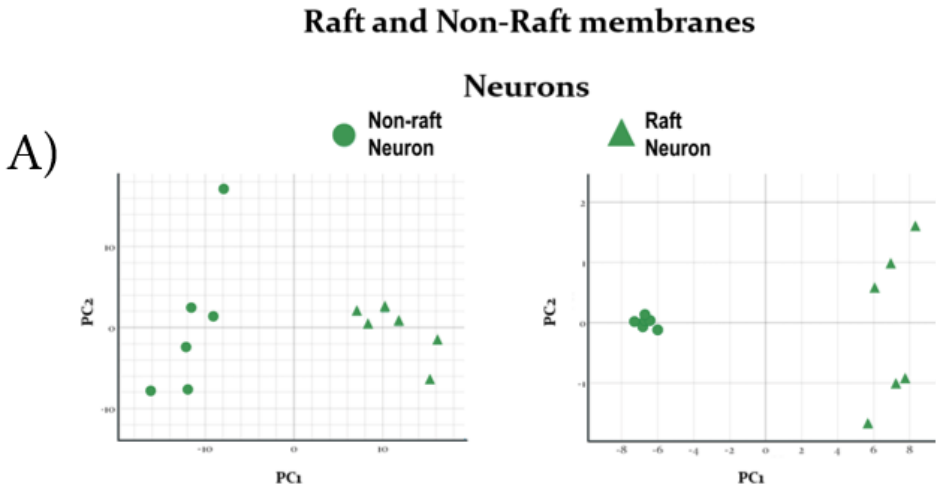

Figure 27: Principal component analysis (PCA) of raft and non-raft domains in human neuronal cell line SH-SY5Y. A) Principal component analysis using the whole lipid spectra. B) Principal component analysis using 50 best-ranked lipids obtained in the one-way ANOVA with α 0.05.

As shown in Figure 27 with the PCA we can distinguish both domains. To validate the classification potential of human neurons lipid fingerprints performed in RMMAs, different algorithms were trained and tested by 10-cross fold validation (Table 14). First, PCA analysis was performed to reduce the variables used for algorithm training by using two datasets: whole lipid content and 50-best ranked variables reduced data set using differences in variance obtained using test ANOVA. With first dataset, 8 Principal Components were obtained, while with second dataset, only 2 were enough to ensure an explained variability of more than 90%. With Principal components of the whole lipid

fingerprint k-NN algorithm achieved best classification of raft and non-raft domains. Nevertheless, with reduced data set's Principal Components perfect classification was obtained with k-NN and Random Forest algorithms. Thus, reduced 50-best ranked lipids can explained the differences between both domains in this printed samples.

In the human neuronal cell line (SH-SY5Y), differences in MS^+ were found between raft and non-raft domains with 94 tentatively assigned lipid species. 28 are GLs, 25 SLs and 41 GPs; in MS^- differences in 10 SLs and 56 GPs were observed. Differences were plotted as the mean rank differences between both groups compared (raft and non-raft domains) and the $-\log_{10}(p\text{-value})$ obtained by Wilcoxon test (Figure 28). In regard to the differences in the tentatively assigned lipids, higher presence of SMs was detected in raft domains, as well as in HexCer and Hex2Cer species. In this case, one Hex2Cer presented significant differences between non-raft and raft domains, Hex2Cer 29:0;O2. In this analysis, differences were generally found in lipid species with less unsaturation.

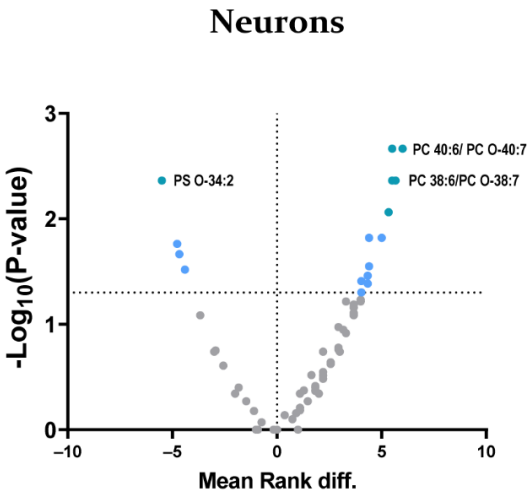

Figure 28: Volcano plot of the differences between raft and non-raft samples from the human neuronal cell line obtained by Wilcoxon-Rank test with α set as 0.05. Statistically significant differences are colored in blue and appear over the dot line.

In regard to GPs, a general increase was observed in tentatively assigned PC, PC O-, LPC and LPC O- in raft domains compared with non-raft membranes. Firstly, the specific mass range of LPC between 28 carbons and 34 carbons coincides with PC range, and LPC 16:0/LPC O-16:1 and LPC O-28:3 were tentatively assigned. A general increase in PSs, PA and PE were observed in raft domains, while a decrease was detected in PA ethers. LPEs with very long odd-numbered chain fatty acid were present in raft domains with a higher relative abundance. LPEs detected were tentatively assigned as LPE O-29:2, O-30:2, O-31:2 and O-31:3. Although, their assignation must be ensured, they did not display a relevant tendency to change between membrane subdomains.

2.2 Lipidomic analysis of raft and non-raft membranes from astrocytes immobilized in microarrays

In the case of the printed raft and non-raft domains from human astrocytic cell line samples we can distinguish both raft and non-raft domains in control situation with the PCA (Figure 29).

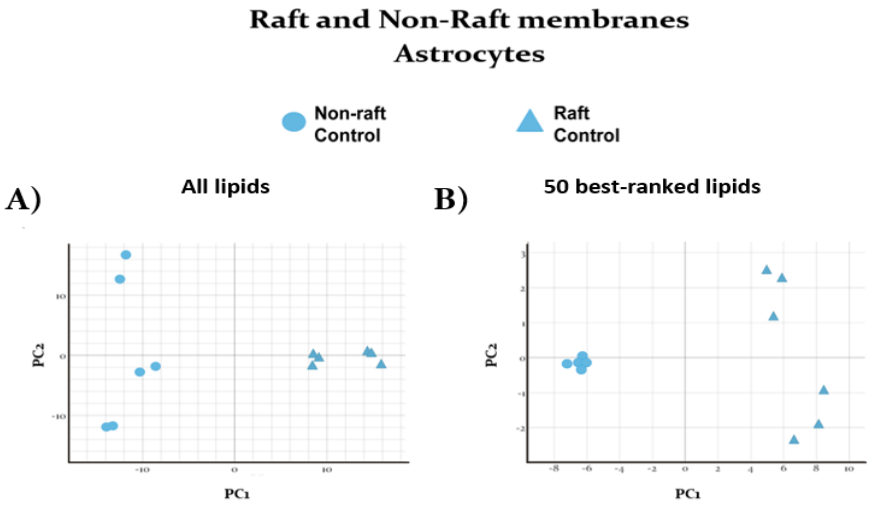

Figure 29: Principal component analysis (PCA) of raft and non-raft domains in human astrocytic cell line 1321N1. A) Principal component analysis using the whole lipid spectra. B) Principal component analysis using 50 best-ranked lipids obtained in the one-way ANOVA with α 0.05.

These differences between lipid composition can lead to a distinguishable lipid fingerprint. To evaluate the classification power of lipid fingerprint obtained from RMMAs several supervised models were trained and tested by 10-fold cross validation. Models were trained using the most explanatory principal components (until reach 90% of variance explained) before and after a variable selection of 50-best ranked lipid species by One-way ANOVA analysis (Table 11). For the complete data set, 9 principal components were used for sample classification, while for reduced dataset 2 principal components were enough for variability explanation. K-nearest neighbor algorithm reached best classification scores in both cases.

In relation to astrocyte's control condition, 60 tentatively assigned lipid adducts presented statistically significant differences, in particular in 21 SLs, 9 GLs, and 15 GPs in MS^+ mode while comparing raft and non-raft domains, whereas in MS^- only differences between 15 SLs were observed. Volcano plot and Wilcoxon test was performed as described above (Figure 30). However, distinguishable fingerprint of both domains was obtained in every condition while analysis positive and negative ion-modes individually or together, with a high capacity of classification using k-NN algorithm.

In general, tentatively assigned SLs showed a relative increase in raft microdomains, as expected, both SMs and HexCer. No significant differences were detected in Hex2Cer. Surprisingly, odd-numbered long-chain lipids seemed to be increased in raft microdomains, as well as lipid species with more than 3 unsaturations. Different GPs displayed differences between both domains, with a general increase in PCs and its ether version (PC and PC O-). Regarding the tentatively assigned lyso-phosphocholines (LPC), LPC 18:1, LPC O-27:3 and LPC O-34:3 were increased in raft domains.

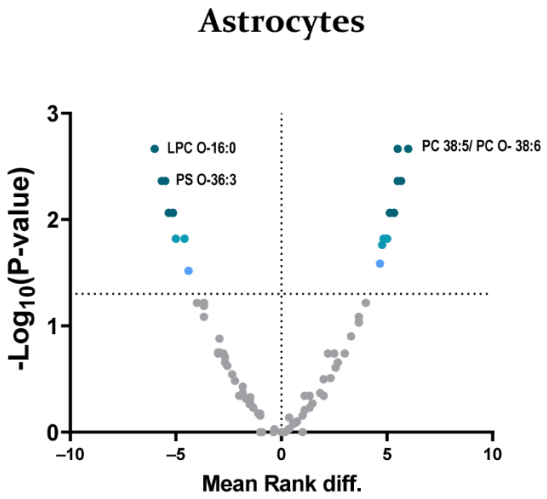

Figure 30: Volcano plot of the differences between raft and non-raft samples from human astrocytoma cell line obtained by Wilcoxon-Rank test with α set as 0.05. Statistically significant differences are colored in blue and appear over the dot line.

Moreover, diacylglycerol (DG) 29:2; O2 decreased in raft domains, as well as other GLs. In contrast, DG O-49:5, DG O-51:5, and TG O-44:8 were increased in raft. No differences were observed in saturated lipid species except in triacylclygerol (TG) 45:0; O3.

Sulfatides (SHexCer) presented a significant increase in control cells' raft domains, as well as the different ceramides. Glycerophosphoserines (PSs) and glycerophosphoinositols (PIs) did now show a general tendency whereas glycerophosphoserine ethers (PSs O-) decreased in raft domains. Glycerophosphoethanolamines (PEs) and glycerophosphates (PAs) displayed a general increase in raft domains. Various lyso-phosphoethanolamines (LPEs) presented differences between both domains, their ether versions from 28 to 33 carbons were found increased in raft domains. Other LGPs, such as LPI 20:3 and LPI 20:4, were increased in raft domains as well as LPG O-28:0 (Figure 30).

2.3 Lipid profile differences from low serum-starved astrocytes using RMMAs

Regarding low serum-starved astrocytes, in printed RMMAs we were able to distinguish both domains (raft and non-raft) using the principal component analysis (PCA) (Figure 31). These differences between lipid composition can lead to a distinguishable lipid fingerprint. To evaluate the classification potential of lipid composition, different algorithms have been trained and tested by 10-fold cross validation, using more explanatory principal components (explained >90% of variance) obtained in the whole lipid dataset and in the reduced dataset of 50 best-ranked lipid species obtained in ANOVA test (Table 12). In whole lipid content data set, 8 principal components were used for algorithm training; whereas in reduced data set only 2 principal components were enough. Among the different algorithm used, K-nearest neighbor algorithm reached best classification scores in both datasets.

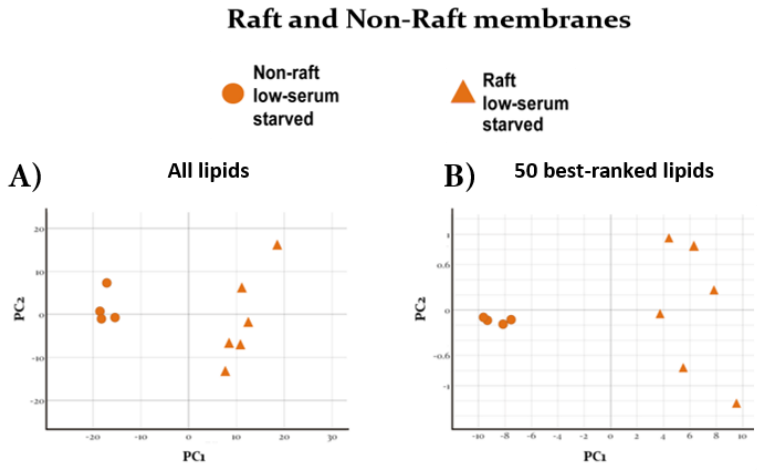

Figure 31: Principal component analysis (PCA) of raft and non-raft domains in human astrocytic cell line 1321N1 in low-serum starvation. A) Principal component analysis using the whole lipid spectra. B) Principal component analysis using 50 best-ranked lipids obtained in the one-way ANOVA with α 0.05.

In particular, in this case 223 tentatively assigned lipid species presented differences, in particular, statistically significant differences were found in 4 SLs, 9 GLs and 20 different GPs in MS^+, also in MS^- differences in 25 SLs and 169 GPs (Figure 32).

In raft printed domains, a general increase of SLs, both HexCer and SM, was observed but not of Hex2Cer. A variety of GPs reach differences between both domains, more in detail, long-chain were increased in raft domains, as well as species with more than 3 unsaturations. In relation to GPs, PCs and LPCs were increased in raft domains, as well as PE, PG and PE ethers, whereas various PI present a decrease. PAs reached a general decrease in non-raft domains. Nevertheless, LPE and LPG lipidic species, can be also

assigned as PA, which is more probable, considering the number of carbons. Finally, Lyso-phosphatidylinositol with arachidonic acid (LPI 20:4) was increased in low serum raft samples, as was observed in control samples.

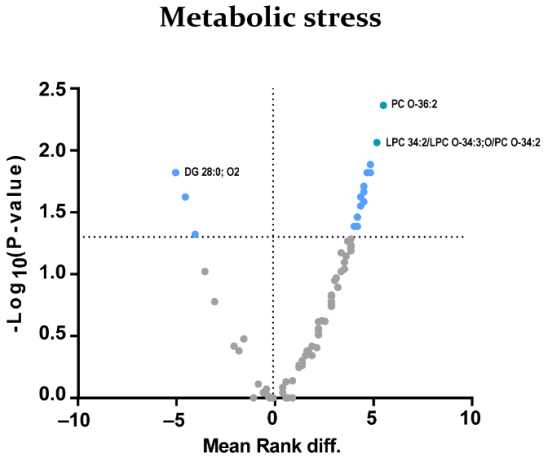

Figure 32: Volcano plot of the differences between raft and non-raft samples from the human astrocytic cell line exposed to low serum starvation obtained by Wilcoxon-Rank test with α set as 0.05. Statistically significant differences are colored in blue and appear over the dot line.

2.4 Lipid profile differences from paraquat-stressed astrocytes using RMMAs

Finally, regarding, the paraquat treatment, we were able to distinguish the raft and non-raft domains in case of paraquat-exposure by their lipid fingerprint with the Principal component analysis (Figure 33).

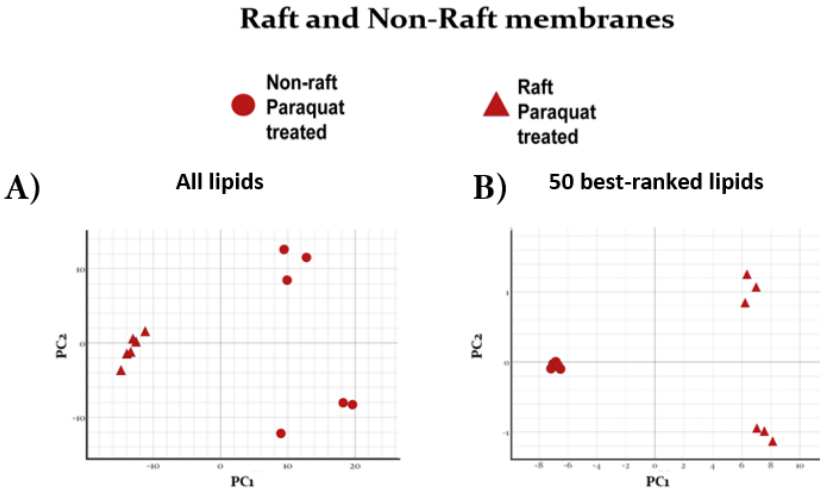

Figure 33: Principal component analysis (PCA) of raft and non-raft domains in human astrocytic cell line 1321N1 in paraquat exposure condition. A) Principal component analysis using the whole lipid spectra. B) Principal component analysis using 50 best-ranked lipids obtained in the one-way ANOVA with α 0.05.

To evaluate the classification potential of lipid fingerprint in an oxidative stress situation, different classification algorithms have been trained (Table 13) and tested by 10-fold cross validation. As before, two datasets were used: whole lipid dataset and 50-best ranked lipid species reduced data set to obtain the principal components that were used in algorithm training. In whole dataset, as in metabolic stress raft and Non-raft classification 8 Principal Components were obtained in whole dataset and 2 Principal Components in reduced dataset. However, in this case, reduced dataset achieved better classification by algorithm trained than whole data set.

In particular inside the tentatively assigned lipids that were found, statistically significant differences were found in with 9 SLs, 19 GLs and 33 GPs in MS^+. As previously observed, SLs present higher relative abundance in raft domains, both in SM, Cer and HexCer. No differences were observed in Hex2Cer (Figure 34).

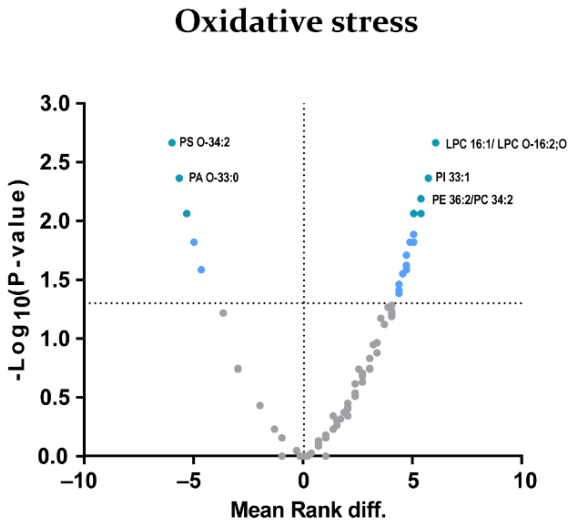

Figure 34: Volcano plot of the differences between raft and non-raft samples from the human astrocytic cell line exposed to paraquat treatment obtained by Wilcoxon-Rank test with α set as 0.05. Statistically significant differences are colored in blue and appear over the dot line.

Different GLs, such as PC and PC O- presented higher relative abundance in raft domains. LPC and LPC O- were also more abundant in raft domains, in particular, LPC O-16:0, 16:1 and 18:1. As well as in low serum starved cells, mass range of PC/LPC might have different lipid assignation, as lipid chains are from 29 carbons. However, differences in LPCs with short chain can correspond to 14:0, 16:1 and 18:0 or to LPC O-14:1, LPC O-16:2 and LPC O-18:1.

Other GPs, such as PG, PE and PA and its ether versions presented higher relative abundance in raft domains, whereas in PI some of them presented higher relative

abundance in non-raft domains. Majority of differences were present in even-numbered long-chain phospholipids, and lipid species with even number of saturations.

LPE from 28 to 31 carbons were detected with higher relative abundance in raft domains, also, LPI 20:4 showed as well higher presence in raft domains, as in other conditions. In case of PG and PE the presence of these long chain lipid adducts with more than 2 unsaturations was increased in raft domains whereas PE 36:1 and PE 36:2 (PE detected with less carbons) decreased. In contrast to low serum and control situation, only DGs with more than 37 carbons were increased in raft domains, moreover only one TG was increased in raft domains.

In the case of SHexCers, in low serum starvation differences in several sulfatides were observed, specifically, in species with more than 2 unsaturations and chains from 32 to 46 carbons. By contrast, in paraquat treated samples, differences were also identified in tentatively assigned saturated sulfatides and chains from 35 to 42 carbons. Sulfatides increases in paraquat-exposed raft domains as in control situation but did not display any significant differences in metabolic stress. Ether version of DG presented more differences in paraquat treatment comparing with low serum starved cells and control cells, mainly in longer-chain species.

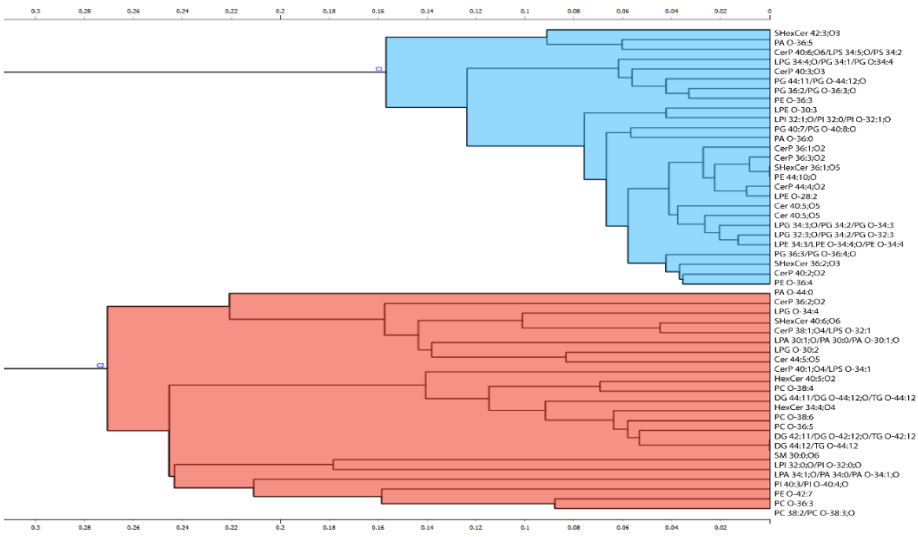

Figure 35: Pearson correlation-based hierarchical cluster of lipidomic fingerprint separating in both non-raft and raft domains of all samples in both ionization modes. Lipid profiles differences between brain cell populations: neurons *versus* astrocytes.

Finally, we evaluate the lipid species that can explain the differences between raft and non-raft domains in printed human astrocytic cell line samples in every case (control situation, low serum-starvation, and paraquat treatment). To evaluate that, we used a hierarchical cluster based on the Pearson correlation, in that case we can distinguish two main groups

with different lipid species (Figure 35). In this case, correlation was performed to obtain lipids with a differential distribution between raft and non-raft domains independently of cell type or condition.

2.5 Detection of lipid fingerprint changes between different cell types in printed RMMAs

Differences in functionality and protein expression between diverse cells populations has been widely studied. Specific lipidomes have been observed in certain tissues and cellular populations, but the specific lipid fingerprint of the different membrane subdomains, such as raft microdomain, remains poorly understood. Lipidic composition in cellular membrane have an effect on cellular signaling, membrane fluidity and protein pathways reactions. To elucidate whether these lipidic changes between different cell populations involve raft lipidome, a Principal Component Analysis (PCA) has been performed with raft and non-raft printed samples from control astrocytic and neuronal cell lines (Figure 36).

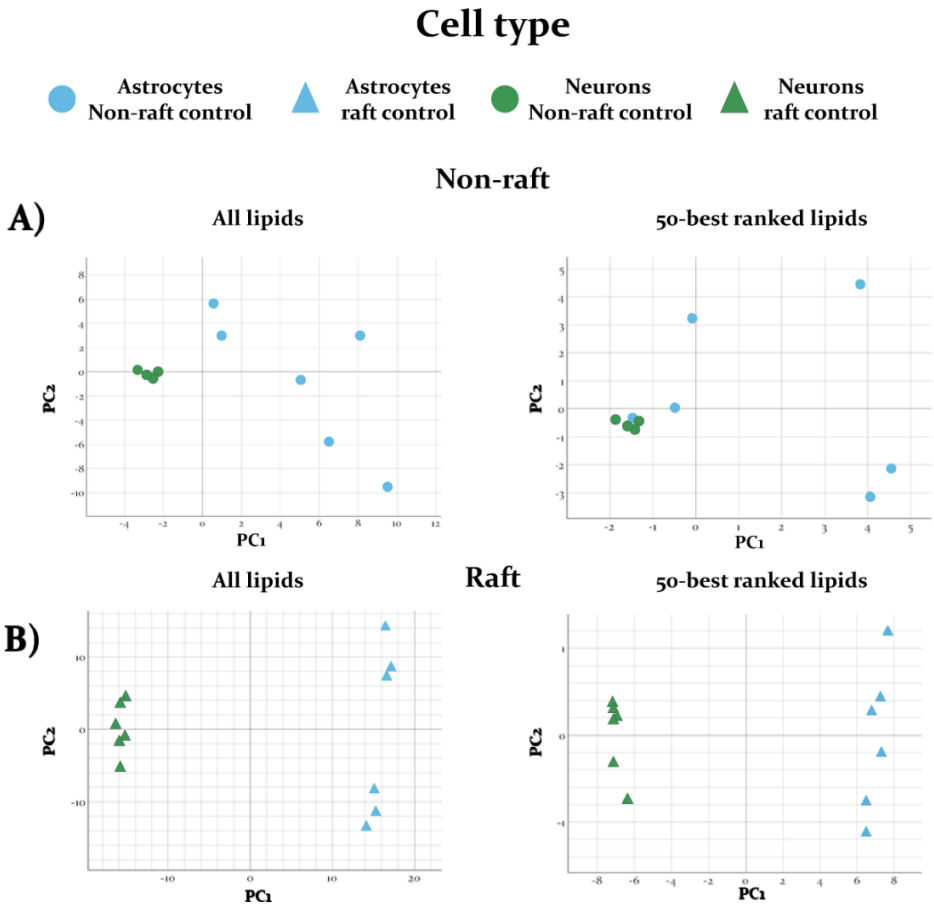

Figure 36: Principal Component Analysis (PCA) between human astrocytic and neuronal cell lines (1321N1 and SHSY-5Y) in raft and non-raft domains. A) PCA of non-raft domains from human astrocytic cell line and human neuronal cell line. B) PCA of raft domains from human astrocytic cell line and human neuronal cell line. In every case, the analysis was carried out using all lipid species or 50 best-ranked lipid species obtained from one-way ANOVA test, two-tailed, with α set as 0.05.

Clear differences have been observed between astrocytes and neuron cell membranes in both raft and non-raft domains. Analysis was carried out with all lipid species and with the 50 best-ranked lipid species obtained by one-way ANOVA two-tailed test, to find out whether there is a specific lipid group that can explain the majority of differences between each lipid profile. For each comparison, all variables were assumed as non-parametric, as the number of data is small, and a Mann-Whitney test was performed with α set as 0.05. Differences between both cell populations were observed, in non-raft domains; more in detail, differences between 58 glycerophospholipids and 2 sphingolipids were observed in MS^- whereas in MS^+ 13 GL, 11 SLs and 26 GPs reached statistically significant differences.

Diacylglycerol and triacylglycerol tentative assigned lipids did not show a clear assignation except for DG 29:2;O2, TG 37:0;O3 and TG O-41:10, first one was increased in neuron cells while the other ones presented a higher relative abundance in astrocytic cell line membranes. In the case of sphingolipids, sphingomyelins with less than 3 unsaturation were found increased in neurons, as well as odd-numbered chain HexCer species. Sulfatide SHexCer36:4;O2 were found increased in astrocytes in contrast to ShexCer 42:6;O4, increased in neurons.

PC and LPC showed a general increased tendency in astrocytic cell line. LPC 16:0/LPC O-16:1 was found increased in control non-raft astrocytes. Moreover, long-chain LPC were also found, more in detail, LPC O-26:3, O-28:3 and O-28:4. In relation to PE, ether PE presented a higher relative abundance in astrocytic non-raft domains in chains with less than 40 carbons, other ones have been observed increased in neuronal non-raft domains. In case of PE adducts with longer carbon chains, their mass range did not show a clear assignation, nevertheless, no general tendency was observed in them. Similar effect happened with PI, only PI 39:10;O, and PI O-32:2;O, and PI 38:4 were clearly assigned due to its mass range, first and second PI were found increased in astrocytes while last one was increased in neurons. Furthermore, lysophospholipids, LPE and LPI presented lower relative abundance in neuron samples, except LPI O-33:0.

Regarding the printed raft domains, differences in tentative assigned 36 glycerolipids, 35 sphingolipids and 71 glycerophospholipids were found in MS^+, whereas in MS^- differences were discovered in 29 sphingolipids and 182 glycerophospholipids. In MS^+, DGs did not show general tendency, whereas its ethers generally increased in astrocyte rafts, except DG O-41:11. In contrast, triacylglycerols were observed generally decrease in astrocytes. On the other hand, sphingomyelins had higher relative abundance in neurons in case of odd-numbered carbon chains with more than 1 unsaturations. Cer compounds also were

detected with higher relative abundance in astrocytes, as well as HexCer species, except Hex2Cer 29:0;O2, which was higher in neuron rafts. Sulfatides did not show general tendency.

Nevertheless, PA and PS ethers, presented a lower relative abundance in neurons, as well as ether PE with less than 38 carbons. PIs were found increased in astrocytes in lipids with more than 38 carbons generally, similar effect occurred with PE adducts which were increased in astrocytic rafts in chains with more than 37 carbons. PCs were general decreased in neurons, as well as its ethers. Lastly, lysophosphocholines were increased in neurons. Moreover, ether LPC were also found increased in neurons, LPC O-16:0, LPC O-16:2, LPC O-26:3, LPC O-27:3, LPC O-28:3, LPC O-28:4 and LPC O-34:3. In contrast, ether LPE were found increased in astrocytic rafts. These differences can lead onto a distinguishable lipid fingerprint. For this purpose, different classification algorithms were trained with whole lipid content and with 50 best-ranked lipid species to elucidate whether different brain cell populations can be identified by their lipidomes (Table 19, Figure 37).

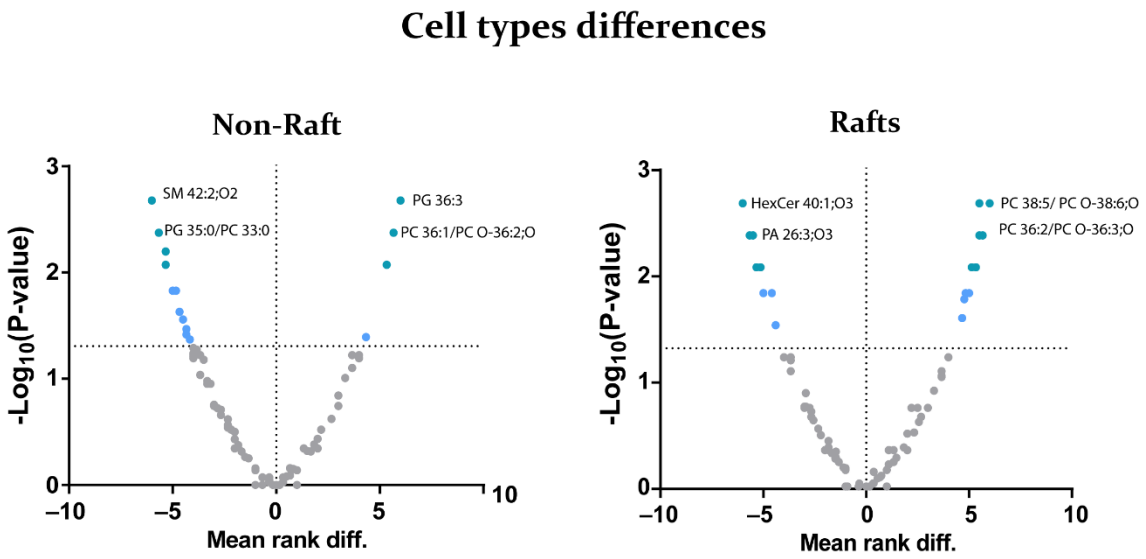

Figure 37: Volcano plot of the differences between the neuronal and astrocytic human cell lines in non-raft (left) and raft (right) obtained by Wilcoxon-Rank test with α set as 0.05. Statistically significant differences are colored in blue and appear over the dot line.

2.6 Lipid fingerprint changes triggered by low serum starvation in printed membrane subdomains from astrocytes

Metabolic stress might involve lipid homeostasis deregulation or lipid oxidation. To elucidate the possible changes in lipid raft and non-raft membranes in these pathological conditions, a principal component analysis (PCA) was performed in both ionization modes separately, along with the whole data set.

A clear grouping depending on the treatment was observed in whole spectra analysis, except in non-raft samples in an oxidative stress situation and metabolic stress non-raft samples (Figure 38). Analysis was carried out using all lipid adducts and with the 50 best-ranked lipid adducts according to one-way ANOVA two-tailed test, to clarify if there is a specific lipid group that can explain the majority of differences between each lipid profile. Comparisons between raft and non-raft domain lipidome were performed in low serum starvation (metabolic stress). For each comparison, all variables were assumed as non-parametric, as the number of data is small, and a Mann-Whitney test was performed with α set as 0.05.

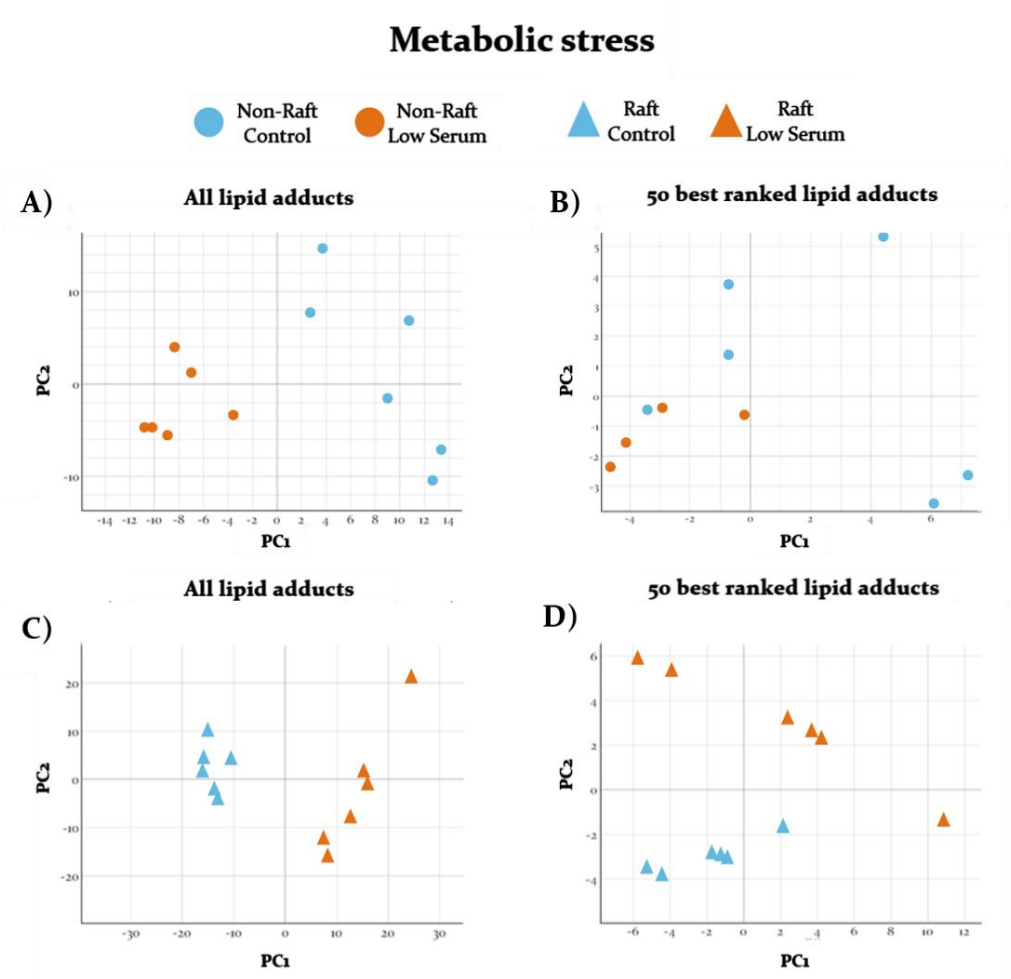

Figure 38: Principal component analysis of whole lipid spectra in raft and non-raft domains from the human astrocytic cell line subject to metabolic stress. PCA of control and low-serum starvation conditions of A) non-raft samples with whole lipid spectra and B) non-raft samples with the 50 best-ranked lipids obtained from one-way ANOVA test, two-tailed, with α set as 0.05. C) raft samples with whole lipid spectra and D) raft samples with 50 best-ranked lipids obtained from one-way ANOVA test, two-tailed, with α set as 0.05.

Between non-raft domains in low serum starvation or control situation general enrichment in control non-raft domain was observed in tentatively assigned GLs (DG and TG), PC and SM. More in detail, DG 28:0;O2 presented a higher presence in low serum starved cells whereas other DG were increased in control situation. Also, possible sulfatide SHexCer35:0;O6 has been found increased in control non-raft domains. In regard to PC and LPC, LPC O-26:3 and LPC O-28:4 were observed increased in control situation. In case of PS, PE and its ether versions were generally decreased in low serum starved non-raft domains, whereas PA and PI or its ethers have not showed any general tendency. Moreover, the only lipids that has been clearly assigned were LPE (LPE O-29:2 and LPE O-31:3), which were increased in control non-raft domains (Figure 38).

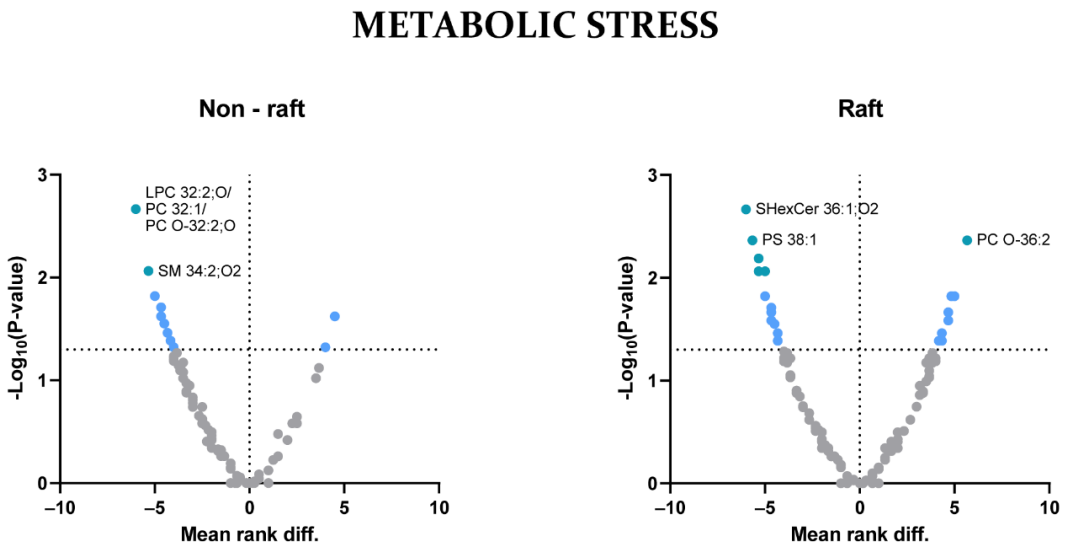

Figure 39: Volcano plot of the differences between the human astrocytic cell line samples exposed to low serum starvation (metabolic stress) and control situation in non-raft (left) and raft (right) domains. Analyzed was performed by Wilcoxon-Rank test with α set as 0.05. Statistically significant differences are colored in blue and appear over the dot line.

In addition, in raft domains, more differences between low serum starvation and control situation were found. Differences between both samples in tentatively assigned lipids were found in: 14 GLs, 31 SLs, and 36 GPs in MS^+ were observe, while differences in 190 GPs and 23 SLs were observed in MS^-. In SLs, HexCer adducts from 28 to 42 carbons were increased in control situation, as well as SM from 29 to 44 carbons with less than 3 unsaturations, the unique possible sulfatide that has differences between control and low serum starvation was found increased in control situation. Ceramides from 40 to 49 carbons were found increased in low serum starvation raft domains, whilst sulfatides does not have a general tendency. In GPs specific mass range, PCs from more than 36 carbons could correspond also to its ether versions. PC/PC O- with more than 3 unsaturations were

increased in control situation, where in low-serum starvation PC 36:2/PC O-36:3;O and PC 38:2 and PC O-38:3;O had higher relative abundance. LPC detected presented a higher relative abundance in raft domains from control cells. In the case of PAs, adducts from less than 43 carbons generally decrease, whereas its ether versions increased independent of the number of carbons. PE and PE O- have not showed a general tendency, whereas PG and PI generally increase in raft from low serum-starved cells. PSs has been observed in higher relative abundance in control domains in adducts with less than 39 carbons, while adducts with more carbons were found increased in low serum-starved cells' raft domains. PS O-40:7;O increased in control domains whereas PS O-42:10 decreased.

Furthermore, differences observed between control and treated situations in both metabolic and oxidative stress situations can lead onto a sample classification due to its lipid fingerprint. To elucidate this, different classification algorithms were trained in both raft and non-raft domains separately (Table 15 and Table 16) with respect to metabolic stress. Non-raft low serum-starved and control samples lipid fingerprint reached better classifications with the 50 best-ranked lipids obtained by ANOVA test (as described above) in case of kNN, Random Forest and Neural network model. Naïve Bayes classification algorithm showed better classification and precision with the whole lipidic content (Table 15). In raft domains, better classification where achieved, as these domains showed a higher number of differences in their membrane lipids. Nevertheless, with the 50 best-ranked lipids limit, the sample classification was perfect in all algorithms, whereas in the whole lipid content, best classification algorithm was k-Nearest Neighbor

2.7 Detection of lipid fingerprint changes triggered by paraquat in printed membrane subdomains from astrocytes

Oxidative stress might involve lipid homeostasis deregulation or lipid oxidation. To elucidate the possible changes in lipid raft and non-raft membranes in these pathological conditions, a principal component analysis (PCA) was performed in both ionization modes separately, along with the whole data set (Figure 40).

On the other hand, in respect of non-raft domains from oxidative stressed astrocytes, only two significant differences were achieved in MS^+ and 5 in MS^- (Figure 41). However, these differences between tentatively assigned lipids had an unclear assignation, one could be either LPC, PC or PC O-; as before, with a long chain, it is more probable to be classified as PC or PC O- 30:2. PG 46:11,O was also found increased in low serum starved non-raft domains, as well as other PE and PI, however, masses obtained did not have unique

tentative assignation. Moreover, differences were achieved in GLs DG or TG 43:12 or SM 29:0. In case of raft domains, differences in 5 GLs, 19 GPs and 18 SLs in MS^+ were found. Differences in DGs were found in those with more than 40 carbons and 10 unsaturations.

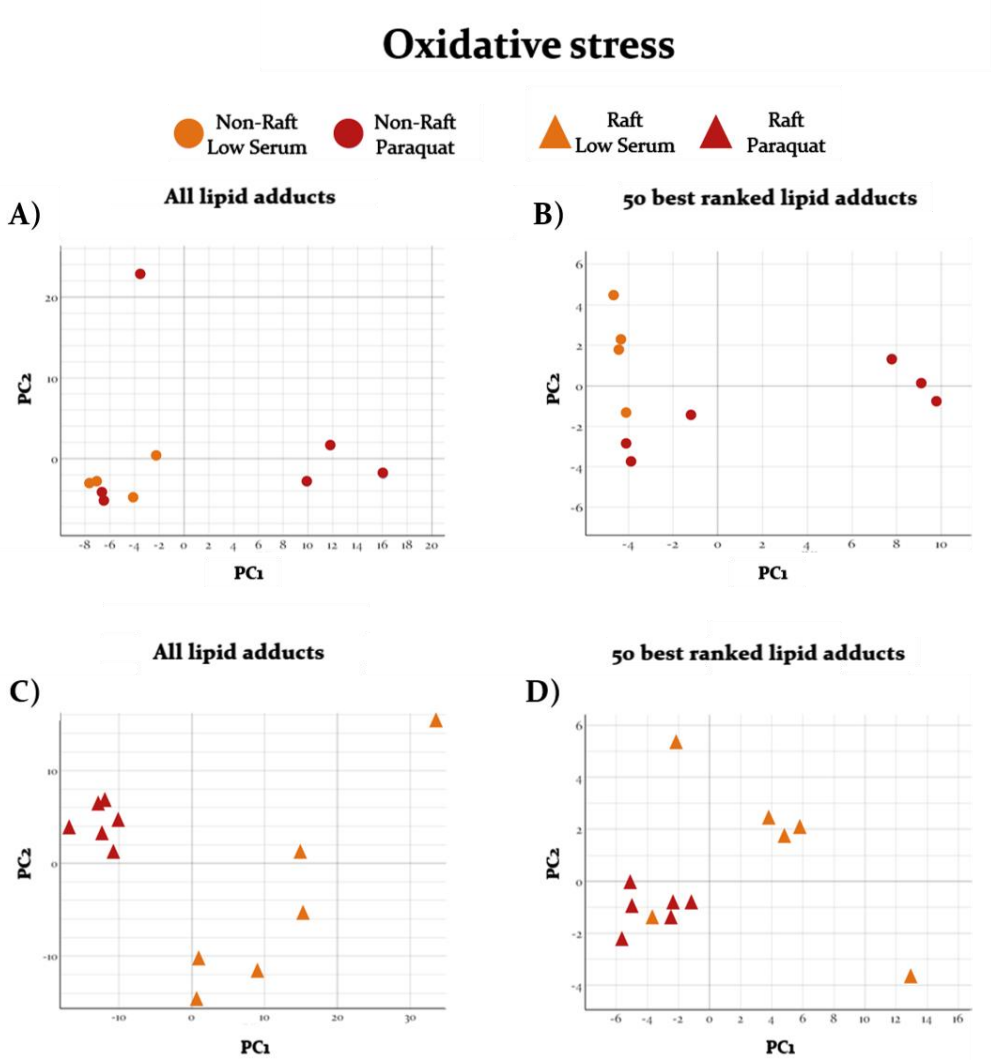

Figure 40: Principal component analysis of whole lipid spectra in raft and non-raft domains from the human astrocytic cell line subject to metabolic stress. PCA of control and low-serum starvation conditions of A) non-raft samples with whole lipid spectra and B) non-raft samples with the 50 best-ranked lipids obtained from one-way ANOVA test, two-tailed, with α set as 0.05. C) raft samples with whole lipid spectra and D) raft samples with 50 best-ranked lipids obtained from one-way ANOVA test, two-tailed, with α set as 0.05.

Also, two saturated TGs were observed increased in raft from paraquat-treated cells surprisingly. Nevertheless, SMs from 32 to 42 carbons were found increased in raft from paraquat-treated cells, whereas these lipidic-adducts presented a higher relative abundance in control situation compared to low serum starvation. HexCer with more than 30 carbons were found with more relative abundance in domains from paraquat treated

astrocytes. Ceramides were found increased in raft from low serum-starved cells, as well as sulfatides, except SHexCer 38:4;O5. Moreover, SHexCer 38:4;O2, same adduct with less oxygen molecules in it has found decreased in raft domains (Figure 41).

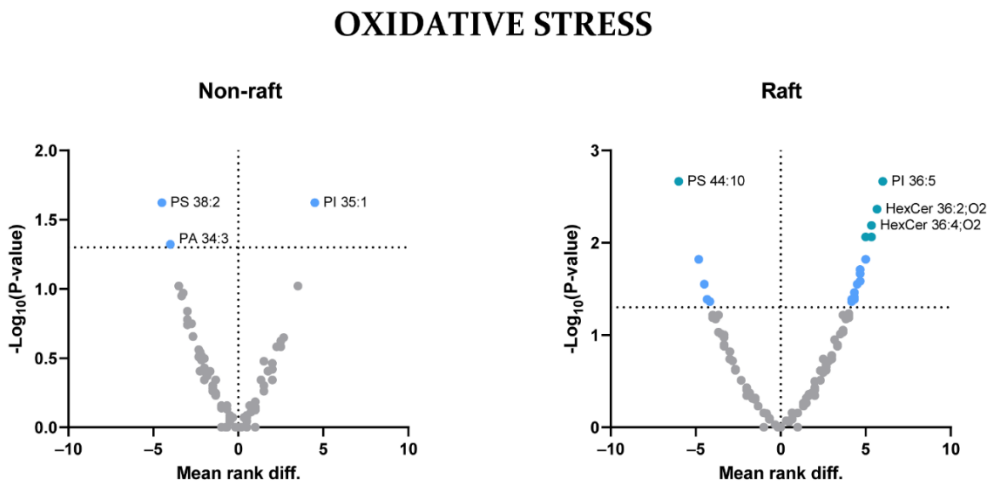

Figure 41: Volcano plot of the differences between the human astrocytic cell line samples exposed to paraquat in low-serum starvation media (oxidative stress) and low-serum starvation without paraquat (metabolic stress) in non-raft (left) and raft (right) domains. Analysis was performed by Wilcoxon-Rank test with α set as 0.05. Statistically significant differences are colored in blue and appear over the dot line.

In addition, LPC were found increased in paraquat-exposed raft domains in LPC O-16:0, LPC O-16:1, LPC O-18:1, LPC O- 26:3, LPC O-27:3, LPC O-28:3, and LPC O-28:4 in comparison with the low serum-starved cells. However, other PC had a lower relative abundance in that domains compared with low serum starvation raft domains, more in detail PC with at least 2 unsaturations, such as tentatively assigned PC 0-36;2 or PC O-34:3. PSs with less than 40 carbons were increased in paraquat-treated cells' raft domains, in contrast to PS with more carbons, which were decreased. Nevertheless, PSs ethers were increased in raft domains except PS O-40:7; O. Regarding PA adducts, the ones with more than 40 carbons were decreased in raft domains, as well as ether PAs, PGs, and ether PEs. On the other hand, PI adducts have been detected with odd and even-numbered chains, these adducts were generally increased in paraquat-treated cell's raft domains. In regard to LGPs, only ether LPE from 28 to 33 carbons have been detected increased in low-serum starved domains, other lipids detected might be classified as long chain LGPs or long chain GP, which is more probable. However, these not clearly assigned lipids generally were generally decreased in paraquat-treated domains, except 6 of them which are in mass range of PI/LPI or ultra-long PAs.

Finally, in regard to the oxidative stress same procedure was performed. The

algorithms trained were used in raft and non-raft domains separately. In non-raft domains, with whole lipid content classification precision was worse than in metabolic stress classification, being Naïve Bayes the algorithm with a better classification precision. However, with best-ranked lipids limitation, higher accuracy was achieved in all cases. raft domains differences in the context of oxidative stress were more clear, perfect classification were achieved with three algorithms (kNN, Neural Network and Naïve Bayes) in the case of best-ranked lipids limitation, whereas in the other case, it was only achieved in kNN model.

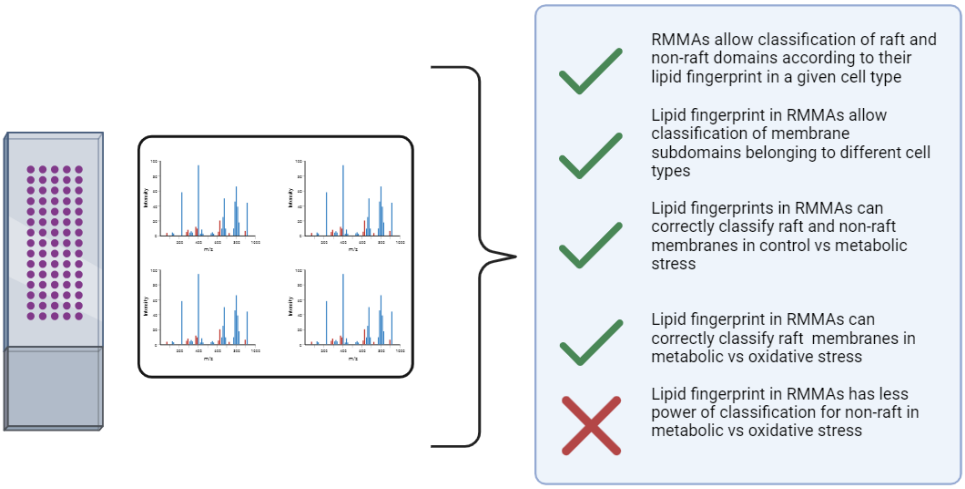

Figure 42: Summary of the potential of performing lipid fingerprint classifications in RMMAs.

CHAPTER 3. ENZYMATIC ACTIVITIES IN MICROARRAYS OF MEMBRANES SEGREGATED IN LIPID RAFT AND NON-RAFT DOMAINS

3 Enzymatic activity assays

The goal of these experiments was to test whether immobilized membrane subdomains retain a native conformation using a set of enzymatic activities as reference.

3.1 NADH – Oxidoreductase enzymatic activity assay in RMMAs

Lipid raft microdomains are known for containing a wide variety of integral and peripheral proteins that can be modified upon different stimuli. Moreover, it has been observed that different complexes of oxidative phosphorylation system may exist in raft (complex I, II, and III) (Kim et al., 2006) in different tissues including brain. To check this activity, a colorimetric assay was performed in presence of NADH, substrate for NADH-oxidoreductases. Three different experimental conditions were used: only with NADH substrate (control situation), or together with the electron carrier, dUQ or with the complex IV inhibitor, sodium azide (net activity of mETC).

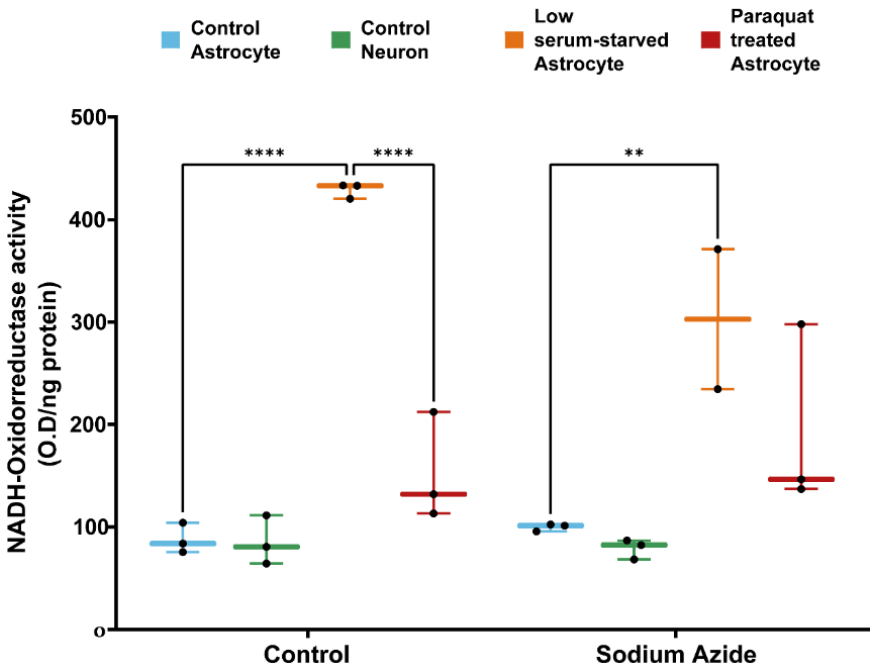

Figure 43: NADH dehydrogenase activity of neuron and astrocyte derived lipid rafts from cell cultures in control condition, and low serum-starved medium with or without paraquat treatment. Higher superoxide production was achieved with or without sodium azide in membranes from metabolically stressed cells (Low serum-starved astrocytes). Two-way ANOVA was performed with Tukey post-hoc α set as 0.05; $p<0.05$ (*), $p<0.01$ (**), $p<0.001$ (***), and $p<0.0001$ (****).

Raft immobilized domains showed higher activity signals within the RMMAs in presence of dUQ. However, no differences were observed with sodium azide complex IV-specific inhibitor, in all conditions (Figure 43). Nevertheless, differences were observed in reactive oxygen species production between low-serum starved astrocytic rafts and control situation-rafts, which in absence of sodium azide achieved 429 ± 7 and 88 ± 15 respectively; whereas in presence of that inhibitor 303 ± 96 and 100 ± 36 respectively. Furthermore, same tendency was observed in presence or absence of sodium azide in paraquat-treated astrocytic rafts and low serum-starved. Nevertheless, no differences were observed between astrocyte and neuron rafts neither in absence (85 ± 24) nor in presence of sodium azide (79 ± 10) (Figure 43).

3.2 Succinate dehydrogenase enzymatic activity assay in RMMAs

Succinate dehydrogenase (SDH) also known as mETC complex II, is a protein whose main action is to transform succinate to fumarate, with the subsequent translocation of electrons to the mitochondrial electron transport chain (Huang & Millar, 2013). As a part of the mETC, SDH is mainly located in the inner mitochondrial membrane. In order to study whether raft domains can contain complexes related to OXPHOS, SDH enzymatic activity was performed in RMMAs in the presence and absence of decylubiquinone, with or without the specific inhibitor of the mETC complex IV, sodium azide.

Enzymatic reactions were carried out as explained in the material and methods section, testing different final pH and phosphate buffer concentrations. However, no signal was achieved in any case, neither in raft nor non-raft domains, whereas in rat cortex (positive control) a normal level of signal was achieved (data not shown).

3.3 GAPDH enzymatic activity assay.

Glyceraldehyde-3-phosphate dehydrogenase (GAPDH) catalyzes the conversion of glyceraldehyde-3-phosphate (G3P) to 1,3-biphosphoglycerate (Bruns & Gerald, 1976; Sirover, 1999). This enzyme is involved in numerous cellular processes but, overall is a key enzyme in the glycolytic pathway. GAPDH not only has been reported in cytosolic fraction, but also in membranes, either in raft or non-raft domains (Kumar et al., 2012).

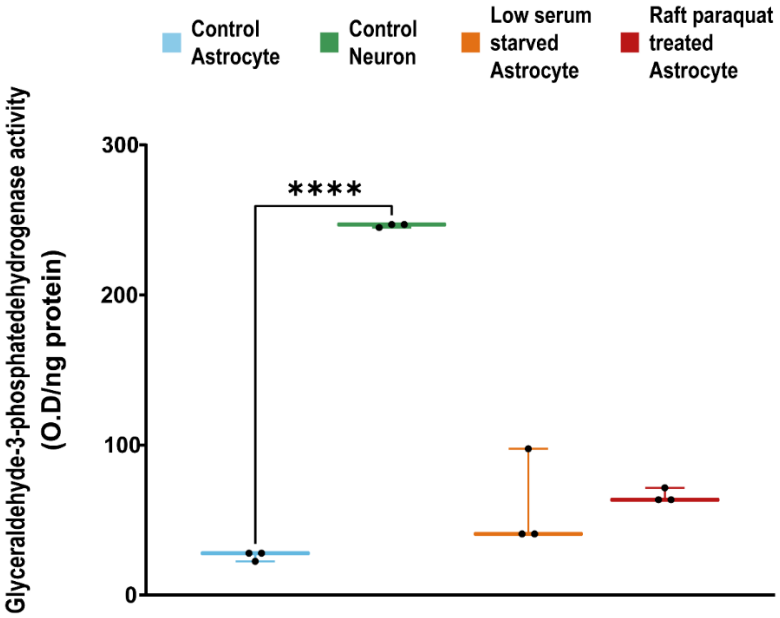

Figure 44: GAPDH activity of neuron and astrocyte derived lipid rafts from cell cultures in control condition, and low serum-starved medium with or without paraquat treatment. Higher superoxide production was achieved in raft from control neuronal cells. One-way ANOVA was performed with Tukey post-hoc α set as 0.05; p<0.05 (*), p<0.01 (**), p<0.001 (***), and p<0.0001 (****).

Significant differences were observed between raft from neuronal (246 ± 1) and astrocytic (26 ± 3) cells in RMMAs. However, slightly differences were observed in RMMAs in low-serum starvation samples with (66 ± 5) and without (60 ± 33) paraquat exposure. Thus, the slight increase in GAPDH activity may be related to metabolic stress (Figure 44).

3.4 Cholinesterase enzymatic activity assay in RMMAs

Cholinesterase (ChE) enzyme family catalyzes the hydrolysis of choline esters, in particular acetylcholinesterase (AchE) catalyzes the hydrolysis of acetylcholine while butyrylcholinesterase (BuChE) does for butyrylcholine. Both enzymes have been related to AD in brain (Darvesh, 2013; Talesa, 2001). In raft printed domains from neurons, total cholinesterase activity reached 247 ± 77 in comparation with 437 ± 86 determined in astrocytes (Figure 45A). However, metabolic stress in astrocytes did not differ from control situation, reaching 414 ± 99. By contrast, the oxidative stress situation triggered by paraquat treatment achieved 613 ± 249. Furthermore, BuChE activity measured using the BW284 acetylcholinesterase inhibitor, revealed that neuron printed rafts (73 ± 31) displayed about half activity compared to the printed raft of control astrocytes (165 ± 19). Control astrocytes also doubled the value of low serum-starved cells' rafts not only in absence (78 ± 35) but also in presence of paraquat (80 ± 32). Regarding acetylcholinesterase activity, neuronal printed rafts (158 ± 64) presented a lower activity than astrocytic rafts (256 ± 97) (Figure 45A). No differences were observed between these control rafts and low

serum-starvation ones (307 ± 86). However, a higher activity of acetylcholinesterase was reported in paraquat-treated rafts (533 ± 249), as happened with the total ChE activity (Figure 45).

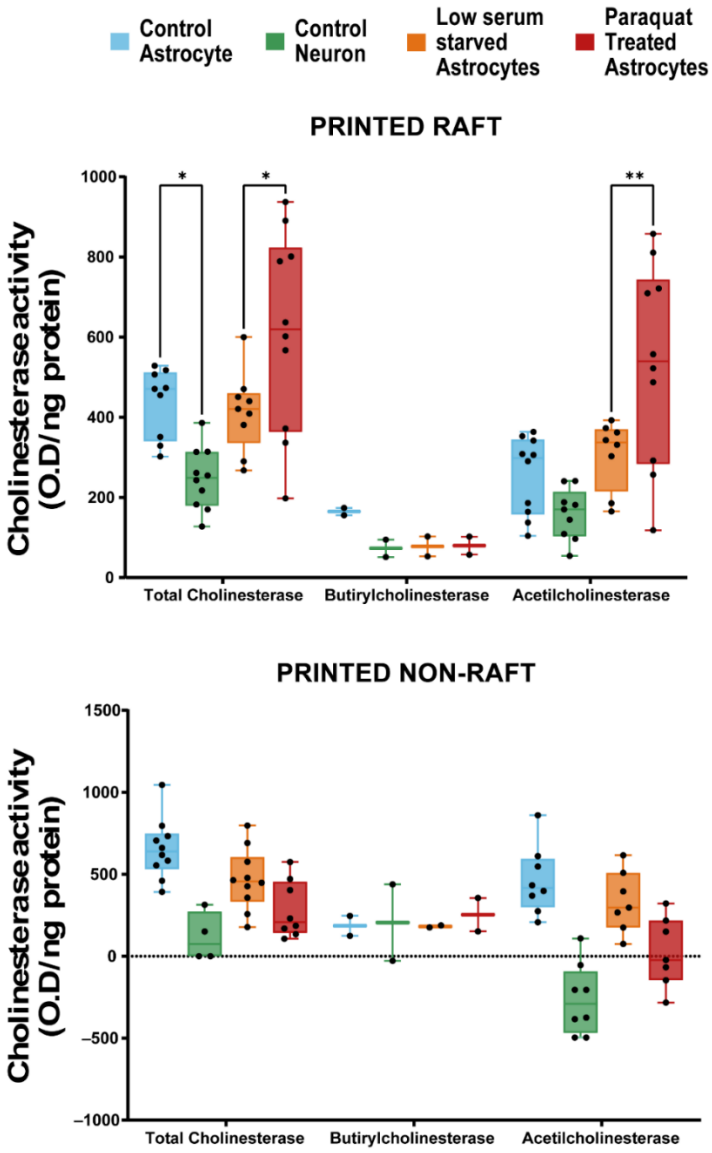

Figure 45: Total cholinesterase activity of neuron and astrocyte derived lipid rafts from cell cultures in control condition, and low serum-starved medium with or without paraquat treatment. Differences in total cholinesterase, butyrylcholinesterase and acetylcholinesterase activities (control situation of neurons and astrocytes, low serum-starved astrocytes, and paraquat-treated astrocytes) in raft printed samples (A) and non-raft printed samples (B). Two-way ANOVA was performed with Tukey post-hoc α set as 0.05; $p<0.05$ (*), $p<0.01$ (**), $p<0.001$ (***), and $p<0.0001$ (****).

In non-raft printed domains, the same tendency was observed between control neurons and astrocytes, with lower activity in neuronal printed non-rafts (116 ± 150) than in astrocytic ones (655 ± 184). Non-raft domains from low serum-starved cells (467 ± 187) did not show any differences with control astrocytes. Although a slight reduction in this activity was observed in paraquat-treated non-raft samples (284 ± 174), reverse tendency

than in raft domains (Figure 45). BuChE activity did not present any significant differences between groups (Figure 45B). Finally, acetylcholinesterase activity displayed a similar behavior to total cholinesterase, not only between types of cells, but also regarding metabolic and oxidative stress (Figure 45).

3.5 Relationships between lipid fingerprints and enzymatic activities in printed raft membrane domains

NADH oxidoreductase and GADPH activity assays displayed specific differences among the samples included in the study, in regard to metabolic stress (Figure 43B) or to cellular origin (Figure 44). In addition, differences between these samples can be observed in their lipid fingerprint. Thus, a Pearson correlation analysis was performed between lipidic spectra of raft samples and their enzymatic activities (APPENDIX I, Figure 60).

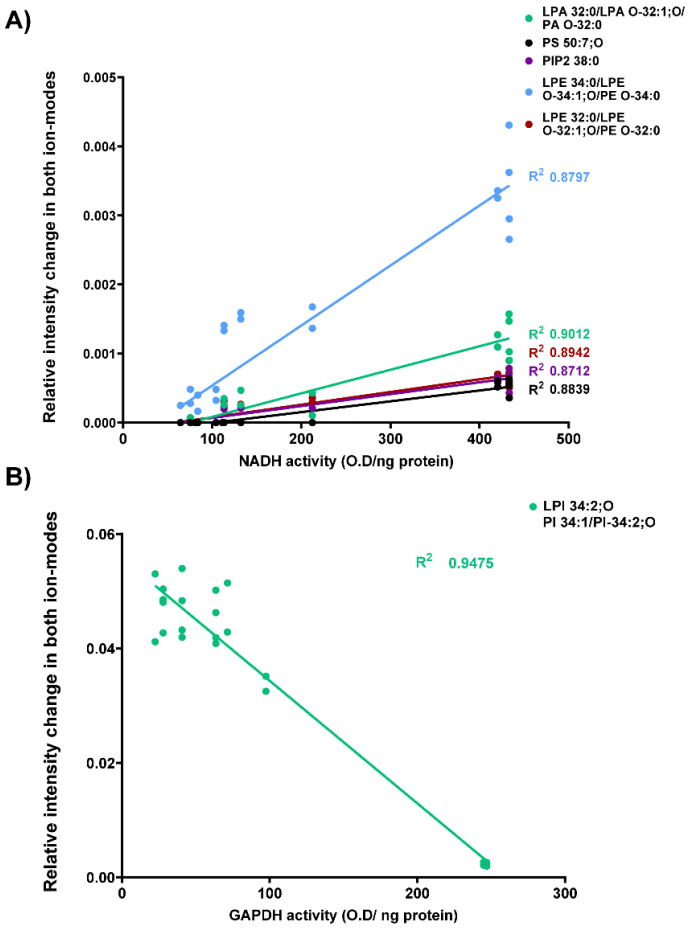

Figure 46: Correlation found between enzymatic activity assays and the relative intensity of a selection of tentatively assigned lipid species. A) Pearson correlation between relative intensity of different m/z (tentative assignation in the legend) and NADH normalized activity (O.D/ng protein). B) Pearson correlation between relative intensity of different m/z (tentative assignation in the legend) and GAPDH normalized activity (O.D/ng protein). Pearson correlation two-tailed was performed with α set as 0.05. All values represented achieved p<0.0001 (****).

Statistically significant correlations were achieved in 252 tentatively assigned lipids with NADH activity and 289 tentatively assigned lipids with GAPDH activity (Table 20). Furthermore, 5-best correlations reached R^2 higher than 0.87 with NADH activity (**Figure 46**A). The lipids that presented correlations with NADH activity were PS 50:7;0, PIP2 38:2, while others lipids which tentative assignation remains elusive, e.g.: LPA 32:0/LPA O-32:1/PA O-32:0; LPE 34:0/LPE O-34:1/PE O-34:0; LPE 32:0/LPE O-32:1/ PE O-32:0 (Figure 46). However, according to the literature, the lipid species that display the highest importance in lipid raft domains are SMs and cholesterol. Therefore, correlations between SM species detected in MALDI-MS and NADH dehydrogenase or GAPDH activities were carried out (Figure 47A).

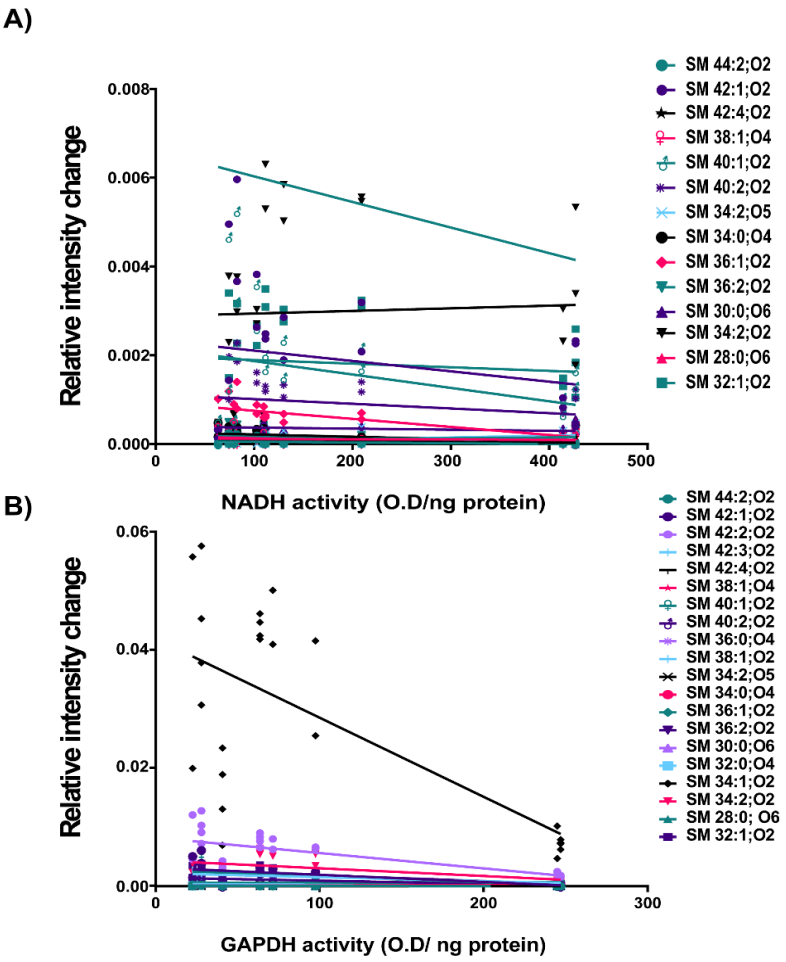

Figure 47: Correlation between sphingomyelins and different enzymatic activities. A) Pearson correlation between relative intensity of different sphingomyelins (tentative assignation in the legend) and NADH normalized activity (O.D/ng protein). B) Pearson correlation between relative intensity of different sphingomyelins (tentative assignation in the legend) and GAPDH normalized activity (O.D/ng protein). Pearson correlation two-tailed was performed with α set as 0.05. All values represented achieved $p<0.0001$ (****).

A statistically significant Pearson correlation was only found with SM 34:1; O2 and NADH activity, being slight or null correlations with the rest of SMs detected (Figure 47B). In line

with this observation, a high correlation was observed between SM 34:1;O2 and GAPDH activity (Figure 47B), but not with other sphingomyelins detected in raft domains. Thus, the alteration in SMs, the SM 34:1 can be related to dysregulation of lipid raft protein functionality. Considering this correlation between activity and lipidomic fingerprint, a Pearson correlation-based hierarchical clustering of the variables was performed, segmenting them into four clusters (Figure 48).

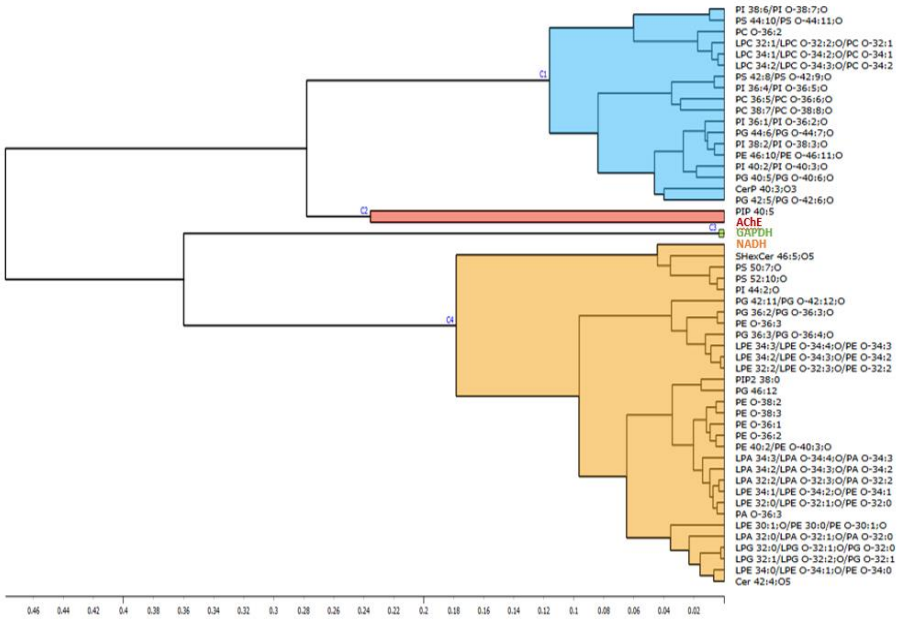

Figure 48: Pearson correlation-based hierarchical cluster of the 52-best ranked variables in ANOVA test, lipidomic composition and enzymatic activity (AChE (green), GAPDH (red), and NADH (blue)).

As a summary, differences in NADH oxidoreductase, GAPDH, AChE enzymatic activities were observed in printed raft domains between treatments and cell populations. Moreover, differences between printed raft and non-raft domains were also observed in the case of neurons (Figure 49).

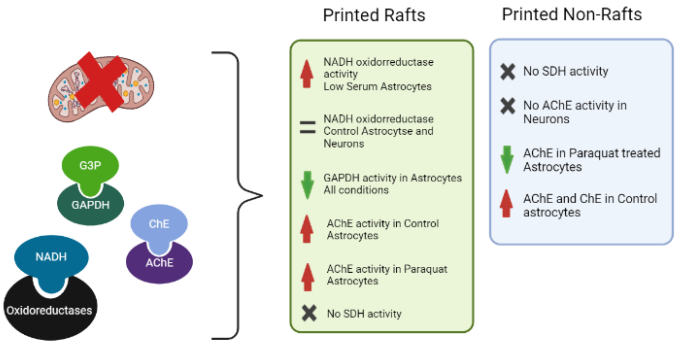

Figure 49: Summary of cell population- and treatment-dependent changes in enzyme activities, grouped into raft and non-raft domains.

DISCUSSION

1 Lipidomic analysis in cell membrane microarrays of the human astrocytic cell line 1321N1

Cellular membranes are a key part of cellular physiology, whose integrity and composition are essential for correct cellular functioning. Membranes are paramount for the maintenance of cellular homeostasis, therefore changes in the cell lipidome are an interesting field for studying the harmful or beneficial effects of different compounds (from pharmacological treatments to environmental contaminants). However, sample quantity can be a major problem for comprehensive research on certain tissues for which only a significantly reduced sample can be available. Setting up systems that can be used for simultaneous analysis of many samples using small amounts of materials is therefore pertinent.

A first approximation is the study of changes in cell membranes that can be observed using complete Cell Membrane Microarrays (CMMAs). CMMA technology was applied for use in lipid studies with cell membranes isolated from plasma membrane and internal organelles under control conditions and subjected to pro-oxidant and antioxidant treatments with paraquat and α-tocopherol, respectively. As a first step in our study, we analyzed cell viability and found that it was enhanced when an α-tocopherol pre-treatment was used prior to paraquat exposure. This antioxidant action against the oxidative stress triggered by paraquat could be due to a protective effect over lipid peroxidation. It is known that tocopherol and tocotrienol compounds prevent lipid peroxidation due to their ROS scavenger properties(Azzi et al., 2003), protecting unsaturated fatty acids and lipid mediators (Zingg, 2019). In addition, α-tocopherol regulates the expression of genes implicated in apoptosis or antioxidant defenses, such as Bcl2-L1 or γ-glutamylcysteine synthetase, (Azzi et al., 2003; Zakharova et al., 2021) or in lipid homeostasis, such as phospholipase A2(Duncan & Suzuki, 2017), which has 1-O-acyl ceramide synthase activity, using ceramides as an acceptor (Shayman & Tesmer, 2019). Thus, we decided to investigate if the changes in the lipid fingerprint due to paraquat exposure could be mitigated by this antioxidant pre-treatment using CMMA technology.

First of all, we demonstrated that our CMMA technology was a good tool to analyze changes in the membrane lipid fingerprint between experimental conditions, using the significantly small amount of sample available. This technology allows the production of thousands of microarrays with minimal total sample amounts. Moreover, this high-throughput technology can be coupled to lipidomic analysis opening the path to future large-scale screenings of many samples at the same time. CMMAs have been used in

different lipidomic studies to analyze the lipid fingerprint of nerve and peripheral tissue in animal models (Fernández et al., 2019; Manuel et al., 2015). An additional advantage of this technology is that protein expression or activity assays can be performed, as the protein-lipid relation and protein functionality is maintained (Astigarraga et al., 2008; Elexpe et al., 2021; Fernández et al., 2019; Hebert-Chatelain et al., 2016; Manuel et al., 2015; Sanchez et al., 2022; Sánchez-Sánchez et al., 2023). Thus, the combination of membrane microarray technology with mass spectrometry results in a powerful technique to determine the effects of different compounds over lipid composition, especially on lipids such as PC, PE, PS, PI, SM and ceramides among others, that shows good ionization on MALDI-MS.

It is known that the ceramide content remains low in non-dividing cells, but can increase due to exposure to stress conditions, such as serum starvation, chemical compound exposure, or oxidative stress conditions (Nikolova-Karakashian & Rozenova, 2010). These SLs, composed of sphingosine group and fatty acid, are primarily produced by de novo synthesis (Hannun & Obeid, 2008), the salvage pathway, or SMase pathways (Ho et al., 2022). In line with these observations, we detected an increase of all tentatively assigned ceramide species in paraquat-treated membranes, whereas, with α-tocopherol pre-treatment, the unsaturated ceramides decreased or remained absent. These bioactive lipid species can participate in diverse signaling pathways themselves or by their hydrolyzation to sphingosine through ceramidase enzymes (Thomas et al., 2022). The higher levels of these lipids observed in the membranes of the paraquat-treated cells, with respect to the control, could indicate that the apoptosis pathway is involved as these molecules are well known second messengers of this pathway (James et al., 2021; Jazvinšćak Jembrek et al., 2015), increasing cell death, as shown in Figure 21. Moreover, the enhancement in ceramide production might be due to an activation of the de novo pathway, and this activation may lead to an increase in other SLs by ceramides transformation, such as SMs by the action of the sphingomyelin synthase (Hannun & Obeid, 2008). The detected ceramides displayed ultra-long chain (ULC) fatty acids, which presence have been related to inflammation and different diseases (Zwara et al., 2021), including neurodegenerative disorders (Panchal et al., 2014; Zwara et al., 2021). The exposure to α-tocopherol increased or triggered the formation of new SM species, such as the tentatively assigned SM 35:1; O2, with respect to the membranes isolated from cells treated only with paraquat. In contrast, some ceramide species decreased with antioxidant pretreatment (Figure 23), which could lead to higher cell survival (Figure 21). In this sense those observations can provide useful information that can be complemented with SMase activity assays using conventional methods by

Holme et al (2018). However, further research must be performed to apply that colorimetric method to CMMA technology.

GPs are particularly sensitive to lipid peroxidation triggered by oxidative stress exposure. In this sense, we observed that PE and their ethers displayed changes upon paraquat treatment. The PE ethers (PE O-) increase might be an adaptive response of the cell, given their antioxidant properties (Poleschuk et al., 2020). PE O- can be precursors of plasmalogen, a lipid species whose oxidative products do not propagate lipid peroxidation (Sindelar et al., 1999), protecting other GPs, lipids, and lipoproteins from oxidative stress (Brites et al., 2004). Thus, the decrease in most ether PE species when α-tocopherol preceded paraquat treatment can reflect a return to basal conditions, where this antioxidant mechanism is not necessary (Drechsler et al., 2016). The antioxidant properties of the PE O- species are mainly attributed to the preferential oxidation of the vinyl ether bond, which results in the protection of the polyunsaturated fatty acids (Messias et al., 2018). In agreement with these observations, paraquat treatment resulted in greater increases in ether forms of PCs, such as tentatively assigned LPC O-16:0 and PC O-32:2, than their non-ether analogs (Figure 22C). Furthermore, and in line with other studies (Drechsler et al., 2016), an increased presence of PE 38:3 was observed in cell membranes upon paraquat treatment. These species only appear in paraquat-treated samples irrespective of the presence of α-tocopherol. Moreover, in paraquat-treated membranes, PCs containing long-chain polyunsaturated fatty acids (LCPUFAs) were increased, while with α-tocopherol pre-treatment some of them disappeared. In this context, important actions of lipids containing LCPUFAs have been demonstrated in brain inflammatory reactions (Janssen & Kiliaan, 2014).

The α-tocopherol pre-treatment that preceded paraquat exposure also triggered an increase in LPI 20:4. This lipid mediator, which contains arachidonic acid, might increase in the membranes due to lower AA release from the membrane phospholipids. As α-tocopherol is a modulator of phospholipase A2 (Duncan & Suzuki, 2017), also involved in raft fission (Staneva et al., 2004), such an effect can be mediated by a reduction this phospholipase activity (Mîinea et al., 2002) or by an increase in the activity of other enzymes such as phospholipase A1 or 2-acyl LPI transferase (Yamashita et al., 2013). Thus, a higher relative content of lipids with AA may be related to a lower free AA content, which excess has been related to neurotoxic effects (Okuda et al., 1994). Moreover LPI 20:4 can be an agonist of GPR55, a G-protein coupled receptor, whose biological activities include the modulation of immune cells and insulin secretion, and also have a potential mitogen

activity in cancer cells (Yamashita et al., 2013). By contrast, LPCs stimulate intracellular ROS production and ATM/Chk2, ATR/Chk1, as well as Akt activation in endothelial cells (Chang et al., 2017). LPC 16:0, which contains a palmitoyl molecule, was present in the samples treated with paraquat, increasing slightly when samples were pre-treated with α-tocopherol. As palmitoylation is particularly important for cell membrane stabilization (Charollais & Van Der Goot, 2009; Koca et al., 2020), its increase in our samples may support the observed effects in cellular viability (Figure 21).

To sum up, CMMAs are useful to detect alterations in the membrane lipidome triggered by different pathological conditions. In this sense, this technology could be used to analyze the changes over lipid fingerprint produced by the action of drugs to better understand the effects of a treatment in different cell types or tissues.

2 Development of Microarrays derived from lipid raft and non-raft domains allows for adequate discrimination of lipid fingerprints in different cell types and conditions

Modifications in the lipid environment not only can alter general membrane composition, but also can modify lipid raft microdomains, which may lead to raft disruption and dysregulation of certain pathways. Raft domains are related with cancer and neurodegenerative diseases, in particular Alzheimer disease as they are involved in the processing of APP (reviewed by Krasnobaev et al., 2022). In this sense astrocytic and neuronal cell line have been selected due to their importance in neurodegenerative diseases (Avila-Muñoz & Arias, 2015). Cell lines can be easily cultured to produce a huge amount of sample for experiments, nevertheless, as lipid rafts are such small microdomains, the amount of sample needed to perform certain experiments can become a major limiting factor.

To address this constraint, this thesis develops the application of microarray technology to raft and non-raft microdomains preparations obtained by different methods. We determined the method that allows their correct immobilization on pre-activated slides, maintaining active proteins and avoiding ionic suppression. First, standard detergent preparation method was performed, using TX-114 and TX-100, with and without subsequent dialysis and concentration. These first approaches resulted in a high concentration of sucrose in the sample that did not allow proper immobilization. This problem was solved by dialysis, but the remaining amount of detergent still prevented proper ionization for MALDI-MS technology and could interfere with the activity of

certain membrane proteins. Subsequently, detergent-free sonication was used followed by an ultracentrifugation protocol for eliminating the excess of sucrose in raft and non-raft preparations. This protocol resulted in minimal loss of sample material through the processing steps.

Once printed, MALDI-MS technology was used to determine a distinguishable lipid fingerprint between raft and non-raft domains obtained from neurons and astrocytes in control conditions or, in astrocyte's case, after cells were exposed to various stress conditions (low-serum starvation and paraquat treatment).

Distinguishable lipid fingerprints were observed when comparing raft and non-raft printed preparations in every condition tested (Figure 27, Figure 29, Figure 31, Figure 33). Non-raft domains presented more differences between them than raft domains, comparing the whole lipid spectra. By contrast with the 50-best ranked lipid analysis, component 2 of the PCA analysis was able to differentiate raft domains among arrays. More in detail, differences between SLs content were observed between raft and non-raft samples in every condition tested. Tentatively assigned SLs were different not only between neurons and astrocytes, but also between experimental situations (control, low serum-starvation, and paraquat). These results obtained using RMMAs technology, can be useful to analyze the differences in raft domains extracted from cells exposed to different drugs.

More in detail, in regard to astrocyte's control situation, tentatively assigned LPCs, LPC 18:1, LPC O-27:3 and LPC O-34:3, were increased in raft domains, with LPC 18:1 containing oleic acid, while the other ones were not common LGPs, as they contain fatty acids with more than 24 carbons. These ultra-long chain fatty acids (ULCFAs) are uncommon but have been detected in humans (Ritchie et al., 2010). This lipid distribution inside the RMMAs was present in raft and non-raft samples (with higher intensity in the first ones) but absent in membranes from rat tissue that were used as internal controls.

Similar results were obtained for LPE and LPI species, presenting acyl chains from 28 to 33 carbons. LPEs can contain ULCFAs as LPCs and were found to increase in raft domains. Regarding LPI, two molecules, LPI 20:3 and LPI 20:4 were identified by their m/z analysis as putatively containing dihomolinolenic acid and arachidonic acid, a common fatty acid in the brain (Rapoport, 2008). Finally, we also detected LPG O-28:0 putatively containing montanic acid, a fatty acid presented in brain and visceral organs in humans (Molzer et al., 1989).

In low serum-starved astrocytes, GP, PC and LPC species were increased in raft domains. However, we must consider that almost all LPC m/z range identified could also be assigned to PC. As the mass range correspond to a long-chain lipid species of more than 30 carbons, PC assignation is more probable. Nevertheless, LPC 18:1 had a unique tentative assignation, and might contain oleic acid (Medina & Tabernero, 2002). Oleic acid is abundant in astrocytic membranes as it is the only fatty acid synthetized by this cell. It is critical for membrane fluidity and it is required also by neurons, which preferentially incorporate oleic acid into membranes rather than storing it in its free form (Medina & Tabernero, 2002, 2002). Therefore, this could explain the relative enrichment of LPC 18:1 in raft domains in neurons. In addition to this species, other LPCs were also increased in raft domains, LPC O-16:0 (palmitic acid) and LPC O-28:4 (octacosatetraenoic acid), a lipid already detected in diverse human tissues (Liu et al., 2010).

Other GPs, such as PG, PE, and PE ether versions, were enriched in the raft domains whereas various PI were decreased. In general, PAs were decreased in non-raft domains. Regarding LPE and LPG species, it should be noted that many can also be assigned as PA, which is more probable, considering the number of carbons. Finally, tentatively assigned LPI 20:4, which might contain arachidonic acid, was increased in raft domains not only in control situation but also in low-serum starvation conditions.

Upon paraquat treatment, as well as in low serum starved cells, the mass range of PC/LPC in printed subdomains might have different lipid assignation in some cases, as lipid chains are 29 carbons or longer. Taking into account this consideration, differences in short chain LPCs can correspond to tetradecanoic (14:0), palmitoleic (16:1) and stearic (18:0) acid or to LPC O-14:1, LPC O-16:2 and LPC O-18:1, with miristoleic acid (14:1) and oleic acid (18:1). LPC O-16:2 contains hexadecadienoic acid, a metabolite of linoleic acid. In this sense, tetradecanoic acid (14:0), is more likely to integrate these molecules, as it is more common than miristoleic acid (14:1). The same consideration can be made with palmitoleic (16:1) as it is more common than hexadecadienoic acid (16:2). Regarding DGs and TGs, only DG species with more than 37 carbons and one TG were enriched in raft domains compared to non-raft membranes. However, as these lipids are detected as adducts (addition of lipid molecule and a positively charged ion), their peaks and assignment cannot be ensured without mass fragmentation, as they exhibit better ionization with sodium or potassium than with cesium. Moreover, spectra present peak duplicity with DG cesium adduct and sodium adduct, thus, for better analysis of TG and DG adducts other displacement method

incubating with sodium solution should be used (Arroyo Negrete et al., 2018).

In the m/z range that can be assigned with ether version of DGs or TGs. In this case, the majority of differences have been observed in lipids with longer chains in paraquat treatment compared both with low serum starved cells and with control cells. Curiously, ether TGs content, as well as other lipids have been observed as aging biomarkers in rats, probably by their implication in antioxidant pathways (Jové et al., 2021). Therefore, the fact that more ether DGs/TGs were detected in oxidized raft domains, compared with low serum-starved or control situations, could be part of a cellular response to mitigate the pro-oxidant effects of paraquat by producing these ether TGs.

In case of the human neuronal cell line SH-SY5Y, there was not unique lipid assignations in the specific mass range of LPC/PC between 28 carbons and 34 carbons, as some LPCs with a long-chain fatty acid can display m/z ratios identical to certain PCs with two short-chain fatty acids. Although these long-chain fatty acids are scarce, ultra-long chain fatty acids (ULCFA) from 30 to 38 carbons have been detected in mammals' brain. In this sense, we detected LPC O-28:3 which is a 28-carbon fatty acid present in small amounts in humans (Poulos et al., 1992). LPC 16:0/LPC O-16:1 were also detected, these molecules contain palmitoic acid (16:0) or palmitoleic fatty acid (16:1) and octacosatrienoic acid, which is a derivate from lineolic acid. The latter LPC (LPC O-28:3) contains a very long chain fatty acid (VLCFA), present in small amount in humans. Furthermore, LPEs with very long odd-numbered chain fatty acid were detected with a higher relative abundance in raft domains. LPE detected were LPE O-29:2, O-30:2, O-31:2 and O-31:3, which may contain nonacosadienoic acid, triacontadienoic acid, and methyl-triacontradienoic acid respectively.

Specific lipid variables were identified to discriminate raft and non-raft printed samples in astrocytic control situation using diverse algorithms. kNN was the one that could best classify raft and non-raft samples in every condition and cell type analyzed. Therefore, RMMAs are a useful platform to analyze the differences in lipid fingerprint in and out of membrane raft microdomains in a variety of conditions, with high reproducibility, negligible amount of sample, and in quick time. In this sense, this technology could be useful to classify samples by their lipid fingerprint, being a powerful technique for drug screening or for distinguish between control or early stages neurodegenerative diseases, for example.

After our comparisons between raft and non-raft domains in each cell type or each condition, we analyzed differences in the lipid fingerprint of lipid rafts caused by

metabolic and oxidative stress. This is relevant, since changes in lipid composition can lead to lipid raft dysregulation. Under metabolic stress ceramides had higher relative intensity in raft domains from low serum-starved cells (Bekhite et al., 2021; Castro et al., 2014). In contrast, HexCers, that are non-bioactive lipid species, were found decreased in low serum starvation raft membranes. These molecules can be transformed into ceramide (Sanchez et al., 2022), as pro-apoptotic second messengers. Thus, a higher HexCer presence in control situation could be due to the lack of pro-apoptotic signaling (Wilkerson et al., 2022).

When comparing oxidative stress *vs* metabolic stress (paraquat-treated cells *vs* low serum-starved cells), ceramides appear to be reduced in raft domains due to paraquat treatment. A low ceramide content could be expected by its involvement in pro-inflammatory and pro-apoptotic responses as a second messenger, such as the activation of IL-1β secretion in NLRP3 dependent manner (Scheiblich et al., 2017). This inflammasome has been reported to be activated by ROS generation and TAG accumulation in cytoplasm (S. Li et al., 2021). However, in certain cells such as spermatogenic cells, ceramides that contains VLCPUFAs can be excluded from raft domains (Santiago Valtierra et al., 2017). In regard to PA species, the ones with more than 40 carbons were decreased in raft domains upon paraquat treatment, as well as ether PA, PGs, and ether PEs. These ultra-long lipids could be fragments of other GPs or cardiolipin fragments.

The lipid variables identified in every case were able to discriminate oxidative stress from metabolic stress in raft printed domains, whereas in non-raft printed samples a worst classification was achieved. Thus, the RMMA technology used to print raft domains provides a useful platform to analyze lipid fingerprint modifications in order to determinate the potential toxicological effect of many compounds such as paraquat.

Last, but not least, we observed that the lipidic pattern present in different tissues was distinguishable, as the cell types analyzed were also distinguishable by this fingerprint, with a better separation in principal component analysis in raft domains. Sulfatides presented a relative increase in astrocytes, compared to neurons, in tentatively assigned species with less than 40 carbons. Small amounts of these molecules are known to be synthetized by astrocytes (Eckhardt, 2008). However, sulfatides with more than 40 carbons were increased in neurons, compared to astrocytes. Sulfatides can be generated from ceramides by the action of UDP-galactose:ceramidegalactosyltransferase (CGT) (Blomqvist et al., 2021). In this sense, an opposite behavior was observed between some ceramides and its sulfatides, such as Cer 42:6 and SHexCer 42:6 that were increased and

decreased in astrocytic raft respectively in comparison with neuronal ones.

In conclusion, metabolic and oxidative stress triggers characteristic lipid changes in lipid raft domains that may be linked to cellular toxicity. The data obtained using RMMAs and MALDI mass spectrometry provide a distinguishable lipid fingerprint that makes possible to distinguish not only between treatments but also between cells types, cell populations, and tissues. Moreover, lipidome changes has been reported as possible biomarkers (Kosek et al., 2020). The RMMA technology is useful for many pertinent analyses using the same platform, which reduce significantly the amount of sample and time for each experiment.

3 Enzymatic activities demonstrate that printed membrane subdomains maintain biologically relevant functionality

Certain enzymatic activities can be used to determine the purity and functionality of lipid rafts, as they are integral or membrane-anchored proteins. These enzymatic activities differ between cell types and cell populations, being their function highly dependent on lipid composition. In this sense, we found that NADH dehydrogenase activity was similar in lipid raft domains from control neurons and astrocytes but was altered due to metabolic stress in the latter cell type. Metabolic stress could increase the production of free-radicals such as superoxide that can trigger the oxidation of NBT to formazan (Y. Zhao et al., 2017). Surprisingly, upon paraquat treatment, less free-radical species were formed in the time studied. The lack of succinate dehydrogenase activity, might indicate the absence of mitochondrial complexes in the printed subdomains, suggesting that paraquat can act through other mechanisms in addition to the inhibition of mitochondrial respiration (W.-S. Choi et al., 2008).

GAPDH, like beta-actin, or beta-tubulin, is considered a housekeeping protein usually used to normalize Western blot results. GAPDH activity has also great interest in neurodegenerative disease research due to its relation with AD, in which different types of oxidative modification can be present, related or not with oxidative stress and ROS production (Butterfield et al., 2010). We observed a slight increase of this activity in raft of paraquat-treated astrocytes, but not enough to have a significant difference. This augmentation could be due to reaction of free radicals triggered by paraquat. Moreover, GAPDH activity was higher in neuronal rafts than in astrocytic ones, where glycolysis normally occurs (Díaz-García et al., 2017). In this sense, it is known that GAPDH seems to interact with proteins related to raft domains such as APP (El Kadmiri et al., 2014).

AChE is another enzyme that has been found in several tissues inside raft domains (Montenegro et al., 2017). This enzyme is related with Parkinson disease, where anticholinergic drugs are used to improve the tremor symptoms (Abusrair et al., 2022; Helmich & Dirkx, 2017; López-Álvarez et al., 2015). In this sense, RMMA technology may be useful to perform screenings of the anticholinergic effects of drugs over a variety of samples. Total cholinesterase activity seemed to be higher in astrocytes compared to neurons in case of total cholinesterase but not significantly in AchE, which can be increased in activated astrocytes (Sáez-Valero et al., 2003). Paraquat astrocytic raft domains achieved higher signal compared with their control in both ChE and AChE activities. This oxidative stress situation can lead into reactive gliosis that would alter the astrocyte functionality (Pekny & Nilsson, 2005). As reported in Figure 45, AChE activity was higher than BuChE in raft printed samples in almost every case. In line with this observation, AChE enzyme has been found inside raft domains in different tissues (Montenegro et al., 2017). By contrast, in non-raft domains from cells in control situation, all the activity observed in the case of neuron was BuChE (Giacobini, 2003), an enzyme found in both astrocyte and neurons in human brain. Thus, the combination of this enzymatic assay with RMMAs technology has shown great potential for the screening of lipid raft protein-targeted drugs, moreover taking into account that certain molecules such as donepezil, an anticholinesterase inhibitor used as AD treatment, can also increase ROS in mitochondria (Goguadze et al., 2019).

Last but not least, the NADH and GAPDH activities present correlations with the changes in GPs and SMs. However, higher correlations were present in GPs as they were more reactive and susceptible to changes due to the exposure to the different treatments. The disruption in NADH dehydrogenase in plants (mETC complex I) has been related with changes in lipidome (Domergue et al., 2022), in particular in GPs such as PAs, PEs, and PCs. In this sense, paraquat has been described as an inhibitor of mETC complex I (Olubodun-Obadun et al., 2022), thus effects of paraquat over the mETC not only affects the mitochondrial function, but also the whole membrane composition. The relationship between enzymatic activity and lipidome composition provides useful information to better understand the effects of a drug or compound on a cell.

To sum up, raft domains printed using RMMA technology maintain their functionality, allowing the study of enzymatic activities, and their close relationship with the membrane composition.

4 Contribution, limitations and future perspectives of the technology developed

This Ph.D. thesis has contributed to develop a novel platform useful for lipidomic and enzymatic assays in isolated membrane subdomains. This technology allows us to measure enzymatic activities as proteins maintain their native conformation mainly due to the preservation of lipid environment in printed raft and non-raft subdomains. Indeed, RMMAs can provide a useful technology for lipid fingerprint analysis. Moreover, our work has contributed to expand the knowledge about the lipidic environment in different cell types and conditions at the scale of membrane subdomains.

One of the limitations of this work is the impossibility of using a quantitative method for lipidomic analysis, that would provide, for example, an interesting view over the different fatty acids that are present in rafts GPLs. Nevertheless, despite this limitation, RMMA technology provide the possibility of analyzing simultaneously many technical replicas and biological samples. The correct classification of neuronal and astrocytic cell lines by the lipid fingerprints obtained in RMMAs makes this technology applicable for the analysis of other cell types and tissues.

A relevant line of work to be pursued is the use of the RMMA technology developed in this thesis for testing effects of drugs over relevant enzymatic activities present in lipid-raft domains. This high-throughput technology can provide useful information for developing a better drug safety profile.

CONCLUSIONS

1. Lipidomic analysis performed in the CMMA system provide distinguishable lipid fingerprints of astrocytic human cell membranes after pro-oxidant and antioxidant treatments.

2. Lipidomic analysis performed in the newly-developed RMMA system provide a distinguishable lipid fingerprint of raft and non-raft membrane subdomains from the astrocytic human cell line in every condition. Likewise, lipidomic analysis in the RMMA system provide a distinguishable lipid fingerprint of both cell types: astrocytic and neuronal cell lines.

3. In this context kNN algorithm can provide an accurate classification of membrane subdomain (raft and non-raft), condition (control, metabolic stress, and oxidative stress) and cell type (astrocytes and neurons).

4. NADH oxidoreductase activity is significantly increased in printed raft domains from metabolically stressed cells, either compared with printed domains from cells in control situation or with oxidative stress situation.

5. GAPDH activity showed no differences between control, metabolic and oxidative stressed conditions in astrocytic printed rafts domains. However, differences in GAPDH activity between both cell types were observed, being higher in neuronal raft membranes.

6. AchE activity showed a decrease in neuronal printed rafts, compared with astrocytic printed rafts. Moreover, raft domains from oxidative stressed astrocytes showed a higher AchE activity.

7. CMMA and RMMA technologies allow the performance of MS and activity assays analysis over whole membranes, and raft and non-raft subdomains, with negligible sample amount. This newly-developed technology is now ready for expanding its use to testing drug effects over several enzymatic activities present in raft and non-raft subdomains.

REFERENCES

REFERENCES

Abusrair, A. H., Elsekaily, W., & Bohlega, S. (2022). Tremor in Parkinson's Disease: From Pathophysiology to Advanced Therapies. *Tremor and Other Hyperkinetic Movements (New York, N.Y.)*, *12*, 29. https://doi.org/10.5334/tohm.712

Adayev, T., Estephan, R., Meserole, S., Mazza, B., Yurkow, E. J., & Banerjee, P. (1998). Externalization of phosphatidylserine may not be an early signal of apoptosis in neuronal cells, but only the phosphatidylserine-displaying apoptotic cells are phagocytosed by microglia. *Journal of neurochemistry*, *71*(5), 1854-1864. https://doi.org/10.1046/J.1471-4159.1998.71051854.X

Almeida, P. F. F., Thompson, T. E., & Vaz, W. L. C. (1992). Lateral Diffusion and Percolation in Two-Phase, Two-Component Lipid Bilayers. Topology of the Solid-Phase Domains In-Plane and Across the Lipid Bilayer. *Biochemistry*, *31*(31), 7198-7210. https://doi.org/10.1021/BI00146A024/ASSET/BI00146A024.FP.PNG_V03

Althoff, T., Mills, D. J., Popot, J.-L., & Kühlbrandt, W. (2011). Arrangement of electron transport chain components in bovine mitochondrial supercomplex I1III2IV1. *The EMBO Journal*, *30*(22), 4652-4664. https://doi.org/10.1038/emboj.2011.324

Alves, A. C. S., Dias, R. A., Kagami, L. P., das Neves, G. M., Torres, F. C., Eifler-Lima, V. L., Carvalho, I., de Miranda Silva, C., & Kawano, D. F. (2018). Beyond the «Lock and Key» Paradigm: Targeting Lipid Rafts to Induce the Selective Apoptosis of Cancer Cells. *Current medicinal chemistry*, *25*(18), 2082-2104. https://doi.org/10.2174/0929867325666180111100601

Anderson, M. R. (1966). Cell surfaces. *British journal of cancer*, *20*(2), 299-306. https://doi.org/10.1038/BJC.1966.38

Angelini, R., Yutuc, E., Wyatt, M. F., Newton, J., Yusuf, F. A., Griffiths, L., Cooze, B. J., El Assad, D., Frache, G., Rao, W., Allen, L. B., Korade, Z., Nguyen, T. T. A., Rathnayake, R. A. C., Cologna, S. M., Howell, O. W., Clench, M. R., Wang, Y., & Griffiths, W. J. (2021). Visualizing Cholesterol in the Brain by On-Tissue Derivatization and Quantitative Mass Spectrometry Imaging. *Analytical Chemistry*, *93*(11), 4932-4943. https://doi.org/10.1021/acs.analchem.0c05399

Angelova, P. R., & Abramov, A. Y. (2018). Role of mitochondrial ROS in the brain: From physiology to neurodegeneration. *FEBS letters*, *592*(5), 692-702. https://doi.org/10.1002/1873-3468.12964

Annesley, S. J., & Fisher, P. R. (2019). Mitochondria in Health and Disease. *Cells*, *8*(7). https://doi.org/10.3390/CELLS8070680

Anthonymuthu, T. S., Kenny, E. M., & Bayır, H. (2016). Therapies targeting lipid peroxidation in traumatic brain injury. *Brain research*, *1640*(Pt A), 57-76. https://doi.org/10.1016/J.BRAINRES.2016.02.006

Antonucci, S., Di Sante, M., Tonolo, F., Pontarollo, L., Scalcon, V., Alanova, P., Menabò, R., Carpi, A., Bindoli, A., Rigobello, M. P., Giorgio, M., Kaludercic, N., & Di Lisa, F. (2021). The Determining Role of Mitochondrial Reactive Oxygen Species Generation and Monoamine Oxidase Activity in Doxorubicin-Induced Cardiotoxicity. *Antioxidants & redox signaling*, *34*(7), 531-550. https://doi.org/10.1089/ARS.2019.7929

Arbor, S. C., LaFontaine, M., & Cumbay, M. (2016). Amyloid-beta Alzheimer targets—Protein processing, lipid rafts, and amyloid-beta pores. *The Yale Journal of Biology and Medicine*, *89*(1), 5-21.

Arroyo Negrete, M. A., Wrobel, K., Acevedo Aguilar, F. J., Yanez Barrientos, E., Corrales Escobosa, A. R., & Wrobel, K. (2018). Determination of fatty acid methyl esters in cosmetic castor oils by flow injection—Electrospray ionization—High resolution mass spectrometry. *International Journal of Cosmetic Science*. https://doi.org/10.1111/ics.12465

Astigarraga, E., Barreda-Gómez, G., Lombardero, L., Fresnedo, O., Castaño, F., Giralt, M. T., Ochoa, B., Rodríguez-Puertas, R., & Fernández, J. A. (2008). Profiling and imaging of lipids on brain and liver tissue by matrix-assisted laser desorption/ ionization mass spectrometry using 2-mercaptobenzothiazole as a matrix. *Analytical chemistry*, *80*(23), 9105-9114. https://doi.org/10.1021/AC801662N

Avila-Muñoz, E., & Arias, C. (2015). Cholesterol-induced astrocyte activation is associated with increased amyloid precursor protein expression and processing. *Glia*, *63*(11), 2010-2022. https://doi.org/10.1002/glia.22874

Azzi, A., Gysin, R., Kempná, P., Ricciarelli, R., Villacorta, L., Visarius, T., & Zingg, J. M. (2003). The role of α-tocopherol in preventing disease: From epidemiology to molecular events. *Molecular Aspects of Medicine*, *24*(6), 325-336. https://doi.org/10.1016/S0098-2997(03)00028-1

Baehner, R. L., Boxer, L. A., & Davis, J. (1976). The biochemical basis of nitroblue tetrazolium reduction in normal human and chronic granulomatous disease polymorphonuclear leukocytes. *Blood*, *48*(2), 309-313.

Baldwin, K. J., & Correll, C. M. (2019). Prion Disease. *Seminars in neurology*, *39*(4), 428-439. https://doi.org/10.1055/S-0039-1687841

Banerjee, R., Purhonen, J., & Kallijärvi, J. (2022). The mitochondrial coenzyme Q junction and complex III: Biochemistry and pathophysiology. *The FEBS Journal*, *289*(22), 6936-6958. https://doi.org/10.1111/febs.16164

Banning, A., Tomasovic, A., & Tikkanen, R. (2011). Functional aspects of membrane association of reggie/flotillin proteins. *Current protein & peptide science*, *12*(8), 725-735. https://doi.org/10.2174/138920311798841708

Baoukina, S., Rozmanov, D., & Tieleman, D. P. (2017). Composition Fluctuations in Lipid Bilayers. *Biophysical journal*, *113*(12), 2750-2761. https://doi.org/10.1016/J.BPJ.2017.10.009

Barnett-Norris, J., Lynch, D., & Reggio, P. H. (2005). Lipids, lipid rafts and caveolae: Their importance for GPCR signaling and their centrality to the endocannabinoid system. *Life sciences*, *77*(14), 1625-1639. https://doi.org/10.1016/J.LFS.2005.05.040

Bedard, K., & Krause, K. H. (2007). The NOX family of ROS-generating NADPH oxidases: Physiology and pathophysiology. *Physiological reviews*, *87*(1), 245-313. https://doi.org/10.1152/PHYSREV.00044.2005

Bekhite, M., González-Delgado, A., Hübner, Haxhikadrija, P., Kretzschmar, K., Müller, T., Wu, J. M., Bekfani, T., Franz, M., Wartenberg, M., Gräler, M., Greber, B., & Schulze, P. C. (2021). The role of ceramide accumulation in human induced pluripotent stem cell-derived cardiomyocytes on mitochondrial oxidative stress and mitophagy. *Free Radical Biology & Medicine*, *167*. https://doi.org/10.1016/j.freeradbiomed.2021.02.016

Bezawork-Geleta, A., Rohlena, J., Dong, L., Pacak, K., & Neuzil, J. (2017). Mitochondrial Complex II: At the Crossroads. *Trends in biochemical sciences*, *42*(4), 312-325. https://doi.org/10.1016/J.TIBS.2017.01.003

Bhatia, S., Knoch, B., Wong, J., Kim, W. S., Else, P. L., Oakley, A. J., & Garner, B. (2012). Selective reduction of hydroperoxyeicosatetraenoic acids to their hydroxy derivatives by apolipoprotein D: Implications for lipid antioxidant activity and Alzheimer's disease. *The Biochemical Journal*, *442*(3), 713-721. https://doi.org/10.1042/BJ20111166

Blanco-Ayala, T., Andérica-Romero, A. C., & Pedraza-Chaverri, J. (2014). New insights into antioxidant strategies against paraquat toxicity. *Free Radical Research*, *48*(6), 623-640. https://doi.org/10.3109/10715762.2014.899694

Bleier, L., & Dröse, S. (2013). Superoxide generation by complex III: From mechanistic rationales to functional consequences. *Biochimica Et Biophysica Acta*, *1827*(11-12), 1320-1331. https://doi.org/10.1016/j.bbabio.2012.12.002

Blomqvist, M., Zetterberg, H., Blennow, K., & Månsson, J.-E. (2021). Sulfatide in health and disease. The evaluation of sulfatide in cerebrospinal fluid as a possible biomarker for neurodegeneration. *Molecular and Cellular Neurosciences*, *116*, 103670. https://doi.org/10.1016/j.mcn.2021.103670

Boveris, A., & Navarro, A. (2008). Brain mitochondrial dysfunction in aging. *IUBMB life*, *60*(5), 308-314. https://doi.org/10.1002/IUB.46

Brieger, K., Schiavone, S., Miller, F. J., & Krause, K. H. (2012). Reactive oxygen species: From health to disease. *Swiss medical weekly*, *142*. https://doi.org/10.4414/SMW.2012.13659

Brites, P., Waterham, H. R., & Wanders, R. J. A. (2004). Functions and biosynthesis of plasmalogens in health and disease. *Biochimica et Biophysica Acta - Molecular and Cell Biology of Lipids*, *1636*(2-3), 219-231. https://doi.org/10.1016/j.bbalip.2003.12.010

Browman, D. T., Resek, M. E., Zajchowski, L. D., & Robbins, S. M. (2006). Erlin-1 and erlin-2 are novel members of the prohibitin family of proteins that define lipid-raft-like domains of the ER. *Journal of cell science*, *119*(Pt 15), 3149-3160. https://doi.org/10.1242/JCS.03060

Brumley, L. M., & Marchase, R. B. (1991). Receptor synthesis and routing to the plasma membrane. *The American Journal of the Medical Sciences*, *302*(4), 238-243. https://doi.org/10.1097/00000441-199110000-00009

Butterfield, D. A., Hardas, S. S., & Lange, M. L. B. (2010). Oxidatively modified glyceraldehyde-3-phosphate dehydrogenase (GAPDH) and Alzheimer's disease: Many pathways to neurodegeneration. *Journal of Alzheimer's Disease: JAD*, *20*(2), 369-393. https://doi.org/10.3233/JAD-2010-1375

Carroll, J., Fearnley, I. M., Skehel, J. M., Shannon, R. J., Hirst, J., & Walker, J. E. (2006). Bovine complex I is a complex of 45 different subunits. *The Journal of biological chemistry*, *281*(43), 32724-32727. https://doi.org/10.1074/JBC.M607135200

Carroll, J., Shannon, R. J., Fearnley, I. M., Walker, J. E., & Hirst, J. (2002). Definition of the Nuclear Encoded Protein Composition of Bovine Heart Mitochondrial Complex I: IDENTIFICATION OF TWO NEW SUBUNITS *. *Journal of Biological Chemistry*, *277*(52), 50311-50317. https://doi.org/10.1074/jbc.M209166200

Casares, D., Escribá, P. V., & Rosselló, C. A. (2019). Membrane Lipid Composition: Effect on Membrane and Organelle Structure, Function and Compartmentalization and Therapeutic Avenues. *International journal of molecular sciences*, *20*(9). https://doi.org/10.3390/IJMS20092167

Castro, B. M., de Almeida, R. F. M., Goormaghtigh, E., Fedorov, A., & Prieto, M. (2011). Organization and dynamics of Fas transmembrane domain in raft membranes and modulation by ceramide. *Biophysical Journal*, *101*(7), 1632-1641. https://doi.org/10.1016/j.bpj.2011.08.022

Castro, B. M., Prieto, M., & Silva, L. C. (2014). Ceramide: A simple sphingolipid with unique biophysical properties. *Progress in Lipid Research*, *54*, 53-67. https://doi.org/10.1016/j.plipres.2014.01.004

Chakraborty, S., Doktorova, M., Molugu, T. R., Heberle, F. A., Scott, H. L., Dzikovski, B., Nagao, M., Stingaciu, L.-R., Standaert, R. F., Barrera, F. N., Katsaras, J., Khelashvili, G., Brown, M. F., & Ashkar, R. (2020). How cholesterol stiffens unsaturated lipid membranes. *Proceedings of the National Academy of Sciences of the United States of America*, *117*(36), 21896-21905. https://doi.org/10.1073/pnas.2004807117

Chan, R. B., Oliveira, T. G., Cortes, E. P., Honig, L. S., Duff, K. E., Small, S. A., Wenk, M. R., Shui, G., & Di Paolo, G. (2012). Comparative lipidomic analysis of mouse and human brain with Alzheimer disease. *The Journal of Biological Chemistry*, *287*(4), 2678-2688. https://doi.org/10.1074/jbc.M111.274142

Chandler, J., Haslam, C., Hardy, N., Leveridge, M., & Marshall, P. (2017). A Systematic Investigation of the Best Buffers for Use in Screening by MALDI–Mass Spectrometry. *SLAS DISCOVERY: Advancing the Science of Drug Discovery*, *22*(10), 1262-1269. https://doi.org/10.1177/1087057116681726

Chang, M. C., Lee, J. J., Chen, Y. J., Lin, S. I., Lin, L. D., Liou, E. J. W., Huang, W. L., Chan, C. P., Huang, C. C., & Jeng, J. H. (2017). Lysophosphatidylcholine induces cytotoxicity/apoptosis and IL-8 production of human endothelial cells: Related mechanisms. *Oncotarget*, *8*(63), 106177. https://doi.org/10.18632/ONCOTARGET.22425

Charollais, J., & Van Der Goot, F. G. (2009). Palmitoylation of membrane proteins (Review). *Molecular membrane biology*, *26*(1), 55-66. https://doi.org/10.1080/09687680802620369

Chaturvedi, R. K., & Beal, M. F. (2013). Mitochondrial diseases of the brain. *Free radical biology & medicine*, *63*, 1-29. https://doi.org/10.1016/J.FREERADBIOMED.2013.03.018

Checa, J., & Aran, J. M. (2020). Reactive Oxygen Species: Drivers of Physiological and Pathological Processes. *Journal of Inflammation Research*, *13*, 1057. https://doi.org/10.2147/JIR.S275595

Chen, Z., & Zhong, C. (2014). Oxidative stress in Alzheimer's disease. *Neuroscience Bulletin*, *30*(2), 271-281. https://doi.org/10.1007/s12264-013-1423-y

Chenna, S., Koopman, W. J. H., Prehn, J. H. M., & Connolly, N. M. C. (2022). Mechanisms and mathematical modeling of ROS production by the mitochondrial electron transport chain. *American Journal of Physiology. Cell Physiology*, *323*(1), C69-C83. https://doi.org/10.1152/ajpcell.00455.2021

Chiu, M. L. (2012). Introduction to membrane proteins. *Current protocols in protein science*, *Chapter 29*(SUPPL.67). https://doi.org/10.1002/0471140864.PS2901S67

Choi, R. Y., Coyner, A. S., Kalpathy-Cramer, J., Chiang, M. F., & Campbell, J. P. (2020). Introduction to Machine Learning, Neural Networks, and Deep Learning. *Translational vision science & technology*, *9*(2). https://doi.org/10.1167/TVST.9.2.14

Choi, W.-S., Kruse, S. E., Palmiter, R. D., & Xia, Z. (2008). Mitochondrial complex I inhibition is not required for dopaminergic neuron death induced by rotenone, MPP+, or paraquat. *Proceedings of the National Academy of Sciences of the United States of America*, *105*(39), 15136-15141. https://doi.org/10.1073/pnas.0807581105

Costa, A., Scholer-Dahirel, A., & Mechta-Grigoriou, F. (2014). The role of reactive oxygen species and metabolism on cancer cells and their microenvironment. *Seminars in cancer biology*, *25*, 23-32. https://doi.org/10.1016/J.SEMCANCER.2013.12.007

Critchley, P., Kazlauskaite, J., Eason, R., & Pinheiro, T. J. T. (2004). Binding of prion proteins to lipid membranes. *Biochemical and Biophysical Research Communications*, *313*(3), 559-567. https://doi.org/10.1016/j.bbrc.2003.12.004

Curnow, P. (2019). Designing minimalist membrane proteins. *Biochemical Society transactions*, *47*(5), 1233-1245. https://doi.org/10.1042/BST20190170

Cuschieri, J., & Maier, R. V. (2007). Oxidative stress, lipid rafts, and macrophage reprogramming. *Antioxidants & redox signaling*, *9*(9), 1485-1497. https://doi.org/10.1089/ARS.2007.1670

Dan Dunn, J., Alvarez, L. A. J., Zhang, X., & Soldati, T. (2015). Reactive oxygen species and mitochondria: A nexus of cellular homeostasis. *Redox biology*, *6*, 472-485. https://doi.org/10.1016/J.REDOX.2015.09.005

Das, M., & Das, D. K. (2009). Lipid Raft in Cardiac Health and Disease. *Current Cardiology Reviews*, *5*(2), 105. https://doi.org/10.2174/157340309788166660

Degli Esposti, M., Ghelli, A., Crimi, M., Estornell, E., Fato, R., & Lenaz, G. (1993). Complex I and complex III of mitochondria have common inhibitors acting as ubiquinone antagonists. *Biochemical and Biophysical Research Communications*, *190*(3), 1090-1096. https://doi.org/10.1006/bbrc.1993.1161

del Caño-Espinel, M. del. (2014). *Relación de la apolipoproteína D y sus homólogos en Drosophila con las membranas biológicas: Estudio de su función en diferentes procesos celulares y de su localización y efectos sobre las balsas lipídicas*. https://doi.org/10.35376/10324/7752

Di Scala, C., Yahi, N., Boutemeur, S., Flores, A., Rodriguez, L., Chahinian, H., & Fantini, J. (2016). Common molecular mechanism of amyloid pore formation by Alzheimer's β-amyloid peptide and α-synuclein. *Scientific Reports 2016 6:1*, *6*(1), 1-10. https://doi.org/10.1038/srep28781

Díaz, M., Fabelo, N., Ferrer, I., & Marín, R. (2018). «Lipid raft aging» in the human frontal cortex during nonpathological aging: Gender influences and potential implications in Alzheimer's disease. *Neurobiology of Aging*, *67*, 42-52. https://doi.org/10.1016/j.neurobiolaging.2018.02.022

Díaz, M., Fabelo, N., Martín, V., Ferrer, I., Gómez, T., & Marín, R. (2015). Biophysical alterations in lipid rafts from human cerebral cortex associate with increased BACE1/AβPP interaction in early stages of Alzheimer's disease. *Journal of Alzheimer's disease : JAD*, *43*(4), 1185-1198. https://doi.org/10.3233/JAD-141146

Díaz-García, C. M., Mongeon, R., Lahmann, C., Koveal, D., Zucker, H., & Yellen, G. (2017). Neuronal Stimulation Triggers Neuronal Glycolysis and Not Lactate Uptake. *Cell Metabolism*, *26*(2), 361-374.e4. https://doi.org/10.1016/j.cmet.2017.06.021

Diaz-Rohrer, B. B., Levental, K. R., Simons, K., & Levental, I. (2014). Membrane raft association is a determinant of plasma membrane localization. *Proceedings of the National Academy of Sciences of the United States of America*, *111*(23), 8500-8505. https://doi.org/10.1073/PNAS.1404582111/-/DCSUPPLEMENTAL

Dobon, B., Rossell, C., Walsh, S., & Bertranpetit, J. (2019). Is there adaptation in the human genome for taste perception and phase I biotransformation? *BMC evolutionary biology*, *19*(1). https://doi.org/10.1186/S12862-019-1366-7

Döhr, O., Paine, M. J. I., Friedberg, T., Roberts, G. C. K., & Wolf, C. R. (2001). Engineering of a functional human NADH-dependent cytochrome P450 system. *Proceedings of the*

National Academy of Sciences of the United States of America, *98*(1), 81-86. https://doi.org/10.1073/PNAS.98.1.81

Domergue, J.-B., Bocca, C., De Paepe, R., Lenaers, G., Limami, A. M., & Tcherkez, G. (2022). Mitochondrial Complex I Disruption Causes Broad Reorchestration of Plant Lipidome Including Chloroplast Lipids. *International Journal of Molecular Sciences*, *24*(1), 453. https://doi.org/10.3390/ijms24010453

Drechsler, R., Chen, S.-W., Dancy, B. C. R., Mehrabkhani, L., & Olsen, C. P. (2016). HPLC-Based Mass Spectrometry Characterizes the Phospholipid Alterations in Ether-Linked Lipid Deficiency Models Following Oxidative Stress. *PLoS ONE*, *11*(11), e0167229. https://doi.org/10.1371/JOURNAL.PONE.0167229

Duncan, K. R., & Suzuki, Y. J. (2017). Vitamin E Nicotinate. *Antioxidants*, *6*(1). https://doi.org/10.3390/ANTIOX6010020

E. Cybulski, L., & de Mendoza, D. (2011). Bilayer hydrophobic thickness and integral membrane protein function. *Current protein & peptide science*, *12*(8), 760-766. https://doi.org/10.2174/138920311798841681

Eckert, G. P., Kirsch, C., Leutz, S., Wood, W. G., & Müller, W. E. (2003). Cholesterol modulates amyloid beta-peptide's membrane interactions. *Pharmacopsychiatry*, *36 Suppl 2*, S136-143. https://doi.org/10.1055/s-2003-43059

Eckhardt, M. (2008). The role and metabolism of sulfatide in the nervous system. *Molecular Neurobiology*, *37*(2-3). https://doi.org/10.1007/s12035-008-8022-3

El Kadmiri, N., Slassi, I., El Moutawakil, B., Nadifi, S., Tadevosyan, A., Hachem, A., & Soukri, A. (2014). Glyceraldehyde-3-phosphate dehydrogenase (GAPDH) and Alzheimer's disease. *Pathologie-Biologie*, *62*(6), 333-336. https://doi.org/10.1016/j.patbio.2014.08.002

Elexpe, A., Nieto, N., Fernández-Cuétara, C., Domínguez-Fernández, C., Morera-Herreras, T., Torrecilla, M., Miguélez, C., Laso, A., Ochoa, E., Bailen, M., González-Coloma, A., Angulo-Barturen, I., Astigarraga, E., & Barreda-Gómez, G. (2021). Study of Tissue-Specific Reactive Oxygen Species Formation by Cell Membrane Microarrays for the Characterization of Bioactive Compounds. *Membranes 2021, Vol. 11, Page 943*, *11*(12), 943. https://doi.org/10.3390/MEMBRANES11120943

Elexpe, A., Sánchez-Sánchez, L., Tolentino-Cortez, T., Astigarraga, E., Torrecilla, M., & Barreda-Gómez, G. (2022). Analysis of Mitochondrial Function in Cell Membranes as Indicator of Tissue Vulnerability to Drugs in Humans. *Biomedicines*, *10*(5).

https://doi.org/10.3390/biomedicines10050980

Ellman, G. L., Courtney, K. D., Andres, V., & Featherstone, R. M. (1961). A new and rapid colorimetric determination of acetylcholinesterase activity. *Biochemical Pharmacology*, *7*(2), 88-95. https://doi.org/10.1016/0006-2952(61)90145-9

Emmelot, P., & van Hoeven, R. P. (1975). Phospholipid unsaturation and plasma membrane organization. *Chemistry and physics of lipids*, *14*(3), 236-246. https://doi.org/10.1016/0009-3084(75)90005-5

Fan, Z., Wang, X., Zhang, M., Zhao, C., Mei, C., & Li, P. (2019). MAPK Pathway Inhibitors Attenuated Hydrogen Peroxide Induced Damage in Neural Cells. *BioMed research international*, *2019*. https://doi.org/10.1155/2019/5962014

Farooqui, A. A., Horrocks, L. A., & Farooqui, T. (2000). Glycerophospholipids in brain: Their metabolism, incorporation into membranes, functions, and involvement in neurological disorders. *Chemistry and physics of lipids*, *106*(1), 1-29. https://doi.org/10.1016/S0009-3084(00)00128-6

Fernández, R., Garate, J., Tolentino-Cortez, T., Herraiz, A., Lombardero, L., Ducrocq, F., Rodríguez-Puertas, R., Trifilieff, P., Astigarraga, E., Barreda-Gómez, G., & Fernández, J. A. (2019). Microarray and Mass Spectrometry-Based Methodology for Lipid Profiling of Tissues and Cell Cultures. *Analytical chemistry*, *91*(24), 15967-15973. https://doi.org/10.1021/ACS.ANALCHEM.9B04529

Formosa, L. E., Dibley, M. G., Stroud, D. A., & Ryan, M. T. (2018). Building a complex complex: Assembly of mitochondrial respiratory chain complex I. *Seminars in cell & developmental biology*, *76*, 154-162. https://doi.org/10.1016/J.SEMCDB.2017.08.011

Frisardi, V., Panza, F., Seripa, D., Farooqui, T., & Farooqui, A. A. (2011). Glycerophospholipids and glycerophospholipid-derived lipid mediators: A complex meshwork in Alzheimer's disease pathology. *Progress in lipid research*, *50*(4), 313-330. https://doi.org/10.1016/J.PLIPRES.2011.06.001

Frisz, J. F., Klitzing, H. A., Lou, K., Hutcheon, I. D., Weber, P. K., Zimmerberg, J., & Kraft, M. L. (2013). Sphingolipid Domains in the Plasma Membranes of Fibroblasts Are Not Enriched with Cholesterol. *The Journal of Biological Chemistry*, *288*(23), 16855-16861. https://doi.org/10.1074/jbc.M113.473207

Frisz, J. F., Lou, K., Klitzing, H. A., Hanafin, W. P., Lizunov, V., Wilson, R. L., Carpenter, K. J., Kim, R., Hutcheon, I. D., Zimmerberg, J., Weber, P. K., & Kraft, M. L. (2013). Direct

chemical evidence for sphingolipid domains in the plasma membranes of fibroblasts. *Proceedings of the National Academy of Sciences of the United States of America*, *110*(8), E613-E622. https://doi.org/10.1073/pnas.1216585110

Gajate, C., & Mollinedo, F. (2014). Lipid rafts, endoplasmic reticulum and mitochondria in the antitumor action of the alkylphospholipid analog edelfosine. *Anti-cancer agents in medicinal chemistry*, *14*(4), 509-527. https://doi.org/10.2174/1871520614666140309222259

Gajate, C., & Mollinedo, F. (2015). Lipid rafts and raft-mediated supramolecular entities in the regulation of CD95 death receptor apoptotic signaling. *Apoptosis : an international journal on programmed cell death*, *20*(5), 584-606. https://doi.org/10.1007/S10495-015-1104-6

Garofalo, T., Matarrese, P., Manganelli, V., Marconi, M., Tinari, A., Gambardella, L., Faggioni, A., Misasi, R., Sorice, M., & Malorni, W. (2016). Evidence for the involvement of lipid rafts localized at the ER-mitochondria associated membranes in autophagosome formation. *Autophagy*, *12*(6), 917-935. https://doi.org/10.1080/15548627.2016.1160971

Gaschler, M. M., & Stockwell, B. R. (2017). Lipid peroxidation in cell death. *Biochemical and Biophysical Research Communications*, *482*(3), 419-425. https://doi.org/10.1016/j.bbrc.2016.10.086

George, K. S., & Wu, S. (2012). Lipid raft: A floating island of death or survival. *Toxicology and applied pharmacology*, *259*(3), 311-319. https://doi.org/10.1016/J.TAAP.2012.01.007

Ghosh, S., Strum, J. C., & Bell, R. M. (1997). Lipid biochemistry: Functions of glycerolipids and sphingolipids in cellular signaling. *FASEB journal : official publication of the Federation of American Societies for Experimental Biology*, *11*(1), 45-50. https://doi.org/10.1096/FASEBJ.11.1.9034165

Giacobini, E. (2003). Cholinesterases: New roles in brain function and in Alzheimer's disease. *Neurochemical Research*, *28*(3-4), 515-522. https://doi.org/10.1023/a:1022869222652

Gimpl, G., Burger, K., & Fahrenholz, F. (1997). Cholesterol as modulator of receptor function. *Biochemistry*, *36*(36), 10959-10974. https://doi.org/10.1021/bi963138w

Girotti, A. W. (2021). Nitric Oxide-elicited Resistance to Antitumor Photodynamic Therapy via Inhibition of Membrane Free Radical-mediated Lipid Peroxidation. *Photochemistry and Photobiology*, *97*(4), 653-663. https://doi.org/10.1111/PHP.13373

Goguadze, N., Zhuravliova, E., Morin, D., Mikeladze, D., & Maurice, T. (2019). Sigma-1 Receptor Agonists Induce Oxidative Stress in Mitochondria and Enhance Complex I Activity in Physiological Condition but Protect Against Pathological Oxidative Stress. *Neurotoxicity Research*, *35*(1), 1-18. https://doi.org/10.1007/s12640-017-9838-2

Griffiths, J. (2008). A Brief History of Mass Spectrometry. *Analytical Chemistry*, *80*(15), 5678-5683. https://doi.org/10.1021/ac8013065

Guengerich, F. P. (2001). Common and uncommon cytochrome P450 reactions related to metabolism and chemical toxicity. *Chemical research in toxicology*, *14*(6), 611-650. https://doi.org/10.1021/TX0002583

Gupta, A., Korte, T., Herrmann, A., & Wohland, T. (2020). Plasma membrane asymmetry of lipid organization: Fluorescence lifetime microscopy and correlation spectroscopy analysis. *Journal of lipid research*, *61*(2), 252-266. https://doi.org/10.1194/JLR.D119000364

Hadrava Vanova, K., Kraus, M., Neuzil, J., & Rohlena, J. (2020). Mitochondrial complex II and reactive oxygen species in disease and therapy. *Redox report : communications in free radical research*, *25*(1), 26-32. https://doi.org/10.1080/13510002.2020.1752002

Halliwell, B., & Chirico, S. (1993). Lipid peroxidation: Its mechanism, measurement, and significance. *The American Journal of Clinical Nutrition*, *57*(5 Suppl), 715S-724S; discussion 724S-725S. https://doi.org/10.1093/ajcn/57.5.715S

Hannaoui, S., Shim, S. Y., Cheng, Y. C., Corda, E., & Gilch, S. (2014). Cholesterol balance in prion diseases and Alzheimer's disease. *Viruses*, *6*(11), 4505-4535. https://doi.org/10.3390/V6114505

Hannun, Y. A., & Obeid, L. M. (2008). Principles of bioactive lipid signalling: Lessons from sphingolipids. *Nature reviews. Molecular cell biology*, *9*(2), 139-150. https://doi.org/10.1038/NRM2329

Harayama, T., & Riezman, H. (2018). Understanding the diversity of membrane lipid composition. *Nature reviews. Molecular cell biology*, *19*(5), 281-296. https://doi.org/10.1038/NRM.2017.138

Hatano, T., Kubo, S.-I., Imai, S., Maeda, M., Ishikawa, K., Mizuno, Y., & Hattori, N. (2007). Leucine-rich repeat kinase 2 associates with lipid rafts. *Human Molecular Genetics*, *16*(6), 678-690. https://doi.org/10.1093/hmg/ddm013

Haughey, N. J., Bandaru, V. V. R., Bae, M., & Mattson, M. P. (2010). Roles for dysfunctional

sphingolipid metabolism in Alzheimer's disease neuropathogenesis. *Biochimica et biophysica acta*, *1801*(8), 878-886. https://doi.org/10.1016/J.BBALIP.2010.05.003

He, L., He, T., Farrar, S., Ji, L., Liu, T., & Ma, X. (2017). Antioxidants Maintain Cellular Redox Homeostasis by Elimination of Reactive Oxygen Species. *Cellular physiology and biochemistry : international journal of experimental cellular physiology, biochemistry, and pharmacology*, *44*(2), 532-553. https://doi.org/10.1159/000485089

Hebert-Chatelain, E., Desprez, T., Serrat, R., Bellocchio, L., Soria-Gomez, E., Busquets-Garcia, A., Pagano Zottola, A. C., Delamarre, A., Cannich, A., Vincent, P., Varilh, M., Robin, L. M., Terral, G., García-Fernández, M. D., Colavita, M., Mazier, W., Drago, F., Puente, N., Reguero, L., … Marsicano, G. (2016). A cannabinoid link between mitochondria and memory. *Nature*, *539*(7630), 555-559. https://doi.org/10.1038/NATURE20127

Hedin, L. E., Illergård, K., & Elofsson, A. (2011). An introduction to membrane proteins. *Journal of proteome research*, *10*(8), 3324-3331. https://doi.org/10.1021/PR200145A

Heerklotz, H. (2002). Triton Promotes Domain Formation in Lipid Raft Mixtures. *Biophysical Journal*, *83*(5), 2693-2701. https://doi.org/10.1016/S0006-3495(02)75278-8

Helmich, R., & Dirkx, M. (2017). Pathophysiology and Management of Parkinsonian Tremor. *Seminars in Neurology*, *37*(02), 127-134. https://doi.org/10.1055/s-0037-1601558

Hicks, D. A., Nalivaeva, N. N., & Turner, A. J. (2012). Lipid rafts and Alzheimer's disease: Protein-lipid interactions and perturbation of signaling. *Frontiers in physiology*, *3*. https://doi.org/10.3389/FPHYS.2012.00189

Hicks, D., John, D., Makova, N. Z., Henderson, Z., Nalivaeva, N. N., & Turner, A. J. (2011). Membrane targeting, shedding and protein interactions of brain acetylcholinesterase. *Journal of neurochemistry*, *116*(5), 742-746. https://doi.org/10.1111/J.1471-4159.2010.07032.X

Higashi, S., Biskup, S., West, A. B., Trinkaus, D., Dawson, V. L., Faull, R. L. M., Waldvogel, H. J., Arai, H., Dawson, T. M., Moore, D. J., & Emson, P. C. (2007). Localization of Parkinson's disease-associated LRRK2 in normal and pathological human brain. *Brain Research*, *1155*(1), 208-219. https://doi.org/10.1016/J.BRAINRES.2007.04.034

Hirst, J. (2013). Mitochondrial complex I. *Annual review of biochemistry*, *82*, 551-575. https://doi.org/10.1146/ANNUREV-BIOCHEM-070511-103700

Hirst, J., Carroll, J., Fearnley, I. M., Shannon, R. J., & Walker, J. E. (2003). The nuclear encoded subunits of complex I from bovine heart mitochondria. *Biochimica Et Biophysica*

Acta, *1604*(3), 135-150. https://doi.org/10.1016/s0005-2728(03)00059-8

Hishikawa, D., Hashidate, T., Shimizu, T., & Shindou, H. (2014). Diversity and function of membrane glycerophospholipids generated by the remodeling pathway in mammalian cells. *Journal of lipid research*, *55*(5), 799-807. https://doi.org/10.1194/JLR.R046094

Ho, Q. W. C., Zheng, X., & Ali, Y. (2022). Ceramide Acyl Chain Length and Its Relevance to Intracellular Lipid Regulation. *International journal of molecular sciences*, *23*(17). https://doi.org/10.3390/IJMS23179697

Holme, M. N., Rana, S., Barriga, H. M. G., Kauscher, U., Brooks, N. J., & Stevens, M. M. (2018). A Robust Liposomal Platform for Direct Colorimetric Detection of Sphingomyelinase Enzyme and Inhibitors. *ACS Nano*, *12*(8), 8197-8207. https://doi.org/10.1021/acsnano.8b03308

Holthuis, J. C. M., & Menon, A. K. (2014). Lipid landscapes and pipelines in membrane homeostasis. *Nature*, *510*(7503), 48-57. https://doi.org/10.1038/NATURE13474

Honigmann, A., & Pralle, A. (2016). Compartmentalization of the Cell Membrane. *Journal of molecular biology*, *428*(24 Pt A), 4739-4748. https://doi.org/10.1016/J.JMB.2016.09.022

Huang, S., & Millar, A. H. (2013). Succinate dehydrogenase: The complex roles of a simple enzyme. *Current opinion in plant biology*, *16*(3), 344-349. https://doi.org/10.1016/J.PBI.2013.02.007

Igbavboa, U., Eckert, G. P., Malo, T. M., Studniski, A. E., Johnson, L. N. A., Yamamoto, N., Kobayashi, M., Fujita, S. C., Appel, T. R., Müller, W. E., Wood, W. G., & Yanagisawa, K. (2005). Murine synaptosomal lipid raft protein and lipid composition are altered by expression of human apoE 3 and 4 and by increasing age. *Journal of the Neurological Sciences*, *229-230*, 225-232. https://doi.org/10.1016/j.jns.2004.11.037

Islam, M. T. (2017). Oxidative stress and mitochondrial dysfunction-linked neurodegenerative disorders. *Neurological research*, *39*(1), 73-82. https://doi.org/10.1080/01616412.2016.1251711

Jakubec, M., Bariås, E., Furse, S., Govasli, M. L., George, V., Turcu, D., Iashchishyn, I., Morozova-Roche, L., & Halskau, Ø. (2019). Cholesterol is a strong promotor of an α-Synuclein membrane binding mode that accelerates oligomerization. *bioRxiv*, 725762. https://doi.org/10.1101/725762

James, B. N., Oyeniran, C., Sturgill, J. L., Newton, J., Martin, R. K., Bieberich, E., Weigel,

C., Maczis, M. A., Palladino, E. N. D., Lownik, J. C., Trudeau, J. B., Cook-Mills, J. M., Wenzel, S., Milstien, S., & Spiegel, S. (2021). CERAMIDE IN APOPTOSIS AND OXIDATIVE STRESS IN ALLERGIC INFLAMMATION AND ASTHMA. *The Journal of allergy and clinical immunology*, *147*(5), 1936. https://doi.org/10.1016/J.JACI.2020.10.024

Janssen, C. I. F., & Kiliaan, A. J. (2014). Long-chain polyunsaturated fatty acids (LCPUFA) from genesis to senescence: The influence of LCPUFA on neural development, aging, and neurodegeneration. *Progress in lipid research*, *53*(1), 1-17. https://doi.org/10.1016/J.PLIPRES.2013.10.002

Jazvinšćak Jembrek, M., Hof, P. R., & Šimić, G. (2015). Ceramides in Alzheimer's Disease: Key Mediators of Neuronal Apoptosis Induced by Oxidative Stress and Aβ Accumulation. *Oxidative Medicine and Cellular Longevity*, *2015*. https://doi.org/10.1155/2015/346783

Jiang, Q. (2014). Natural forms of vitamin E: metabolism, antioxidant, and anti-inflammatory activities and their role in disease prevention and therapy. *Free Radical Biology & Medicine*, *72*, 76-90. https://doi.org/10.1016/j.freeradbiomed.2014.03.035

Jin, J., Zhi, X., Wang, X., & Meng, D. (2021). Protein palmitoylation and its pathophysiological relevance. *Journal of Cellular Physiology*, *236*(5), 3220-3233. https://doi.org/10.1002/jcp.30122

Jin, S., Zhou, F., Katirai, F., & Li, P. L. (2011). Lipid raft redox signaling: Molecular mechanisms in health and disease. *Antioxidants & redox signaling*, *15*(4), 1043-1083. https://doi.org/10.1089/ARS.2010.3619

Jones, D. P. (2008). Radical-free biology of oxidative stress. *American journal of physiology. Cell physiology*, *295*(4). https://doi.org/10.1152/AJPCELL.00283.2008

Jové, M., Cabré, R., Mota-Martorell, N., Martin-Garí, M., Obis, È., Ramos, P., Canales, I., Galo-Licona, J. D., Sol, J., Nogueras, L., Torres, P., Portero-Otín, M., Ayala, V., Ferrer, I., & Pamplona, R. (2021). Age-Related Changes in Lipidome of Rat Frontal Cortex and Cerebellum Are Partially Reversed by Methionine Restriction Applied in Old Age. *International Journal of Molecular Sciences*, *22*(22), 12517. https://doi.org/10.3390/ijms222212517

Kaiser, H. J., Lingwood, D., Levental, I., Sampaio, J. L., Kalvodova, L., Rajendran, L., & Simons, K. (2009). Order of lipid phases in model and plasma membranes. *Proceedings of the National Academy of Sciences of the United States of America*, *106*(39), 16645-16650. https://doi.org/10.1073/PNAS.0908987106

Kan, A., Mohamedali, A., Tan, S. H., Cheruku, H. R., Slapetova, I., Lee, L. Y., & Baker, M. S. (2013). An improved method for the detection and enrichment of low-abundant membrane and lipid raft-residing proteins. *Journal of Proteomics*, *79*, 299-304. https://doi.org/10.1016/j.jprot.2012.11.019

Karas, M., & Hillenkamp, F. (1988). Laser desorption ionization of proteins with molecular masses exceeding 10,000 daltons. *Analytical Chemistry*, *60*(20), 2299-2301. https://doi.org/10.1021/ac00171a028

Karnovsky, M. J., & Roots, L. (1964). A «DIRECT-COLORING» THIOCHOLINE METHOD FOR CHOLINESTERASES. *Journal of Histochemistry & Cytochemistry*, *12*(3), 219-221. https://doi.org/10.1177/12.3.219

Kim, S. I., Yi, J. S., & Ko, Y. G. (2006). Amyloid beta oligomerization is induced by brain lipid rafts. *Journal of cellular biochemistry*, *99*(3), 878-889. https://doi.org/10.1002/JCB.20978

Kim, Y. C., Lee, J., Lee, D. W., & Jeong, B. H. (2021). Large-scale lipidomic profiling identifies novel potential biomarkers for prion diseases and highlights lipid raft-related pathways. *Veterinary research*, *52*(1), 105. https://doi.org/10.1186/S13567-021-00975-1

Koca, T., Canatan, D., Örmeci, A. R., Koca, Y. S., Duman, H., Baykal, A., & Akçam, M. (2020). Amino acids and fatty acids in patients with beta thalassemia major. *Acta Bio Medica : Atenei Parmensis*, *91*(1), 79. https://doi.org/10.23750/ABM.V91I1.7266

Kosek, V., Heczkova, M., Novak, F., Meisnerova, E., Novákova, O., Zelenka, J., Bechynska, K., Vrzacova, N., Suttnar, J., Hlavackova, A., Dankova, H., Bratova, M., Daskova, N., Malinska, H., Oliyarnyk, O., Wohl, P., Bastova, H., Hajslova, J., & Cahova, M. (2020). The ω-3 Polyunsaturated Fatty Acids and Oxidative Stress in Long-Term Parenteral Nutrition Dependent Adult Patients: Functional Lipidomics Approach. *Nutrients*, *12*(8), 2351. https://doi.org/10.3390/nu12082351

Krasnobaev, V. D., Galimzyanov, T. R., Akimov, S. A., & Batishchev, O. V. (2022). Lysolipids regulate raft size distribution. *Frontiers in Molecular Biosciences*, *9*, 1021321. https://doi.org/10.3389/fmolb.2022.1021321

Kubo, S. I., Hatanos, T., & Hattori, N. (2015). Lipid rafts involvement in the pathogenesis of Parkinson's disease. *Frontiers in bioscience (Landmark edition)*, *20*(2), 263-279. https://doi.org/10.2741/4308

Kudryavtseva, A. V., Krasnov, G. S., Dmitriev, A. A., Alekseev, B. Y., Kardymon, O. L.,

Sadritdinova, A. F., Fedorova, M. S., Pokrovsky, A. V., Melnikova, N. V., Kaprin, A. D., Moskalev, A. A., & Snezhkina, A. V. (2016). Mitochondrial dysfunction and oxidative stress in aging and cancer. *Oncotarget*, *7*(29), 44879. https://doi.org/10.18632/ONCOTARGET.9821

Kusumi, A., Fujiwara, T. K., Tsunoyama, T. A., Kasai, R. S., Liu, A.-A., Hirosawa, K. M., Kinoshita, M., Matsumori, N., Komura, N., Ando, H., & Suzuki, K. G. N. (2020). Defining raft domains in the plasma membrane. *Traffic (Copenhagen, Denmark)*, *21*(1), 106-137. https://doi.org/10.1111/tra.12718

Lai, Y.-H., Cai, Y.-H., Lee, H., Ou, Y.-M., Hsiao, C.-H., Tsao, C.-W., Chang, H.-T., & Wang, Y.-S. (2016). Reducing Spatial Heterogeneity of MALDI Samples with Marangoni Flows During Sample Preparation. *Journal of the American Society for Mass Spectrometry*, *27*(8), 1314-1321. https://doi.org/10.1007/s13361-016-1406-0

Lambeth, J. D. (2004). NOX enzymes and the biology of reactive oxygen. *Nature reviews. Immunology*, *4*(3), 181-189. https://doi.org/10.1038/NRI1312

Larsen, A. H., John, L. H., Sansom, M. S. P., & Corey, R. A. (2022). Specific interactions of peripheral membrane proteins with lipids: What can molecular simulations show us? *Bioscience Reports*, *42*(4). https://doi.org/10.1042/BSR20211406

Lee, A. (2001). Membrane structure. *Current biology : CB*, *11*(20). https://doi.org/10.1016/S0960-9822(01)00491-2

Lee, S. I., Jeong, W., Lim, H., Cho, S., Lee, H., Jang, Y., Cho, J., Bae, S., Lin, Y. T., Tsai, L. H., Moon, D. W., & Seo, J. (2021). APOE4-carrying human astrocytes oversupply cholesterol to promote neuronal lipid raft expansion and Aβ generation. *Stem Cell Reports*, *16*(9), 2128. https://doi.org/10.1016/J.STEMCR.2021.07.017

Lenaz, G., Tioli, G., Falasca, A. I., & Genova, M. L. (2016). Complex I function in mitochondrial supercomplexes. *Biochimica et biophysica acta*, *1857*(7), 991-1000. https://doi.org/10.1016/J.BBABIO.2016.01.013

Levental, I., Grzybek, M., & Simons, K. (2010). Greasing their way: Lipid modifications determine protein association with membrane rafts. *Biochemistry*, *49*(30), 6305-6316. https://doi.org/10.1021/BI100882Y

Levental, I., Levental, K. R., & Heberle, F. A. (2020). Lipid Rafts: Controversies Resolved, Mysteries Remain. *Trends in cell biology*, *30*(5), 341-353. https://doi.org/10.1016/J.TCB.2020.01.009

Lewis, V., & Hooper, N. M. (2011). The role of lipid rafts in prion protein biology. *Frontiers in bioscience (Landmark edition)*, *16*(1), 151-168. https://doi.org/10.2741/3681

Li, B., Qin, Y., Yu, X., Xu, X., & Yu, W. (2022). Lipid raft involvement in signal transduction in cancer cell survival, cell death and metastasis. *Cell proliferation*, *55*(1). https://doi.org/10.1111/CPR.13167

Li, N., Shaw, A. R. E., Zhang, N., Mak, A., & Li, L. (2004). Lipid raft proteomics: Analysis of in-solution digest of sodium dodecyl sulfate-solubilized lipid raft proteins by liquid chromatography-matrix-assisted laser desorption/ionization tandem mass spectrometry. *PROTEOMICS*, *4*(10), 3156-3166. https://doi.org/10.1002/pmic.200400832

Li, S., Wang, L., Xu, Z., Huang, Y., Xue, R., Yue, T., Xu, L., Gong, F., Bai, S., Wu, Q., Liu, J., Lin, B., Zhang, H., Xue, Y., Xu, P., Hou, J., Yang, X., Jin, T., Zhou, R., … Bai, L. (2021). ASC deglutathionylation is a checkpoint for NLRP3 inflammasome activation. *The Journal of Experimental Medicine*, *218*(9), e20202637. https://doi.org/10.1084/jem.20202637

Li, Y., Bai, H., Li, C., & Shi, G. (2011). Colorimetric Assays for Acetylcholinesterase Activity and Inhibitor Screening Based on the Disassembly–Assembly of a Water-Soluble Polythiophene Derivative. *ACS Applied Materials & Interfaces*, *3*(4), 1306-1310. https://doi.org/10.1021/am200101n

Li, Y. C., Park, M. J., Ye, S. K., Kim, C. W., & Kim, Y. N. (2006). Elevated levels of cholesterol-rich lipid rafts in cancer cells are correlated with apoptosis sensitivity induced by cholesterol-depleting agents. *The American journal of pathology*, *168*(4), 1107-1118. https://doi.org/10.2353/AJPATH.2006.050959

Li, Y., Park, J.-S., Deng, J.-H., & Bai, Y. (2006). Cytochrome c oxidase subunit IV is essential for assembly and respiratory function of the enzyme complex. *Journal of Bioenergetics and Biomembranes*, *38*(5-6), 283-291. https://doi.org/10.1007/s10863-006-9052-z

Lin, M. T., & Beal, M. F. (2006). Mitochondrial dysfunction and oxidative stress in neurodegenerative diseases. *Nature*, *443*(7113), 787-795. https://doi.org/10.1038/NATURE05292

Liu, A., Chang, J., Lin, Y., Shen, Z., & Bernstein, P. S. (2010). Long-chain and very long-chain polyunsaturated fatty acids in ocular aging and age-related macular degeneration. *Journal of Lipid Research*, *51*(11), 3217-3229. https://doi.org/10.1194/jlr.m007518

López-Álvarez, J., Zea Sevilla, M. A., Agüera Ortiz, L., Fernández Blázquez, M. Á., Valentí Soler, M., & Martínez-Martín, P. (2015). Effect of anticholinergic drugs on cognitive

impairment in the elderly. *Revista de Psiquiatría y Salud Mental (English Edition)*, *8*(1), 35-43. https://doi.org/10.1016/j.rpsmen.2015.03.001

Lu, S. M., & Fairn, G. D. (2018). Mesoscale organization of domains in the plasma membrane—Beyond the lipid raft. *Critical reviews in biochemistry and molecular biology*, *53*(2), 192-207. https://doi.org/10.1080/10409238.2018.1436515

Lucero, H. A., & Robbins, P. W. (2004). Lipid rafts–protein association and the regulation of protein activity. *Archives of Biochemistry and Biophysics*, *426*(2), 208-224. https://doi.org/10.1016/J.ABB.2004.03.020

Lucken-Ardjomande Hasler, S. (2012). Cholesterol, cardiolipin, and mitochondria permeabilisation. *Anti-Cancer Agents in Medicinal Chemistry*, *12*(4), 329-339. https://doi.org/10.2174/187152012800228724

Malaplate-Armand, C., Florent-Béchard, S., Youssef, I., Koziel, V., Sponne, I., Kriem, B., Leininger-Muller, B., Olivier, J.-L., Oster, T., & Pillot, T. (2006). Soluble oligomers of amyloid-β peptide induce neuronal apoptosis by activating a cPLA2-dependent sphingomyelinase-ceramide pathway. *Neurobiology of Disease*, *23*(1), 178-189. https://doi.org/10.1016/j.nbd.2006.02.010

Mallajosyula, J. K., Kaur, D., Chinta, S. J., Rajagopalan, S., Rane, A., Nicholls, D. G., Di Monte, D. A., Macarthur, H., & Andersen, J. K. (2008). MAO-B elevation in mouse brain astrocytes results in Parkinson's pathology. *PloS one*, *3*(2). https://doi.org/10.1371/JOURNAL.PONE.0001616

Manuel, I., Barreda-Gomez, G., González De San Román, E., Veloso, A., Fernández, J. A., Giralt, M. T., & Rodriguez-Puertas, R. (2015). Neurotransmitter receptor localization: From autoradiography to imaging mass spectrometry. *ACS chemical neuroscience*, *6*(3), 362-373. https://doi.org/10.1021/CN500281T

Marin, R., Fabelo, N., Fernández-Echevarría, C., Canerina-Amaro, A., Rodríguez-Barreto, D., Quinto-Alemany, D., Mesa-Herrera, F., & Díaz, M. (2016). Lipid Raft Alterations in Aged-Associated Neuropathologies. *Current Alzheimer research*, *13*(9), 973-984. https://doi.org/10.2174/1567205013666160314150017

Marquardt, D., Kučerka, N., Wassall, S. R., Harroun, T. A., & Katsaras, J. (2016). Cholesterol's location in lipid bilayers. *Chemistry and Physics of Lipids*, *199*, 17-25. https://doi.org/10.1016/j.chemphyslip.2016.04.001

Marquer, C., Devauges, V., Cossec, J. C., Liot, G., Lécart, S., Saudou, F., Duyckaerts, C.,

Lévêque-Fort, S., & Potier, M. C. (2011). Local cholesterol increase triggers amyloid precursor protein-Bace1 clustering in lipid rafts and rapid endocytosis. *FASEB journal : official publication of the Federation of American Societies for Experimental Biology*, *25*(4), 1295-1305. https://doi.org/10.1096/FJ.10-168633

Martellucci, S., Santacroce, C., Santilli, F., Manganelli, V., Sorice, M., & Mattei, V. (2020). Prion Protein in Stem Cells: A Lipid Raft Component Involved in the Cellular Differentiation Process. *International journal of molecular sciences*, *21*(11), 1-12. https://doi.org/10.3390/IJMS21114168

Martellucci, S., Santacroce, C., Santilli, F., Piccoli, L., Monache, S. D., Angelucci, A., Misasi, R., Sorice, M., & Mattei, V. (2019). Cellular and Molecular Mechanisms Mediated by recPrPC Involved in the Neuronal Differentiation Process of Mesenchymal Stem Cells. *International Journal of Molecular Sciences*, *20*(2), 345. https://doi.org/10.3390/IJMS20020345

Martosella, J., Zolotarjova, N., Liu, H., Moyer, S. C., Perkins, P. D., & Boyes, B. E. (2006). High Recovery HPLC Separation of Lipid Rafts for Membrane Proteome Analysis. *Journal of Proteome Research*, *5*(6), 1301-1312. https://doi.org/10.1021/pr060051g

Matsuki, H., Goto, M., & Tamai, N. (2019). Membrane States of Saturated Glycerophospholipids: A Thermodynamic Study of Bilayer Phase Transitions. *Chemical & pharmaceutical bulletin*, *67*(4), 300-307. https://doi.org/10.1248/CPB.C18-00954

Mattei, V., Martellucci, S., Santilli, F., Manganelli, V., Garofalo, T., Candelise, N., Caruso, A., Sorice, M., Scaccianoce, S., & Misasi, R. (2017). Morphine Withdrawal Modifies Prion Protein Expression in Rat Hippocampus. *PloS one*, *12*(1). https://doi.org/10.1371/JOURNAL.PONE.0169571

Medina, J. M., & Tabernero, A. (2002). Astrocyte-synthesized oleic acid behaves as a neurotrophic factor for neurons. *Journal of Physiology-Paris*, *96*(3), 265-271. https://doi.org/10.1016/S0928-4257(02)00015-3

Megha, & London, E. (2004). Ceramide Selectively Displaces Cholesterol from Ordered Lipid Domains (Rafts): IMPLICATIONS FOR LIPID RAFT STRUCTURE AND FUNCTION *. *Journal of Biological Chemistry*, *279*(11), 9997-10004. https://doi.org/10.1074/jbc.M309992200

Mesa-Herrera, F., Taoro-González, L., Valdés-Baizabal, C., Diaz, M., & Marín, R. (2019). Lipid and Lipid Raft Alteration in Aging and Neurodegenerative Diseases: A Window for

the Development of New Biomarkers. *International journal of molecular sciences*, *20*(15). https://doi.org/10.3390/IJMS20153810

Messias, M. C. F., Mecatti, G. C., Priolli, D. G., & De Oliveira Carvalho, P. (2018). Plasmalogen lipids: Functional mechanism and their involvement in gastrointestinal cancer. *Lipids in Health and Disease*, *17*(1), 1-12. https://doi.org/10.1186/S12944-018-0685-9/FIGURES/3

Mîinea, C., Kuruvilla, R., Merrikh, H., & Eichberg, J. (2002). Altered arachidonic acid biosynthesis and antioxidant protection mechanisms in Schwann cells grown in elevated glucose. *Journal of neurochemistry*, *81*(6), 1253-1262. https://doi.org/10.1046/J.1471-4159.2002.00912.X

Miyazawa, T., Burdeos, G. C., Itaya, M., Nakagawa, K., & Miyazawa, T. (2019). Vitamin E: Regulatory Redox Interactions. *IUBMB Life*, *71*(4), 430-441. https://doi.org/10.1002/iub.2008

Mohamed, A., Robinson, H., Erramouspe, P. J., & Hill, M. M. (2018). Advances and challenges in understanding the role of the lipid raft proteome in human health. *Expert Review of Proteomics*, *15*(12), 1053-1063. https://doi.org/10.1080/14789450.2018.1544895

Mollinedo, F., & Gajate, C. (2015). Lipid rafts as major platforms for signaling regulation in cancer. *Advances in biological regulation*, *57*, 130-146. https://doi.org/10.1016/J.JBIOR.2014.10.003

Mollinedo, F., & Gajate, C. (2020). Lipid rafts as signaling hubs in cancer cell survival/death and invasion: Implications in tumor progression and therapy: Thematic Review Series: Biology of Lipid Rafts. *Journal of lipid research*, *61*(5), 611-635. https://doi.org/10.1194/JLR.TR119000439

Molzer, B., Kainz-Korschinsky, M., Sundt-Heller, R., & Bernheimer, H. (1989). Phytanic acid and very long chain fatty acids in genetic peroxisomal disorders. *Journal of Clinical Chemistry and Clinical Biochemistry. Zeitschrift Fur Klinische Chemie Und Klinische Biochemie*, *27*(5), 309-314.

Montenegro, M. F., Cabezas-Herrera, J., Campoy, F. J., Muñoz-Delgado, E., & Vidal, C. J. (2017). Lipid rafts of mouse liver contain nonextended and extended acetylcholinesterase variants along with M3 muscarinic receptors. *FASEB Journal: Official Publication of the Federation of American Societies for Experimental Biology*, *31*(2), 544-555. https://doi.org/10.1096/fj.201600609R

Moral-Naranjo, M. T., Montenegro, M. F., Muñoz-Delgado, E., Campoy, F. J., & Vidal, C. J. (2008). Targeting of acetylcholinesterase to lipid rafts of muscle. *Chemico-biological interactions*, *175*(1-3), 312-317. https://doi.org/10.1016/J.CBI.2008.04.018

Morris, G., Walder, K., Puri, B. K., Berk, M., & Maes, M. (2016). The Deleterious Effects of Oxidative and Nitrosative Stress on Palmitoylation, Membrane Lipid Rafts and Lipid-Based Cellular Signalling: New Drug Targets in Neuroimmune Disorders. *Molecular neurobiology*, *53*(7), 4638-4658. https://doi.org/10.1007/S12035-015-9392-Y

Morrow, I. C., Rea, S., Martin, S., Prior, I. A., Prohaska, R., Hancock, J. F., James, D. E., & Parton, R. G. (2002). Flotillin-1/reggie-2 traffics to surface raft domains via a novel golgi-independent pathway. Identification of a novel membrane targeting domain and a role for palmitoylation. *The Journal of biological chemistry*, *277*(50), 48834-48841. https://doi.org/10.1074/JBC.M209082200

Murphy, M. P. (2009). How mitochondria produce reactive oxygen species. *The Biochemical Journal*, *417*(1), 1-13. https://doi.org/10.1042/BJ20081386

Nash, Y., Schmukler, E., Trudler, D., Pinkas-Kramarski, R., & Frenkel, D. (2017). DJ-1 deficiency impairs autophagy and reduces alpha-synuclein phagocytosis by microglia. *Journal of Neurochemistry*, *143*(5), 584-594. https://doi.org/10.1111/jnc.14222

Nicolson, G. L., & Ferreira de Mattos, G. (2021). A Brief Introduction to Some Aspects of the Fluid–Mosaic Model of Cell Membrane Structure and Its Importance in Membrane Lipid Replacement. *Membranes*, *11*(12), 947. https://doi.org/10.3390/membranes11120947

Niki, E. (2008). Lipid peroxidation products as oxidative stress biomarkers. *BioFactors (Oxford, England)*, *34*(2), 171-180. https://doi.org/10.1002/biof.5520340208

Niki, E., & Noguchi, N. (2021). Antioxidant action of vitamin E in vivo as assessed from its reaction products with multiple biological oxidants. *Free Radical Research*, 55(4), 352-363. https://doi.org/10.1080/10715762.2020.1866181

Nikolova-Karakashian, M. N., & Rozenova, K. A. (2010). Ceramide in stress response. *Advances in Experimental Medicine and Biology*, *688*, 86-108. https://doi.org/10.1007/978-1-4419-6741-1_6

Nolfi-Donegan, D., Braganza, A., & Shiva, S. (2020). Mitochondrial electron transport chain: Oxidative phosphorylation, oxidant production, and methods of measurement. *Redox biology*, *37*. https://doi.org/10.1016/J.REDOX.2020.101674

Ohlendieck, K. (1996). Extraction of membrane proteins. *Methods in molecular biology (Clifton, N.J.), 59*, 293-304. https://doi.org/10.1385/0-89603-336-8:293

Okamoto, Y. (1994). High-sensitivity microwave-induced plasma mass spectrometry for trace element analysis. *Journal of Analytical Atomic Spectrometry*, *9*(7), 745-749. https://doi.org/10.1039/JA9940900745

Okuda, S., Saito, H., & Katsuki, H. (1994). Arachidonic acid: Toxic and trophic effects on cultured hippocampal neurons. *Neuroscience*, *63*(3), 691-699. https://doi.org/10.1016/0306-4522(94)90515-0

Olubodun-Obadun, T. G., Ishola, I. O., & Adeyemi, O. O. (2022). Impact of environmental toxicants exposure on gut-brain axis in Parkinson disease. *Drug Metabolism and Personalized Therapy*, *37*(4), 329-336. https://doi.org/10.1515/dmpt-2021-0144

Op den Kamp, J. A. (1979). Lipid asymmetry in membranes. *Annual review of biochemistry*, *48*, 47-71. https://doi.org/10.1146/ANNUREV.BI.48.070179.000403

Owen, D. M., Williamson, D. J., Magenau, A., & Gaus, K. (2012). Sub-resolution lipid domains exist in the plasma membrane and regulate protein diffusion and distribution. *Nature Communications 2012 3:1*, *3*(1), 1-8. https://doi.org/10.1038/ncomms2273

Oyewole, A. O., & Birch-Machin, M. A. (2015). Mitochondria-targeted antioxidants. *FASEB journal : official publication of the Federation of American Societies for Experimental Biology*, *29*(12), 4766-4771. https://doi.org/10.1096/FJ.15-275404

Panchal, M., Gaudin, M., Lazar, A. N., Salvati, E., Rivals, I., Ayciriex, S., Dauphinot, L., Dargère, D., Auzeil, N., Masserini, M., Laprévote, O., & Duyckaerts, C. (2014). Ceramides and sphingomyelinases in senile plaques. *Neurobiology of disease*, *65*, 193-201. https://doi.org/10.1016/J.NBD.2014.01.010

Pascua Maestro, R. (2018). *Identification of a new mechanism for preserving lysosomal functional integrity upon oxidative stress*. https://doi.org/10.35376/10324/33119

Patel, H. H., Murray, F., & Insel, P. A. (2008). G-protein-coupled receptor-signaling components in membrane raft and caveolae microdomains. *Handbook of experimental pharmacology*, *186*(186), 167-184. https://doi.org/10.1007/978-3-540-72843-6_7

Pekny, M., & Nilsson, M. (2005). Astrocyte activation and reactive gliosis. *Glia*, *50*(4), 427-434. https://doi.org/10.1002/glia.20207

Picaud, V., Giovannelli, J. F., Truntzer, C., Charrier, J. P., Giremus, A., Grangeat, P., &

Mercier, C. (2018). Linear MALDI-ToF simultaneous spectrum deconvolution and baseline removal. *BMC bioinformatics*, *19*(1). https://doi.org/10.1186/S12859-018-2116-3

Poleschuk, T. S., Sultanov, R. M., Ermolenko, E. V., Shulgina, L. V., & Kasyanov, S. P. (2020). Protective action of alkylglycerols under stress. *Stress (Amsterdam, Netherlands)*, *23*(2), 213-220. https://doi.org/10.1080/10253890.2019.1660316

Popov-Čeleketic, D., & van Bergen en Henegouwen, P. M. P. (2014). Membrane domain formation-a key factor for targeted intracellular drug delivery. *Frontiers in physiology*, *5*(Nov). https://doi.org/10.3389/FPHYS.2014.00462

Poulos, A., Beckman, K., Johnson, D. W., Paton, B. C., Robinson, B. S., Sharp, P., Usher, S., & Singh, H. (1992). Very Long-Chain Fatty Acids in Peroxisomal Disease. En N. G. Bazan, M. G. Murphy, & G. Toffano (Eds.), *Neurobiology of Essential Fatty Acids* (pp. 331-340). Springer US. https://doi.org/10.1007/978-1-4615-3426-6_30

Quinlivan, V. H., Wilson, M. H., Ruzicka, J., & Farber, S. A. (2017). An HPLC-CAD/fluorescence lipidomics platform using fluorescent fatty acids as metabolic tracers. *Journal of Lipid Research*, *58*(5), 1008-1020. https://doi.org/10.1194/jlr.D072918

Quinn, P. J. (2002). Plasma membrane phospholipid asymmetry. *Sub-cellular biochemistry*, *36*, 39-60. https://doi.org/10.1007/0-306-47931-1_3

Ramana, K. V., Srivastava, S., & Singhal, S. S. (2014). Lipid peroxidation products in human health and disease 2014. *Oxidative Medicine and Cellular Longevity*, *2014*, 162414. https://doi.org/10.1155/2014/162414

Rapoport, S. I. (2008). Arachidonic Acid and the Brain. *The Journal of Nutrition*, *138*(12), 2515-2520.

Ray, P. D., Huang, B. W., & Tsuji, Y. (2012). Reactive oxygen species (ROS) homeostasis and redox regulation in cellular signaling. *Cellular signalling*, *24*(5), 981. https://doi.org/10.1016/J.CELLSIG.2012.01.008

Rehling, P., Brandner, K., & Pfanner, N. (2004). Mitochondrial import and the twin-pore translocase. *Nature reviews. Molecular cell biology*, *5*(7), 519-530. https://doi.org/10.1038/NRM1426

Rich, P. R., & Maréchal, A. (2010). The mitochondrial respiratory chain. *Essays in biochemistry*, *47*, 1-23. https://doi.org/10.1042/BSE0470001

Ritchie, S. A., Ahiahonu, P. W., Jayasinghe, D., Heath, D., Liu, J., Lu, Y., Jin, W.,

Kavianpour, A., Yamazaki, Y., Khan, A. M., Hossain, M., Su-Myat, K. K., Wood, P. L., Krenitsky, K., Takemasa, I., Miyake, M., Sekimoto, M., Monden, M., Matsubara, H., … Goodenowe, D. B. (2010). Reduced levels of hydroxylated, polyunsaturated ultra long-chain fatty acids in the serum of colorectal cancer patients: Implications for early screening and detection. *BMC Medicine*, *8*(1), 13. https://doi.org/10.1186/1741-7015-8-13

Rodriguez-Puertas, R., Barreda-Gómez, G., Fernández González, J. A., Astigarraga, E., Aranzabe García, A., Marcaide Rodríguez, A., & Gómez Plaza, D. (2009). *Method for the surface treatment of solid substrated*.

Rothfield, L., & Finkelstein, A. (1968). Membrane biochemistry. *Annual review of biochemistry*, *37*, 463-496. https://doi.org/10.1146/ANNUREV.BI.37.070168.002335

Sáez-Valero, J., Fodero, L. R., White, A. R., Barrow, C. J., & Small, D. H. (2003). Acetylcholinesterase is increased in mouse neuronal and astrocyte cultures after treatment with beta-amyloid peptides. *Brain Research*, *965*(1-2), 283-286. https://doi.org/10.1016/s0006-8993(02)04159-8

Sainani, K. L. (2014). Introduction to principal components analysis. *PM & R : the journal of injury, function, and rehabilitation*, *6*(3), 275-278. https://doi.org/10.1016/J.PMRJ.2014.02.001

Sanchez, V., Galor, A., Jensen, K., Mondal, K., & Mandal, N. (2022). Relationships between ocular surface sphingomyelinases, Meibum and Tear Sphingolipids, and clinical parameters of meibomian gland dysfunction. *The Ocular Surface*, *25*, 101-107. https://doi.org/10.1016/j.jtos.2022.06.003

Sánchez-Sánchez, L., García, J., Fernández, Roberto, Noskova, E., Egiguren-Ortiz, J., Gulak, M., Ochoa, E., Laso, A., Oiarbide, M., Santos, J. I., Andrés, M. F., González-Coloma, A., Adell, A., Astigarraga, E., & Barreda-Gómez, G. (2023, febrero 14). Characterization of the Antitumor Potential of Extracts of Cannabis sativa Strains with High CBD Content in Human Neuroblastoma. *International Journal of Molecular Sciences*, *24*(4). https://www.mdpi.com/1422-0067/24/4/3837

Santiago Valtierra, F. X., Mateos, M. V., Aveldaño, M. I., & Oresti, G. M. (2017). Sphingomyelins and ceramides with VLCPUFAs are excluded from low-density raft-like domains in differentiating spermatogenic cells. *Journal of Lipid Research*, *58*(3), 529-542. https://doi.org/10.1194/jlr.M072595

Schägger, H. (2001). Respiratory chain supercomplexes. *IUBMB Life*, *52*(3-5), 119-128.

https://doi.org/10.1080/15216540152845911

Schägger, H., & Pfeiffer, K. (2001). The ratio of oxidative phosphorylation complexes I-V in bovine heart mitochondria and the composition of respiratory chain supercomplexes. *The Journal of biological chemistry*, *276*(41), 37861-37867. https://doi.org/10.1074/JBC.M106474200

Scheiblich, H., Schlütter, A., Golenbock, D. T., Latz, E., Martinez-Martinez, P., & Heneka, M. T. (2017). Activation of the NLRP3 inflammasome in microglia: The role of ceramide. *Journal of Neurochemistry*, *143*(5), 534-550. https://doi.org/10.1111/jnc.14225

Schmid, F. (2017). Physical mechanisms of micro- and nanodomain formation in multicomponent lipid membranes. *Biochimica et Biophysica Acta (BBA) - Biomembranes*, *1859*(4), 509-528. https://doi.org/10.1016/J.BBAMEM.2016.10.021

Schütze, S., Potthoff, K., Machleidt, T., Berkovic, D., Wiegmann, K., & Krönke, M. (1992). TNF activates NF-kappa B by phosphatidylcholine-specific phospholipase C-induced «acidic» sphingomyelin breakdown. *Cell*, *71*(5), 765-776. https://doi.org/10.1016/0092-8674(92)90553-O

Schwall, C. T., Greenwood, V. L., & Alder, N. N. (2012). The stability and activity of respiratory Complex II is cardiolipin-dependent. *Biochimica et Biophysica Acta (BBA) - Bioenergetics*, *1817*(9), 1588-1596. https://doi.org/10.1016/j.bbabio.2012.04.015

Scialò, F., Fernández-Ayala, D. J., & Sanz, A. (2017). Role of Mitochondrial Reverse Electron Transport in ROS Signaling: Potential Roles in Health and Disease. *Frontiers in Physiology*, *8*, 428. https://doi.org/10.3389/fphys.2017.00428

Sebastian, T. T., Baldridge, R. D., Xu, P., & Graham, T. R. (2012). Phospholipid flippases: Building asymmetric membranes and transport vesicles. *Biochimica et biophysica acta*, *1821*(8), 1068-1077. https://doi.org/10.1016/J.BBALIP.2011.12.007

Selvin, P. C., & Fujii, T. (2001). Lithium ion attachment mass spectrometry: Instrumentation and features. *Review of Scientific Instruments*, *72*(5), 2248-2252. https://doi.org/10.1063/1.1362439

Senoner, T., & Dichtl, W. (2019). Oxidative Stress in Cardiovascular Diseases: Still a Therapeutic Target? *Nutrients*, *11*(9). https://doi.org/10.3390/nu11092090

Sezgin, E., Levental, I., Mayor, S., & Eggeling, C. (2017). The mystery of membrane organization: Composition, regulation and roles of lipid rafts. *Nature reviews. Molecular*

cell biology, *18*(6), 361-374. https://doi.org/10.1038/NRM.2017.16

Shayman, J. A., & Tesmer, J. J. G. (2019). Lysosomal phospholipase A2. *Biochimica et biophysica acta. Molecular and cell biology of lipids*, *1864*(6), 932. https://doi.org/10.1016/J.BBALIP.2018.07.012

Shindo, Y., Witt, E., Han, D., Epstein, W., & Packer, L. (1994). Enzymic and non-enzymic antioxidants in epidermis and dermis of human skin. *The Journal of investigative dermatology*, *102*(1), 122-124. https://doi.org/10.1111/1523-1747.EP12371744

Shinoda, T., Shinya, N., Ito, K., Ishizuka-Katsura, Y., Ohsawa, N., Terada, T., Hirata, K., Kawano, Y., Yamamoto, M., Tomita, T., Ishibashi, Y., Hirabayashi, Y., Kimura-Someya, T., Shirouzu, M., & Yokoyama, S. (2016). Cell-free methods to produce structurally intact mammalian membrane proteins. *Scientific Reports*, *6*. https://doi.org/10.1038/SREP30442

Simons, K., & Ikonen, E. (1997). Functional rafts in cell membranes. *Nature*, *387*(6633), 569-572. https://doi.org/10.1038/42408

Sindelar, P. J., Guan, Z., Dallner, G., & Ernster, L. (1999). The protective role of plasmalogens in iron-induced lipid peroxidation. *Free radical biology & medicine*, *26*(3-4), 318-324. https://doi.org/10.1016/S0891-5849(98)00221-4

Smith, S. M. (2017). Strategies for the Purification of Membrane Proteins. *Methods in molecular biology (Clifton, N.J.)*, *1485*, 389-400. https://doi.org/10.1007/978-1-4939-6412-3_21

Song, Y. S., Annalora, A. J., Marcus, C. B., Jefcoate, C. R., Sorenson, C. M., & Sheibani, N. (2022). Cytochrome P450 1B1: A Key Regulator of Ocular Iron Homeostasis and Oxidative Stress. *Cells*, *11*(19). https://doi.org/10.3390/CELLS11192930

Sorice, M., Manganelli, V., Matarrese, P., Tinari, A., Misasi, R., Malorni, W., & Garofalo, T. (2009). Cardiolipin-enriched raft-like microdomains are essential activating platforms for apoptotic signals on mitochondria. *FEBS letters*, *583*(15), 2447-2450. https://doi.org/10.1016/J.FEBSLET.2009.07.018

Souda, P., Ryan, C. M., Cramer, W. A., & Whitelegge, J. (2011). Profiling of integral membrane proteins and their post translational modifications using high-resolution mass spectrometry. *Methods (San Diego, Calif.)*, 55(4), 330. https://doi.org/10.1016/J.YMETH.2011.09.019

Sousa, J. S., D'Imprima, E., & Vonck, J. (2018). Mitochondrial Respiratory Chain Complexes.

Sub-cellular biochemistry, *87*, 167-227. https://doi.org/10.1007/978-981-10-7757-9_7

Spector, A. A., & Yorek, M. A. (1985). Membrane lipid composition and cellular function. *Journal of Lipid Research*, *26*(9), 1015-1035.

Stephan, K., & Ott, M. (2020). Timing of dimerization of the bc1 complex during mitochondrial respiratory chain assembly. *Biochimica Et Biophysica Acta. Bioenergetics*, *1861*(5-6), 148177. https://doi.org/10.1016/j.bbabio.2020.148177

Sviridov, D., Mukhamedova, N., & Miller, Y. I. (2020). Lipid rafts as a therapeutic target. *Journal of lipid research*, *61*(5), 687-695. https://doi.org/10.1194/JLR.TR120000658

Tanaka, K., Waki, H., Ido, Y., Akita, S., Yoshida, Y., Yoshida, T., & Matsuo, T. (1988). Protein and polymer analyses up tom/z 100 000 by laser ionization time-of-flight mass spectrometry. *Rapid Communications in Mass Spectrometry*, *2*(8), 151-153. https://doi.org/10.1002/rcm.1290020802

Tengstrand, E. A., Miwa, G. T., & Hsieh, F. Y. (2010). Bis(monoacylglycerol)phosphate as a non-invasive biomarker to monitor the onset and time-course of phospholipidosis with drug-induced toxicities. *Expert Opinion on Drug Metabolism & Toxicology*, *6*(5), 555-570. https://doi.org/10.1517/17425251003601961

Thomas, J. M., Sudhadevi, T., Basa, P., Ha, A. W., Natarajan, V., & Harijith, A. (2022). The Role of Sphingolipid Signaling in Oxidative Lung Injury and Pathogenesis of Bronchopulmonary Dysplasia. *International Journal of Molecular Sciences*, *23*(3), 23. https://doi.org/10.3390/IJMS23031254

Tipton, K. F. (2018). 90 years of monoamine oxidase: Some progress and some confusion. *Journal of neural transmission (Vienna, Austria : 1996)*, *125*(11), 1519-1551. https://doi.org/10.1007/S00702-018-1881-5

Trumpower, B. L. (1991). The three-subunit cytochrome bc1 complex of Paracoccus denitrificans. Its physiological function, structure, and mechanism of electron transfer and energy transduction. *Journal of Bioenergetics and Biomembranes*, *23*(2), 241-255. https://doi.org/10.1007/BF00762220

Tsuchiya, H., & Mizogami, M. (2020). Interaction of drugs with lipid raft membrane domains as a possible target. *Drug target insights*, *14*(1), 34-47. https://doi.org/10.33393/DTI.2020.2185

Udagawa, J., & Hino, K. (2022). Plasmalogen in the brain: Effects on cognitive functions

and behaviors attributable to its properties. *Brain research bulletin*, *188*, 197-202. https://doi.org/10.1016/J.BRAINRESBULL.2022.08.008

Usmanov, D. T., Ninomiya, S., Chen, L. C., Saha, S., Mandal, M. K., Sakai, Y., Takaishi, R., Habib, A., Hiraoka, K., Yoshimura, K., Takeda, S., Wada, H., & Nonami, H. (2017). Desorption in Mass Spectrometry. *Mass Spectrometry*, *6*(Spec Iss), S0059. https://doi.org/10.5702/massspectrometry.S0059

Van Der Goot, F. G., & Harder, T. (2001). Raft membrane domains: From a liquid-ordered membrane phase to a site of pathogen attack. *Seminars in Immunology*, *13*(2), 89-97. https://doi.org/10.1006/smim.2000.0300

Vandenabeele, P., & Fiers, W. (1991). Is amyloidogenesis during Alzheimer's disease due to an IL-1-/IL-6-mediated 'acute phase response' in the brain? *Immunology Today*, *12*(7), 217-219. https://doi.org/10.1016/0167-5699(91)90032-O

Vatner, S. F., Zhang, J., Oydanich, M., Berkman, T., Naftalovich, R., & Vatner, D. E. (2020). Healthful aging mediated by inhibition of oxidative stress. *Ageing research reviews*, *64*. https://doi.org/10.1016/J.ARR.2020.101194

Vetrivel, K. S., Cheng, H., Lin, W., Sakurai, T., Li, T., Nukina, N., Wong, P. C., Xu, H., & Thinakaran, G. (2004). Association of γ-secretase with lipid rafts in post-golgi and endosome membranes. *Journal of Biological Chemistry*, *279*(43), 44945-44954. https://doi.org/10.1074/jbc.M407986200

Vorobyov, I., & Allen, T. W. (2011). On the role of anionic lipids in charged protein interactions with membranes. *Biochimica Et Biophysica Acta*, *1808*(6), 1673-1683. https://doi.org/10.1016/j.bbamem.2010.11.009

Wahrle, S., Das, P., Nyborg, A. C., McLendon, C., Shoji, M., Kawarabayashi, T., Younkin, L. H., Younkin, S. G., & Golde, T. E. (2002). Cholesterol-dependent γ-secretase activity in buoyant cholesterol-rich membrane microdomains. *Neurobiology of Disease*, *9*(1), 11-23. https://doi.org/10.1006/nbdi.2001.0470

Wang, M., Gu, X., Zhang, G., Zhang, D., & Zhu, D. (2009). Continuous Colorimetric Assay for Acetylcholinesterase and Inhibitor Screening with Gold Nanoparticles. *Langmuir*, *25*(4), 2504-2507. https://doi.org/10.1021/la803870v

Wang, X., Sun, J., Zhao, X.-E., Xu, Y., Sun, L., Zhu, S., You, J., & Wang, X. (2019). Stable isotope labeling derivatization coupled with magnetic dispersive solid phase extraction for the determination of hydroxyl-containing cholesterol and metabolites by in vivo

microdialysis and ultra-high performance liquid chromatography tandem mass spectrometry. *Journal of Chromatography. A*, *1594*, 23-33. https://doi.org/10.1016/j.chroma.2019.02.021

Wilkerson, J. L., Basu, S. K., Stiles, M. A., Prislovsky, A., Grambergs, R. C., Nicholas, S. E., Karamichos, D., Allegood, J. C., Proia, R. L., & Mandal, N. (2022). Ablation of Sphingosine Kinase 1 Protects Cornea from Neovascularization in a Mouse Corneal Injury Model. *Cells*, *11*(18). https://doi.org/10.3390/cells11182914

Wodlej, C., Riedl, S., Rinner, B., Leber, R., Drechsler, C., Voelker, D. R., Choi, J.-Y., Lohner, K., & Zweytick, D. (2019). Interaction of two antitumor peptides with membrane lipids—Influence of phosphatidylserine and cholesterol on specificity for melanoma cells. *PloS One*, *14*(1), e0211187. https://doi.org/10.1371/journal.pone.0211187

Wollnik, H. (1993). Time-of-flight mass analyzers. *Mass Spectrometry Reviews*, *12*(2), 89-114. https://doi.org/10.1002/mas.1280120202

Wong, E., Liao, G. P., Chang, J. C., Xu, P., Li, Y.-M., & Greengard, P. (2019). GSAP modulates γ-secretase specificity by inducing conformational change in PS1. *Proceedings of the National Academy of Sciences of the United States of America*, *116*(13), 6385-6390. https://doi.org/10.1073/pnas.1820160116

Yahi, N., Di Scala, C., Chahinian, H., & Fantini, J. (2022). Innovative treatment targeting gangliosides aimed at blocking the formation of neurotoxic α-synuclein oligomers in Parkinson's disease. *Glycoconjugate journal*, *39*(1). https://doi.org/10.1007/S10719-021-10012-0

Yamashita, A., Oka, S., Tanikawa, T., Hayashi, Y., Nemoto-Sasaki, Y., & Sugiura, T. (2013). The actions and metabolism of lysophosphatidylinositol, an endogenous agonist for GPR55. *Prostaglandins & Other Lipid Mediators*, *107*, 103-116. https://doi.org/10.1016/J.PROSTAGLANDINS.2013.05.004

Yang, S., & Lian, G. (2020). ROS and diseases: Role in metabolism and energy supply. *Molecular and cellular biochemistry*, *467*(1-2). https://doi.org/10.1007/S11010-019-03667-9

Yokoyama, H., & Matsui, I. (2020). The lipid raft markers stomatin, prohibitin, flotillin, and HflK/C (SPFH)-domain proteins form an operon with NfeD proteins and function with apolar polyisoprenoid lipids. *Critical reviews in microbiology*, *46*(1), 38-48. https://doi.org/10.1080/1040841X.2020.1716682

Youdim, M. B. H., Edmondson, D., & Tipton, K. F. (2006). The therapeutic potential of

monoamine oxidase inhibitors. *Nature reviews. Neuroscience*, *7*(4), 295-309. https://doi.org/10.1038/NRN1883

Yu, H., Wakim, B., Li, M., Halligan, B., Tint, G. S., & Patel, S. B. (2007). Quantifying raft proteins in neonatal mouse brain by «tube-gel» protein digestion label-free shotgun proteomics. *Proteome Science*, *5*, 17. https://doi.org/10.1186/1477-5956-5-17

Yu, L., Fan, J., Zhou, C., & Xu, C. (2021). Sterols are required for the coordinated assembly of lipid droplets in developing seeds. *Nature Communications*, *12*(1), Article 1. https://doi.org/10.1038/s41467-021-25908-6

Yusupov, M., Wende, K., Kupsch, S., Neyts, E. C., Reuter, S., & Bogaerts, A. (2017). Effect of head group and lipid tail oxidation in the cell membrane revealed through integrated simulations and experiments. *Scientific Reports*, *7*(1), 5761. https://doi.org/10.1038/s41598-017-06412-8

Zakharova, I. O., Bayunova, L. V., Zorina, I. I., Sokolova, T. V., Shpakov, A. O., & Avrova, N. F. (2021). Insulin and α-tocopherol enhance the protective effect of each other on brain cortical neurons under oxidative stress conditions and in rat two-vessel forebrain ischemia/reperfusion injury. *International Journal of Molecular Sciences*, *22*(21). https://doi.org/10.3390/IJMS222111768/S1

Zhang, N., Shaw, A. R. E., Li, N., Chen, R., Mak, A., Hu, X., Young, N., Wishart, D., & Li, L. (2008). Liquid chromatography electrospray ionization and matrix-assisted laser desorption ionization tandem mass spectrometry for the analysis of lipid raft proteome of monocytes. *Analytica Chimica Acta*, *627*(1), 82-90. https://doi.org/10.1016/j.aca.2008.05.058

Zhang, P.-Y., Xu, X., Li, X.-C., & Zhang, P. (2014). Cardiovascular diseases: Oxidative damage and antioxidant protection. *Eur Rev Med Pharmacol Sci*, *18*, 3091-3096.

Zhao, R.-Z., Jiang, S., Zhang, L., & Yu, Z.-B. (2019). Mitochondrial electron transport chain, ROS generation and uncoupling (Review). *International Journal of Molecular Medicine*, *44*(1), 3-15. https://doi.org/10.3892/ijmm.2019.4188

Zhao, Y., Hu, X., Liu, Y., Dong, S., Wen, Z., He, W., Zhang, S., Huang, Q., & Shi, M. (2017). ROS signaling under metabolic stress: Cross-talk between AMPK and AKT pathway. *Molecular Cancer*, *16*(1), 79. https://doi.org/10.1186/s12943-017-0648-1

Ziegler, A. B., & Tavosanis, G. (2019). Glycerophospholipids—Emerging players in neuronal dendrite branching and outgrowth. *Developmental biology*, *451*(1), 25-34.

https://doi.org/10.1016/J.YDBIO.2018.12.009

Zingg, J. M. (2019). Vitamin E: Regulatory Role on Signal Transduction. *IUBMB life*, *71*(4), 456-478. https://doi.org/10.1002/IUB.1986

Zwara, A., Wertheim-Tysarowska, K., & Mika, A. (2021). Alterations of Ultra Long-Chain Fatty Acids in Hereditary Skin Diseases-Review Article. *Frontiers in medicine*, *8*. https://doi.org/10.3389/FMED.2021.730855

APPENDIX

APPENDIX I

Table 6: List of all lipids identified in paraquat-treated and non-treated samples using MALDI-MS. Changes are expressed as change-percentage of paraquat-treated samples respect control.

PARAQUAT-TREATED ASTROCYTES VS CONTROL							
Lipid adduct	**Regulation**	**Lipid adduct**	**Regulation**	**Lipid adduct**	**Regulation**	**Lipid adduct**	**Regulation**
Cer 40:0;O3	Up	PC 28:0	Up	PC O-32:0	Up	PE O-38:7	Up
Cer 40:1;O3	Up	PC 29:0	No changes	PC O-32:1	Up	PE O-40:5	No changes
Cer 40:2;O3	Up	PC 29:1	Up	PC O-32:2	Up	PE O-40:6	Up
DG 37:0	Up	PC 30:0	Down	PC O-33:0	No changes	PG 21:1;O	Up
DG 42:11	Up	PC 30:1	Up	PC O-34:1	Up	PG 32:0	Up
DG 44:11	No changes	PC 31:0	Up	PC O-34:2	Up	PG 32:1	Up
DG 44:12	Up	PC 31:1	Up	PC O-34:3	Up	PG 34:0	Up
DG O-34:1	No changes	PC 31:2	Up	PC O-36:1	Up	PG 34:2	Up
HexCer 32:2;O3	Up	PC 32:0	Down	PC O-36:2	Up	PG 36:1	Up
HexCer 37:1;O3	Up	PC 32:1	Up	PC O-36:3	Up	PG 36:2	Up
LPC 14:0/PC O-14:0	Up	PC 32:2	Up	PC O-36:4	Up	PG 44:10	Up
LPC 16:0/PC O-16:0	Up	PC 33:0	Up	PC O-36:5	Up	PG O-40:7	Down
LPC 16:1	Up	PC 33:1	Up	PC O-38:5	Up	PI 32:0	Up
LPC 18:0/PC O-18:0	No changes	PC 33:2	Up	PC O-38:6	Up	PI 32:1	Up
LPC 18:1/PC O-18:1	Up	PC 33:4	No changes	PC O-38:7	Up	PI 32:2	Up
LPC 18:2	No changes	PC 33:5	No changes	PC O-40:4	Up	PI 34:1	Down
LPC O-16:0	Up	PC 34:1	Up	PC O-40:5	No changes	PI 34:2	Up
LPC O-16:1	Up	PC 34:2	Up	PC O-40:7	No changes	PI 35:1	Up
LPI 16:0	Up	PC 34:3	Up	PE 32:0	Up	PI 35:2	Up
LPI 16:1	Up	PC 35:1	Up	PE 32:1	Up	PI 36:1	Down
LPI 18:0	Up	PC 35:2	Up	PE 32:2	Up	PI 36:2	Up
LPI 18:1/PG 21:1;O2	Up	PC 35:3	Up	PE 34:0	Up	PI 36:3	Up
LPI 20:4	Up	PC 35:4	Up	PE 34:1	Down	PI 36:4	Up
PA 24:2;O3	Up	PC 35:5	Up	PE 34:2	Up	PI 37:2	Up
PA 30:0	Up	PC 35:6	Up	PE 35:1	Up	PI 38:2	Up
PA 30:1	Up	PC 36:1	Up	PE 35:2	Up	PI 38:4	Down
PA 31:0	Up	PC 36:2	Up	PE 36:1	Down	PI 38:5	Up
PA 32:0	Up	PC 36:4	Up	PE 36:2	Down	SM 32:1;O2	Up
PA 32:1	Up	PC 36:5	Up	PE 36:3	Up	SM 33:1;O2	Up
PA 32:2	Up	PC 37:2	Up	PE 36:4/PE O-36:5;O	Up	SM 33:2;O2	Up
PA 33:1	Up	PC 37:6	Up	PE 37:1	Up	SM 34:1;O2	Up
PA 34:1	Up	PC 37:7	Up	PE 37:2	Up	SM 34:2;O2	Up
PA 34:2	Up	PC 38:1	No changes	PE 38:1	Up	SM 35:1;O2	No changes
PA 34:3	Up	PC 38:2	Up	PE 38:2	Down	SM 36:1;O2	Down
PA 35:1	Up	PC 38:3	Up	PE 38:3	Up	SM 36:2;O2	No changes
PA 35:2	Up	PC 38:4	Up	PE 38:4/PE O-38:5;O	Up	SM 38:1;O2	No changes
PA 36:1	Up	PC 38:5	Up	PE 38:5/PE O-38:6;O	Up	SM 40:1;O2	Up
PA 36:2	Down	PC 38:6	Up	PE O-32:1	Up	SM 40:2;O2	Up
PA 36:3	Up	PC 38:7	No changes	PE O-32:2	Up	SM 41:1;O2	No changes
PA 36:4	Up	PC 39:7	No changes	PE O-34:0	Up	SM 41:2;O2	No changes
PA 36:7	No changes	PC 40:5	Up	PE O-34:1	Up	SM 42:1;O2	Up
PA 38:2	Up	PC 40:6	Up	PE O-34:2	Up	SM 42:2;O2	Up
PA 38:3	Up	PC 40:7	Up	PE O-34:3	Up	SM 42:3;O2	Up
PA 40:6	Up	PC O-14:0	Up	PE O-36:1	Up	TG 45:5	Up
PA 41:6	Up	PC O-16:0	Up	PE O-36:2	Up		
PA 43:6	Up	PC O-18:0	No changes	PE O-36:3	Up		
PA O-32:1	Up	PC O-18:1	Up	PE O-36:5	Up		
PA O-34:2	Up	PC O-30:0	Up	PE O-36:6	Up		
PA O-36:0	Up	PC O-30:1	Up	PE O-38:5	Up		
PC 19:1	Up	PC O-31:0	No changes	PE O-38:6	Up		

Table 7: List of all lipids identified in paraquat-treated samples with or without α-tocopherol pre-treatment using MALDI-MS. Changes are expressed as change-percentage of α-tocopherol pre-treated respect non-pre-treated paraquat-treated samples.

α-TOCOPHEROL PRE-TREATED VS NON-PRE-TREATED PARAQUAT-TREATED CELLS

Lipid adduct	Regulation	Lipid adduct	Regulation	Lipid adduct	Regulation	Lipid adduct	Regulation
Cer 40:0;O3	Up	PC 28:0	Up	PC O-32:0	Up	PE O-38:7	Down
Cer 40:1;O3	Down	PC 29:0	No changes	PC O-32:1	Up	PE O-40:5	Up
Cer 40:2;O3	Down	PC 29:1	Down	PC O-32:2	Up	PE O-40:6	Up
DG 37:0	Down	PC 30:0	Up	PC O-33:0	Up	PG 21:1;O	Down
DG 42:11	Up	PC 30:1	Up	PC O-34:1	Up	PG 32:0	Down
DG 44:11	Up	PC 31:0	Up	PC O-34:2	Up	PG 32:1	Down
DG 44:12	Up	PC 31:1	Up	PC O-34:3	Down	PG 34:0	Down
DG O-34:1	No changes	PC 31:2	Up	PC O-36:1	Up	PG 34:2	Down
HexCer 32:2;O3	Up	PC 32:0	Up	PC O-36:2	Up	PG 36:1	Up
HexCer 37:1;O3	Up	PC 32:1	Up	PC O-36:3	Up	PG 36:2	Down
LPC 14:0/PC O-14:0	Up	PC 32:2	Up	PC O-36:4	Up	PG 44:10	Down
LPC 16:0/PC O-16:0	Up	PC 33:0	Down	PC O-36:5	Up	PG O-40:7	No changes
LPC 16:1	Up	PC 33:1	Up	PC O-38:5	Up	PI 32:0	Up
LPC 18:0/PC O-18:0	Up	PC 33:2	Down	PC O-38:6	Up	PI 32:1	Down
LPC 18:1/PC O-18:1	Up	PC 33:4	Up	PC O-38:7	Up	PI 32:2	Down
LPC 18:2	No changes	PC 33:5	No changes	PC O-40:4	Down	PI 34:1	Down
LPC O-16:0	Up	PC 34:1	Up	PC O-40:5	Up	PI 34:2	Down
LPC O-16:1	Up	PC 34:2	Up	PC O-40:7	No changes	PI 35:1	Down
LPI 16:0	Down	PC 34:3	Up	PE 32:0	Down	PI 35:2	Down
LPI 16:1	Down	PC 35:1	Up	PE 32:1	Up	PI 36:1	Down
LPI 18:0	Down	PC 35:2	Down	PE 32:2	Down	PI 36:2	Down
LPI 18:1/PG 21:1;O2	Down	PC 35:3	Down	PE 34:0	Down	PI 36:3	Down
LPI 20:4	Up	PC 35:4	Down	PE 34:1	Up	PI 36:4	Down
PA 24:2;O3	Down	PC 35:5	Down	PE 34:2	Up	PI 37:2	Down
PA 30:0	Up	PC 35:6	Up	PE 35:1	Up	PI 38:2	Down
PA 30:1	Up	PC 36:1	Down	PE 35:2	Up	PI 38:4	Down
PA 31:0	Up	PC 36:2	Up	PE 36:1	Up	PI 38:5	Down
PA 32:0	Down	PC 36:4	Down	PE 36:2	Up	SM 32:1;O2	Up
PA 32:1	Up	PC 36:5	Up	PE 36:3	Up	SM 33:1;O2	Up
PA 32:2	Up	PC 37:2	Down	PE 36:4/PE O-36:5;O	Down	SM 33:2;O2	Up
PA 33:1	Up	PC 37:6	Up	PE 37:1	Up	SM 34:1;O2	Up
PA 34:1	Up	PC 37:7	Down	PE 37:2	Up	SM 34:2;O2	Up
PA 34:2	Up	PC 38:1	No changes	PE 38:1	Up	SM 35:1;O2	Up
PA 34:3	Up	PC 38:2	Up	PE 38:2	Up	SM 36:1;O2	Up
PA 35:1	Up	PC 38:3	Up	PE 38:3	Up	SM 36:2;O2	Up
PA 35:2	Up	PC 38:4	Up	PE 38:4/PE O-38:5;O	Up	SM 38:1;O2	Up
PA 36:1	Down	PC 38:5	Up	PE 38:5/PE O-38:6;O	Up	SM 40:1;O2	Up
PA 36:2	Up	PC 38:6	Up	PE O-32:1	Down	SM 40:2;O2	Up
PA 36:3	Up	PC 38:7	Up	PE O-32:2	Down	SM 41:1;O2	No changes
PA 36:4	Up	PC 39:7	Up	PE O-34:0	Down	SM 41:2;O2	Up
PA 36:7	No changes	PC 40:5	Down	PE O-34:1	Up	SM 42:1;O2	Up
PA 38:2	Down	PC 40:6	Down	PE O-34:2	Down	SM 42:2;O2	Up
PA 38:3	Up	PC 40:7	Up	PE O-34:3	Up	SM 42:3;O2	Up
PA 40:6	Down	PC O-14:0	Up	PE O-36:1	Down	TG 45:5	Up
PA 41:6	Down	PC O-16:0	Up	PE O-36:2	Up		
PA 43:6	Up	PC O-18:0	Up	PE O-36:3	Up		
PA O-32:1	Up	PC O-18:1	Up	PE O-36:5	Down		
PA O-34:2	Up	PC O-30:0	Up	PE O-36:6	Down		
PA O-36:0	Down	PC O-30:1	Up	PE O-38:5	Down		
PC 19:1	Up	PC O-31:0	No changes	PE O-38:6	Up		

APPENDIX II

Table 8: Pearson Correlation R coefficients from correlation between spectra in negative ion-mode.

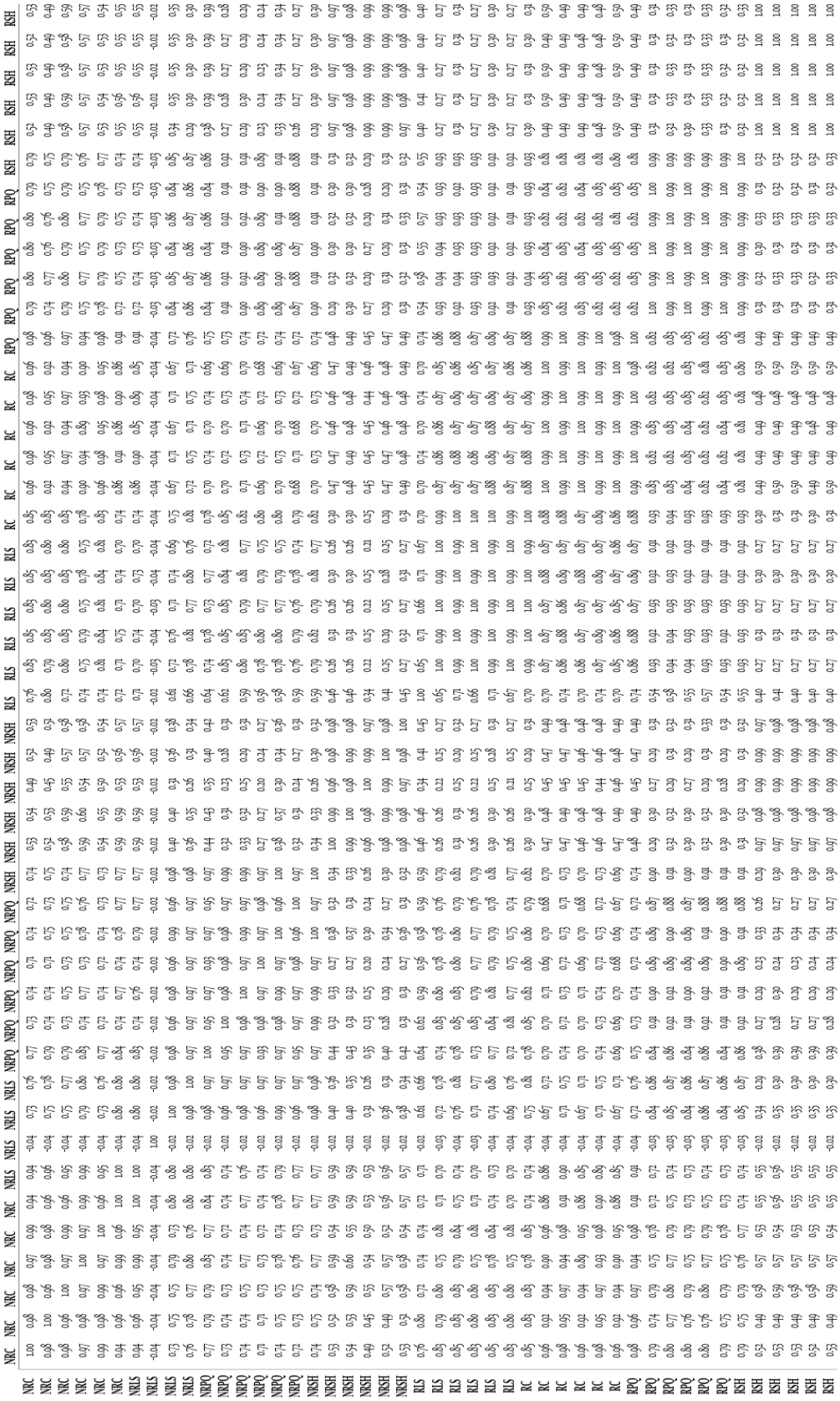

Table 9: Pearson Correlation R coefficients from correlation between spectra in positive ion-mode.

	NRC	NRC	NRC	NRC	NRLS	NRLS	NRLS	NRLS	NRPQ	NRPQ	NRPQ	NRPQ	NRSH	NRSH	NRSH	NRSH	RC	RC	RC	RC	RLS	RLS	RLS	RLS	RPQ	RPQ	RPQ	RPQ	RSH	RSH	RSH	RSH
NRC	1.00	0.96	1.00	0.95	0.94	0.93	0.97	0.85	0.90	0.75	0.93	0.96	0.97	0.85	0.83	0.79	0.81	0.99	0.99	0.98	0.99	0.99	0.92	0.93	0.92	0.94	0.93	0.98	0.98	0.98	0.85	0.86	0.85	0.85
NRC	0.96	1.00	0.97	0.99	0.97	0.95	0.94	0.97	0.88	0.73	0.95	0.96	0.96	0.90	0.85	0.82	0.85	0.97	0.96	0.95	0.96	0.97	0.95	0.98	0.95	0.94	0.97	0.98	0.94	0.94	0.88	0.88	0.84	0.88
NRC	1.00	0.97	1.00	0.95	1.00	0.94	0.93	0.97	0.94	0.95	0.93	0.96	0.97	0.96	0.95	0.91	0.94	1.00	1.00	0.98	0.99	0.99	0.93	0.94	0.93	0.95	0.95	0.98	0.95	0.95	0.85	0.85	0.85	0.85
NRC	0.95	0.99	0.95	1.00	0.98	0.95	0.95	0.91	0.86	0.75	0.93	0.96	0.97	0.84	0.82	0.78	0.82	0.95	0.96	0.93	0.94	0.94	0.99	0.99	0.96	0.93	0.97	0.93	0.91	0.94	0.93	0.87	0.85	0.87
NRC	0.94	0.99	0.94	1.00	1.00	0.98	0.93	0.96	0.93	0.93	0.96	0.94	0.95	0.94	0.93	0.88	0.93	0.94	0.95	0.91	0.93	0.93	0.99	0.97	0.99	0.97	1.00	0.98	0.93	0.93	0.93	0.84	0.82	0.84
NRC	0.93	0.97	0.93	0.98	1.00	0.93	0.96	0.88	0.93	0.93	0.96	0.94	0.95	0.94	0.93	0.88	0.93	0.95	0.96	0.93	0.96	0.96	0.99	0.99	0.99	0.99	0.99	0.94	0.93	0.94	0.94	0.85	0.83	0.82
NRLS	0.94	0.95	0.93	0.95	0.93	1.00	0.98	0.93	0.96	0.93	0.96	0.94	0.95	0.94	0.94	0.91	0.94	0.95	0.96	0.94	0.95	0.96	0.90	0.90	0.91	0.92	0.91	0.92	0.93	0.93	0.93	0.97	0.96	0.97
NRLS	0.97	0.97	0.97	0.96	0.96	0.98	1.00	0.90	0.93	0.88	0.95	0.96	0.96	0.90	0.84	0.87	0.90	0.98	0.98	0.96	0.97	0.97	0.93	0.93	0.93	0.95	0.94	0.95	0.97	0.97	0.97	0.92	0.91	0.92
NRLS	0.95	0.97	0.95	0.93	0.92	0.96	0.97	1.00	0.88	0.94	0.97	0.96	0.97	0.96	0.95	0.94	0.95	0.97	0.97	0.96	0.97	0.97	0.93	0.93	0.93	0.95	0.94	0.95	0.97	0.97	0.97	0.93	0.92	0.93
NRLS	0.91	0.96	0.91	0.89	0.84	0.90	0.96	0.88	1.00	0.87	0.94	0.91	0.94	0.91	0.90	0.87	0.90	0.94	0.94	0.91	0.94	0.94	0.90	0.90	0.90	0.91	0.90	0.91	0.94	0.94	0.94	0.91	0.90	0.91
NRLS	0.90	0.88	0.90	0.88	0.84	0.90	0.88	0.94	0.87	1.00	0.93	0.94	0.95	0.94	0.93	0.90	0.93	0.96	0.96	0.94	0.96	0.96	0.92	0.92	0.92	0.93	0.92	0.93	0.94	0.94	0.94	0.92	0.91	0.92
NRPQ	0.75	0.73	0.76	0.77	0.86	0.75	0.83	0.75	0.55	0.57	1.00	0.90	0.67	0.68	0.65	0.66	0.61	0.65	0.52	0.62	0.76	0.71	0.69	0.76	0.71	0.76	0.69	0.81	0.83	0.83	0.83	0.66	0.65	0.68
NRPQ	0.93	0.95	0.93	0.96	0.96	0.94	0.97	0.86	0.93	0.82	1.00	1.00	0.91	0.91	0.85	0.83	0.80	0.91	0.82	0.91	0.92	0.92	0.90	0.96	0.94	0.96	0.94	0.96	0.95	0.95	0.95	0.85	0.84	0.85
NRPQ	0.96	0.96	0.96	0.96	0.94	0.97	0.96	0.86	0.93	0.82	1.00	1.00	0.91	0.98	0.88	0.88	0.84	0.91	0.82	0.91	0.97	0.97	0.95	0.97	0.96	0.97	0.96	0.97	0.96	0.96	0.96	0.86	0.84	0.86
NRPQ	0.97	0.96	0.97	0.95	0.93	0.96	0.96	0.97	0.96	0.96	0.91	0.91	1.00	0.98	0.98	0.98	0.98	0.98	0.97	0.98	0.98	0.98	0.97	0.98	0.97	0.98	0.97	0.98	0.98	0.98	0.98	0.97	0.96	0.97
NRPQ	0.85	0.90	0.86	0.89	0.86	0.90	0.94	0.85	0.94	0.94	0.88	0.90	0.98	1.00	0.99	0.99	0.99	0.99	0.99	0.99	0.99	0.99	0.99	0.99	0.99	0.99	0.99	0.99	0.99	0.99	0.99	0.99	0.99	0.99
NRPQ	0.97	0.96	0.97	0.95	0.93	0.91	0.96	0.85	0.94	0.94	0.88	0.89	0.98	0.99	1.00	0.99	0.99	0.99	0.99	0.99	0.99	0.99	0.99	0.99	0.99	0.99	0.99	0.99	0.99	0.99	0.99	0.99	0.99	0.99
NRSH	0.85	0.87	0.84	0.86	0.82	0.91	0.97	0.91	0.90	0.90	0.85	0.89	0.97	0.99	0.99	1.00	0.99	0.99	0.99	0.99	0.99	0.99	0.99	0.99	0.99	0.99	0.99	0.99	0.99	0.99	0.99	0.99	1.00	1.00
NRSH	0.83	0.85	0.82	0.84	0.81	0.91	0.96	0.85	0.85	0.85	0.83	0.86	0.98	0.99	0.99	1.00	0.98	0.99	0.99	0.98	0.99	0.99	0.99	0.99	0.99	0.99	0.99	0.99	0.99	0.99	0.99	0.99	0.99	0.99
NRSH	0.79	0.82	0.78	0.82	0.79	0.94	0.94	0.87	0.85	0.85	0.83	0.86	0.98	1.00	1.00	0.98	1.00	0.98	0.98	0.98	0.98	0.98	0.98	0.98	0.98	0.98	0.98	0.98	0.98	0.98	0.98	0.98	0.98	0.98
NRSH	0.82	0.85	0.82	0.85	0.81	0.96	0.94	0.88	0.88	0.88	0.88	0.88	0.99	0.99	0.99	0.99	0.99	0.99	0.99	0.99	0.99	0.99	0.99	0.99	0.99	0.99	0.99	0.99	0.99	0.99	0.99	0.99	0.99	0.99
NRSH	0.79	0.82	0.78	0.81	0.79	0.91	0.94	0.88	0.86	0.86	0.85	0.89	0.97	0.98	0.97	0.95	0.95	0.98	0.98	0.97	0.98	0.98	0.98	0.98	0.98	0.98	0.98	0.98	0.98	0.98	0.98	0.98	0.98	0.98
NRSH	0.81	0.83	0.81	0.80	0.78	0.89	0.93	0.87	0.87	0.87	0.85	0.89	0.97	0.98	0.97	0.96	0.96	0.98	0.98	0.97	0.98	0.98	0.98	0.98	0.98	0.98	0.98	0.98	0.98	0.98	0.98	0.98	0.98	0.98
RC	0.99	0.97	0.99	0.96	0.94	0.97	0.96	0.88	0.94	0.94	0.88	0.90	0.98	1.00	1.00	0.98	1.00	1.00	1.00	1.00	1.00	1.00	1.00	1.00	1.00	1.00	1.00	1.00	1.00	1.00	1.00	1.00	1.00	1.00
RC	0.99	0.96	1.00	0.95	0.92	0.96	0.97	0.86	0.91	0.91	0.90	0.91	0.98	1.00	1.00	0.98	1.00	1.00	1.00	1.00	1.00	1.00	1.00	1.00	1.00	1.00	1.00	1.00	1.00	1.00	1.00	1.00	1.00	1.00
RC	0.99	0.97	1.00	0.96	0.93	0.95	0.97	0.89	0.92	0.92	0.90	0.91	0.98	1.00	1.00	0.98	1.00	1.00	1.00	1.00	1.00	1.00	1.00	1.00	1.00	1.00	1.00	1.00	1.00	1.00	1.00	1.00	1.00	1.00
RC	0.98	0.95	0.98	0.93	0.91	0.89	0.93	0.94	0.89	0.89	0.90	0.94	0.98	0.98	0.98	0.98	0.98	0.98	0.98	0.98	0.98	0.98	0.98	0.98	0.98	0.98	0.98	0.98	0.98	0.98	0.98	0.98	0.98	0.98
RC	0.99	0.95	0.99	0.94	0.93	0.94	0.94	0.96	0.90	0.90	0.91	0.94	0.98	0.99	0.99	0.99	0.99	0.99	0.99	0.99	0.99	0.99	0.99	0.99	0.99	0.99	0.99	0.99	0.99	0.99	0.99	0.99	0.99	0.99
RC	0.99	0.96	0.99	0.94	0.93	0.94	0.96	0.96	0.91	0.91	0.91	0.94	0.98	0.99	0.99	0.99	0.99	0.99	0.99	0.99	0.99	0.99	0.99	0.99	0.99	0.99	0.99	0.99	0.99	0.99	0.99	0.99	0.99	0.99
RLS	0.92	0.99	0.92	0.96	0.94	0.98	0.98	0.90	0.94	0.94	0.90	0.94	0.97	0.98	0.98	0.97	0.98	0.98	0.98	0.98	0.98	0.98	0.98	0.98	0.98	0.98	0.98	0.98	0.98	0.98	0.98	0.98	0.98	0.98
RLS	0.93	0.98	0.93	0.96	0.97	0.96	0.96	0.95	0.97	0.97	0.93	0.96	0.98	0.98	0.98	0.98	0.98	0.98	0.98	0.98	0.98	0.98	0.98	0.98	0.98	0.98	0.98	0.98	0.98	0.98	0.98	0.98	0.98	0.98
RLS	0.92	0.95	0.93	0.96	0.99	0.91	0.96	0.85	0.94	0.94	0.89	0.92	0.98	0.98	0.98	0.98	0.98	0.98	0.98	0.98	0.98	0.98	0.98	0.98	0.98	0.98	0.98	0.98	0.98	0.98	0.98	0.98	0.98	0.98
RLS	0.94	0.99	0.95	0.99	0.99	0.92	0.96	0.87	0.93	0.93	0.89	0.93	0.98	0.99	0.99	0.99	0.99	0.99	0.99	0.99	0.99	0.99	0.99	0.99	0.99	0.99	0.99	0.99	0.99	0.99	0.99	0.99	0.99	0.99
RLS	0.93	0.97	0.93	0.97	0.98	0.92	0.96	0.87	0.92	0.92	0.89	0.92	0.98	0.99	0.99	0.99	0.99	0.99	0.99	0.99	0.99	0.99	0.99	0.99	0.99	0.99	0.99	0.99	0.99	0.99	0.99	0.99	0.99	0.99
RPQ	0.98	0.94	0.98	0.93	0.94	0.93	0.97	0.85	0.94	0.94	0.88	0.91	0.98	0.99	0.99	0.99	0.99	0.99	0.99	0.99	0.99	0.99	0.99	0.99	0.99	0.99	0.99	0.99	0.99	0.99	0.99	0.99	0.99	0.99
RPQ	0.97	0.92	0.97	0.91	0.93	0.92	0.97	0.85	0.95	0.95	0.91	0.94	0.98	0.99	0.99	0.99	0.99	0.99	0.99	0.99	0.99	0.99	0.99	0.99	0.99	0.99	0.99	0.99	0.99	0.99	0.99	0.99	0.99	0.99
RPQ	0.98	0.94	0.98	0.94	0.93	0.93	0.97	0.86	0.95	0.95	0.91	0.94	0.98	0.99	0.99	0.99	0.99	0.99	0.99	0.99	0.99	0.99	0.99	0.99	0.99	0.99	0.99	0.99	0.99	0.99	0.99	0.99	0.99	0.99
RPQ	0.99	0.94	0.99	0.93	0.92	0.93	0.97	0.86	0.95	0.95	0.91	0.94	0.98	0.99	0.99	0.99	0.99	0.99	0.99	0.99	0.99	0.99	0.99	0.99	0.99	0.99	0.99	0.99	0.99	0.99	0.99	0.99	0.99	0.99
RPQ	0.98	0.95	0.98	0.94	0.94	0.93	0.97	0.86	0.95	0.95	0.91	0.94	0.98	0.99	0.99	0.99	0.99	0.99	0.99	0.99	0.99	0.99	0.99	0.99	0.99	0.99	0.99	0.99	0.99	0.99	0.99	0.99	0.99	0.99
RPQ	0.94	0.86	0.94	0.85	0.85	0.87	0.92	0.88	0.88	0.88	0.85	0.88	0.98	0.99	0.99	0.99	0.99	0.99	0.99	0.99	0.99	0.99	0.99	0.99	0.99	0.99	0.99	0.99	0.99	0.99	0.99	0.99	0.99	0.99
RPQ	0.94	0.88	0.94	0.87	0.85	0.87	0.92	0.88	0.88	0.88	0.85	0.88	0.98	0.99	0.99	0.99	0.99	0.99	0.99	0.99	0.99	0.99	0.99	0.99	0.99	0.99	0.99	0.99	0.99	0.99	0.99	0.99	0.99	0.99
RSH	0.85	0.88	0.85	0.87	0.84	0.85	0.87	0.85	0.85	0.85	0.82	0.85	0.98	0.99	0.99	0.99	0.99	0.99	0.99	0.99	0.99	0.99	0.99	0.99	0.99	0.99	0.99	0.99	0.99	0.99	0.99	0.99	0.99	0.99
RSH	0.86	0.88	0.86	0.85	0.85	0.85	0.87	0.85	0.86	0.86	0.82	0.85	0.98	0.99	0.99	0.99	0.99	0.99	0.99	0.99	0.99	0.99	0.99	0.99	0.99	0.99	0.99	0.99	0.99	0.99	0.99	0.99	0.99	0.99
RSH	0.85	0.88	0.85	0.87	0.84	0.85	0.87	0.85	0.86	0.86	0.82	0.85	0.98	0.99	0.99	0.99	0.99	0.99	0.99	0.99	0.99	0.99	0.99	0.99	0.99	0.99	0.99	0.99	0.99	0.99	0.99	0.99	0.99	0.99
RSH	0.84	0.86	0.85	0.85	0.82	0.82	0.96	0.91	0.85	0.85	0.84	0.84	0.98	0.99	0.99	0.99	0.99	0.99	0.99	0.99	0.99	0.99	0.99	0.99	0.99	0.99	0.99	0.99	0.99	0.99	0.99	0.99	0.99	0.99
RSH	0.85	0.88	0.85	0.87	0.84	0.85	0.97	0.92	0.89	0.89	0.85	0.89	0.98	0.99	0.99	0.99	0.99	0.99	0.99	0.99	0.99	0.99	0.99	0.99	0.99	0.99	0.99	0.99	0.99	0.99	0.99	0.99	0.99	0.99
RSH	0.85	0.87	0.85	0.86	0.83	0.82	0.97	0.92	0.87	0.88	0.85	0.89	0.98	0.99	0.99	0.99	0.99	0.99	0.99	0.99	0.99	0.99	0.99	0.99	0.99	0.99	0.99	0.99	0.99	0.99	0.99	0.99	0.99	0.99

APPENDIX

Table 10: Pearson correlation coefficient between samples from two arrays: Samples with number 1 correspond to first array measured and 2 with second array measured.

	NRC 1	NRLS 1	NRPQ 1	RAFTC 1	RAFTLS 1	RAFTPQ 1	NRC 2	NRLS 2	NRPQ 2	RAFTC 2	RAFTLS 2	RAFTPQ 2	NRSH 1	NRSH 2	RAFTSH 1	RAFTSH 2
NRC 1	1.00	0.87	0.77	0.95	0.87	0.88	0.99	0.78	0.74	0.96	0.83	0.79	0.71	0.53	0.54	0.54
NRLS 1	0.87	1.00	0.96	0.82	0.79	0.87	0.90	0.96	0.95	0.79	0.75	0.85	0.72	0.45	0.45	0.44
NRPQ 1	0.77	0.96	1.00	0.78	0.81	0.89	0.78	0.98	0.99	0.72	0.80	0.90	0.62	0.32	0.32	0.32
RAFTC 1	0.95	0.82	0.78	1.00	0.94	0.95	0.91	0.78	0.77	0.98	0.94	0.89	0.61	0.42	0.44	0.44
RAFTLS 1	0.87	0.79	0.81	0.94	1.00	0.90	0.83	0.81	0.77	0.88	0.95	0.86	0.57	0.35	0.36	0.36
RAFTPQ 1	0.88	0.87	0.89	0.95	0.90	1.00	0.85	0.87	0.88	0.91	0.95	0.99	0.60	0.36	0.38	0.38
NRC 2	0.99	0.90	0.78	0.91	0.83	0.85	1.00	0.79	0.76	0.93	0.77	0.77	0.74	0.55	0.56	0.56
NRLS 2	0.78	0.96	0.98	0.78	0.81	0.87	0.79	1.00	0.98	0.73	0.78	0.87	0.61	0.31	0.30	0.30
NRPQ 2	0.74	0.95	0.99	0.77	0.77	0.88	0.76	0.98	1.00	0.70	0.78	0.90	0.58	0.28	0.28	0.28
RAFTC 2	0.96	0.79	0.72	0.98	0.88	0.91	0.93	0.73	0.70	1.00	0.87	0.83	0.63	0.47	0.49	0.49
RAFTLS 2	0.83	0.75	0.80	0.94	0.95	0.95	0.77	0.78	0.78	0.87	1.00	0.92	0.48	0.26	0.28	0.28
RAFTPQ 2	0.79	0.85	0.90	0.89	0.86	0.99	0.77	0.87	0.90	0.83	0.92	1.00	0.55	0.30	0.32	0.32
NRSH 1	0.71	0.72	0.62	0.61	0.57	0.60	0.74	0.61	0.58	0.63	0.48	0.55	1.00	0.93	0.92	0.92
NRSH 2	0.53	0.45	0.32	0.42	0.35	0.36	0.55	0.31	0.28	0.47	0.26	0.30	0.93	1.00	0.99	0.99
RAFTSH 1	0.54	0.45	0.32	0.44	0.36	0.38	0.56	0.30	0.28	0.49	0.28	0.32	0.92	0.99	1.00	1.00
RAFTSH 2	0.54	0.44	0.32	0.44	0.36	0.38	0.56	0.30	0.28	0.49	0.28	0.32	0.92	0.99	1.00	1.00

	NRC 1	NRLS 1	NRPQ 1	NRSH 1	RaftC 1	RaftLS 1	RaftPQ 1	RaftSH 1	NRC 2	NRLS 2	NRPQ 2	NRSH 2	RaftC 2	RaftLS 2	RaftPQ 2	RaftSH 2
NRC 1	1.00	0.98	0.85	0.86	0.99	0.97	0.97	0.87	0.97	0.96	0.98	0.84	0.99	0.96	0.98	0.87
NRLS 1	0.98	1.00	0.88	0.94	0.96	0.95	0.95	0.95	0.96	0.96	0.97	0.92	0.97	0.95	0.96	0.94
NRPQ 1	0.85	0.88	1.00	0.74	0.81	0.90	0.90	0.76	0.90	0.80	0.79	0.71	0.87	0.93	0.89	0.75
NRSH 1	0.86	0.94	0.74	1.00	0.85	0.80	0.82	1.00	0.84	0.89	0.89	0.99	0.85	0.81	0.82	1.00
RaftC 1	0.99	0.96	0.81	0.85	1.00	0.94	0.97	0.86	0.94	0.96	0.99	0.84	0.99	0.93	0.98	0.86
RaftLS 1	0.97	0.95	0.90	0.80	0.94	1.00	0.93	0.83	1.00	0.90	0.92	0.78	0.93	1.00	0.93	0.81
RaftPQ 1	0.97	0.95	0.90	0.82	0.97	0.93	1.00	0.83	0.94	0.93	0.95	0.80	0.99	0.94	1.00	0.83
RaftSH 1	0.87	0.95	0.76	1.00	0.86	0.83	0.83	1.00	0.85	0.90	0.90	0.99	0.87	0.83	0.84	1.00
NRC 2	0.97	0.96	0.90	0.84	0.94	1.00	0.94	0.85	1.00	0.92	0.94	0.81	0.94	0.99	0.94	0.84
NRLS 2	0.96	0.96	0.80	0.89	0.96	0.90	0.93	0.90	0.92	1.00	0.97	0.88	0.96	0.90	0.94	0.89
NRPQ 2	0.98	0.97	0.79	0.89	0.99	0.92	0.95	0.90	0.94	0.97	1.00	0.88	0.97	0.91	0.95	0.89
NRSH 2	0.84	0.92	0.71	0.99	0.84	0.78	0.80	0.99	0.81	0.88	0.88	1.00	0.84	0.78	0.81	0.99
RaftC 2	0.99	0.97	0.87	0.85	0.99	0.93	0.99	0.87	0.94	0.96	0.97	0.84	1.00	0.94	1.00	0.86
RaftLS 2	0.96	0.95	0.93	0.81	0.93	1.00	0.94	0.83	0.99	0.90	0.91	0.78	0.94	1.00	0.94	0.82
RaftPQ 2	0.98	0.96	0.89	0.82	0.98	0.93	1.00	0.84	0.94	0.94	0.95	0.81	1.00	0.94	1.00	0.84
RaftSH 2	0.87	0.94	0.75	1.00	0.86	0.81	0.83	1.00	0.84	0.89	0.89	0.99	0.86	0.82	0.84	1.00

Table 11: Sample classification control cells' raft and non-raft control astrocyte samples algorithms by lipid fingerprint.

CONTROL ASTROCYTE RAFT AND NON-RAFT CLASSIFICATION

All lipid adducts

Model	Area under ROC	Classification accuracy	F-1	Precision	Recall
k-Nearest Neighbor	1.0	1.0	1.0	1.0	1.0
Random Forest	1.0	0.8333	0.8285	0.8750	1.0
Neural Network	0.8880	0.9166	0.9166	0.9285	0.9166
Naïve Bayes	1.0	0.9166	0.9166	0.9285	0.9166
	Nº of Principal components	**Variability explained**		**Sampling type**	
	9	95%		Stratified 10- fold cross validation	

50 best ranked lipid adducts

Model	Area under ROC	Classification accuracy	F-1	Precision	Recall
k-Nearest Neighbor	1.0	1.0	1.0	1.0	1.0
Random Forest	1.0	1.0	1.0	1.0	1.0
Neural Network	1.0	1.0	1.0	1.0	1.0
Naïve Bayes	0.9722	0.9166	0.9160	0.9285	0.9166
	Nº of Principal components	**Variability explained**		**Sampling type**	
	2	92%		Stratified 10- fold cross validation	

Table 12: Sample classification Low serum- starved cells' raft and non-raft samples algorithms by lipid fingerprint.

LOW SERUM ASTROCYTES RAFT AND NON-RAFT CLASSIFICATION

All lipid adducts

Model	Area under ROC	Classification accuraty	F-1	Precision	Recall
k-Nearest Neighbor	1.0	1.0	1.0	1.0	1.0
Random Forest	1.0	1.0	1.0	1.0	1.0
Neural Network	0.8333	0.8333	0.8333	0.8333	0.8333
Naïve Bayes	0.9722	0.9167	0.9161	0.9286	0.9167
	№ of Principal components	**Variability explained**	**Sampling type**		
	8	95%	Stratified 10- fold cross validation		

50 best ranked lipid adducts

Model	Area under ROC	Classification accuracy	F-1	Precision	Recall
k-Nearest Neighbor	1.0	1.0	1.0	1.0	1.0
Random Forest	1.0	0.9167	0.9161	0.9286	0.9167
Neural Network	1.0	0.8333	0.8286	0.8750	0.8333
Naïve Bayes	1.0	1.0	1.0	1.0	1.0
	№ of Principal Components	**Variability explained**	**Sampling type**		
	2	99%	Stratified 10- fold cross validation		

Table 13: Sample classification paraquat exposed raft and non-raft samples algorithms by lipid fingerprint.

PARAQUAT TREATED RAFT AND NON-RAFT CLASSIFICATION

All lipid adducts

Model	Area under ROC	Classification accuracy	F-1	Precision	Recall
k-Nearest Neighbor	1.0	1.0	1.0	1.0	1.0
Random Forest	1.0	1.0	1.0	1.0	1.0
Neural Network	0.8889	0.6666	0.6250	0.8000	0.6666
Naïve Bayes	1.0	0.9167	0.9161	0.9286	0.9167
	№ of Principal components	**Variability explained**	**Sampling type**		
	8	93%	Stratified 10- fold cross validation		

50 best ranked lipid adducts

Model	Area under ROC	Classification accuracy	F-1	Precision	Recall
k-Nearest Neighbor	1.0	1.0	1.0	1.0	1.0
Random Forest	1.0	1.0	1.0	1.0	1.0
Neural Network	1.0	1.0	1.0	1.0	1.0
Naïve Bayes	1.0	1.0	1.0	1.0	1.0
	№ of Principal components	**Variability explained**	**Sampling type**		
	2	98%	Stratified 10- fold cross validation		

APPENDIX

Table 14: Sample classification control situation raft and non-raft samples from neuron cell line. Algorithms used for lipid fingerprint classification.

CONTROL NEURON RAFT AND NON-RAFT CLASSIFICATION

All lipid adducts

Model	Area under ROC	Classification accuracy	F-1	Precision	Recall
k-Nearest Neighbor	1.0	1.0	1.0	1.0	1.0
Random Forest	0.8888	0.6666	0.6571	0.6875	0.6660
Neural Network	0.6388	0.5000	0.4857	0.5000	0.5000
Naïve Bayes	0.8333	0.8333	0.8285	0.8750	0.8333
	№ of Principal components	**Variability explained**		**Sampling type**	
	8	90%		Stratified 10- fold cross validation	

50 best ranked lipid adducts

Model	Area under ROC	Classification accuracy	F-1	Precision	Recall
k-Nearest Neighbor	1.0	1.0	1.0	1.0	1.0
Random Forest	1.0	1.0	1.0	1.0	1.0
Neural Network	0.9999	1.0	1.0	1.0	1.0
Naïve Bayes	0.9444	0.8333	0.8333	0.8333	0.8333
	№ of Principal components	**Variability explained**		**Sampling type**	
	2	92%		Stratified 10- fold cross validation	

Table 15: Non-raft domains from cells in metabolic stress situation. Classification algorithms in both whole lipid content and 50 best-ranked lipid adducts.

METABOLIC STRESS- NON-RAFT LOW SERUM STARVED AND CONTROL SITUATION CLASSIFICATION

All lipid adducts

Model	Area under ROC	Classification accuracy	F-1	Precision	Recall
k-Nearest Neighbor	1.0	0.7500	0.7333	0.8333	0.7500
Random Forest	0.9166	0.7500	0.7482	0.7571	0.7500
Neural Network	0.5833	0.5833	0.5555	0.6111	0.5833
Naïve Bayes	1.0	0.9166	0.9160	0.9285	0.9166
	№ of Principal components	**Variability explained**		**Sampling type**	
	8	92%		Stratified 10- fold cross validation	

50 best ranked lipid adducts

Model	Area under ROC	Classification accuracy	F-1	Precision	Recall
k-Nearest Neighbor	1.0	1.0	1.0	1.0	1.0
Random Forest	0.9444	0.9166	0.9160	0.9286	0.9166
Neural Network	1.0	1.0	1.0	1.0	1.0
Naïve Bayes	0.7500	0.5833	0.5804	0.5857	0.5833
	№ of Principal components	**Variability explained**		**Sampling type**	
	4	91%		Stratified 10- fold cross validation	

Table 16: raft domains from metabolic stressed cells. Classification algorithms in both whole lipid content and 50 best-ranked lipid adducts.

METABOLIC STRESS- RAFT DOMAIN FROM PARAQUAT EXPOSED AND LOW SERUM STARVED ASTROCYTES CLASSIFICATION

All lipid adducts

Model	Area under ROC	Classification accuracy	F-1	Precision	Recall
k-Nearest Neighbor	1.0	1.0	1.0	1.0	1.0
Random Forest	0.8055	0.8333	0.8285	0.8750	0.8333
Neural Network	0.5833	0.5000	0.4857	0.5000	0.5000
Naïve Bayes	0.9	0.8333	0.8285	0.8750	0.8333

Nº of Principal components	**Variability explained**	**Sampling type**
8	94%	Stratified 10- fold cross validation

50 best ranked lipid adducts

Model	Area under ROC	Classification accuracy	F-1	Precision	Recall
k-Nearest Neighbor	1.0	1.0	1.0	1.0	1.0
Random Forest	1.0	1.0	1.0	1.0	1.0
Neural Network	1.0	1.0	1.0	1.0	1.0
Naïve Bayes	1.0	1.0	1.0	1.0	1.0

Nº of Principal components	**Variability explained**	**Sampling type**
2	98%	Stratified 10- fold cross validation

Table 17: Oxidative stress. Non-raft samples from paraquat exposed and low serum starved cells. Classification algorithms in both whole lipid content and 50 best-ranked lipid adducts.

OXIDATIVE STRESS – NON-RAFT PARAQUAT EXPOSURE AND LOW SERUM STARVATION CLASSIFICATION

All lipid adducts

Model	Area under ROC	Classification Accuracy	F-1	Precision	Recall
k-Nearest Neighbor	0.5	0.6	0.6	0.6	0.6
Random Forest	0.5000	0.5833	0.5804	0.5857	0.5833
Neural Network	0.4444	0.5833	0.5555	0.6111	0.0000
Naïve Bayes	0.8888	0.8333	0.8285	0.8750	0.5833

Nº of Principal components	**Variability explained**	**Sampling type**
8	94%	Stratified 10- fold cross validation

50 best-ranked lipid adducts

Model	Area under ROC	Classification Accuracy	F-1	Precision	Recall
k-Nearest Neighbor	0.8750	0.7500	0.7333	0.8333	0.7500
Random Forest	0.6944	0.6666	0.6571	0.6875	0.6666
Neural Network	0.6666	0.7500	0.7333	0.8333	0.7500
Naïve Bayes	0.8888	0.8333	0.8333	0.8333	0.8333

Nº of Principal components	**Variability explained**	**Sampling type**
4	91%	Stratified 10- fold cross validation

APPENDIX

Table 18: Oxidative stress. raft samples from paraquat exposed and low serum starved cells. Classification in both whole lipid content and 50 best-ranked lipid adducts.

OXIDATIVE STRESS – RAFT PARAQUAT EXPOSED AND LOW SERUM STARVED CLASSIFICATION

All lipid adducts

Model	Area under ROC	Classification accuracy	F-1	Precision	Recall
k-Nearest Neighbor	1.0	1.0	1.0	1.0	1.0
Random Forest	0.8888	0.9167	0.9160	0.9285	0.9167
Neural Network	0.7500	0.5000	0.4857	0.5000	0.5000
Naïve Bayes	0.7500	0.6666	0.6571	0.6875	0.6666

№ of Principal components	**Variability explained**	**Sampling type**
8	94%	Stratified 10- fold cross validation

50 best ranked lipid adducts

Model	Area under ROC	Classification accuracy	F-1	Precision	Recall
k-Nearest Neighbor	1.0	1.0	1.0	1.0	1.0
Random Forest	1.0	0.9166	0.9160	0.9286	0.9166
Neural Network	1.0	1.0	1.0	1.0	1.0
Naïve Bayes	1.0	1.0	1.0	1.0	1.0

№ of Principal components	**Variability explained**	**Sampling type**
2	96%	Stratified 10- fold cross validation

Table 19: Astrocyte and neuron cell line lipid fingerprint classification, both raft and non-raft domains from control situation cells.

ASTROCYTE AND NEURON RAFT AND NON-RAFT CLASSIFICATION

All lipid adducts

Model	Area under ROC	Classification accuracy	F-1	Precision	Recall
k-Nearest Neighbor	1.0	1.0	1.0	1.0	1.0
Random Forest	1.0	1.0	1.0	1.0	1.0
Neural Network	1.0	1.0	1.0	1.0	1.0
Naïve Bayes	1.0	1.0	1.0	1.0	1.0

№ of Principal components	**Variability explained**	**Sampling type**
17	93%	Stratified 20- fold cross validation

50 best ranked lipid adducts

Model	Area under ROC	Classification accuracy	F-1	Precision	Recall
k-Nearest Neighbor	1.0	1.0	1.0	1.0	1.0
Random Forest	1.0	1.0	1.0	1.0	1.0
Neural Network	1.0	1.0	1.0	1.0	1.0
Naïve Bayes	1.0	1.0	1.0	1.0	1.0

№ of Principal components	**Variability explained**	**Sampling type**
4	95%	Stratified 20- fold cross validation

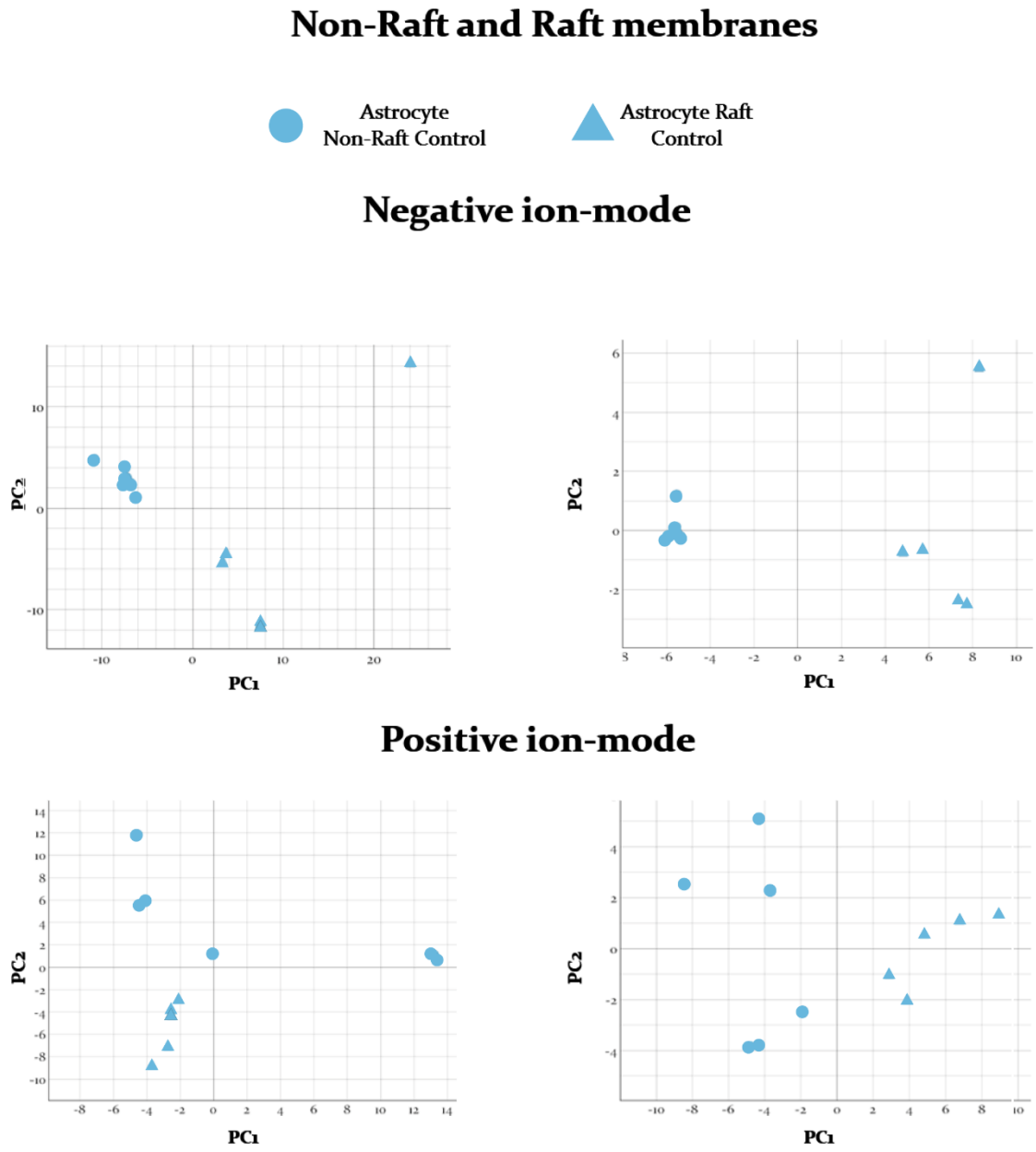

Figure 50: Principal Component Analysis (PCA) of non-raft and raft domains from astrocytes in control situation in positive and negative ion-mode separately.

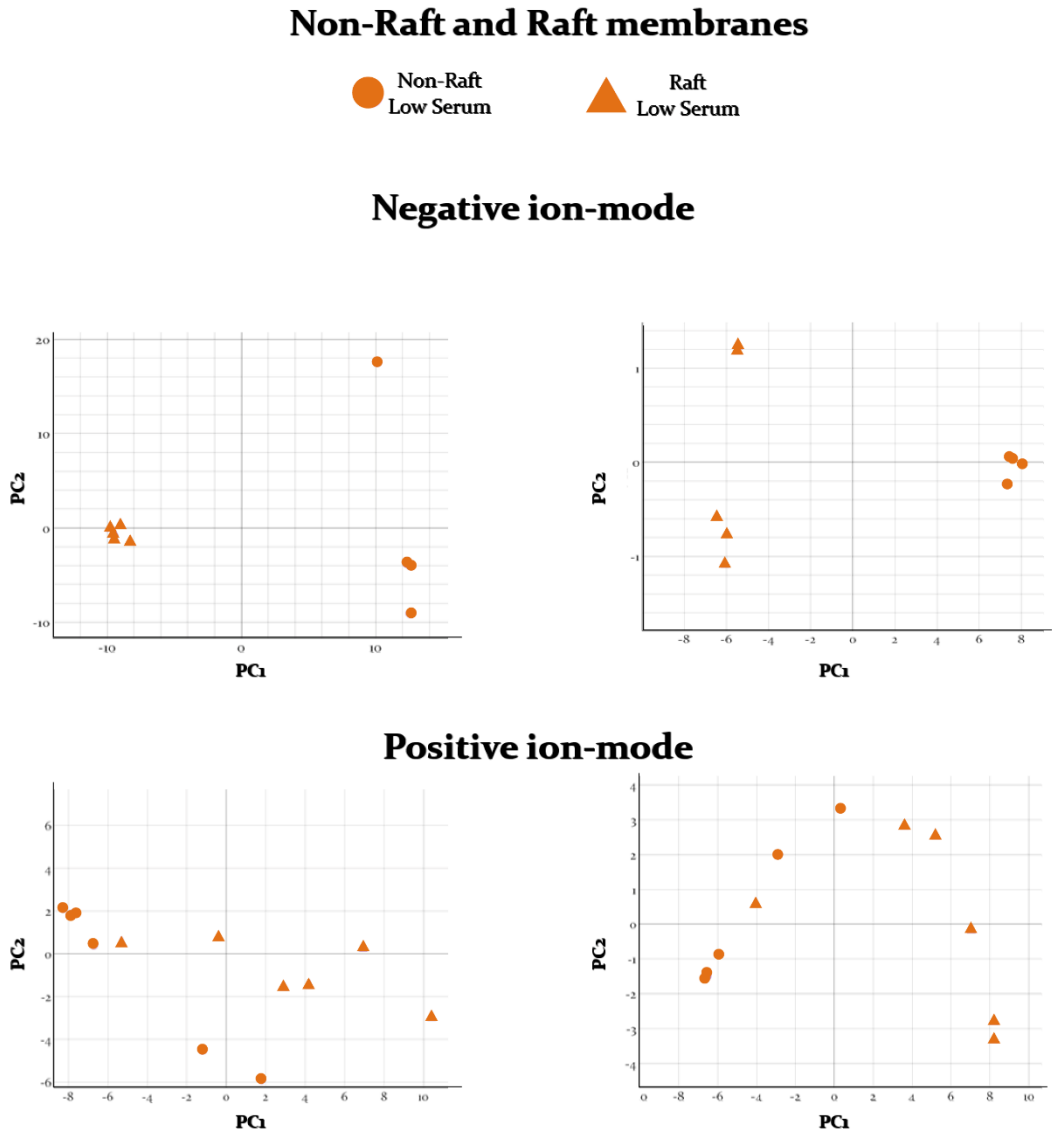

Figure 51: Principal Component Analysis (PCA) of non-raft and raft domains from astrocytes in low serum starvation in positive and negative ion-mode separately.

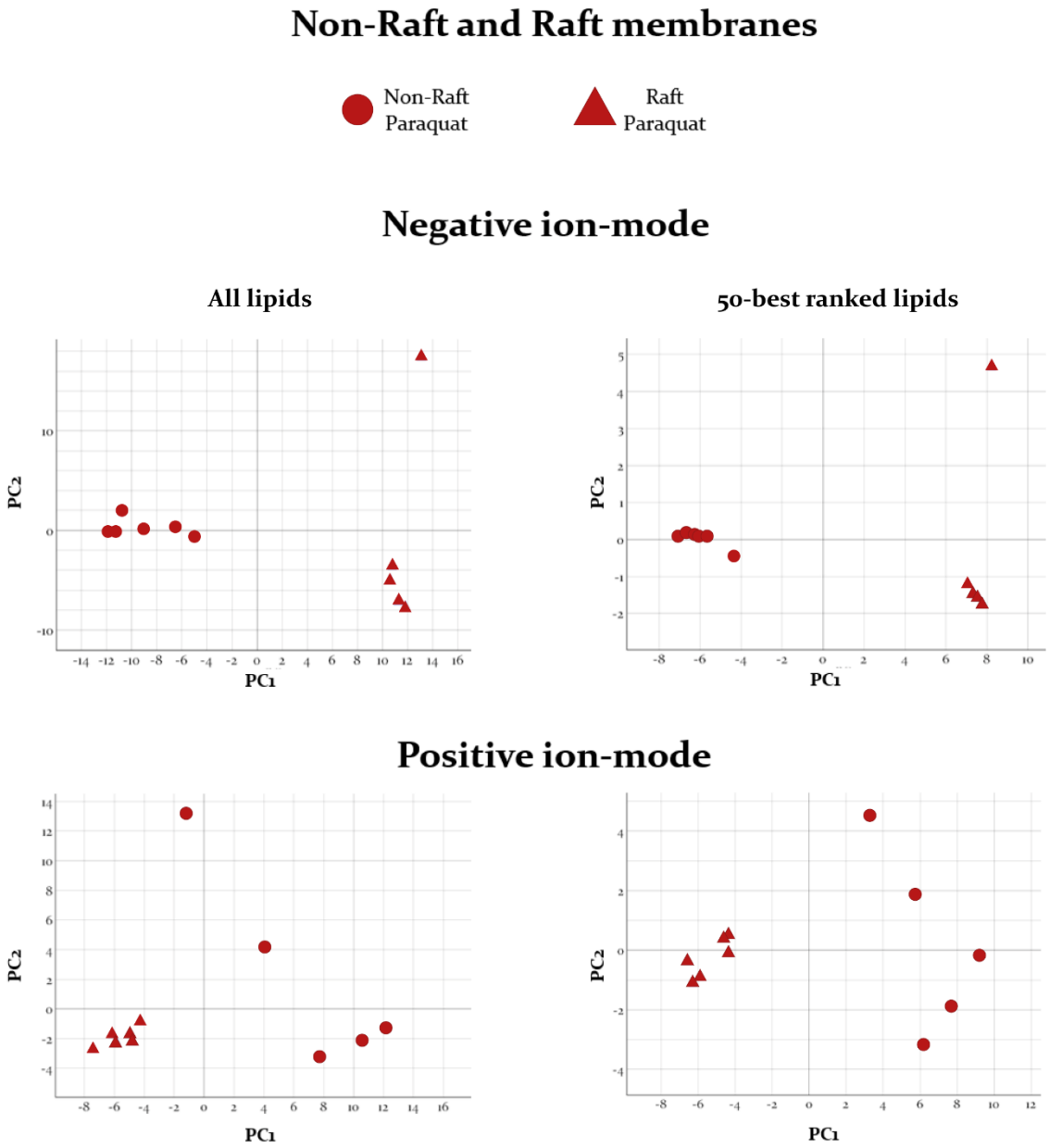

Figure 52: Principal Component Analysis (PCA) of non-raft and raft domains from paraquat exposed astrocytes in positive and negative ion-mode separately.

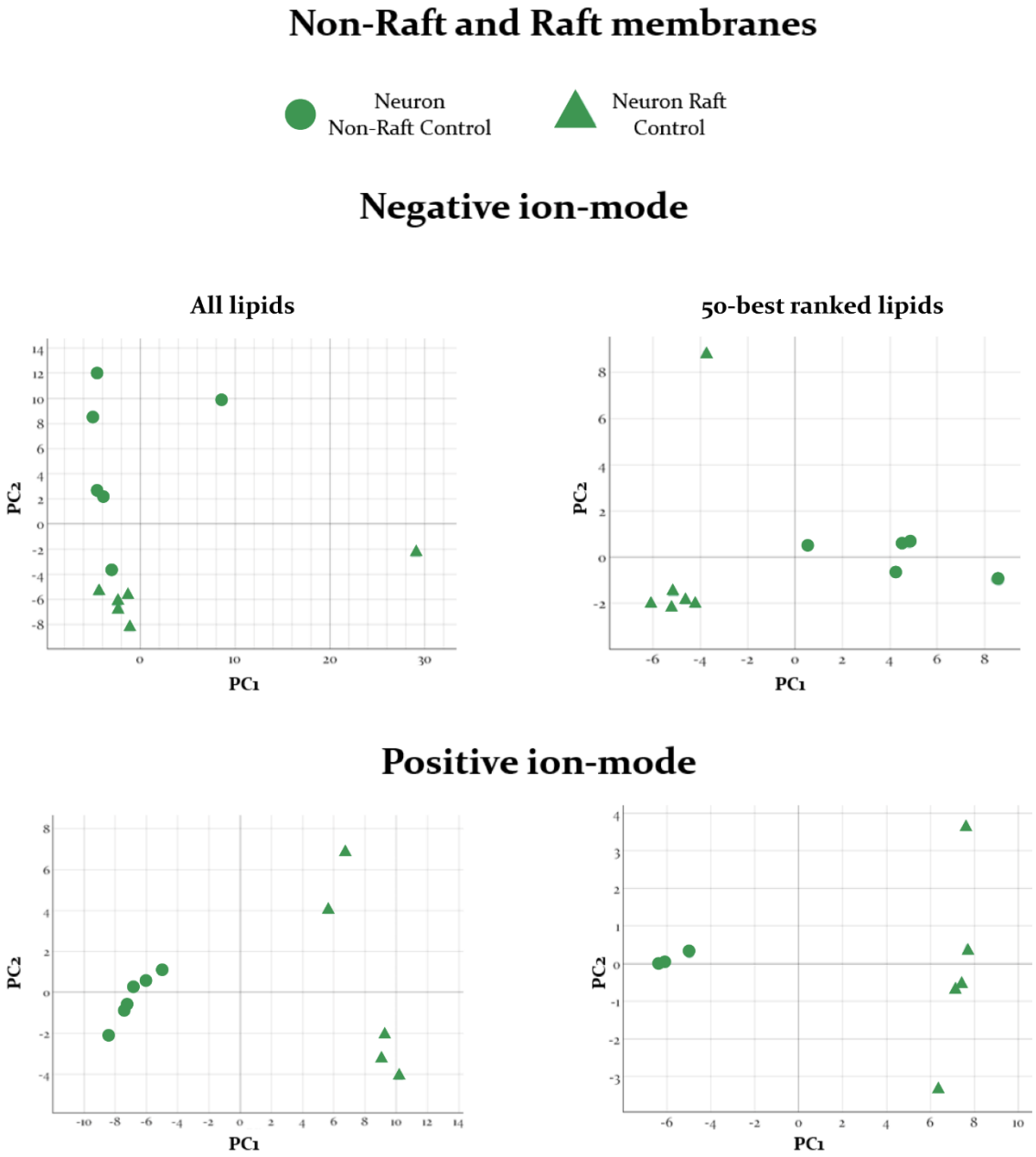

Figure 53: Principal Component Analysis (PCA) of non-raft and raft domains from human neurons in control situation in positive and negative ion-mode separately.

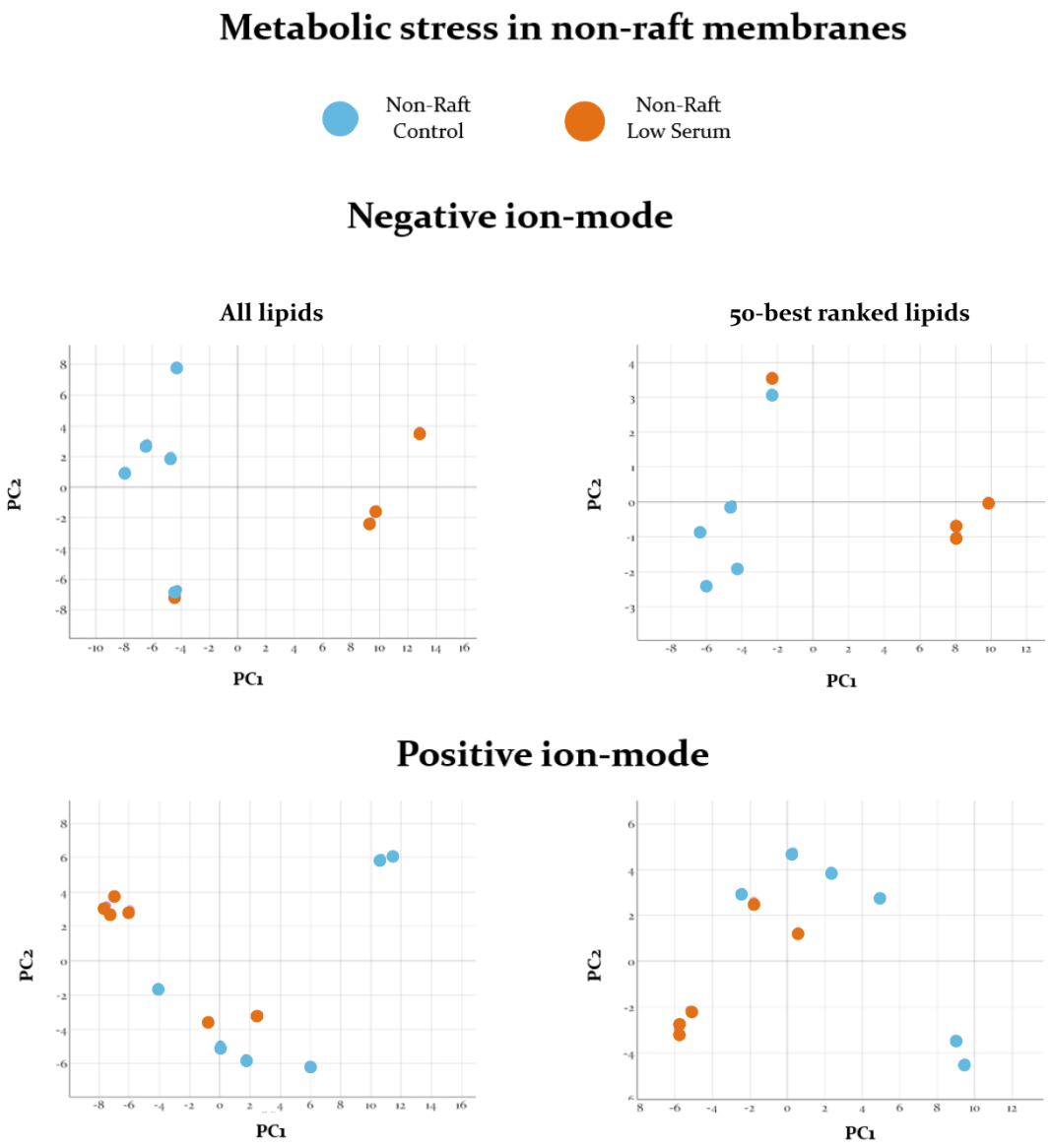

Figure 54: Principal Component Analysis (PCA) of non-raft domains from human astrocytes in control situation and low serum starvation in positive and negative ion-mode separately.

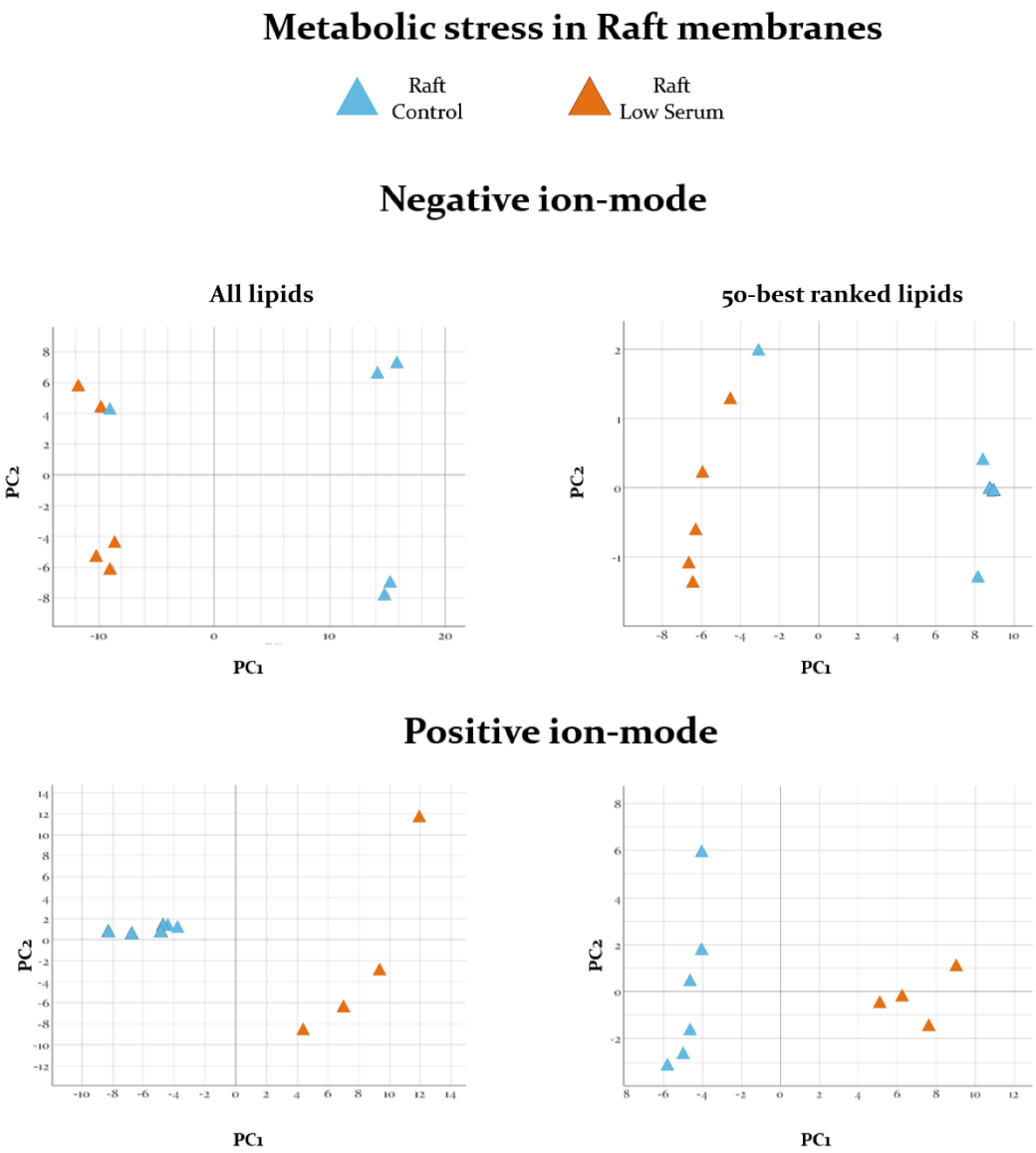

Figure 55: Principal Component Analysis (PCA) of raft domains from human astrocytes in control situation and low serum starvation in positive and negative ion-mode separately.

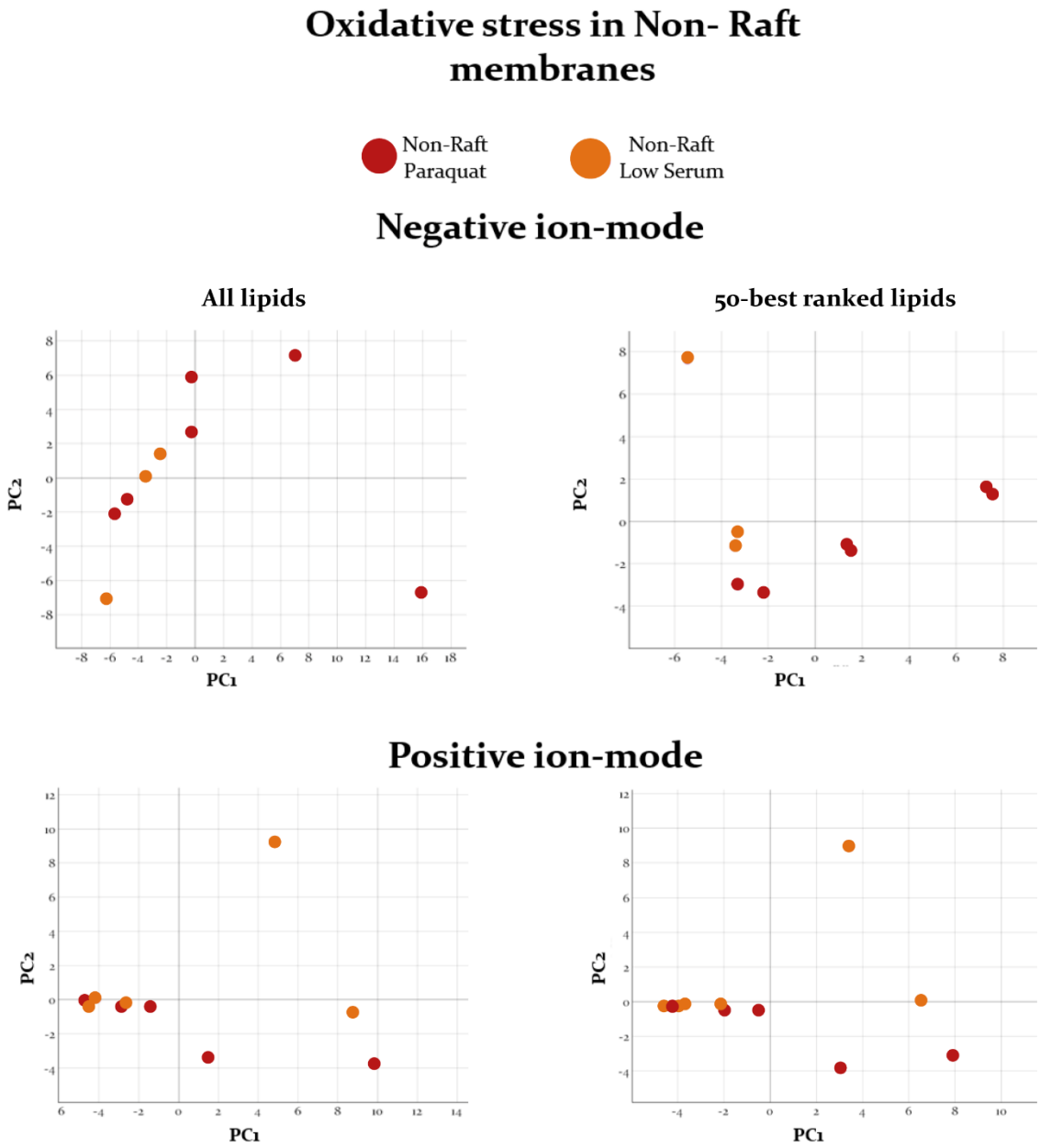

Figure 56: Principal Component Analysis (PCA) of non-raft domains from human astrocytes in low serum starvation and paraquat exposure in positive and negative ion-mode separately.

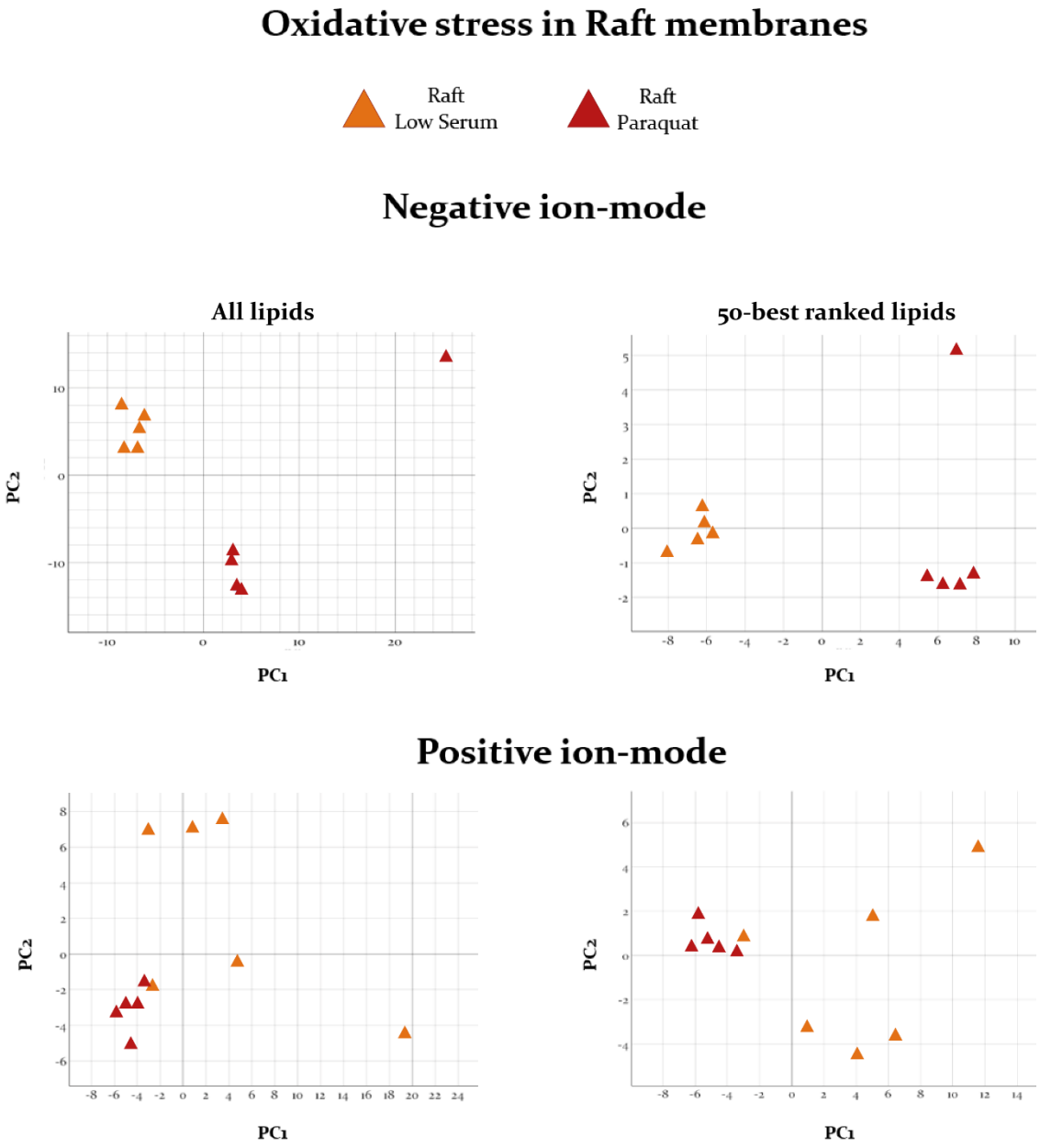

Figure 57: Principal Component Analysis (PCA) of raft domains from human astrocytes in low serum starvation and paraquat exposure in positive and negative ion-mode separately.

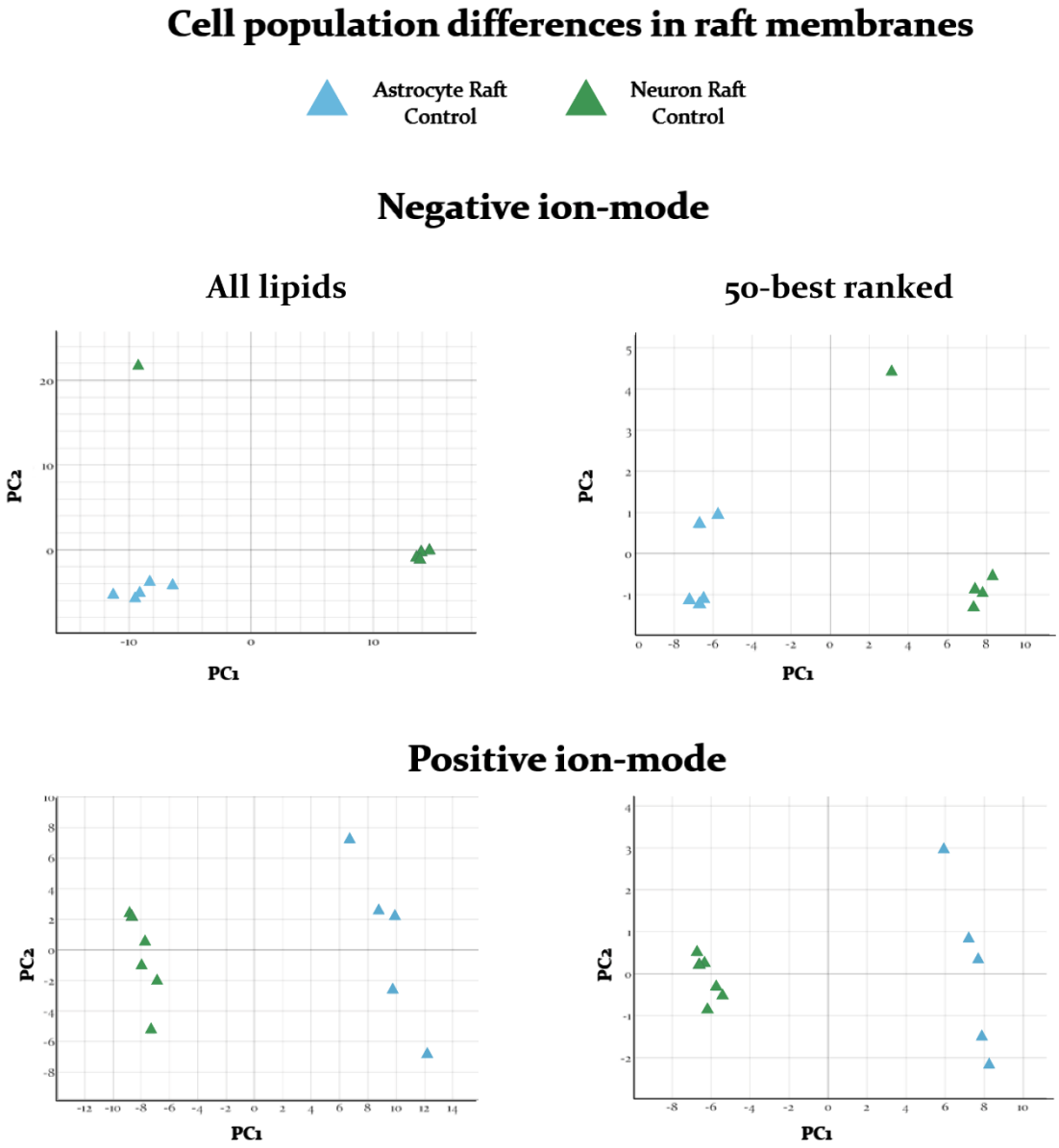

Figure 58: Principal Component Analysis (PCA) of raft domains from human astrocytes and human neurons in control situation in positive and negative ion-mode separately.

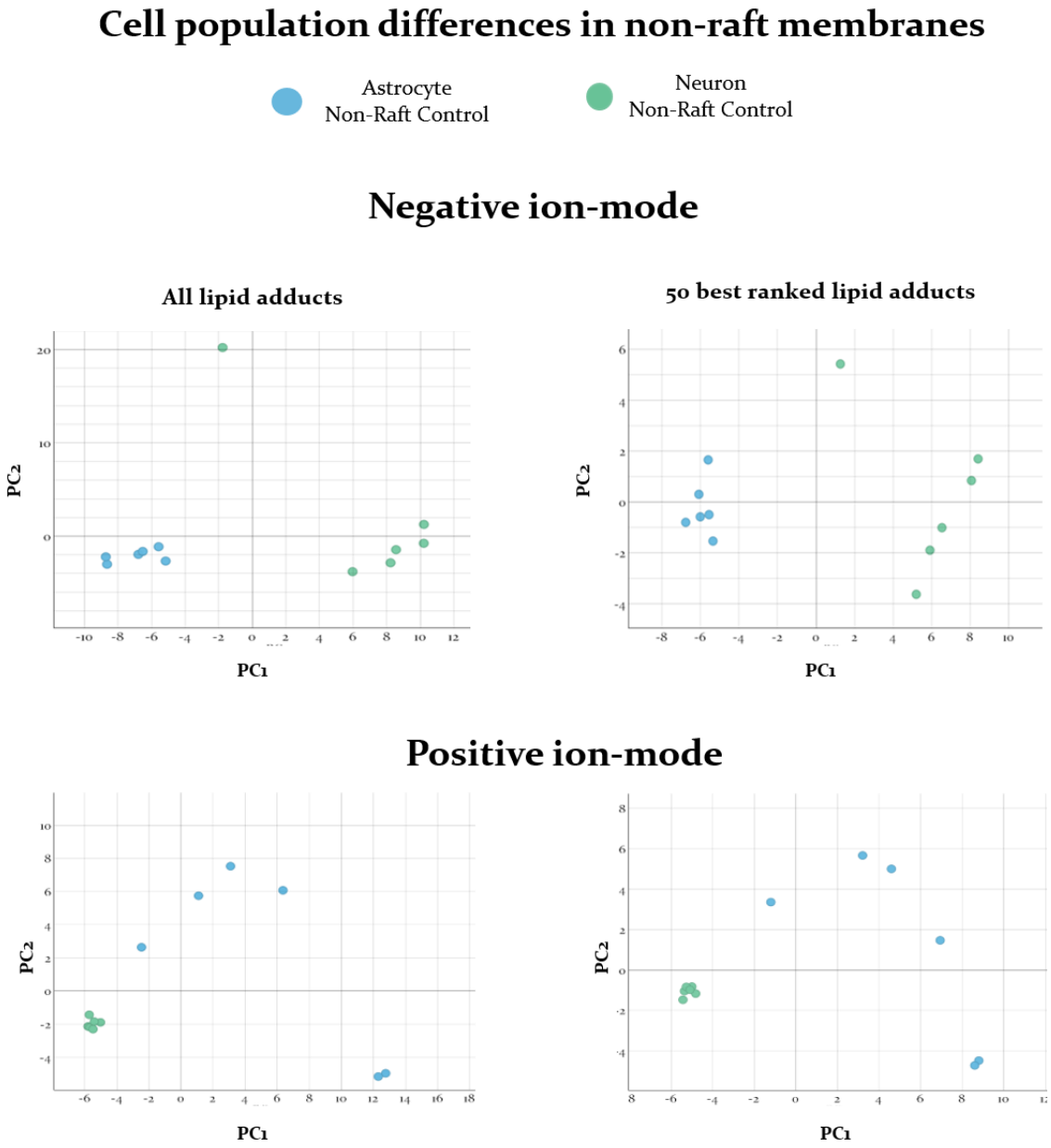

Figure 59: Principal Component Analysis (PCA) of non- raft domains from human astrocytes and human neurons in control situation in positive and negative ion-mode separately.

APPENDIX III

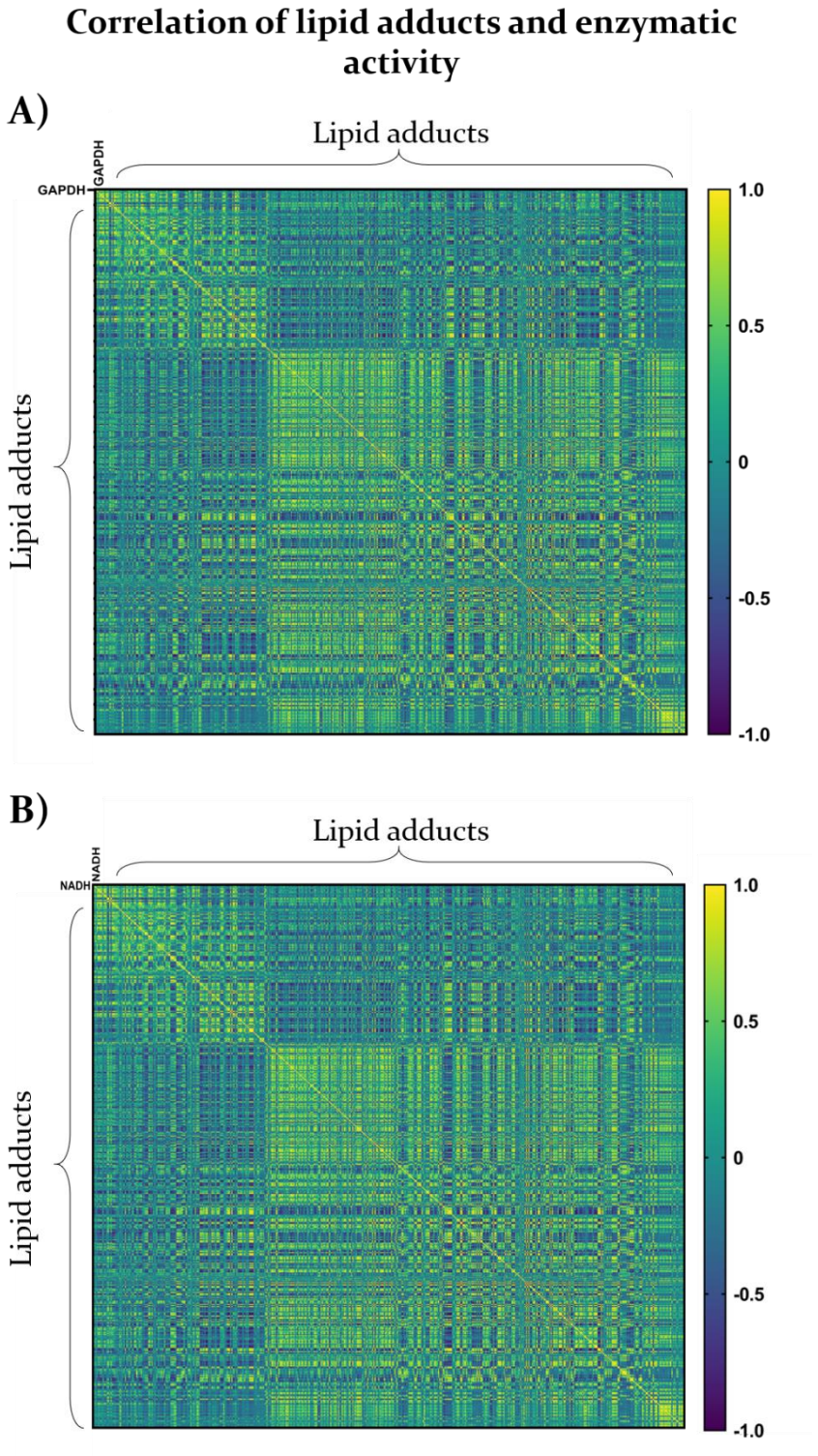

Figure 60: Correlation matrix of NADH or GAPDH activity assays and m/z values of lipidic adducts. A) Correlation matrix of different m/z values of lipid adducts with NADH oxidoreductase activity. B) Correlation matrix of different m/z values of lipid adducts with GAPDH activity.

APPENDIX

Table 20: Correlation of GAPDH and NADH activity and diverse tentatively-assigned sphingomyelins obtained in lipid raft domains.

CORRELATION GAPDH - SM					CORRELATION NADH - SM				
m/z	**Lipid adduct**	**R^2**	**p-value**	**sig.**	**m/z**	**Lipid aduct**	**R^2**	**p-value**	**sig.**
790,62	SM 38:1;O4	0,2606	0,0108	*	684,469	SM 28:0;O6	0,1874	0,0346	*
808,6458	SM 42:4;O2	0,2204	0,0206	*	708,5418	SM 32:0;O4	0,2491	0,013	*
840,7084	SM 44:2;O2	0,1701	0,0452	*	736,5731	SM 34:0;O4	0,2093	0,0246	*
700,5519	SM 34:2;O2	0,3258	0,0036	**	728,5832	SM 36:2;O2	0,3347	0,0031	**
712,5003	SM 30:0;O6	0,3054	0,0051	**	730,5989	SM 36:1;O2	0,5406	<0,0001	****
758,6302	SM 38:1;O2	0,2872	0,0069	**					
786,6615	SM 40:1;O2	0,3551	0,0021	**					
674,5363	SM 32:1;O2	0,4725	0,0002	***					
702,5676	SM 34:1;O2	0,4459	0,0004	***					
784,6458	SM 40:2;O2	0,457	0,0003	***					
810,6615	SM 42:3;O2	0,4383	0,0004	***					
812,6771	SM 42:2;O2	0,4103	0,0007	***					
814,6928	SM 42:1;O2	0,4194	0,0006	***					

NOTES